INVESTIGATIONS ON PERFORMANCE IMPROVEMENT OF SOLAR PHOTOVOLTAIC SYSTEM FED ASYNCHRONOUS MOTOR DRIVE

A THESIS

submitted by

PAKKIRAIAH B
(Regd. No. 131FG06201)

for the award of the degree

of

DOCTOR OF PHILOSOPHY

under the guidance of

Dr. G. DURGA SUKUMAR

VIGNAN'S
FOUNDATION FOR SCIENCE, TECHNOLOGY AND RESEARCH
(Deemed to-be University U/s 3 of the UGC Act, 1956)
Accredited by NAAC with 'A' Grade

**DEPARTMENT OF ELECTRICAL AND ELECTRONICS ENGINEERING
VIGNAN'S FOUNDATON FOR SCIENCE TECHNOLOGY AND RESEARCH
UNIVERSITY, VADLAMUDI
GUNTUR – 522 213, ANDHRA PRADESH, INDIA**

MAY 2017

Dedicated

to

My guide &
My family members!

DECLARATION

I certify that

a. The work contained in the thesis is original and has been done by myself under the general supervision of my supervisor.

b. I have followed the guidelines provided by the Institute in writing the thesis.

c. I have conformed to the norms and guidelines given in the Ethical Code of Conduct of the Institute.

d. Whenever I have used materials (data, theoretical analysis, and text) from other sources, I have given due credit to them by citing them in the text of the thesis and giving their details in the references.

e. Whenever I have quoted written materials from other sources, I have put them under quotation marks and given due credit to the sources by citing them and giving required details in the references.

f. The thesis has been subjected to plagiarism check using professional software and found to be within the limits specified by the University.

g. The work has not been submitted to any other Institute for any degree or diploma.

(PAKKIRAIAH B)

(131FG06201)

CERTIFICATE

This is to certify that the thesis entitled **'INVESTIGATIONS ON PERFORMANCE IMPROVEMENT OF SOLAR PHOTOVOLTAIC SYSTEM FED ASYNCHRONOUS MOTOR DRIVE'** submitted by **PAKKIRAIAH B** to the Vignan's Foundation for Science, Technology and Research University, Vadlamudi. Guntur for the award of the degree of **Doctor of Philosophy** is a bonafide record of the research work done by him under my supervision. The contents of this thesis, in full or in parts, have not been submitted to any other Institute or University for the award of the doctoral degree.

Dr. G. Durga Sukumar   Place: Vadlamudi
Research Guide   Date: 26 May 2017
Professor, Dept. of Electrical and Electronics Engineering
VFSTR University, Andhra Pradesh, India-522 213.

ACKNOWLEGEMENTS

<div align="right">

PAKKIRAIAH B

</div>

x

ABSTRACT

INVESTIGATIONS ON PERFORMANCE IMPROVEMENT OF SOLAR PHOTOVOLTAIC SYSTEM FED ASYNCHRONOUS MOTOR DRIVE

Solar energy is rapidly gaining prominence as an important renewable energy resource. However, only a minuscule portion of the available solar energy is harnessed by the technology till date. Using Conventional Si based photovoltaic modules results a mere conversion of solar energy into electricity is 15%. The factors of conversion can be increased up to 40% by using higher efficiency solar cells under high concentration. The new capacity installation decisions today are becoming more complicated in many parts of the world because of difficulty in finding sites for new generation and transmission facilities. Hence, a research is to be carried out to design and develop various solar plants with MPPT based controller for a PV array with a low cost and battery less electric drive. The system is connected to an asynchronous motor drive where, power is fed to DC-DC boost converter and an inverter from photovoltaic panels.

There are advantages with the use of batteries that are used for maintaining the efficiency of power conversion chain from the PV panel to the asynchronous motor drive. Solar energy is the best option for electricity generation, as it is available everywhere, free and harmless. On an average the sunshine in India is about 6 hrs in a day and annually the sun shine is about 9 months in a year. Electricity from the sun can be generated through the solar photovoltaic modules (SPV). The SPV comes in various power output to meet the load requirement. The photovoltaic (PV) is even more modular than the wind. It allows installations in stages as needed without losing the economy. It can be sized to any capacity, as the solar arrays are priced directly by the peak generating capacity in watts and indirectly by square foot. For small grids, the modularity of the PV and wind systems is having more importance.

Local renewable power plants can also benefit small power systems by moving generation near the load, thereby reducing voltage drop at the end of a long overloaded line. In the developing countries like China and India, the demand for

solar energy has been rising at 10 percent growth rate or more. This growth rate, when viewed with the large population based, makes these two countries rapidly growing electrical power markets for all sources of electrical energy. Major advantages of the photovoltaic power are, Short lead time to design and install for starting a new plant. Power output matches very well with peak load demands. As it is a static structure, no moving parts, hence, no noise and high power capability per unit of weight. Thus, the system has longer life with little maintenance. Highly mobile and portable because of light weight. Researchers in the field of photovoltaic are dealing with the task of making solar energy more efficient.

There exists a variety of avenues in making this type of technology more productive. For example, one branch of research deals with the solid state properties of the materials used in solar cells. This type of research focuses primarily on the properties of thin film silicon and finding methods to manufacture high quality silicon at lower costs. This research is motivated by the fact, that the high quality semiconductor materials are having a significant effect on the energy efficiency of the solar panels themselves. A photovoltaic (PV) system may be a combination of several components such as a battery system, DC/AC conversion circuits and other power conditioning devices in addition to the solar panels. It is environmentally wise to enhance the power output of renewable energy sources. In addition to enhancing efficiency, power conditioning is also used to facilitate energy storage. For example, some battery charging systems may require power conditioning circuitry to provide a desired current to charge batteries effectively.

For this type of system, the use of an electronic circuit called a DC/DC converter is required to control the current supplied by the photovoltaic array to the battery. To prevent battery damage, the charging current supplied to the battery by the DC/DC converter will be determined by the batteries state of charge. In other less sophisticated systems, circuitry may manage battery charging by simply connecting or disconnecting the solar panels. It focuses on the impact of large solar plants on power systems due to rapid variation in power injection caused by various factors such as the intermittency of solar radiation, changes in temperature and tripping out of power electronic based converters connected to the system. It presents a strategy for tracking the maximum power point (MPP) for several solar insolation levels. Here, a voltage based maximum power point tracking scheme is developed for the inverters.

Mathematical models are formulated and then a tracking algorithm is evolved. Maximum power point tracking algorithm that optimizes solar array performance and adapts to rapidly varying irradiance conditions. The Maximum Power Point Tracking (MPPT) system is implemented with the boost DC-DC converter to extract maximum power from the solar PV array.

Here, the research work is carried out with three different types of MPPT techniques such as, P&O, Artificial Neural Network (ANN) based MPPT and Adaptive Neuro Fuzzy Inference System (ANFIS) based algorithms. These algorithms are simulated in Matlab/Simulink and implemented with dSPACE DS-1104 hard ware set up. In particular, a new modified MPPT controller that utilizes the natural inverter, the ripple content is observed and tested on a simulated solar array with an inverter. The new modified algorithm is benchmarked against the perturb and observe (P&O) method using high variance irradiance data gathered on a rooftop array experiment with the help of Space Vector Modulation (SVM) technique in inverter for PV generation system.

PV generation system based on a nonlinear maximum power point tracking method and SVM control scheme for three-phase voltage source inverter is built in Matlab-simulink software. Simulation results show the feasibility and effectiveness of the proposed method. And also it is needed to observe on the impact of large solar plants on power systems due to rapid variation in power injection caused by various factors such as the intermittency of solar radiation, changes in temperature and tripping out of power electronic based converters connected to the system. Here the control algorithm design for a three-phase PV inverter is to achieve either MPPT or a certain amount of real power injection as well as the voltage/var control. The switching between MPPT control mode and a certain amount of real power control mode is automatic and seamless.

DC/DC converters are also useful in circuitry designed to draw maximum power from solar panels with the help of MPP trackers. The great deal of the solar panel's electrical power may be dissipated in the form of heat depending on the load connected directly to solar panels in the absence of an MPPT. In the interest of maximizing energy efficiency, MPPTs are connected between the solar panels and load to ensure that the solar panels are producing their maximum power despite variations in light intensity and/or other factors that may vary within the system. The

power point tracker is developed and tested successfully with the help of Matlab-simulink. MPPT is used in PV systems to maximize the photovoltaic array output power, irrespective of the temperature and irradiation conditions and of the load characteristics. A new modified MPPT system has been developed, consisting of a boost type DC/DC converter. The proposed MPPT system and other techniques are used in the PV array to increase the output power with the help of DC/DC boost converter and inverter.

The main attribute of the boost converter and inverter is to generate an AC output voltage larger than the DC input one, depending on the instantaneous duty cycle. Both the solar panels and batteries supplies DC voltages but most of the electronic devices require AC supply to provide power for them, circuitry is usually required to convert this DC voltage into an AC voltage with the help of an inverters. Once the DC voltage is converted into a 50 Hz waveform with proper amplitude, the AC voltage can then be introduced into a power grid or to the available AC loads. The presence of the inverter makes it possible to use solar energy to power electronic device that runs on AC power. The Dissertation report I am presenting in this work concentrates more on the electronic means of enhancing energy efficiency in a PV system as well as to convert the variable DC from sun into AC to fed AC loads.

This branch of power electronics is generally called power conditioning and in the present case, it is used to describe the management of electrical energy and to charge the batteries effectively, by tracking the maximum power from the solar panels, or to provide a high quality AC output. The controlling purpose is to track the maximum available solar power in a photovoltaic array that is interfaced to an electric utility via a line commutated inverter. Due to its ability to handle nonlinear functions, regardless of the derivative information the Evolutionary Programming (EP) is envisaged to be very effective for MPPT of photovoltaic cell. The ANFIS based MPPT improves the system efficiency even at abnormal weather conditions. Here, a lot of reduction in torque and current ripple contents is obtained with the help of ANFIS based MPPT for an asynchronous motor drive.

Also the better performance of an asynchronous motor drive is analyzed with the comparison of conventional and proposed ANFIS MPPT controller using Matlab-simulation along with experimental implementation. The experimental implementation of MPPT with hardware setup is done using dSPACE real time

controller. Data acquisition and codes of the successfully simulated model can be linked and loaded directly to the dSPACE DS-1104 controller for real-time hardware operation. The advantage of ANFIS is a linguistic controller and does not require a precise and accurate mathematical model of an asynchronous motor drive. The major problem in a conventional system is the presence of ripples in the motor developed torque and stator flux.

One of the methods to reduce ripples in torque and flux with less complexity and cost is space vector modulation strategy. The phase voltages and currents required in the control of asynchronous motor drive which is reconstructed using the DC-link voltage and DC-link current, instead of the stator phase voltages sensed from asynchronous motor drive and hence the number of sensors required is minimized.

TABLE OF CONTENTS

LIST OF TABLES

LIST OF FIGURES

LIST OF SYMBOLS AND ABBRIVATIONS

E_{DR}	Rotational induced voltage
I_{DR}	D-axis rotor current
I_{DS}	D-axis stator current
I_{QR}	Q-axis rotor current
I_{QS}	Q-axis stator current
L_{lR}	Rotor self inductance
L_{lS}	Stator self inductance
V_{DR}	D-axis rotor voltage
V_{DS}	D-axis stator voltage
V_{QR}	Q-axis rotor voltage
V_{QS}	Q-axis stator voltage
w_R	Rotor speed
w_{Sl}	Slip speed
Ψ_{DM}	D-axis mutual flux linkages
Ψ_{DR}	D-axis rotor flux linkages
Ψ_{DS}	D-axis stator flux linkages
Ψ_Q	Total armature flux linkages at Q-axis
Ψ_{QM}	Q-axis mutual flux linkages
Ψ_{QR}	Q-axis rotor flux linkages
Ψ_{QS}	Q-axis stator flux linkages
D^M	'M' pattern's desired output
Y^M	"M" pattern's actual obtained output
Y_N^M	Actual obtained output
AC	Alternating current
ADC	Analog to digital converter
ANFIS	Adaptive neuro fuzzy inference system
ANN	Artificial neural network
C	Capacitor
°C	Degree centigrade
C_{MIN}	Minimum capacitance
D	Duty cycle

DAC	Digital to analog converter
DC	Direct current
dSPACE	Digital signal processing and control engineering
e	Exponential
E_{GO}	Semiconductor band gap energy
EML	Emulated MPP locus
FMPPT	Fuzzy based maximum power point tracking
FNN	fuzzy neural network
FOC	Field oriented control
FPGA	Field programmable gate array
f_S	Switching frequency
GUI	Graphical user interface
I_A	Array current
I_C	Capacitor current
ICs	Integrated circuits
I_D	Diode current
IGBT	Isolated gate bipolar transistor
I_L	Inductor current
I_M	Module current
I_{MPP}	Maximum power point current
INC	Incremental and conductance
I_{OCELL}	Reverse saturation current
I_{OUT}	Output current
I_{PVCELL}	Photon generated current
I_{SAT}	Saturation current
I_{SCR}	Short circuit current
I_{SE}	Series current
I_{SH}	Shunt current
K	Boltzmann's constant
KCL	Kirchhoff's current law
KHz	Kilo hertz
L	Inductor
LGRNN	Limited general regression neural network
L_{MIN}	Minimum inductance

LSE	Least square estimation
MLP	Multilayer perceptron
MMF	Magneto motive force
MOSFET	Metal oxide semiconductor field effect transistor
MPP	Maximum power point
MPPT	Maximum power point tracking
MRE	Mean relative error
N	diode ideality factor
NPC	Neutral point clamped
N_{PR}	No. of parallel cells
N_{SE}	No. of series cells
N_T	No. of total cells
Opp-Amp	Operational amplifier
P&O	Perturb and observation
P_{AP}	Applied temperature
P_{ARRAY}	Array power
PI	Proportional integral
P_{MPP}	Maximum power point power
P_{REF}	Reference irradiance
PV	Photovoltaic
PWM	Pulse width modulation
Q	Electron charge
RCC	Ripple correlation control
RPM	Revolutions per minute
R_R	Rotor resistance
R_{SE}	Series resistance
R_{SH}	Shunt resistance
RTDS	Real time digital simulation
RTI	Real time interface
RTW	Real time workshop
SCR	Silicon controlled rectifier
SSE	Sum of squared errors
STC	Standard test conditions
SVM	Space vector modulation

SVPWM	Space vector pulse width modulation
SVR	Support vector regression
T_{AP}	Applied temperature
T_e	Electromagnetic torque
THD	Total harmonic distortions
T_{REF}	Reference temperature
T_{SCI}	Short circuit temperature co-efficient
V	Voltage
V_{IN}	Input voltage
V_L	Inductor voltage
V_M	Module voltage
V_{MPP}	Maximum power point voltage
V_{OC}	Open circuit voltage
V_{OUT}	Output voltage
V_T	Thermal voltage
Z	Dimension of the output vector
θ_E	Estimated rotor angle

CHAPTER-1

INTRODUCTION AND LITERATURE SURVEY

1.1 General Introduction

Separately excited DC motors were majorly used as drive loads for various research applications over decades because of their simple construction, variable speed, control of torque and flux by the decoupled armature and field currents. Systems that are employed for controlling the motion are called as drives such as robots, pumps and transportation etc... Drive requires the prime movers such as hydraulic motors, electric motors, petrol engines and diesel engines to provide the motion. An electric drive is an electromechanical device which converts electrical energy into mechanical energy and also imparts the motion to the machines and mechanisms for various controlling processes. Since electrical sources are uncontrollable, it is necessary to control the power flow by using power modulators. But complexity in the control unit majorly depends on the desired performance of the drive and motors used. The controller unit can be very simple as operational amplifiers (Opp-Amp) and digital ICs. It can also be complex, by the combinations of computers and digital signal processors.

Asynchronous motor drives play a vital role in industrial applications as they are used worldwide because for their simple installation process, robustness, simple structure, ruggedness, durability, better controlness, reasonable cost, less weight & inertia, low maintenance and comfortable for more applications. Undeniably, for industrial applications, approximately 70% of the entire available electrical power is being consumed by the electric loads, i.e. mostly by asynchronous motor drives. It is quite difficult to get the required task for a peculiar application without a proper speed control. Moreover, asynchronous motor drive is advantageous as it does not require any interfacing between the stationary and rotating parts distinct as that of DC motors. It also does not require any external devices like commutator and brushes in order to have a neat establishment without any sparkling effect.

Thus, it resembles the low maintenance and cost efficient. This superiority made it to be used in various industrial applications. Hence, it is becoming as the perfect

rotational energy conversion machine for variable speed applications. Nowadays, it has numerous applications incorporated with automation techniques for speed control. The variable speed drive with variable frequency can control the speed of the motor that drives such as conveyor belt, pump and fan. Though the asynchronous motor drive has above mentioned merits and advantages, but it has the drawback in controlling its speed. To overcome this drawback, it is incorporated with the variable frequency pulse width modulation (PWM) controlled techniques. Most preferably space vector modulation (SVM) controlling technique for the inverters.

Because, this electric drive has an advantage that by which, its speed can be matched with set reference value if it gets deviates from the provided value due to other disturbances. This can be overcome with the help of feedback closed loop so as to make the motor speed to the set reference value. Due to this, the overall performance of the motor drive is ameliorated a lot by reducing its ripple content in the stator phase current and torque, reaching of early steady state response with attaining of better speed response and minimization of harmonics etc.., which indirectly helps the stability and efficiency of the motor drive. This is possible with the consideration of very important factors as:

- ❖ Invention and design of eminently efficient and completely controllable power semiconductor devices like MOSFET, SCR, IGBT etc….
- ❖ New topologies for soft switching converters.
- ❖ Design of AC machine new control strategies like SVPWM and ANN & ANFIS based MPPT and SVM controlling techniques etc…
- ❖ Analysis for the optimized control solutions for ANN, ANFIS and genetic algorithms etc….

The asynchronous motor drive also needs the variable voltage because; its impedance minimizes the frequency and constantly regulates the current by varying the applied voltage. To obtain the variable supply voltage for the motor drive, it should be provided by the two level inverter that is controlled by the SVM controlling technique. To which the input is supplied by the DC-DC boost converter. For optimization of outputs in this research it is carried out with modified maximum power point tracking (MPPT), ANN based MPPT and ANFIS based MPPT incorporated with the DC-DC boost converter and inverter with SVM controlling

technique. Apart from SVM, many other controlling techniques are also observed in the literature survey.

1.2 Literature Survey

The complete literature survey carried out during this research study is on modeling of photovoltaic systems, working of MPPT controlling techniques, DC-DC boost converters, inverters with controlling techniques and modeling of asynchronous motor drive.

1.2.1   Representation of photovoltaic generation

Electricity is generates by a solid state semiconductor Photovoltaic system (PV) system when it is exposed to sun light. Group of solar cells are gathered to form a solar panel, where, such panels are connected in series and parallel combinations to form a solar PV module to obtain the rated output voltage, current and power. Modules are connected in series and parallel combinations to form solar PV array. Series connection of modules produces the maximum output current where as the parallel connection gives the maximum required voltage.

Due to advantages of PV systems, such as, maintenance free and long life time benefit, they have been commercialized for many countries. Major challenge of PV power generation systems is to control the non-linear characteristics of an array. These characteristic curves are majorly caused by the variable irradiance levels for different climatical conditions like passing clouds, variable temperature, shadows of neighboring buildings and trees. The layout of PV generation is illustrated in Fig.1.1.
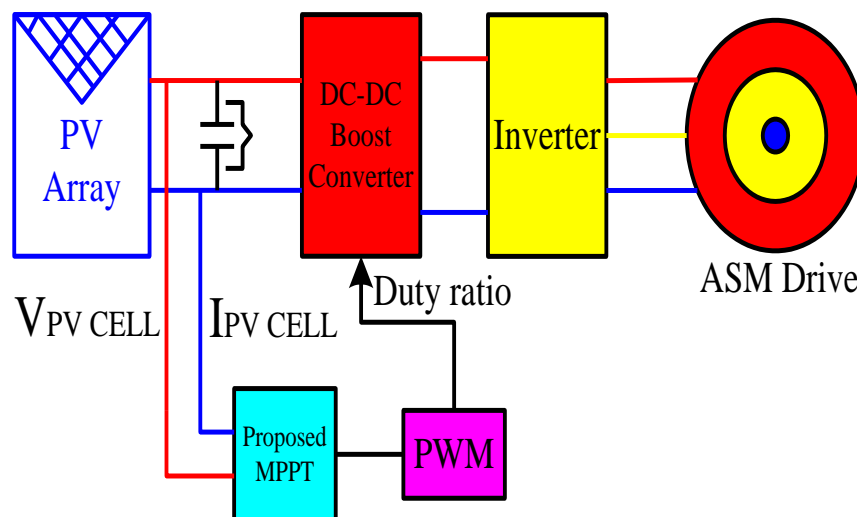
Fig. 1.1 Block diagram representation of photovoltaic generation with a load

Categorization of PV systems will be done based on their operation of systems, functionality, component configurations and the connected equipment to the electrical loads. Mainly classified systems are as, stand alone systems and grid connected systems that are designed to dispense the DC and AC power services to operate independently by connecting them to the electric sources and storage systems.

1.2.1.1   PV system with grid connection

PV systems with grid connection are designed to operate parallelly by connecting it to the electric utility grid systems. It mainly consists of inverter to convert the array DC power into AC power with the voltage and power quality requirements. Between the PV system, AC output circuits and electric utility network, a bi-directional interface is made to allow the AC power either to supply or to feed back to the grid from the on-site distribution panel or service entrance, if the PV system output is greater than load demand (S. Kamaruzzaman, 2009). Grid connected PV system's block diagram is represented Fig. 1.2.
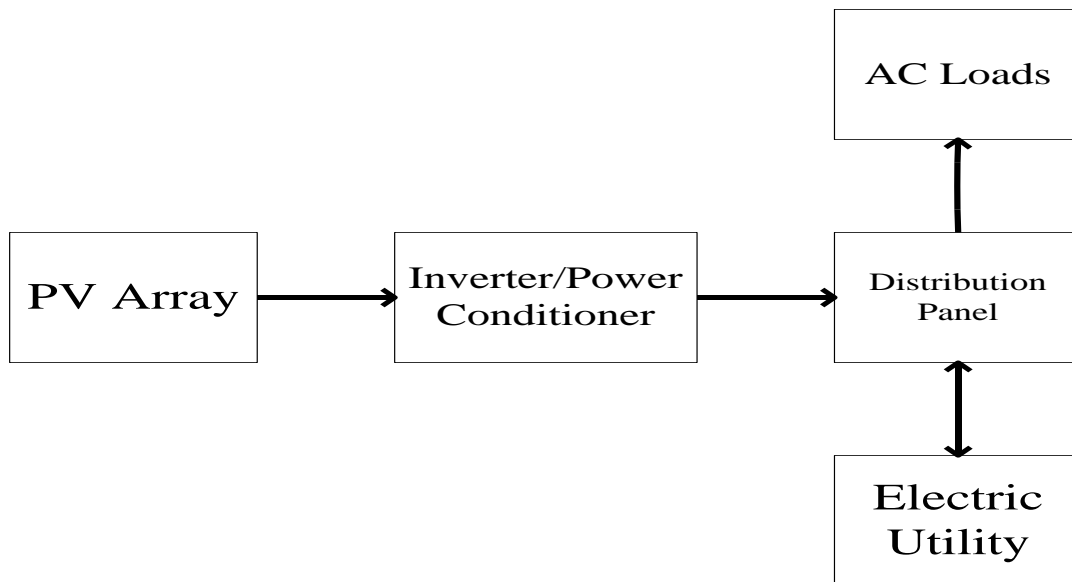
Fig. 1.2 Block diagram representation of PV system with the grid connection

Using boosts converters and multilevel inverters, PV systems are capable of operating at grid connected and stand alone modes, with extracting the maximum power to feed the utility grid as well as to the stand alone systems (C. Liu et al, 2004).

1.2.1.2   Stand alone PV systems

These are mainly delineated to operate independently on the electric utility grid to supply certain DC or AC electric loads. Direct coupled system is the simple type of

standalone PV system that operates only during the sun light hours and that energy is no where stored in the battery system. Major applications of these systems include ventilation fans, water pumps, small pumps for solar thermal water heating systems (S. Kamaruzzaman, 2009). Diagrammatic representation of a direct coupled PV system is available in the Fig. 1.3.
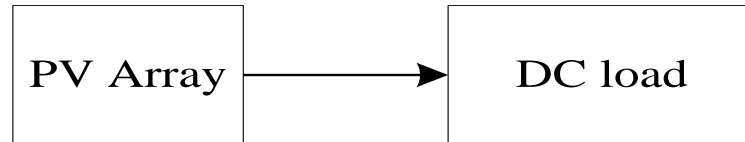
Fig. 1.3 Direct coupled photovoltaic system

Various analysis like, geographical location, climatic conditions, continuous variations of solar radiation, quality of load matching, degree of utilization and accurate sizing are to be considered for various loads in designing the direct-coupled PV systems (J. Appelbaum, 1987, M. M. Saied et al, 1989, K. Y. Kouzam, 1990, K. Y. Kouzam et al, 1991, Q. Kou, et al, 1998). (L. Cristaldi et al, 2012) has observed the working performance of switched-mode converter and MPPT algorithm with the direct-coupled PV system.

Characteristics of the panel with and without MPPT have been observed. In this research, the design methodology is majorly on the variable solar radiations, because, for the provided specific radiation, these results cannot be safely applied over a period of time. Supplying of power for DC and AC loads with battery storage is explained by the stand alone PV systems. (T. D. Hund et al, 1997) as depicted in Fig. 1.4.
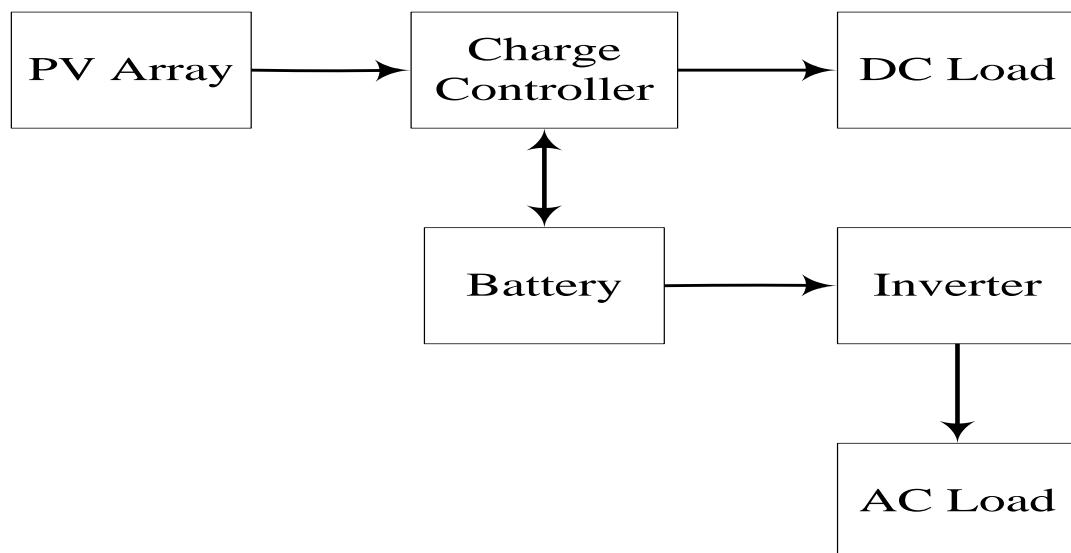
Fig. 1.4 Standalone PV systems with battery storage and loads

Another type is PV hybrid system, which forms by the combination of PV system with the wind turbines (diesel generators), that are used for the grid backup purpose. (Subramanian Krithiga et al, 2014). The layout of such PV hybrid system is represented in the Fig. 1.5.
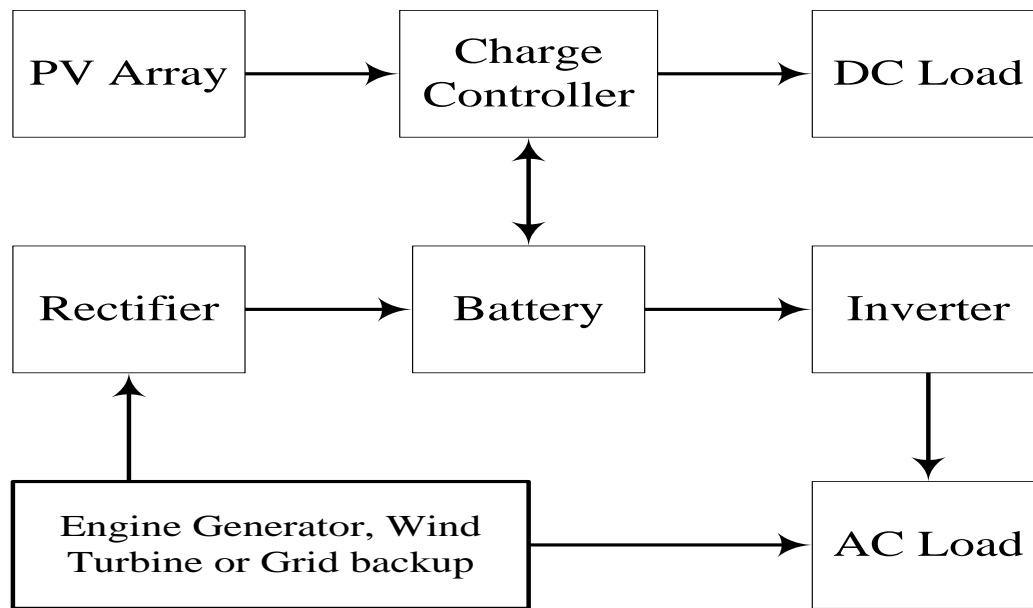
Fig. 1.5 Block diagram of Hybrid type PV system

Series and parallel combinations of solar panels are connected to the boost converter in order to meet the inverter requirement. Difference in panel voltages occurs during partial and fully shaded atmospheric conditions and causes the problems like, location of global MPPs at different positions. To overcome this, suitable optimizers are installed on each panel to work independently from one another, optimize the energy output and make us to monitor the performance of each module. Stand alone system consists of photovoltaic panel, regulator, energy storage system and the load. (S. Duryea et al, 2001).

According to (R. Giral et al, 2010), active voltage sharing minimizes the shadow effect in a two-section module PV system, where, the active bypass does not produce any losses under non-shadow matching conditions. (H. A. B. Siddique et al, 2013) to increase the overall plant output by reducing the overall cost, the loss analysis in the conventional ac configuration for large PV farms & proposed DC collector grid configurations are observed in making it a potentially viable option to increase the energy production and revenue of the plant.

(G. H. Yordanov et al, 2013) the analysis of series resistance corrected load ideality factor, between the MPP open circuit, for various types of crystalline-silicon methodologies are explained. This observation is made to learn more about the PV device performances. (L. H. et al, 2012) based on MPPT technologies with the stable and accurate maximum power points by improving the control precision, the mathematical modeling of photovoltaic cell with its characteristic curves are being analyzed. And also the disturbances based on four corners module perceiving, delay, opening and closing characteristics are discussed.

(A. O. Ibrahim et al, 2013) proposed the multistage SVR (support vector regression) algorithm to avoid outdoor irradiation and temperature. It consists of three stage algorithm for irradiation, temperature and voltage with incentive ambient temperature variations. Here, the implementation and performance of partial shading effect of PV array is not carried out.

1.3 Maximum Power Point Tracking Controlling Techniques

Maximum power point tracking control algorithm is majorly used to extract the maximum capable of PV modules power with the respective solar irradiance and temperature at particular instant of time by MPPT controller. For efficient tracking, numbers of algorithms are developed to track maximum power point. Slow tracking is the most commonly observed drawback in most of the existing algorithms, due to which, the utilization efficiency is reduced.

Three types of modified MPPT control techniques are analyzed and observed to improve the solar energy efficiency in this research. Such as, modified Hill Climbing or Perturbation & Observation (P&O), modified Artificial Neural Network (ANN) with back propagation technique and modified Adaptive Neuro Fuzzy Inference System (ANFIS) based MPPT. The appearance of multi peak output curves during abnormal weather changes in a PV arrays is common, where the development of an algorithm for accurately tracking the true MPPs of the complex and non-linear output curves is crucial and quite difficult.

(W. Libo et al, 2007) says that the MPPT regulates the output obtained from the PV system and provides that output to the DC converter and inverter. If the PV output

voltage is higher than MPP then the power transferred to the load or network is increased.

(L. Piegari et al, 2010) discussed the MPPT techniques for different applications for different individual systems. The MPPT efficiency varies depending on cell temperature and fill factor. (N. A. Azli et al, 2008) proposes the MPPT performance improves with the temperature of the PV system; the 4% of the efficiency is affected by the variations of the fill factor with the climatic conditions and features of geographic region. (M. Tauseef et al, 2012) presented the modeling of MPPT with buck converter with oscillations less than 0.5% in the output power. Also the PV cell with two diode model for MPPT controller which relies on the fact that the ratio of V_{MPP}/V_{OC} does not strongly depend on the environmental conditions.

(P. Mattavelli et al, 2010) implemented the single chip IC circuit for MPPT to interface the PV panel with batteries, inverters to utility grid and the transient response of the system was verified with the step dc voltage to check the MPPT response for PV short-circuit current variations. (H. Al-Bahaldi et al, 2013) discusses the computer simulation to evaluate the performance of MPPT algorithm for PV energy system to carry different PV technologies. Also to demonstrate an excellent and flexible environment for studying various PV solar cells operating at different environments of irradiance and temperature. (Xiaojin Wu et al, 2009) proposed the MPPT method performances to the MPPT structure and cost in the common insolation condition is to reach the efficiency of 98% of the real maximum output power.

(E. Michael et al, 2009) discussed the aspects of PV inverters accuracy consisting of detection behavior and the action of maximum power point tracker response to grid voltage and frequency fluctuations introduced by the PV array. (G. Brando et al, 2007) explained the sensor-less control of H bridge multi-level converter for MPPT in grid connected PV systems to deliver maximum power for variations of incident irradiations on PV arrays with the H-bridge 5 level converter to reduce the current oscillations up to 1% though the voltage slope changes. (S. A. Khan et al, 2010) explained the implementation of MPP algorithm in a 8-bit microcontroller to generate optimized real time code in C.

(R. Kadri et al, 2011) discussed the voltage control MPPT to reduce the power losses caused by dynamic tracking errors under rapid weather changing conditions. Also the grid current components for reflecting the power grid side and the signal error of a PI outer voltage regulation to reflect the change in power by the irradiation variation for identifying the correct direction of MPP. (Nguyen Gia Minh Thao et al, 2013) proposed a method to the controller for PV 1-phase grid connected system with rated power 1 kW for great performances in seeking the MPP of the PV array which regulates the DC link voltage and also reaches unity power factor even if the solar irradiance and temperature vary abruptly.

1.3.1   Perturbation and observe based MPPT

The Perturb and Observe MPPT algorithm is easy to implement, it works based on the PV array is perturbed of a radiation of direction. If the power drained from the array increases the operating point varies towards the MPP which in turn suits therefore the working voltage in the similar direction. if the power drained from the PV array decreases, the operating point varies away from the MPP, thus the direction of the working voltage perturbation have to be overturned (Ajay Patel et al, 2013, T. H. Tuffaha et al, 2014, M. Quamuzzam et al, 2014, Nicola Femia Giovanni Spagnuolo et al, 2005).

A disadvantage of P&O MPPT method is at steady state. The operating point oscillates in the region of the MPP give rise to the waste of energy. A number of improvements of the P&O algorithm have been deliberate in order to decrease the oscillations in steady state, but this slows down the speed of response of the algorithm during the atmospheric changes. (I. K. Song, 2011) discusses power oscillations in P&O algorithm is that the array terminal voltage is perturbed every MPPT cycle. (R. B. A. Koad et al, 2014) proposed to solve decoupling the PV power fluctuations caused by the hill climbing P&O process from the variations of the irradiance to solve the oscillation problem.

In this the incremental change in power ΔP is measured. If the ΔP value is positive, the operating voltage is increased to get MPP, if the value of ΔP is negative, the direction of voltage adjustment is reversed and operating point in trying to make it is the closed to MPP (A. Yafaoui et al, 2007). The flow chart algorithm is shown in Fig. 1.6.
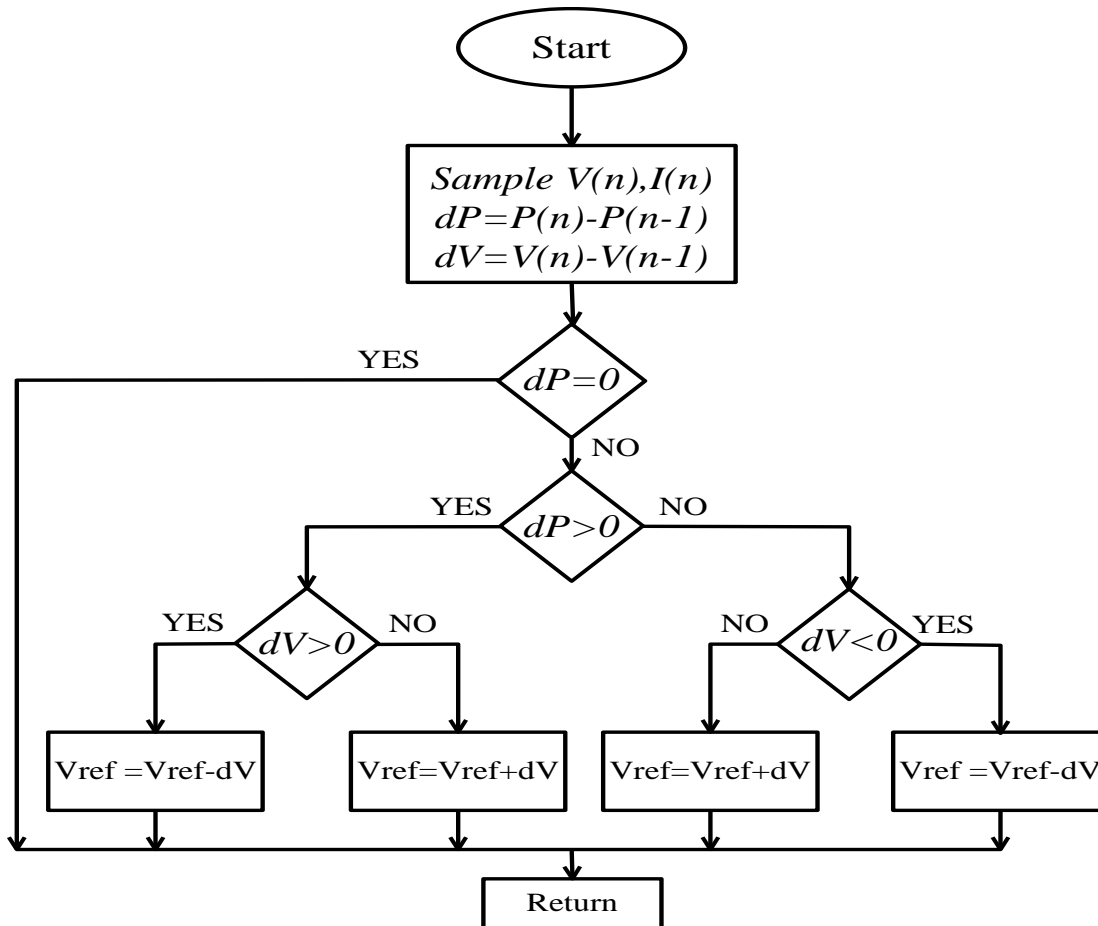
Fig. 1.6 Flow chart of perturb and observation method

However, the applications of analog circuits using P&O algorithm is presented in (J. M. Enrique et al, 2010). (A. Al-Amoudi et al, 1998) proposed a variable step-size that gradually moves towards MPP. But this method is not adaptive because the steps are varied in predetermined way. A model based approach is given by (L. Zhang et al, 2000) to measure the PV array temperature and irradiance. In the specific set of irradiance and temperature measurements, a DC voltage value is predicted so that PV array can deliver maximum output. A variable perturb is proposed in (H. Patel et al, 2009), in this four power ranges are adopted, A specific perturb value is used in each range, but it changes in continuous in a real time.

Therefore, this method is not fully adaptive. Fast tracking is obtained using larger step-size due to this greater oscillations are obtained in (J. M. Kwon et al, 2009, C. Liu et al, 2010).Where converter duty ratio is perturbed instead of array voltage or current. (G. Petrone et al, 2011) discussed a multivariable P&O MPPT techniques for single stage PV inverter. Though it performs well, the need for controlling more than one variable increases the complexity of the operation. (Youngseok Jung et al, 2005)

proposed the improved perturbation and observation method with adaptive algorithm to adjust the reference voltage step size and hysteresis in constant or slowly varying atmospheric conditions to reduce the PV output power up to 5% than the traditional P&O in the unsettled weather conditions.

(J. Suganya et al, 2012) modeled and analyzed the photo voltaic system based on Perturb & Observation MPPT method to maximize the PV array output power by tracking the MPP continuously. It improved the MPPT algorithm under same irradiation condition. (H. Radwan et al, 2012) discussed optimizing of P&O algorithm parameters to get the dynamic behavior of the PV system. Here also some drawbacks are observed, about the oscillations of the operating point around the MPP. In practical the non-ideality of the DC-DC converter are considered for customizing the P&O MPPT algorithm parameters in order to avoid the instability of the algorithm. (Liang-Rui Chen et al, 2010) proposed the biological swam chasing PV MPPT algorithm to improve the MPPT performance.

On comparing with a typical P&O algorithm the efficiency of the MPPT is improved to 12.19% in the transient state. (Wang Nian Chun et al, 2011) proposed the PV model based mathematical models of photo-voltaic array on the basis of P&O method. In this the characteristics of photo voltaic arrays are analyzed. (N. M. Razali et al, 2011) presents the experimental works on a standalone solar system with P&O MPPT algorithm. (Guo Xiao Yun et al, 2011) analyzed the equivalent model of PV cells based on Real Time Digital Simulation (RTDS) and studies the output characteristics of PV cells. In this control of 3-phase PWM inverter controls the output active & reactive power with maintaining of DC bus voltage to a limited reference value.

1.3.2 Artificial neural network based MPPT

In this technique, a multi layered feed-back neural networks with back propagation trained network is used. A two-stage off-line trained artificial neural network based MPPT with two cascaded ANNs to estimate the temperature & irradiance levels from the PV array voltage, current signals. This technique gives the better performance even under rapidly changing environmental conditions for both steady and transient instants with reducing the training set usually a three layer RBFN NN is adopted for implementing the MPPT. (L. Ciabattoni et al, 2013) presented the

home energy management system using neural network monitors the home loads, forecasts photovoltaic production, home consumptions and influences the users on their energy choice.(Lian Jiang et al, 2013) implemented the two stages MPPT to improve non uniform irradiance on the PV modules. In this solar array model a blocking diode is connected in series to PV string to prevent reverse current flow from load, a bypass diode is also used to improve the power capture and prevent hotspots.

Hong hee lee et al, 2010) presented the ANN based MPPT 2 stages method for MPP, this algorithm independent of time dependency and trade property due to this, MPP can be tracked without time increment through PV characteristics changes. (M. Sheraz et al, 2012) to overcome the problem nonlinear characteristics of PV array with rapidly changing irradiation and temperature using differential Evolution (DE) and ANN along with conventional MPPT to track the maximum power point. (Phan Quoc Dzung et al, 2010) implemented the ANN based MPPT and Incremental Conductance method for searching maximum power point based using feedback voltage and current without PV array characteristics.

This method solves the time dependence and trade off as tracking time is very fast. Experimental valuation is carried out using dSPACE 1104. (Jinbang Xu et al, 2011) has presented a new ANN based MPPT algorithm by using the traditional Incremental Conductance using sensors to get better performance. Compared with the Incremental Conductance & the P&O controller it is much faster to the sudden change of the weather combinations. To evaluate the effectiveness of the training network the mean square error is introduced to give the better performance and accuracy of the network. (Long Jie et al, 2011) implemented the 2-level neural network-genetic algorithm to estimate battery power influencing factors as light intensity, temperature, battery junction temperature.

Maximum power point of photovoltaic system can be controlled by online with the use of transform technology of semiconductor memory. (A. Durgadevi et al, 2011) studied V-I & P-V characteristics of PV cell with ANFIS model and empirical model for various temperature, illumination ageing effects of equipment. In this when compared to empirical model, ANFIS model gives better results. (L. M. Elobaid et al, 2012) proposed the two-stage artificial neural network based MPPT to estimate the temperature and irradiance levels from array voltage, current signals in order to

determine the optimum peak operating point. This technique gives the better performance even under rapidly changing environmental conditions for both steady and transient instants.

(Lian Jiang et al, 2013) proposed the two diode PV array model to improve the accuracy under low irradiance and to reduce computational time, irradiance. (Nian Zhang et al, 2013) presented the recurrent neural network model trained by a Particle Swarm Optimization (PSO) for solar radiation monitoring & controlling and to predict accurate the solar radiation of standalone systems and of hybrid power systems. (Yi-Hsum Chiu et al, 2012) presented the ANN based for piecewise line segments (PLS) to approximate the maximum power point locus. It is of high speed, low-complexity MPPT technique.In this a separate high speed voltage is applied to regulate the PV panel output voltage and to follow the emulated MPP locus (EML), a good response due to sudden changes of irradiance levels and helps to improve the tracking efficiency.

This method is simple and achieves the good static and dynamic tracking. (K. Yamauchi et al, 2012) proposed the MPPT using a limited general regression neural network (LGRNN) for testing of two series connected solar panels if one of the panels is under shading condition. The LGRNN is used for learning the each panel output at instances with a limited memory capacity. (S. D. Anitha et al, 2011) presented Artificial Neural Network based MPPT controller for the PV system in order to overcome the drawback of slow, wrong tracking and to operate it at maximum point, and reduce oscillations during rapidly changing weather conditions. In this a with the help of boost converter, inverter are used to provide maximum output voltage to the load. Here back propagation feed forward trained networks are introduced to overcome the non-linearities of PV arrays.

(Zhao Yang et al, 2012) presented the ANN based MPPT control to track the MPP at different weather, irradiance. This network is used to overcome slow tracking speed, more output oscillations and power oscillations. (Ramaprabha et al, 2009) discussed about the 3 layered ANN with back propagation algorithm based MPPT for boost converter for standalone PV system to minimize the long term system losses and to increase the conversion efficiency. Even under variable temperature it gives optimum output voltage.

1.3.3   Fuzzy logic controller based MPPT

Fuzzy logic control is a convenient way to map an input space to output space. Fuzzy logic uses fuzzy set theory, in which a variable is a member of one or more sets, with a specified degree of membership. A fuzzy logic controller basically includes three blocks named as Fuzzification, Inference and De-fuzzification. (H. Afghoul et al, 2013) implemented the hybrid Adaptive Neuro-fuzzy inference system to find operating point near the MPP. (S. Sreekumar et al, 2013) implemented fuzzy logic to obtain maximum MPP operating voltage fluctuations using mamdani method. This method tracks the maximum power rapidly compared to conventional algorithm. (M. Adly et al, 2012) compared the Incremental Conductance and Fuzzy MPPT techniques for the PV model under fast changing environmental conditions.

Here, DC-DC converter is used as an isolation stage for a load connected PV module. (A. Mellit et al, 2007) predicted the daily total solar radiation data from sunshine duration and ambient temperature based on ANFIS model. Here mean relative error (MRE) produces very accurate estimation between the actual and predicted data with not exceeding of 1%. (M. I. Hossain et al, 2011) proposed the intelligent method for maximum power point tracking of a PV system under variable temperature and insolation conditions. In order to overcome non-linearity characteristics of PV cell fuzzy logic control is implemented the duty cycle for the converter is calculated based on fuzzy logic control algorithm.

(A-Al Nabulsi et al, 2011) made a comparison between two controllers as Hill Climbing, two input fuzzy controller and single input fuzzy controller for tracking maximum power point. The basic idea behind these MPPT techniques is to find the optimum duty cycle that results maximum power delivered from the PV panel through DC/DC converter to the load. In this Hill Climbing method controls the operating point of PV array that oscillates around the MPP with causing of power loss, fuzzy with 2 inputs require more calculation with N*N rules in addition to two inputs and output gains but single input fuzzy controller is implemented with least settling time and acceptable oscillations around MPP.

(S. Hadjammar et al, 2013) introduced the Fuzzy Logic based MPPT to extract the maximum power and to feed a three level Neural Point Clamped (NPC) VSI from the photovoltaic system, where this gives the more number of levels of output

waveforms with lower dV/dT, less harmonic distortion & lower switching frequencies. In this multilevel inverter with grid connected PV system using MPPT extracts maximum power, controls active and regulate the reactive power injected into the grid. (A. Mellit et al, 2006) presented ANFIS modeling of a photo voltaic power supply systems under variable climatic conditions, variable radiation, temperature and humidity.

(Yuan Wang et al, 2011) presented the PV plug in hybrid electric vehicles power supply system as the energy storage by replacing the battery and treating as power source for the intelligent community by using of hierarchical fuzzy control with reducing the number of fuzzy rules. Here HFC maintains the output power & reliability of grid from load fluctuations. (Chia Seet Chin et al, 2012) discussed about the optimization of PV system under partially shaded conditions with the P&O algorithm to overcome a low accuracy, fuzzy logic algorithm has been implemented to obtain faster MPP control and more stable output power under transient and steady state conditions. The tracking and settling time with FMPPT is very low compared to P&O algorithm and also to conventional MPPT.

Thus FMPPT gives better efficiency. (A. Iqbal et al, 2010) presented the maximum power with fast response in the available solar irradiance and temperature. Here MPPT are used for the voltage adjustments of PV modules by changing duty ratio of boost converter which is used for calculation of solar irradiance & temperature. ANFIS controller outputs the crisp value of maximum power, where this power is calculated by the multiplication algorithm of sensed voltage & current, the error in power is processed through PI controller by giving its output to the PWM blocks DC-DC converter to adjust the operating PV module. (A. A. Kulaksiz et al, 2012) have presented ANFIS controller for a PV system, in order to control of DC-DC buck converter by providing the duty cycle for the DC-DC buck converter.

(O. Cigdem et al, 2011) presented the sliding mode control to overcome the drawbacks of long convergence process in case of uncertainties and disturbances. In this it tunes ANN & FNN algorithms in online. (Chian-Song Chiu et al, 2011) developed a Sugeno fuzzy MPPT method for PV system. Here maximum power voltage-based control (MPV) direct maximum power (DMP) are used to control the output PV voltage to the reference PV voltage V_{ref} from MPP decision maker and to

control the power slope. (A. Subiyanto et al, 2009) proposed fuzzy logic controller to overcome the draw backs of non-linearities of PV output due to changes in temperature and irradiation. Output obtained from the PV array along with controller techniques will be given to the DC-DC boost converter in order to boost up the PV output up to the load requirement. Few of the literature review points about DC-DC boost converter are stated below.

1.4 MPPT with Boost Converter

(S. Chin et al, 2003) presented a DC-DC converter to transfer maximum power from the solar PV module to the load. This is achieved by module by changing the duty cycle of a converter so that the load impedance is varied and matched at the point of peak power with the source. (G. Spiazzi et al, 2009) discussed about ripple correlation control (RCC) technique on correlation existing between PV panel power, voltage, current ripples and can exploit the AC signals caused by switching action of the converter. It is mainly used to equilibrium point in case of non-sinusoidal and to analyze the simple effects of reactive parasitic components like panel shunts capacitance and series inductance. Finally it is observed that the combined effects of reactive parasitic components can lead to the unacceptable errors in the MPP tracking capability where a high frequency DC-DC converter is used.

(J. Huusari et al, 2012) proposed the distributed maximum power point tracking in order to overcome the effect of shading which used to reduce the output power. Each PV module is connected by a DC-DC converter to extract maximum power where its output is connected to the grid connected inverter. It is also discussed about the terminal constraints, topological constraints and dynamic constraints to get maximum output voltage. (Weiping Luo et al, 2009) studied the MPPT with MCU control system in a grid connected photovoltaic generation system by introducing DC-DC conversion techniques. (S. Patel et al, 2011) gives an analysis of the PV module characteristics and determination of short-circuit current to get converging maximum power point tracking control.

It is observed by connecting the DC-DC converter between the PV source and the load with pulse width modulation control of the converter. In this the short circuit current, open circuit voltage and load voltage at MPP determined.

Here the boost converter is turned to ensure the operation of PV array at its maximum power point regardless of atmospheric conditions and load variations. (A. Trejos et al, 2012) presented the DC link voltage oscillation compensations in grid connected PV systems based on three different DC/DC converters such a Cuk converters, SEPIC converters and Zeta converters.

These high order converters are suitable for reducing the current ripple injected in the PV array and load. (E. Koutroulis et al, 2001) proposed low power consumption MPPT for battery charging which consisting of a high efficiency DC/DC buck type converter. A micro-controller based unit is used to control the DC/DC converter directly from the PV array output power. (Zhigang Liang et al, 2012) introduced a switching capacitor buck-boost DC/DC converter to process of energy operated by PV module. (A. F. Cupertino et al, 2012) presented the control in a maximum power tracker boost converter for a grid connected photo voltaic system using two topologies.

In this active power injected in the grid is close to generated value besides the control of the inverter which reduces the harmonic distortion. (Jun Pan et al, 2009) proposed the MPPT strategy to charge the photovoltaic system. This charging needs PV array, DC/DC controller, battery. As the output characteristics of PV array varies with the change in solar radiation, ambient temperature due to this constant voltage and constant current are not suitable for PV charging system. Here DC/DC converter is used to track the output current and adjusts the perturb step to achieve fast accurate tracking. In the charging management an optimal charging strategy, which integrates MPPT charging with variable intermittent current charging to increase the battery's charging acceptance and level of state of charge.

Boosted output from DC-DC converter is fed to the two level inverter for the convertification of DC quantity into AC quantity so as to provide the required supply to the asynchronous motor drive. For the better outputs of the inverter with less ripple and total harmonic distortions (THD), that the inverter is incorporated with the space vector modulation (SVM) controlling technique. Output of inverter is fed to the asynchronous motor drive and its performance is evaluated by the matlab-simulation along with experimental validation. Platform used for the experimental validation is dSPACE RTI-1104.

1.5 SVM Controlling Technique

Solar energy is a vital untapped resource in a tropical country like ours. India plans to produce 20 Giga watts of solar by 2020. A MPPT controller with the inverter is connected to the asynchronous motor drive with space vector modulation technique to get the better performance with the PV system. Various strategies are used for selecting the order of vectors with zero vectors to reduce the harmonic content and the switching losses (J. J. Joshi et al, 2013, M. Aleenejad et al, 2012).

The space vector modulation diagram of an inverter is composed of number of sub hexagons. The sector identification can be done by determining the triangle which encloses the tip of the reference space vector diagram with forming of six regions (C. Sreeja et al, 2011, A. Mbarushimana et al, 2011). To overcome the distortions in the inverter output voltage and currents, single phase SVM based cascaded bridge inverter is used for PV system to improve the quality of power even under abnormal weather conditions.

The reduced torque ripple and the performance are obtained with the help of particle swarm optimization method for the optimal torque control of an asynchronous motor drive (Dong Hwa Kim et al, 2007). A comparison of neuro fuzzy based space vector modulation with neural network and conventional based system has been presented (Durga Sukumar et al, 2014), it proposes that the direct adaptive fuzzy sliding mode control is employed to control a class of under-actuated uncertain systems which can be regarded as a combination of several subsystems with one same control input by using the hierarchical sliding control approach (Shun-Feng Su et al, 2015).

(J. Selvaraj et al, 2009, S. Mekhilef et al, 2002) developed DSP TMS320F2812 and FPGA based photovoltaic converters for the controlling techniques. However, these converters need the developed software programming for controlling purpose. In addition to a simulation model, the experimental validations were also being implemented. A different method for PV inverters is approached with the help of dSPACE RTI-1104 control technique to implement the Matlab/Simulink model for the simulation and experimental validations. The dSPACE RTI-1104 control platform simplifies the controlling technique using its control library. Moreover, the data and

codes of successfully simulated model are linked directly to the controller board for real-time experimental implementations.

In this paper, adaptive neuro fuzzy inference system (ANFIS) based MPPT method is implemented for the experimental validation along with the simulation. The experimental implementation (validation) is done with the help of dSPACE RTI-1104 real time controller with the hardware setup. The benefit of this ANFIS based MPPT is to control the operating point even at the uneven climatical conditions with higher tracking and conversion efficiency. Asynchronous motor drive performance parameters are clearly explained in the individual respective chapters with the specified respective methods.

1.6 Thesis Main Objectives

The main purpose of this research work is mentioned below

- ❖ To develop the PV array mathematical modeling with the parameters of voltage, current, temperature, irradiance, ideality factor, series resistance, shunt resistance and total number of cells.
- ❖ To develop the conventional MPPT, modified MPPT.
- ❖ To develop the artificial neural network and adaptive neuro fuzzy inference system based MPPTs with the obtained data pattern values from the modified MPPT controller to get better performance.
- ❖ To develop the SVM controlling technique for the two level inverter.
- ❖ To develop the simulink modeling of an asynchronous motor drive with the observable performance parameters and also
- ❖ The performance of the simulation system is compared with experimental validations using dSPACE RTI-1104 hardware setup along with PV array practical set up, MPPT controller with boost converter module, inverter module incorporated SVM controlling technique and asynchronous motor drive.

1.7 Organization of the Thesis

This thesis work is divided into seven chapters and the organization of the research work is represented as:

Chapter-1 represents the general introduction of the research problem along with the previous investigations report or research carried out knee points in the literature survey and the main objectives of the thesis.

Mathematical modeling of PV array with its working performance for different temperature and different irradiance conditions at different instants of time is discussed in chapter-2.

Performances of PV system with the conventional perturb & observation based MPPT and modified MPPT controlling techniques are explained in chapter-3 along with the DC-DC boost converter design.

Mathematical modeling of asynchronous motor drive, development of space vector modulation (SVM) technique with the two level inverter and the performance of an asynchronous motor drive with the modified MPPT, developed inverter and SVM controlling technique is detected in chapter-4.

ANN based MPPT is designed and the performance of the asynchronous motor drive with the ANN based MPPT and two level inverter incorporated with the SVM controlling technique is observed in chapter-5.

Chapter-6 analyzes about the enhanced performance of an asynchronous motor drive parameters with the simulink developed ANFIS based MPPT along with the SVM controlling technique of the two level inverter. In this chapter, the experimental validation is also carried out by the hardware set up of dSPACE RTI-1104 platform.

The concluding remarks with the future scope are stated in chapter-7.

1.8 Conclusion

General introduction of the identified research problem is represented along with the previous investigations report notes or various researches carried out techniques (knee points) in the literature survey. And also the main objectives of the entire thesis are clearly mentioned along with the brief notes of each individual chapter by the thesis organization.

CHAPTER-2

MATHEMATICAL MODELING OF PV SYSTEM

2.1 Introduction

The Photovoltaic cell is a semiconductor device that converts light energy into electrical energy by photoelectric effect. If the energy of photon of light is greater than the band gap then the electron is emitted and the flow of electrons generates electricity in a clean, quiet and reliable way. Photovoltaic systems are comprised of photovoltaic cells. The word 'photovoltaic' comes from **'photo'** means **light** and **'voltaic'** refers to **producing the electricity**. Therefore, the photovoltaic process is producing the electricity directly from sunlight, which is often referred to as PV. In this mathematical modeling of the poly photovoltaic system is described with respect to the irradiance and temperature along with the effects of series and shunt resistances.

2.2 Mathematical Modeling of PV Array

PV cells are made of semiconductor materials with crystalline, thin film, amorphous, multi-junction and organic or photochemical as the dominant materials. The majority of PV-cells are silicon based but in the near future other thin film materials are likely going to surpass silicon PV cells in terms of cost and performance. The use of equivalent electric circuits makes it possible to model characteristics of a PV cell. The method used here is implemented in MATLAB program for simulations. The same modeling technique is also applicable for modeling a PV module and PV array. PV module is formed by the series and parallel connections of PV cells. Similarly PV array consists of several photovoltaic modules in series and parallel connections. Series connections are responsible for increasing the voltage of an array whereas the parallel connection is responsible for increasing the current in the array.

2.2.1 Modeling of ideal PV cell

A single PV cell produces an output voltage less than 1 V i.e. each Si Photovoltaic cell will give the output voltage of around 0.7 V under open circuit condition and 0.5 V under working condition. No. of cells are connected in series and

parallel to form a PV module and No. of modules are connected in series and parallel to produce the required output. Using Si based photovoltaic modules the PV system converts only 15% of solar energy into electricity. Ideal solar PV cell is modeled by a current source and an inverted diode connected in parallel to it as shown in Fig. 2.1.
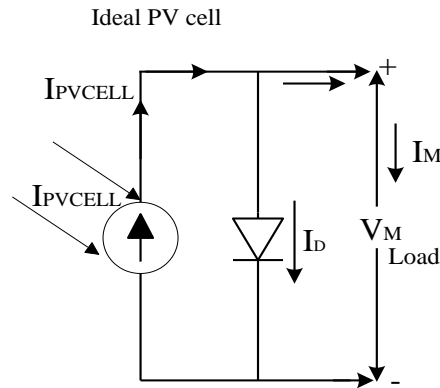
Ideal PV cell

Fig. 2.1 Ideal PV cell equivalent circuit

The current source represents the current generated by photons denoted as I_{PVCELL} and its output is constant under constant temperature and constant light incident radiation. The practical behavior of cell is deviated from ideal due to the optical and electrical losses. There are two key parameters as short circuit current (I_{SCR}) and open circuit voltage (V_{OC}) that are frequently used to characterize a PV cell. By short circuiting the terminals of the cell the photon generated current (I_{PVCELL}) as shown in Fig. 2.2 (a), flows out of the cell called as a short circuit current (I_{SCR}).

Thus, we can say that $I_{PVCELL} = I_{SCR}$ as the current I_{PVCELL} is flowing in a single series circuit. As the terminals are short circuited then the voltage across the circuit is equal to zero i.e. $V_{OC} = 0$ and the short circuit current (I_{SCR}) is the PV cell load current (I_M) or the output current which is very maximum as equal to that of current source or photovoltaic photon generated current (I_{PVCELL}) i.e. $I_{PVCELL} = I_{SCR} = I_M$. Similarly when the terminals are open circuited i.e. no load and nothing is connected as represented in 2.2 (b), the load current of a PV cell (I_M) becomes zero.

And the load voltage of a PV cell is equal to the maximum applied source voltage or open circuit voltage i.e. ($V_M = V_{OC}$). When there is no connection to the PV cell then the photon generated current is shunted internally by the intrinsic p-n junction diode to give the open circuit voltage (V_{OC}). The PV module or cell manufacturer usually provides the values of these parameters in their datasheets.

22

(a) PV cell at short circuit condition   (b) PV cell at open circuit condition

Fig. 2.2 PV cell at different working conditions
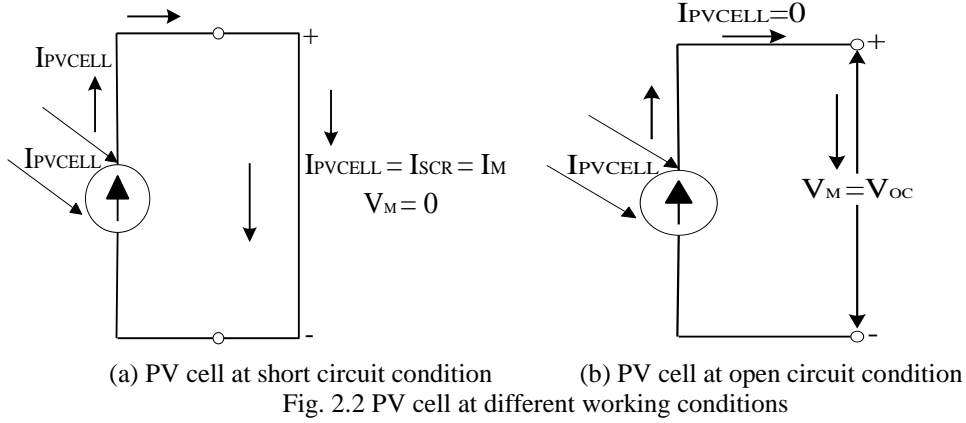
The output current (I_M) from the PV cell is found by applying the Kirchhoff's current law (KCL) on the equivalent circuit as shown in Figure 2.1.

$$I_M = I_{PVCELL} - I_D \tag{2.1}$$

Here: I_D is the diode current, I_M is the PV cell load current or output current and I_{PVCELL} is the photon generated current.

The diode current I_D is given by the Shockley's diode equation as:

$$I_D = I_{OCELL}(e^{\left(\frac{QV}{KT_{AP}}\right)} - 1) \tag{2.2}$$

Where:

I_{OCELL} the reverse saturation current of diode in Amps,

Q is the electron charge (1.602×10^{-19}) in Coulombs,

V is the voltage of the PV cell across the diode in Volts.

K is the Boltzmann's constant 1.381×10^{-23} in J/K,

T_{AP} is the junction temperature in Kelvin (K).

By replacing of I_D in Eq. 2.1 it gives the current voltage relationship of the PV cell as shown below:

$$I_M = I_{PVCELL} - I_{OCELL}[\, e^{\left(\frac{QV}{KT_{AP}}\right)} - 1] \tag{2.3}$$

Here: V is the PV cell voltage, and I_M is the output current from the cell.

The diode reverse saturation current (I_{OCELL}) is constant under the constant temperature and irradiance that is calculated by the open circuit condition of PV cell

as illustrated in Fig. 2.2(b). From the Eq. (2.3) it is observed that $I_M = 0$ (no output current i.e. open circuited) and solve for I_{OCELL}.

$$0 = I_{PVCELL} - I_{OCELL} \left(e^{\left(\frac{QV}{KT_{AP}} \right)} - 1 \right) \tag{2.4}$$

$$I_{PVCELL} = I_{OCELL} \left(e^{\left(\frac{QV}{KT_{AP}} \right)} - 1 \right) \tag{2.5}$$

$$I_{OCELL} = \frac{I_{SCR}}{\left(e^{\left(\frac{QV}{KT_{AP}} \right)} - 1 \right)} \tag{2.6}$$

The photon generated current is directly proportional to the irradiance and temperature, whereas the voltage is directly proportional to the irradiance and inversely proportional to the temperature. The value of I_{SCR} is provided by the manufacturer datasheet at STC (standard test condition). At STC, the working temperature and irradiance are 25°C and 1000 W/m^2 respectively.

2.2.2 Modeling of practical PV module and array with PV cell

In practical there is no existence of ideal cell i.e. all the cells are additionally connected to series and shunt resistances. The series resistance is due to hindrance in the path of flow of electrons from n to p junction and parallel resistance is due to the leakage current. This model is generalized to take into consideration the series, shunt and recombination losses. The practical photovoltaic cell is illustrated in Fig. 2.3.
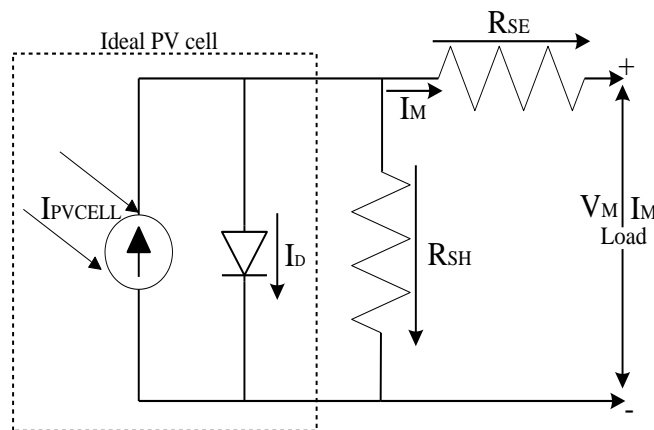
Fig. 2.3 Practical PV cell equivalent circuit

From the Kirchhoff's current law (KCL) that the output current I_M produced by the PV cell is

24

$$I_M = I_{PVCELL} - I_D - I_{SH} \qquad (2.7)$$

Here:

I_M is the PV output current in amps

I_D is the diode current in amps and

I_{SH} is the shunt current across the shut resistance.

As the practical cell consists of additional resistances, the effects of the resistances are also to be considered. PV cells are grouped to form PV module and modules are grouped to form PV array. 60 PV cells are connected in series and parallel combinations to form the PV module i.e. 10 cells are connected in series and such 6 combinations are connected in parallel. In general, for charging a 12 V battery, the required voltage used to be provided by the 36 cell PV module and similarly for 24 V batteries charging a 72 cell solar PV module was used appropriately. Because, large usage of photovoltaic systems are with batteries as a backup for the system. But here, 60 cells PV modules are used.

Furthermore, the advent of high efficiency dc-dc converters has alleviated the need for modules with specific voltages. When the PV cells are connected together in series, then the current output is the same as the single cell, but the voltage output is the sum of the voltage of all cells. Multiple modules are connected together in series and parallel to deliver the required voltage and current levels (Roberto Faranda et al, 2008). Matlab-simulink design of photovoltaic system is made as per provided data sheet parameters from the SSI-3M6-250W poly-crystalline solar PV module at standard test conditions (STC) i.e. at 25°C and 1000 W/m^2 as shown in Appendix A.

2.3 Effect of Series and Shunt Resistances

Shunt resistance has negative relation to the shunt leakage current and the variations in series resistance are affecting the photovoltaic output.

2.3.1 Effect of series resistance

The series resistance (R_{SE}) of the PV module has a large impact on the slope of the I-V curve near the open-circuit voltage (V_{OC}). Hence the value of R_{SE} is calculated by evaluating the slope of $\frac{dV_M}{dI_M}$ of the I-V curve at the open circuit voltage (V_{OC}). The

equation for R_{SE} is derived by differentiating the Equation (2.8) and then rearranging it in terms of R_{SE}.

$$I_M = I_{PVCELL} - I_{OCELL}\left[e^{\frac{Q(V_M + I_M R_{SE})}{N_T K N T_{AP}}} - 1\right] \qquad (2.8)$$

$$dI_M = 0 - I_{OCELL}.Q\left(\frac{dV + R_{SE}.dI_M}{N_T K N T_{AP}}\right).e^{Q(\frac{V_M + I_M R_{SE}}{N_T K N T_{AP}})} \qquad (2.9)$$

$$R_{SE} = -\frac{dV_M}{dI_M} - \frac{\frac{N_T K N T_{AP}}{Q}}{I_{OCELL}.e^{Q(\frac{V_M + I_M R_{SE}}{N_T K N T_{AP}})}} \qquad (2.10)$$

The Equation (2.10) is evaluated at the open circuit voltage i.e. at $V_M = V_{OC}$ with making $I_M = 0$ because at open circuit, the current remains zero to get series resistance value as:

$$R_{SE} = -\frac{dV_M}{dI_M}|V_{OC} - \frac{\frac{N_T K N T_{AP}}{Q}}{I_{OCELL}.e^{Q(\frac{V_{OC}}{N_T K N T_{AP}})}} \qquad (2.11)$$

Here: $\frac{dV_M}{dI_M}|V_{OC}$ is the slope of the I-V curve at the V_{OC} by using the I-V curve with the provided data sheet and then divide it by the number of cells in series.

Finally, it is possible to solve the Equation (2.8) for I-V characteristics. It is, however complex because the solution of current is recursive by inclusion of a series resistance in the model. Although it may be possible to find the answer by the simple iterations, the Newton's method is chosen for rapid convergence of the answer (Fangrui Liu et al, 2008). The Newton's method is described as:

$$x_{n+1} = x_n - \frac{f(x_n)}{f'(x_n)} \qquad (2.12)$$

Here: f'(x) is the derivative of the function,

f (x) = 0,

x_n is a present value and

x_{n+1} is a next value.

By rewriting the Equation (2.8) it gives the following Equations as:

$$f(I_M) = I_{SCR} - I_M - I_{OCELL}\left[e^{\frac{Q(V_M + I_M R_{SE})}{N_T K N T_{AP}}} - 1\right] = 0 \qquad (2.13)$$

$$I_{n+1} = I_n - \frac{I_{OCELL}\left[e^{\frac{Q(V_M + I_M R_{SE})}{N_T K N T_{AP}}} - 1\right]}{-1 - I_{OCELL}\left(\frac{Q(R_{SE})}{N_T K N T_{AP}}\right).(e^{\frac{Q(V_M + I_M R_{SE})}{N_T K N T_{AP}}})} \qquad (2.14)$$

2.3.2 Effect of shunt resistance

The effect of shunt resistance (R_{SH}) is very small in a single module, thus, the PV model does not include it. To make a better model it also includes temperature affects on the short circuit current (I_{SCR}) and the reverse saturation current of a diode (I_{OCELL}) using a single diode with the diode ideality factor (N) set to achieve the best V-I curve match. This is also called 'parallel resistance'. It is a loss associated with a small leakage of current through a resistive path in parallel with the intrinsic device represented by a shunt resister (R_{SH}). Its effect is much less conspicuous in a PV module compared to the series resistance and it will only become noticeable when a number of PV modules are connected in parallel for a larger system. Shunt current (I_{SH}) is calculated from the below Equation (2.15)

$$I_{SH} = \frac{V_M + I_M R_{SE}}{R_{SH}} \qquad (2.15)$$

2.3.3 Combination of series and shunt resistance effects

Recombination in the depletion region of PV cells provides non-ohmic current paths in parallel with the intrinsic PV cell. As shown in Figure 2.3 this can be represented by the diode in the equivalent circuit. Summarizing these effects the current-voltage relationship of PV cell is written as:

$$I_M = I_{PVCELL} - I_{OCELL}\left[e^{\frac{Q(V_M + I_M R_{SE})}{N_T K N T_{AP}}} - 1\right] - \frac{V_M + I_M R_{SE}}{R_{SH}} \qquad (2.16)$$

Where:

I_M = current of designed PV module in amps

I_{PVCELL} = current generated by the incident light in amps

I_{OCELL} = diode's reverse saturation current in amps

Q = electron charge (1.602×10^{-19}) in Coulombs

N_T = no. of total cells in a photovoltaic module

27

K = Boltzmann constant in (1.381×10⁻²³) J/^{o}K

T_{AP} = temperature applied in Kelvin

V_M = voltage produced by the module in Volts

R_{SE} = resistance connected in series in ohms

R_{SH} = resistance connected in parallel in ohms

N = Ideality factor of a diode (taken from data sheet). Generally its value is taken between 1 and 2, for ideal diode N = 1. Its value is estimated by the manufacturer, unless until the most accurate curve fitting of the PV module is obtained after taking the several trails or experimental validations. Ideality factor value gets varied from material to material i.e. for different type of material its estimated value is different. For Silicon poly crystalline material its value is chosen as 1.3 and those different values are represented in Appendix B.

2.4 Effect of Irradiance and Temperature on PV System

❖ Current generated by light (I_{PVCELL}) depends linearly on solar radiation and also on temperature.

❖ Whereas voltage produced by the PV module is inversely proportional to the temperature and somewhat directly proportional to the irradiance that can be enumerated in the next sub topics.

2.4.1 Effect of irradiance

There are two important factors to be taken into consideration are the temperature and the irradiance (insolation). The term 'Irradiance' means the measure of energy-density of sunlight collected at the surface of the earth which is measured in watt per meter square (W/m^2) and milli watts per centimeter square (mW/cm^2). 'Watts' is defined as a measure of the light power or brightness concentration of the light. The term 'Irradiance' and 'Irradiation' are related to solar components. As the solar insolation keeps on changing throughout the day then the I-V and P-V characteristics varies as depicted in Fig. 2.4 and in Fig. 2.5. As a result the maximum power point varies during the day and as such the maximum power point (MPP) must constantly be tracked and ensure that the maximum available power is always being reached from the panel.

The photo generated current is directly proportional to the irradiance level i.e. an increment in the irradiation level that takes place & then leads to a higher photo

generated current. The short circuit current which is directly proportional to the photo generated current and is directly proportional to the irradiance as well. When the operating point is not short circuited then no power is generated. The photo generated current is also the main factor in the PV current. In practice, the voltage dependency on the irradiation is often neglected. As the effect on both the current and the voltage are having directly proportional relationship i.e. both increase when the irradiation rises and the effect on the power is also increased. If there is more irradiation, then the power generated is also more.

In a very bright weather day at afternoon time (12 pm) the irradiance reaching the surface, faces the sun radiation about 1000 W/m^2 is called full sun. Prescribed modules are modeled (depicted) for charging 12 V batteries. However about, minimum of 13 V charging is needed to provide the connection between the terminals of the battery, which should rise to about 15 V for a lead-acid battery for reaching the full charge. Where the system losses are taken into concern then the charging voltage is more than 15 V i.e. 16 V is preferred to be adequate.
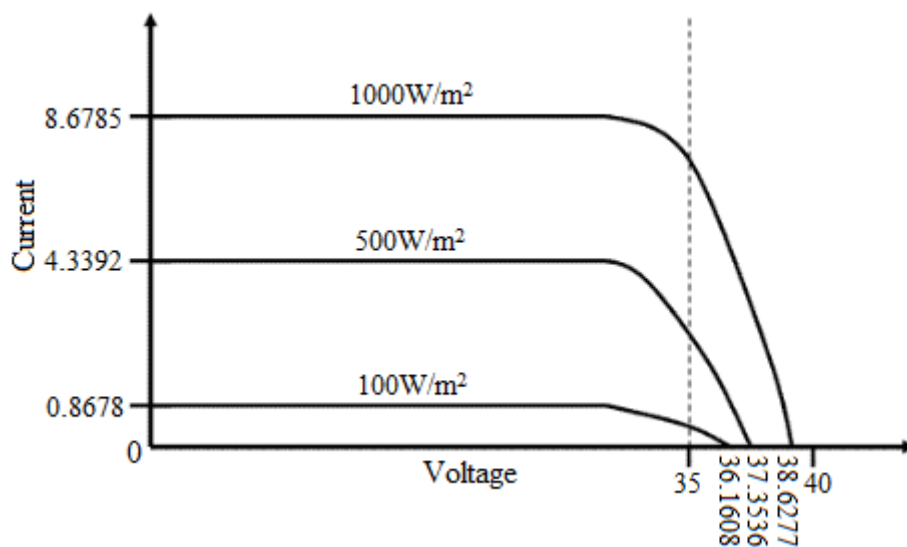
Fig. 2.4 I-V characteristic curves at various irradiance levels.

From the above figure it shows that the I-V curves for 100, 500 and 1000 W/m^2, for the I-V curve at 1000 W/m^2, that the module experiences the solar radiation directly. When the sun is exactly up above in the right location in tropical countries, then the module should be in slant position with some angle of inclination to get utmost current. When the radiation intensity is low in the sky at 30° above, then the module should be tilted towards the sun at an angle of 60° from plane surface.

However, modules are at fixed position facing the sun directly then the reaching of maximum intensity becomes difficulty in some times, especially at before 10 am and after 4 pm, because the irradiance intensity gets slowly decreases, i.e. the irradiance is about half the value of maximum irradiance. The effect is observed with the 500 W/m^2 I-V characteristic curve. Therefore, the output produced by the module gets varied by the variation of sun place (location) throughout the day. When the weather condition is bad with gloomy and covered by clouds then the irradiance is further reduced i.e. reduced to 100 W/m^2 or less. The obtained values of current and voltage are observed in the 100 W/m^2 I-V characteristic curve.

2.4.2   Temperature effect

When the temperature plays another major factor in finding the solar cell efficiency. As the temperature increases the rate of photon current generation increases thus, reverse saturation current increases quickly and this decreases the band gap. Hence this leads to slight changes in current & major changes in voltage. The open circuit voltage is linearly dependent on the temperature. The effect of the temperature on voltage, it is inversely proportional i.e. when the temperature increases then the voltage gets reduced and vice-versa.

And the cell voltage is decreased by 2.2 V per one degree rise of temperature. Fast increase of temperature gives the drawback, in reducing the performance of solar system. Therefore, the better performance solar cell is given during cold and sunny days rather than hot and sunny weather. Nowadays, solar panels are made of non-silicon solar cells which are temperature insensitive. The current increases very slightly with the temperature rise and vice-versa, but it could unable to indemnify the reduction in voltage that is caused due to the temperature rise. Due to this reason, the total produced power is getting decreased.

Because of this the PV panel manufacturers are providing the limited coefficients for the temperature in their data sheets, to provide the information about the voltage and current parameters that are going to varied with respect to the temperature variations. Due to the effect of the temperature, that the observed current variations are very small, sometimes it may be negotiable. As represented earlier, that the temperature and the irradiations are factors of atmosphere, and they are, surely depends on climatical conditions which is not constant throughout the year or during a

single day. They gets vary instantly due to fast changing weather conditions, such as gloomy or cloud formations in the atmosphere etc…Due to this maximum power point (MPP) or operating point is also going to be varied.

Then it becomes as a quite problem in tracking the maximum power point during these variations. If the operating point is not close to the MPP then it causes the more variations in obtained outputs. Hence, it is essential to track the MPP in any condition and it should ensure that, whether the maximum available power of the PV panel is being reached or not. Due to this, the modern solar power converters are entrusted to the maximum power point tracking (MPPT) controlling techniques.
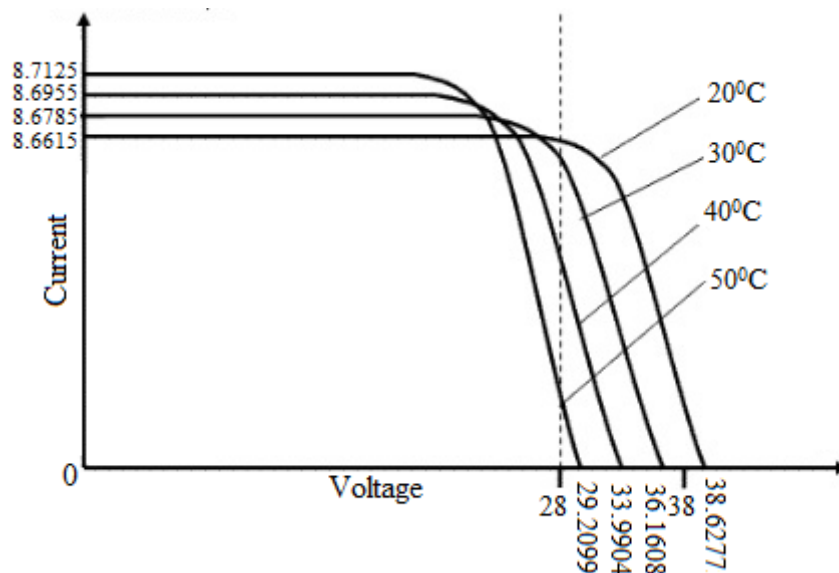
Fig. 2.5 I-V characteristic curves at various temperatures

From the above represented figure with the 1000 W/m^2 I-V characteristic curve, it resembles effect of cell temperature. And here, that temperature is getting increased from 20°C to 50℃, when compared to the prior curve that the V_{OC} is getting decreased drastically while I_{SC} is getting increased slightly higher. However, the graph represents the fall of voltage (V_{OC}). In order to get the maximum output current, that the modules are arranged to be in parallel connection.

I-V characteristic curves are generally represented for different temperatures from 20°C- 50°C as shown in Fig. 2.5. It is also observed that, for the production of output current the solar panels are required to have sufficient amount of sunlight. In order to increase the irradiance during abnormal weather conditions i.e. to meet the

requirement of 1000 W/m^2, sometimes suitable lenses and mirrors are preferred to increase the solar radiation concentration.

However, it does not support all the time, because there is chance for damage occurrence for the solar panel due to overheating by the fall of heavy concentrated solar radiations during abnormal weather conditions. The strategy for modeling the PV cell and the PV module is same for the provided parameters. The difference is majorly occurs between modules and cell current, as well as module and cell voltage. Current generated by light (I$_{PVCELL}$) is proportional to the provided irradiance and temperature and it is obtained from the Eq. (2.17)

$$I_{PVCELL} = \frac{P_{AP}[I_{SCR}+T_{SCI}(T_{AP}-T_{REF})]}{P_{REF}} \tag{2.17}$$

Where:

P_{AP} = solar irradiance applied in W/m^2 (it is provided during the experiment)

P_{REF} = reference irradiance in W/m^2 (1000 W/m^2 is taken under STC)

I_{SCR} = short circuit current of a PV module (taken from the data sheet)

T_{SCI} = short circuit current temperature coefficient in A/^{o}K (got from data sheet)

T_{AP} = temperature applied for the PV module in Kelvin

T_{REF} = reference temperature 298 in Kelvin i.e. 273+25=298 at (25^0 C)

The calculated values of I$_{PVCELL}$ at different irradiance and different temperature from the above noted mathematical modeling Eq. (2.17) is tabulated in Table 2.1.

Table 2.1 Calculated module current (I$_{PVCELL}$) values at different irradiance and different temperatures

S. No	Irradiance in (W/m^2)	Temperature (in ℃)				
		20	30	40	50	60
1	1000	8.6615	8.6785	8.6955	8.7125	8.7295
2	800	6.9292	6.9428	6.9564	6.97	6.9836
3	500	4.3307	4.3392	4.3477	4.3562	4.3647
4	250	2.1653	2.1696	2.1738	2.1781	2.1823
5	100	0.8661	0.8678	0.8695	0.8712	0.8729
6	50	0.4330	0.4339	0.4347	0.4356	0.4364

6 Modules are connected to form an array i.e. two modules are connected in series and such three pairs are connected in parallel in order to meet the voltage,

current and power requirements. The array current is calculated by the given equation (2.18) and the values at different instants i.e. at different irradiance and different temperatures are tabulated in Table 2.2. Currents generated by the module and array are directly proportional to the irradiance as well as temperature.

$$I_A = N_{PV}\, I_{PVCELL} - N_{PR} I_{OCELL}\left[e^{\frac{Q}{N_T KN T_{AP}}\left(\frac{V_M}{N_{SE}} + \frac{I_M R_{SE}}{N_{PR}}\right)} - 1\right] - \frac{1}{R_{SH}}\left[\frac{N_{PR} V_M}{N_{SE}} + I_M R_{SE}\right]$$

$$(2.18)$$

Here:

I_A is the PV array current in amps,

R_{SE} is the series resistance in ohms,

R_{SH} is the shunt resistance in ohms,

$I_M\, R_{SE}$ is the voltage drop due to the series resistance in volts,

N_{SE} is the number of solar cells connected in series and

N_{PR} is the number of solar cells connected in parallel.

Table 2.2 Calculated array current (I_A) values at different irradiance and different temperatures

S. No	Irradiance in (W/m²)	Temperature (in °C)				
		20	30	40	50	60
1	1000	26.0015	26.0185	26.0355	26.0525	26.0695
2	800	20.8012	20.8148	20.8284	20.8420	20.8556
3	500	13.0007	13.0092	13.0177	13.0262	13.0347
4	250	6.5003	6.5046	6.5088	6.5131	6.5173
5	100	2.6001	2.6018	2.6035	2.6052	2.6069
6	50	1.30	1.3009	1.3017	1.3026	1.3034

Reverse saturation current of a diode in a module (I_{OCELL}) at different conditions for the provided temperature and irradiance is given by Eq. (2.19). The reverse saturation current (I_{OCELL}) is also a temperature dependent and the calculated values of module and array are tabulated in the Table 2.3 and in Table 2.4 respectively.

$$I_{OCELL} = \frac{I_{SCR}}{e^{\left(\frac{QV_{OC}}{N_T KN T_{AP}}\right)} - 1}$$

$$(2.19)$$

Here:

I_{OCELL} = diode's reverse saturation current in amps

N_T = no. of total cells in a photovoltaic module

Table 2.3 Calculated module reverse saturation current (I_{OCELL}) values at different irradiance and different temperatures

S. No	Irradiance in (W/m²)	Temperature (in °C)				
		20	30	40	50	60
1	1000	1.5178×10^{-16}	5.4233×10^{-16}	1.7863×10^{-15}	5.4650×10^{-15}	1.5633×10^{-14}
2	800	1.2142×10^{-16}	4.3386×10^{-16}	1.4290×10^{-15}	4.3720×10^{-15}	1.2506×10^{-14}
3	500	7.5893×10^{-17}	2.7116×10^{-16}	8.9316×10^{-16}	2.7325×10^{-15}	7.8166×10^{-15}
4	250	3.7946×10^{-17}	1.3558×10^{-16}	4.4658×10^{-16}	1.3662×10^{-15}	3.9083×10^{-15}
5	100	1.5178×10^{-17}	5.4233×10^{-17}	1.7863×10^{-16}	5.4650×10^{-16}	1.5366×10^{-15}
6	50	7.5893×10^{-18}	2.7116×10^{-17}	8.9316×10^{-17}	2.7325×10^{-16}	7.8166×10^{-10}

Table 2.4 Calculated array reverse saturation current (I_{OCELL}) values at different irradiance and different temperatures

S. No	Irradiance in (W/m²)	Temperature (in °C)				
		20	30	40	50	60
1	1000	4.5536×10^{-16}	1.6270×10^{-15}	5.3590×10^{-15}	1.6395×10^{-14}	4.69×10^{-14}
2	800	3.6428×10^{-16}	1.3016×10^{-15}	4.2872×10^{-15}	1.3116×10^{-14}	3.752×10^{-14}
3	500	2.2768×10^{-16}	8.135×10^{-16}	2.6795×10^{-15}	8.1975×10^{-15}	2.345×10^{-14}
4	250	1.1384×10^{-16}	4.0675×10^{-16}	1.3397×10^{-15}	4.0987×10^{-15}	1.1725×10^{-14}
5	100	4.5536×10^{-17}	1.6270×10^{-16}	5.3590×10^{-16}	1.6395×10^{-15}	4.69×10^{-15}
6	50	2.2768×10^{-17}	8.1350×10^{-17}	2.6795×10^{-16}	8.1975×10^{-16}	2.345×10^{-15}

The reverse saturation current of diode has its major effect on the saturation current (I_{SAT}) of a diode. Unless the reverse saturation current value is obtained, the saturation current of the diode cannot be obtained, as saturation current is majorly dependent on reverse saturation current along with the applied and the reference temperatures. Its value is calculated by the equation (2.20) and the calculated values of the module and array are tabulated in the Table 2.5 and in Table 2.6 respectively.

$$I_{SAT} = I_{OCELL} \times \left(\frac{T_{AP}}{T_{REF}} \right)^3 \times e^{\left\{ \frac{QE_{GO}}{NK} \left(\frac{1}{T_{REF}} - \frac{1}{T_{AP}} \right) \right\}} \tag{2.20}$$

Here:

I_{SAT} = Saturation current of a diode in amps and

E_{GO} = Semiconductor band gap energy of the module in J/C (for silicon it is about 1.12 eV)

Table 2.5 The module saturation current values of a diode (I_{SAT}) at different irradiance and different temperatures

S. No	Irradiance in (W/m²)	Temperature (in °C)				
		20	*30*	*40*	*50*	*60*
1	1000	$8.1303*10^{-17}$	$9.8760*10^{-16}$	$1.0321*10^{-14}$	$9.2930*10^{-14}$	$7.4250*10^{-13}$
2	800	$6.5042*10^{-17}$	$7.9008*10^{-16}$	$8.2568*10^{-15}$	$7.4344*10^{-14}$	$5.940*10^{-13}$
3	500	$4.0651*10^{-17}$	$4.9380*10^{-16}$	$5.1605*10^{-15}$	$4.6465*10^{-14}$	$3.7125*10^{-13}$
4	250	$2.0325*10^{-17}$	$2.4690*10^{-16}$	$2.5805*10^{-15}$	$2.3232*10^{-14}$	$1.8562*10^{-13}$
5	100	$8.1303*10^{-18}$	$9.8760*10^{-17}$	$1.0321*10^{-15}$	$9.2930*10^{-15}$	$7.4250*10^{-14}$
6	50	$4.0651*10^{-18}$	$4.9380*10^{-17}$	$5.1605*10^{-16}$	$4.6465*10^{-15}$	$3.7125*10^{-14}$

Table 2.6 The array saturation current values of a diode (I_{SAT}) at different irradiance and different temperatures

S. No	Irradiance in (W/m²)	Temperature (in °C)				
		20	*30*	*40*	*50*	*60*
1	1000	$2.4391*10^{-16}$	$2.9628*10^{-15}$	$3.0963*10^{-14}$	$2.7879*10^{-13}$	$2.2275*10^{-12}$
2	800	$1.9512*10^{-16}$	$2.3702*10^{-15}$	$2.4770*10^{-14}$	$2.2303*10^{-13}$	$1.782*10^{-12}$
3	500	$1.2195*10^{-16}$	$1.4814*10^{-15}$	$1.5481*10^{-14}$	$1.3939*10^{-13}$	$1.1137*10^{-12}$
4	250	$6.0977*10^{-17}$	$7.407*10^{-16}$	$7.7407*10^{-15}$	$6.9697*10^{-14}$	$5.5687*10^{-13}$
5	100	$2.4391*10^{-17}$	$2.9628*10^{-16}$	$3.0963*10^{-15}$	$2.7879*10^{-14}$	$2.2275*10^{-13}$
6	50	$1.2195*10^{-17}$	$1.4814*10^{-16}$	$1.5481*10^{-15}$	$1.3939*10^{-14}$	$1.1137*10^{-13}$

The equations for the reverse saturation current and the saturation currents are modeled and their respective currents are calculated in order to find out the effects of diode current in the PV system. The diode current is formed unless until those two current equations are formed. PV module diode current is calculated with the effects of series and shunt resistances by the equation (2.21). And the values of diode module and array currents at different irradiance with the working room temperature are tabulated in the Table 2.7 below.

$$I_D = I_{OCELL}\left[e^{\frac{Q(V_M+I_M R_{SE})}{N_T KN T_{AP}}} - 1\right] \tag{2.21}$$

Table 2.7 Module and array current values of a diode (I$_D$) at different irradiance with constant temperature

S. No	Irradiance in (W/m^2)	Temperature (in °C)	
		Module current (in Amps)	Array current (in Amps)
1	1000	$1.0606*10^{-15}$	$3.1821*10^{-15}$
2	800	$8.4848*10^{-16}$	$2.5456*10^{-15}$
3	500	$5.3030*10^{-16}$	$1.5910*10^{-15}$
4	250	$2.6515*10^{-16}$	$7.9552*10^{-16}$
5	100	$1.0606*10^{-16}$	$3.1821*10^{-16}$
6	50	$5.3030*10^{-17}$	$1.5910*10^{-16}$

In order to find out the total module or array current, we need to consider the leakage current across the shunt resistance (R$_{SH}$). The respective shunt current is calculated from the equation (2.15). And the values of module and array shunt currents at different irradiance with the constant working temperature are tabulated in the Table 2.8.

Table 2.8 Module and array shunt current values (I$_{SH}$) at different irradiance with constant temperature

S. No	Irradiance in (W/m^2)	Temperature (in °C)	
		Module current (in Amps)	Array current (in Amps)
1	1000	0.0751	0.2254
2	800	0.060	0.1803
3	500	0.0375	0.1127
4	250	0.0187	0.0563
5	100	$7.510*10^{-3}$	0.0225
6	50	$3.7550*10^{-3}$	0.0112

Here, the voltage of the PV module gets decreases as the applied temperature goes on increasing that can be obtained from the Eq. (2.22). Calculated module and array current values are tabulated in the Table 2.9 and in Table 2.10 respectively.

$$V_M = \frac{N_T K N T_{AP}}{Q} \times \ln\left[\frac{I_{PVCELL} - I_{RS}}{I_{RS}}\right] \qquad (2.22)$$

Table 2.9 The module voltage values at different irradiance and different temperatures

S. No	Irradiance in (W/m²)	Temperature (in ℃)				
		20	*30*	*40*	*50*	*60*
1	1000	38.6278	35.3536	36.1608	35.0420	33.9904
2	800	38.1478	34.8636	35.6408	34.5320	33.4704
3	500	37.6678	34.3236	35.1308	34.0120	32.9604
4	250	37.1878	33.8136	34.6108	33.5020	32.4404
5	100	36.7078	33.3336	34.1008	32.9820	31.9304
6	50	36.2348	32.8606	33.5808	32.4720	31.4104

Table 2.10 The array voltage values at different irradiance and different temperatures

S. No	Irradiance in (W/m²)	Temperature (in ℃)				
		20	*30*	*40*	*50*	*60*
1	1000	77.2556	74.2072	71.3217	68.5840	65.9808
2	800	76.7756	73.7272	70.8407	68.1030	65.4998
3	500	76.2956	73.2472	70.3597	67.6220	65.0178
4	250	75.8156	72.7672	69.8787	67.1410	64.5368
5	100	75.3356	72.2872	69.3977	66.6580	64.0548
6	50	74.8556	71.8072	68.9167	66.1770	63.5738

2.5 Comparison of I$_{PVCELL}$ Values with the Modified Model

Module and array current values with the modified model parameters are compared with the existed model and that are tabulated in the Table 2.11 and in Table 2.12 respectively at different temperature and different irradiance.

Table 2.11 The module current values with conventional and modified model

Irradiance in W/m²	Temperature (in ℃)					
	30		40		50	
	modified	conventional	modified	conventional	modified	conventional
1000	8.6785	8.3820	8.6955	8.4750	8.7125	8.5160
800	6.9428	6.7056	6.9564	6.780	6.970	6.8128
500	4.3392	4.1910	4.3477	4.2375	4.3562	4.2580
250	2.1696	2.0955	2.1738	2.1237	2.1187	2.2190
100	0.8678	0.8382	0.8695	0.8475	0.8712	0.8516

Table 2.12 The array current values with conventional and modified model

Irradiance in W/m²	Temperature (in °C)					
	30		40		50	
	modified	conventional	modified	conventional	modified	conventional
1000	26.0355	25.1460	26.0865	25.4250	26.1375	25.5480
800	20.8284	20.1168	20.8692	20.340	20.910	20.4384
500	13.0177	12.5730	13.0432	12.7125	13.0687	12.7740
250	6.5088	6.2865	6.5216	6.3562	6.3561	6.6570
100	2.6035	2.5146	2.6086	2.5425	2.6136	2.5548

2.6 Summary and Conclusion

A detailed mathematical modeling of solar cells has been described by considering the series, shunt and recombination resistance effects. Matlab-simulink modeling has been described based on the provided data sheet. PV module and PV array is modeled under different conditions and the values calculated for each modeling parameters are tabulated at different irradiance and different temperature. When the irradiance level of light changes the number of photons, the energy entering the PV device changes along with the number of electrons released transferring to electrical energy. Changes in irradiance significantly affect output current with a much smaller effect on voltage.

The current is directly proportional to light intensity and the voltage varies more slowly in a logarithmic relationship. The operating temperatures of solar cells are important. If the temperatures are operating higher, it typically results in lower power outputs and efficiencies with the slight decrease of solar life time. As temperature increases, the current also increases slightly. However, it significantly decreases the net produced power. Manufacturers of modules anticipate the loss of voltage in hot conditions in real world and compensate by building modules with enough cells in series and parallel, so that the modules have the enough voltage to charge batteries and to operate the any system load.

PERFORMANCE OF PHOTOVOLTAIC SYSTEM WITH THE MODIFIED MPPT CONTROLLER

3.1 Introduction

Maximum power point tracking (MPPT) algorithm is used mainly to extract the maximum possible power of PV modules for the provided irradiance and temperature at particular instant of time by the MPPT controller. The MPPT controller is to find out the maximum power point (MPP) of the solar photovoltaic system. The controller is fed with the measured output voltage and current of the solar PV system under the provided irradiance and temperature. The actual value of the PV system is to be transformed in to a required value based on the panel data sheet values with the help of tracking controller while performing its execution process. To generate the output, the controller always adjusts the duty cycle to its optimum value, due to which the DC-DC converter's switching is controlled. The DC-DC boost converter is used to produce the maximum rated output voltage and currents to the inverter. MPPT working with its topology and its major functions are discussed below.

3.2 Controller Topology

Maximum power point tracking technique internal working and its implementation with the photovoltaic (PV) system and DC-DC boost converter mainly requires its controller topology. The controller topology of the MPPT is represented with the major required functions.

3.2.1 PWM generator

It compares the reference signal i.e. control signal (which is generated by the photovoltaic system) with that of the carrier signal i.e. triangular wave signal. The input for the PWM generator is the module generated output signal, where the generated duty cycle from the controller is given to PWM signal generator. Based upon this input, the PWM generator generates the required switching signals to send subsequently for the switching device of the DC-DC converter. Working and implementation of MPPT are explained below.

3.3 PV Panel I-V and P-V Characteristic Curves at Different Instants

When the temperature and the irradiance, both are increased, then the PV panel current is increased and voltage is also increased slightly till the irradiance rise and vice-versa. Similarly, if the temperature increases, then the current gets increased and the voltage gets decreased drastically. During the irradiance rise, power obtained from the PV system is increased as voltage and current are getting increased and vice-versa. Similarly, during the temperature rise, the net PV system power is decreased as the voltage drastically decreases. These results are presented in Fig. 3.1-3.2.
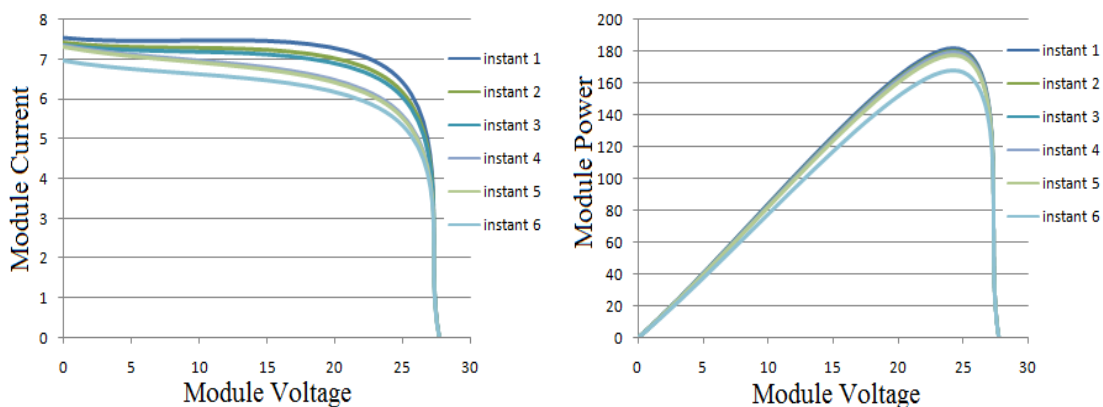
Fig. 3.1 PV module I-V & P-V characteristic curves at different instants
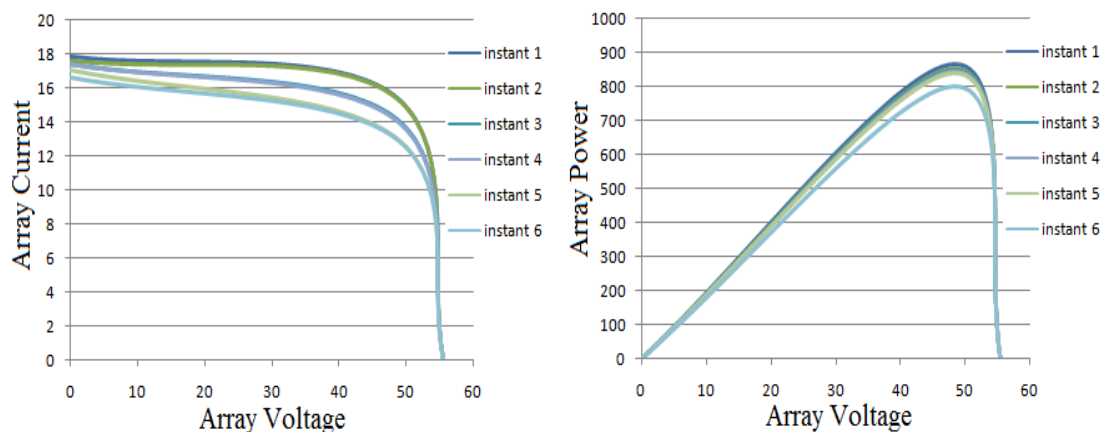
Fig. 3.2 PV array I-V & P-V characteristic curves at different instants

At different time instants, the power, voltage and currents obtained from the module and array during morning 8:00 am to evening 16:00 pm are tabulated in the Table 3.1-3.2. The maximum current, voltage and powers are 5.9667 amps, 26.40 volts and 144.394 watts respectively. Similarly, the array values at different time instants from morning 8:00 am to evening 16:30 pm are tabulated in Table 3.2. The

maximum PV array produced output current, voltage and powers are 17.90 amps, 53.80 volts and 866.36 watts respectively.

Table 3.1 PV module output values without MPPT at different instants

Time in (Hours)	Temperature in (^{0}C)	Irradiance in (W/m^2)	Voltage in (Volts)	Current in (Amps)		Power in (Watts)	
				Theoretical	Practical	Theoretical	Practical
08.00	30.75	188.70	27.75	1.6374	1.133	45.4378	31.4407
09.06	33.35	642.94	26.35	5.5744	4.06	146.8854	106.981
10.00	38.25	725.62	25.55	6.3031	4.73	161.0442	120.851
11.00	39.55	839.61	24.55	7.3003	5.70	179.2223	139.935
12.00	40.50	853.60	24.25	7.4234	5.8667	180.0174	142.267
12.10	40.68	866.36	26.40	7.5346	5.9667	182.3373	144.394
13.00	41.35	801.78	24.15	6.9691	5.53	168.3037	133.54
14.00	40.08	662.70	23.50	5.7627	4.70	135.4234	110.45
15.00	38.42	611.00	23.50	5.3113	4.3333	124.8155	101.832
16.00	37.32	453.12	23.60	3.9381	3.20	92.9391	75.52

Table 3.2 PV array voltage, current and power values without MPPT at different instants

Time in (Hours)	Temperature in (^{0}C)	Module Voltage in (Volts)	Array Voltage in (Volts)	Module Current in (Amps)	Array Current in (Amps)	Module Power in (Watts)	Array Power in (Watts)
08.00	30.75	27.75	55.50	1.6374	03.40	45.4378	188.70
09.06	33.35	26.35	52.70	5.5744	12.20	146.8854	642.94
10.00	38.25	25.55	51.10	6.3031	14.20	161.0442	725.62
11.00	39.55	24.55	49.10	7.3003	17.10	179.2223	839.61
12.00	40.50	24.25	48.50	7.4234	17.60	180.0174	853.60
12.10	40.68	24.20	53.80	7.5346	17.90	182.3373	866.36
13.00	41.35	24.15	48.30	6.9691	16.60	168.3037	801.78
14.00	40.08	23.50	47.00	5.7627	14.10	135.4234	662.70
15.00	38.42	23.50	47.00	5.3113	13.00	124.8155	611.00
16.00	37.32	23.60	47.20	3.9381	09.60	92.9391	453.12
16.30	37.06	23.55	47.10	3.3155	08.10	78.0800	381.51

3.4 Locus of Practically Calculated PV Array Output Power at Different Instants in A Day

Out of 252 validations in a day with the variations of irradiance and temperatures, the locus of the plotted power is obtained from PV array during the observation in several days from morning 8:00 am to evening 5:30 pm. Upon all the

validations & one day observed power, values are plotted as shown in Fig. 3.3. These validations have been taken to observe the working performance of the installed PV system at the university campus.
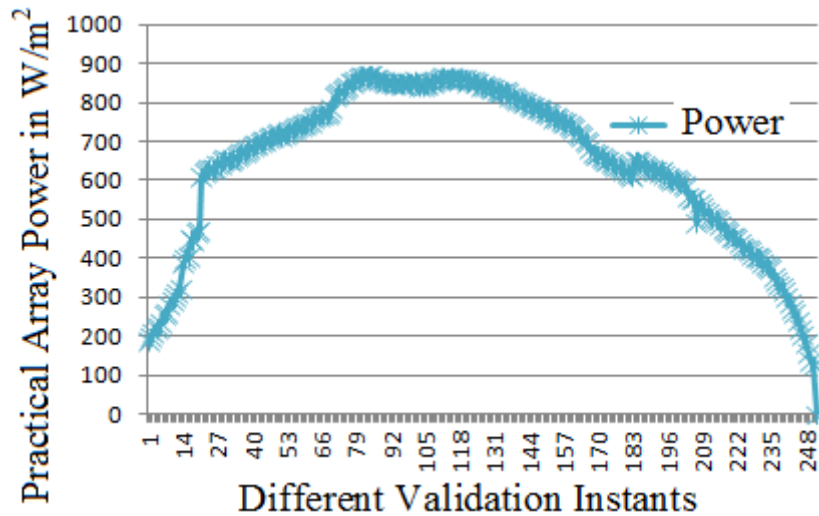
Fig. 3.3 Locus of practically calculated PV array output power at different instants

3.5 Maximum Power Point Tracking (MPPT) Controller Working and Implementation

Maximum power point tracking algorithm is mainly used to extract maximum capable power with the respective solar irradiance and temperature at particular instant of time with the help of MPPT controller. The tracking controller or sometimes just MPPT is used to enhance the power outcome generally in wind turbines and photovoltaic (PV) solar systems under all suitable working conditions. A typical solar panel converts only 30-40 percent of the incident solar irradiation into electrical energy.

Maximum power point tracking is used to increase the efficiency of the panel. The requirement to get the maximum power is that the source resistance should be equal to that of the load resistance. Solar PV systems are generally available in different layouts with respect to their relationship in inverter systems, external grids, battery banks, or other electrical loads. In spite of the ultimate destination of the solar power, the major problem occurred by MPPT is that, the efficiency of power transfer of the solar cell depends on, the amount of sunlight falling on the solar panel and the electrical behavior of the electric loads. The connected load with PV system and the MPPT controller is represented in Fig. 3.4.

42
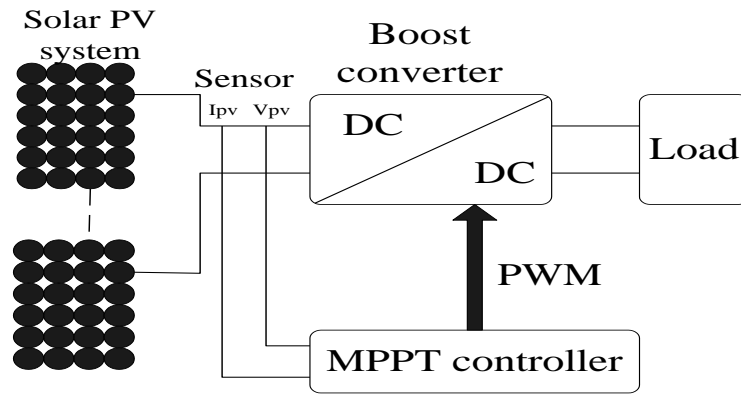
Fig. 3.4 MPPT with solar PV system and load

In the source side, a boost converter is connected to a solar panel in order to enhance the output voltage so that it would be used for different applications like motor loads by changing the duty cycle for the boost converter. As the quantity of sunlight gets varied, then the load characteristic curve also gives the much variations in the power transfer efficiency. Such that the efficiency of the system also gets varied, when the load characteristic changes. The operating point of PV module will be at the intersection of its V-I curve and the load line which is the V-I relationship of load. The points indicating module voltage V_{MPP} and current I_{MPP} at maximum Power P_{MAX} are obtained. The location of the maximum power point (MPP) on the V-I curve always changes vigorously based on the availability of irradiance and temperature. These are observable voltage shifts while the occurrence of MPP. Therefore, the MPP is required to be located by tracking technique which is the sole of MPPT controller. Different algorithms help to track the peak power point of the solar PV module automatically. Although there are conventionally two types of MPPT algorithms like Incremental Conductance and Perturb and Observe (P&O) algorithms, here the working and implementation of the Perturb and Observe (P&O) algorithm is carried out.

Because the incremental conductance method is a very slow tracking method. This algorithm uses the instantaneous conductance I/V and dI/dV for MPPT. Using these two values, the algorithm determines the location of the operating point of the PV module in the P-V curve shows that the PV module operates at the MPP along with left, right sides of the MPP in the P-V curve. The MPP is tracked by searching the peak of the P-V curve (Kok Soon Tey et al, 2014, M. Qiang et al, 2011, L. Fangrui et al, 2008, A. Safari et al, 2011, Y. Zhou et al, 2008, C. Bo-Chiau et al, 2011).

However, the cost of INC method is high due to requirements of high sampling compliance and speed control as a result of complex structure. Classically, INC method is the mostly used technique as a part in hill climbing algorithm, but it has the drawback in decision making as the speed increases in proportion to the step size of the error. A large step size of the voltage change helps the system to rapidly approach the MPPs. On the other hand, this large value generally induces persisting oscillations around the MPP if no other special countermeasures are taken. The issues using a small step size of voltage change are the opposite (S. Kazmi et al, 2009). The operating point of PV array oscillates around the MPP with causing power loss. To overcome all the above mentioned drawbacks of incremental conductance method that the perturb and observation (P&O) method is considered.

3.6 Conventional Perturb and Observation based MPPT Controlling Technique

The Perturb and Observe MPPT algorithm is easy to implement as it works based on the PV array, which is perturbed of a radiation of direction. If the power drained from the array increases, the operating point varies towards the MPP which in turn suits to the working voltage in the similar direction. If the power drained from the PV array decreases, the operating point varies away from the MPP, thus the direction of the working voltage perturbation has to be overturned (reversed). Though there are many algorithms are developed most of them are suffering from slow tracking and wrong tracking. Due to which, the utilization efficiency gets reduced. To overcome this problem, perturb and observe (P&O) tracking algorithm is implemented. In this conventional MPPT, that the algorithm senses the voltage and currents of PV array and compares with that of the maximum operating voltage (V_{MPP}) and current (I_{MPP}) to calculate the power at each instant. And it compares the power obtained in the present instant to the previous instant. If the power difference is more positive then the algorithm tracking process is continued in the same direction until the power difference becomes zero.

If the power increases during the perturbation, it is an indication that the maximum power has not been obtained so the iteration process has to be continued in the same direction. During this perturbation, if the algorithm crosses the maximum rated power, then, it compares the power with the previous iteration and calculates the

power difference. At that moment if the power difference is negative then it is an indication to the algorithm so as to make the iteration process in the reverse direction. In order to have a very keen observation of power difference, that the perturbation size has to be chosen very low. This process is to be continued till the algorithm reaches its maximum rated value. The moment when it reaches the maximum rated value then the MPPT is said to be attained the steady state. When the steady state is reached, the power point oscillates around the peak point. This is observed from the performance of the controller as tabulated in Table 3.3.

Table 3.3 Performance of conventional P&O

Perturbation	Change in power	Next perturbation
Reverse direction	-ve	Forward direction
Reverse direction	+ve	Reverse direction
Forward direction	-ve	Reverse direction
Forward direction	+ve	Forward direction

❖ If dP > 1, then the operating point of PV panel is close to MPP.

❖ If dP <-1, then the operating point of PV panel is further away from MPP. The flow chart representation of the conventional MPPT depicted in Fig. 3.5.
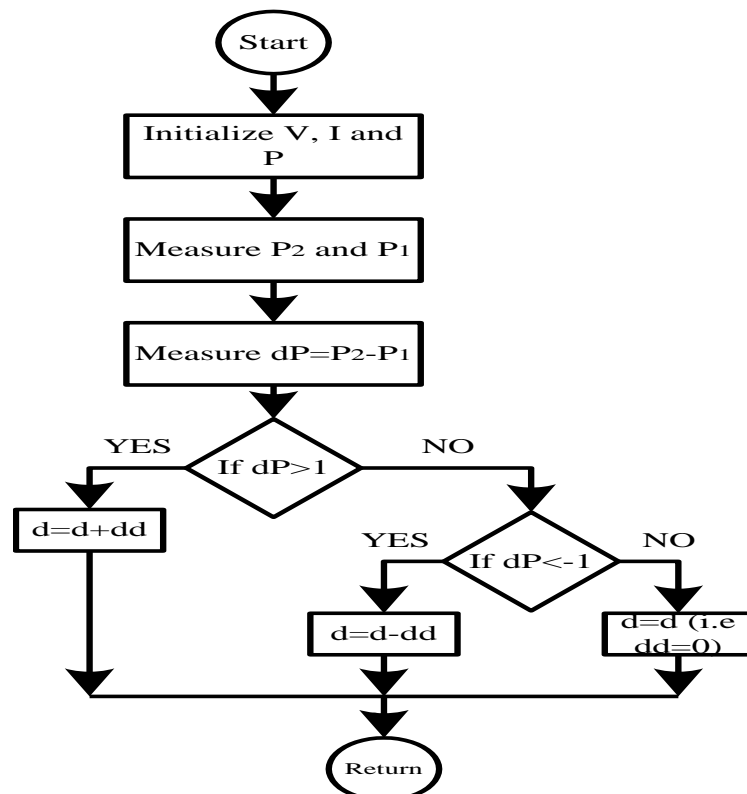
Fig. 3.5 Representation of conventional MPPT in a flow chart

45

The conventional MPPT algorithm takes the practical obtained values from the PV array i.e. V, I_L and calculates the maximum tracked available power P_1. This calculated power P_1 is considered as a initial reference value in the algorithm for this iteration. After a time instant of 0.01 seconds, it takes another set of values V & I_L and calculates P_2. After, calculating P_1 and P_2, the differential power $dP = P_2-P_1$ is calculated. This calculated 'dP' is used for the formation of duty cycle D and this can be used for providing of gating pulse for boost converter. For the next iteration P_2 is consider initial reference and the process is repeated. The flow chart for the algorithm is given in Fig. 5. Where 'dd' is the differential duty ratio corresponding to the differential power of particular iteration and 'd' is the duty ratio of the prior time instant.

3.6.1 PV array I-V and P-V characteristic curves with the conventional MPPT at various instants

Voltage, current and power values are increased with the conventional MPPT technique when compared to without MPPT values and I-V and P-V characteristic curves are formed with the respective obtained outputs. Voltage, current and powers are increased as the irradiance increases and decreases as the irradiance decreases. Here, the theoretical and practical power characteristic curves are represented below in Fig. 3.6.

a) Theoretical I-V characteristics   b) Practical P-V curves   c) Theoretical & practical power curves
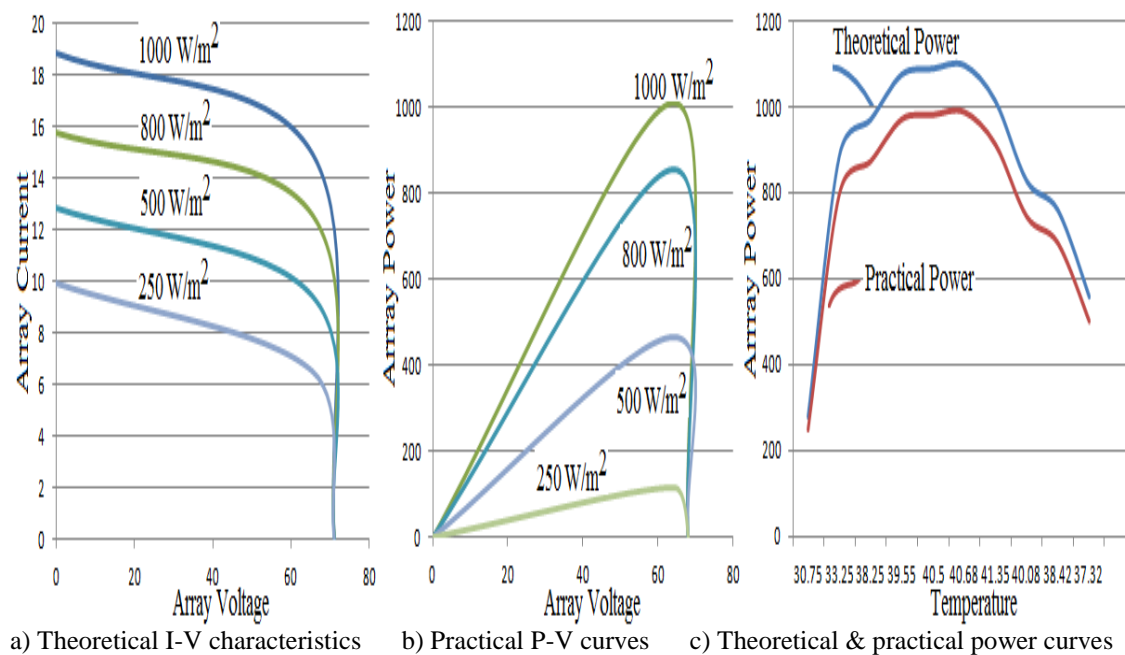
Fig. 3.6 Theoretical and practical power curves with PV array I-V, and P-V characteristic curves at different instants

46

The maximum theoretical and practical power obtained with the conventional MPPT at different instants with different irradiance and temperatures from morning 8:00 am to evening 16:00 pm are tabulated in Table 3.4. Maximum theoretical and practical output powers produced by the PV array with the conventional MPPT are 1097.073 watts and 1016.274 watts respectively.

Table 3.4 PV array power values at different irradiance and different temperatures

Time in (Hours)	Temperature in (^{0}C)	Irradiance in (W/m^2)	Array Power in (Watts)	
			Theoretical	Practical
08.00	30.75	200.80	276.1242	248.2518
09.06	33.35	655.05	884.6328	795.294
10.00	38.25	737.72	969.4848	871.572
11.00	39.55	851.71	1075.3338	969.516
12.00	40.50	865.70	1088.967	979.936
12.10	40.68	878.46	1097.073	1016.274
13.00	41.35	813.88	1012.866	910.572
14.00	40.08	674.80	826.6062	743.136
15.00	38.42	623.10	757.9326	681.396
16.00	37.32	465.22	556.8078	500.58

3.6.2   Drawbacks of conventional P&O MPPT

Though the MPPT controlling technique tracks the maximum available power with respect to irradiance and temperature, it has the following drawbacks:

❖ Due to slow tracking, the outcome of the PV system is reduced.

❖ The efficiency is also affected by the variations of the fill factor along with the climatic conditions.

❖ Decision making is difficult as the speed increases in proportion to error at each iteration. However, if the error is high, efficiency is reduced.

❖ When the steady state is reached, the power point oscillates around the peak point.

❖ Large perturbation value induces the persisting oscillations around the MPP due to which the operating point of PV array will vary resulting in power loss.

❖ A number of improvements of the P&O algorithm have been deliberated in order to decrease the oscillations in steady state; however, this slows down the

speed of response of the algorithm during the atmospheric changes.

❖ Due to this PV output voltage is lower than MPP, and the power transferred to the load is insufficient.

❖ One of the major difficulties in implementing this method is the selection of the fixed voltage change at each iteration for simultaneously satisfying the tracking speed and maintaining the MPP.

In order to overcome the above mentioned drawbacks, a modified MPPT algorithm is implemented.

3.7 Modified MPPT Controller

Here, a modified MPPT algorithm is being proposed to calculate the differential power 'dP' with the considerations of 'dV' and 'dI'. In case of conventional MPPT methods for iterations there will be a chance of occurring of very large and very small differential power 'dP'. Due to this it creates the large changes in the magnitude of pulses with creating uneven changes in duty angle.

This produces more distortions in the out puts of the boost converter and inverter due variations in the duty ratio produced by the MPPT algorithm. To overcome this, 'dV' and 'dI' are chosen to the modified MPPT algorithm. These 'dV' and 'dI' observe the power differences in a better way than the existed methods in order to manage the changes in the duty pulses with reducing the distortions in the outputs of both boost converter and inverter. Here voltage and current are sensed for the calculation of the power at each iteration.

Perturbation size of the algorithm is also chosen less than 0.01 seconds for a very keen observation while measuring the power differences at the each iteration. The iteration process is continued as per the conditions given in the flow chart diagram. If the power difference is not equal to zero, then constant supply is provided to the asynchronous motor drive to observe the accurate responses with less distortions and THD. The modified MPPT algorithm flow chart is represented in Fig. 3.7.
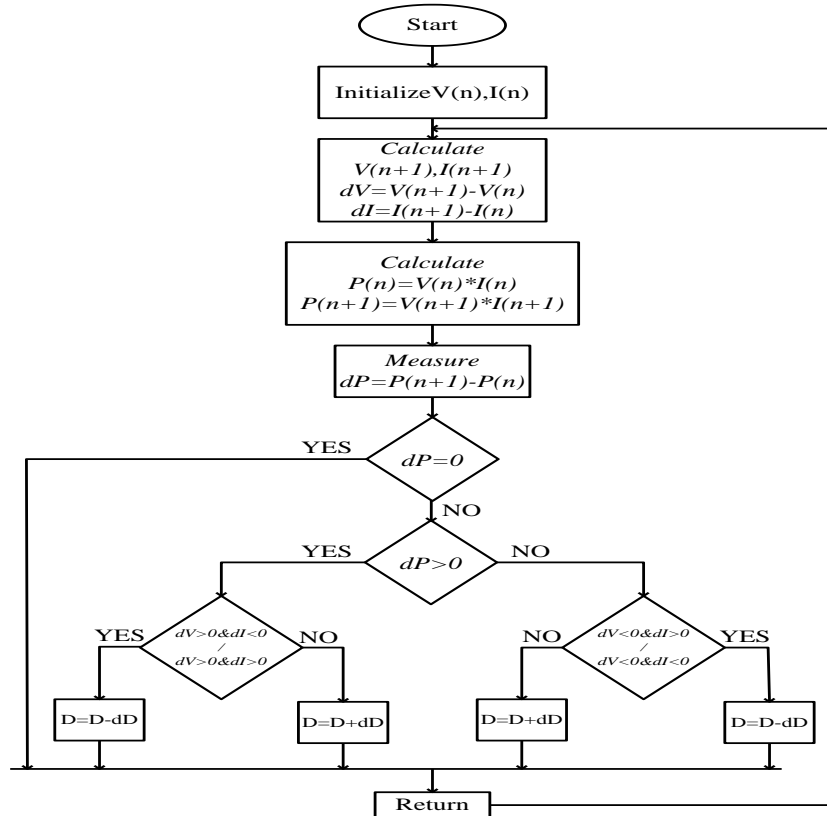
Fig. 3.7 Modified MPPT flow chart representation

- ❖ 'dV' and 'dI' are chosen to the modified MPPT algorithm in order to reduce the large power variations with respect to V and I, when compared to next iteration power with the previous iteration power.

- ❖ These 'dV' and 'dI' observe the power differences in a better way than the existed methods in order to manage the changes in the duty pulses.

- ❖ These results increase the maximum possible output power of the PV system, i.e. at most to reach the rated power.

- ❖ Due to this, the load requirement can be met sufficiently with the help of a boost converter and an inverter.

A PV array is formed with the series and the parallel combination of PV modules in order to generate the required voltage and current. If the voltage requirement is more, then the modules are connected in series and if the current requirement is more, the PV modules will be connected in parallel. This mismatching between a PV module and the load requires further over sizing of the PV array, increasing the overall system cost. With the modified MPPT algorithm, the maximum power tracking efficiency is increased to 94-98 % by the optimized duty cycle. From the modified MPPT controller, it is observed that, $I_{PVCELL} \gg I_{OCELL}$ and the maximum

power point current I_{MPP} is calculated with thermal voltage is as:

$$I_{MPP=}I_{PVCELL} - I_{OCELL}e^{\left(\frac{V_{MPP}}{V_{TH}}\right)} \quad\quad (3.1)$$

Then I_{OCELL} becomes as:

$$I_{OCELL} = \frac{I_{SCR}}{e^{\left(\frac{V_{OC}}{V_{TH}}\right)}} \quad\quad (3.2)$$

With the consideration of V_{OC} and V_{TH} the calculation of I_{MPP} is as:

$$I_{MPP} = I_{SCR}\left[1 - e^{\left(\frac{V_M-V_{OC}}{V_{TH}}\right)}\right] \qu\quad (3.3)$$

Then the thermal voltage V_{TH} is calculated as:

$$V_{TH} = \frac{V_{MPP}-V_{OC}}{\ln^{\left(\frac{I_{SCR}-I_{MPP}}{I_{SCR}}\right)}} \qu\quad (3.4)$$

So Array power can be calculated as:

$$P_{ARRAY} = V_{MPP} \times I_{MPP} = I_{PVCELL} \times V - I_{OCELL}[e^{\left(\frac{V}{V_{TH}}\right)} - 1] \times V \qu\quad (3.5)$$

By deriving the above equation w.r.t. the voltage, the maximum array power as:

$$P_{ARRAY\ MAX} = \frac{\partial P_{ARRAY}}{\partial V} = I_{OCELL}\left[e^{\left(\frac{V}{V_{TH}}\right)} - 1\right] + I_{OCELL} \times \frac{V}{V_{TH}}\left[e^{\left(\frac{V}{V_{TH}}\right)} - 1\right] \qu\quad (3.6)$$

From the above equation it is observed that the maximum voltage which gives the maximum array power is $V=V_{MPP}$. So that:

$$\frac{\partial P_{ARRAY}}{\partial V} \text{ at } V = V_{MPP} = 0 \qu\quad (3.7)$$

Then it gives the

$$I_{MPP} - \frac{V_{MPP}}{V_{TH}} \times I_D = 0 \qu\quad (3.8)$$

When a load is directly connected to the PV system, the operating point of the system is sporadically available at the maximum power. The internal panel impedance

50

derives the operating point of the solar panel. Thus by varying the impedance, the operating point also gets changed and with equalizing the impedance it moves towards peak power point. Since panels are DC devices, hence DC-DC converters are used to transform the impedance from source to load. By varying the duty cycle of the converter, impedance of the PV system also gets varied. At a particular impedance or duty ratio, the operating point reaches the maximum power. The I-V curve of the PV system is changed prominently by the uneven weather conditions such as radiance and temperature. Therefore, it is not suitable (workable) to fix the duty cycle for variable operating points. This MPPT technique regularly observes PV system voltages and currents in order to adjust the duty ratio up to the requirement. At last the maximum obtained power (P_{MPP}) is calculated is by the product of the voltage (V_{MPP}) and current (I_{MPP}). Array values at different instants are tabulated in a Table 3.5.

Table 3.5 Array values at different irradiance and different temperature with modified MPPT

Time in (Hrs)	Temperature in (^{0}C)	Irradiance in (W/m^2)	Voltage in (Volts)		Current in (Amps)		Power in (Watts)	
			Theoretical	Practical	Theoretical	Practical	Theoretical	Practical
08.00	30.75	143.55	66.48	60.90	3.9010	3.81	259.33	232.02
08.30	32.55	285.64	68.42	61.60	7.4060	7.72	478.94	475.55
09.06	33.35	408.50	69.43	62.30	10.6036	10.93	695.68	680.93
09.30	35.25	475.73	69.86	63.80	12.3547	12.41	815.96	791.75
10.00	38.25	494.11	69.95	64.20	12.8358	12.83	848.49	823.68
10.30	39.35	513.48	70.05	64.70	13.3409	13.22	883.33	855.33
11.00	39.55	552.65	70.27	65.20	14.3609	14.12	954.96	920.62
11.30	40.02	605.10	70.53	65.80	15.7270	15.33	1048.07	1008.71
12.00	40.50	631.65	70.65	66.10	16.4187	15.91	1096.48	1051.65
12.10	40.68	666.39	70.81	66.40	17.3233	16.71	1159.15	1109.54
12.30	41.10	695.60	70.93	67.30	18.0843	17.22	1212.19	1158.90
13.00	41.35	724.29	71.05	68.10	18.8315	17.73	1264.69	1207.41
13.30	40.45	666.39	70.81	66.80	17.3230	16.62	1159.15	1110.21
14.00	40.08	608.13	70.54	65.70	15.8057	15.43	1053.86	1013.75
14.30	39.00	552.75	70.27	64.30	14.3630	14.31	953.56	920.13
15.00	38.42	479.56	69.86	63.80	12.4570	12.51	822.25	798.13
15.30	37.95	384.05	69.22	63.20	9.9703	10.12	652.05	639.58
16.00	37.32	308.32	68.59	61.70	7.9986	8.32	518.54	513.34
16.30	37.06	147.91	66.46	59.70	3.8229	3.98	240.73	237.60
17.08	33.25	74.63	64.55	58.40	1.9149	2.06	122.74	120.30
17.30	32.85	28.84	61.79	57.90	0.7235	0.79	46.35	45.74

Therefore, the theoretical maximum voltage, current and power values with the modified MPPT are observed as 71.05 Volts, 18.8315 Amps and 1264.69 Watts respectively. Similarly, the practical maximum voltage, current and power values are obtained as 68.10 Volts, 17.73 Amps and 1207.41 Watts respectively at different instants in a day from morning 8:00 AM to evening 5:30 PM

3.8 Simulation Results with Modified MPPT

From the Matlab-simulink designed modified MPPT model, the temperature and the irradiances are given as the inputs to the model at standard test conditions (STC). At STC the basic requirements of irradiance and temperature are 1000 W/m^2 and 25^0 C respectively. Each PV module has 60 cells to produce the 250 watt power. Here, six modules are arranged in series and parallel combinations in order to form solar PV array. Two panels are connected in series and all the three series combinations are connected in parallel.

From simulation results we got the module open circuit voltage as 37.98 volts, the short circuit current about 8.67 amps and power around 250 watts. Similarly the open circuit voltage of array is 75.96 volts with short circuit current of 26.01 amps and the maximum power obtained at MPP is about 1500 watts. These results with the PV array modified MPPT simulation model, I-V, P-V characteristic curves, voltage responses and current responses are presented in Fig. 3.8-3.10 and in Table 3.6.
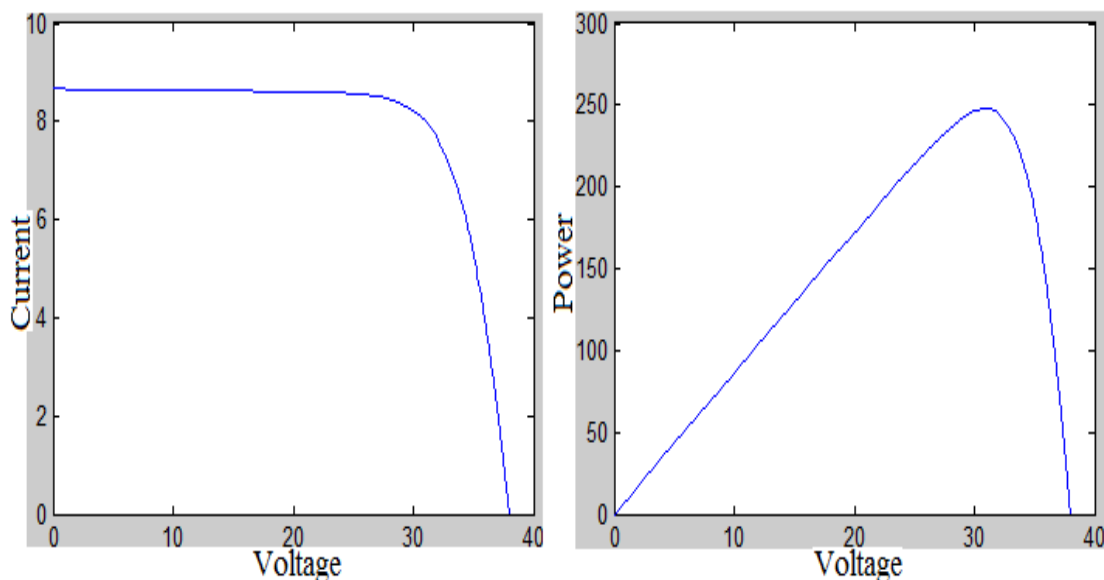
Fig. 3.8 Modified MPPT I-V and P-V characteristic curves of a module
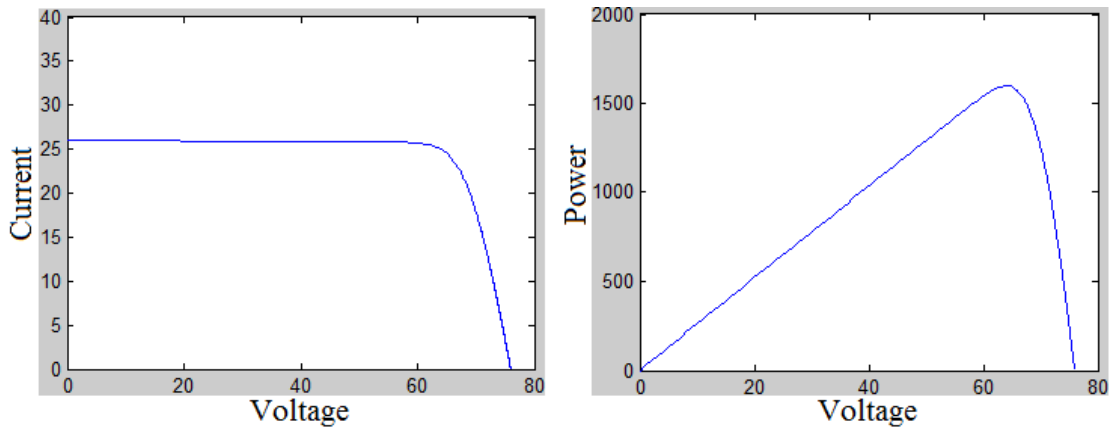
Fig. 3.9 Modified MPPT I-V and P-V characteristic curves of an array
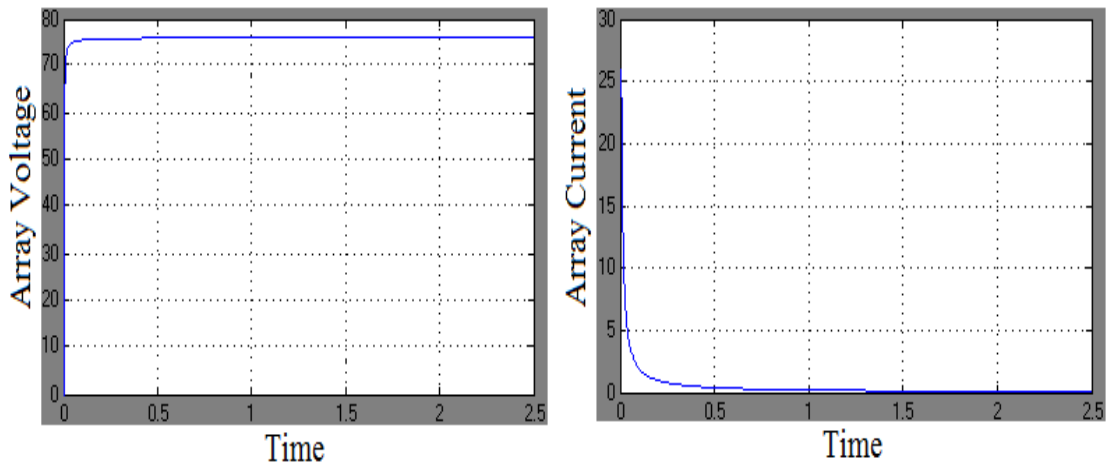
Fig. 3.10 Array output voltage and current responses by the modified MPPT

Table 3.6 PV module and array values from simulation results

Parameter	Module values	Array values
Rated power (P rated)	250 watts	1500 watts
Maximum power point voltage (V_{MPP})	30.68 volts	61.36 volts
Maximum power point current (I_{MPP})	8.14 amps	24.42 amps
Open circuit voltage (V_{OC})	37.98 volts	75.96 volts
Short circuit current (I_{SCR})	8.67 amps	26.01 amps

3.9 Inductance and Capacitance Calculations for Boost Converter Designing

DC-DC boost converter increases the array output voltage with increasing the maximum utilization of PV system by operating at maximum power point. Reactive components like 'shunt capacitance' and 'series inductances' are used to acquire the required load current and voltage respectively. PV array with modified MPPT is connected to DC-DC boost converter to feed the required output to the inverter and loads.

The DC-DC converter converts the DC input voltage to another DC output voltage. Here, the boost converter is used is increase the voltage in order supply the inverter for which the voltage requirement is higher than the output voltage of the solar panel. The three main components are: the inductor; the MOSFET switching device and the diode. When the switch is open as depicted in Fig. 3.12, the current from the source charges the inductor and the inductor stores the part of energy (in the form of magnetic field) that is being supplied by the source. When the switch is closed as shown in Fig. 3.13, the energy stored in the inductor adds to the source and thus increases the output voltage. The duty cycle of a PWM signal determines the ratio between the input and the output voltage. In case of an ideal switching device and when losses are neglected, the ratio between input voltage (V_{IN}) and output voltage (V_{OUT}) can be calculated as shown in Eq. 3.9. From this Equation 3.9 the term 'D' represents the duty cycle of the PWM signal and it has the value between 0 and 1. The output voltage (V_{OUT}) increases as the duty cycle increases. This property is used to adjust the operating point of the MPPT.

$$\frac{V_{OUT}}{V_{IN}} = \frac{1}{1-D} \tag{3.9}$$

As the point of operation of the PV array's MPPT is adjusted by varying the duty cycle, the output voltage of the converter gets increased as the duty cycle increases. So the converter boosts up the output voltage and feeds it to the inverter. The schematic layout of the boost converter with its operating states is represented in the Fig. 3.11-3.13
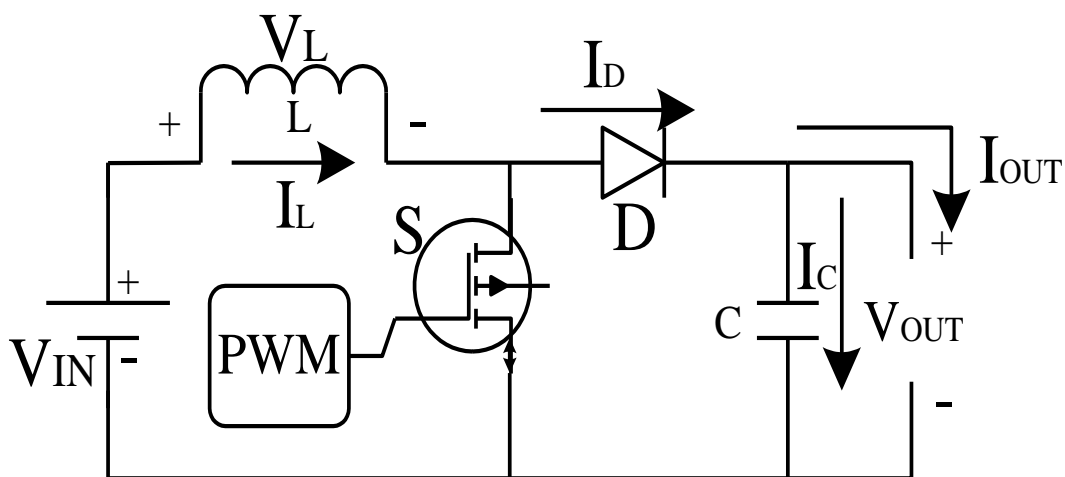
Fig. 3.11 Boost Converter
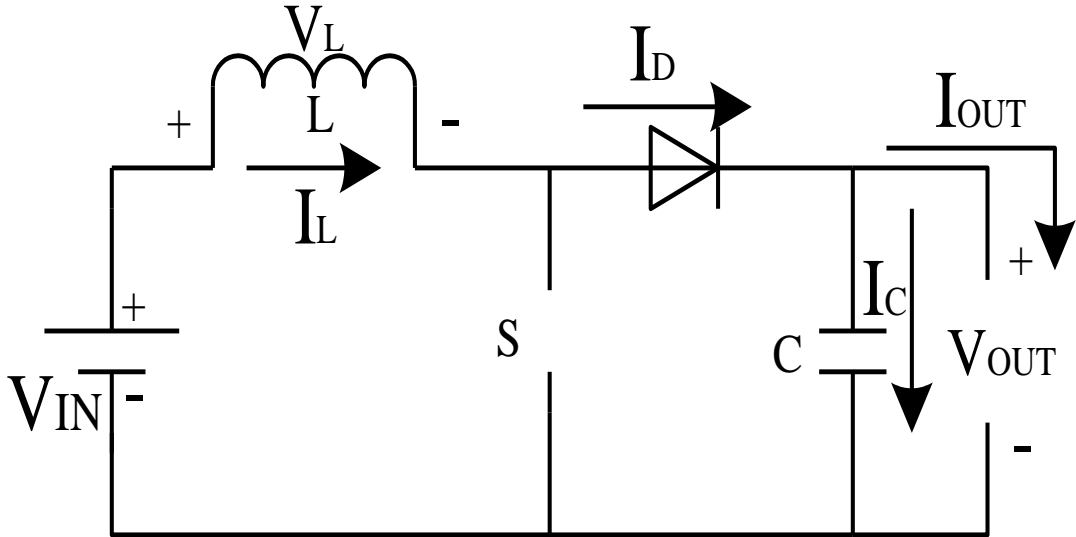
Fig. 3.12 Representation of boost converter while the switch is at open circuit condition
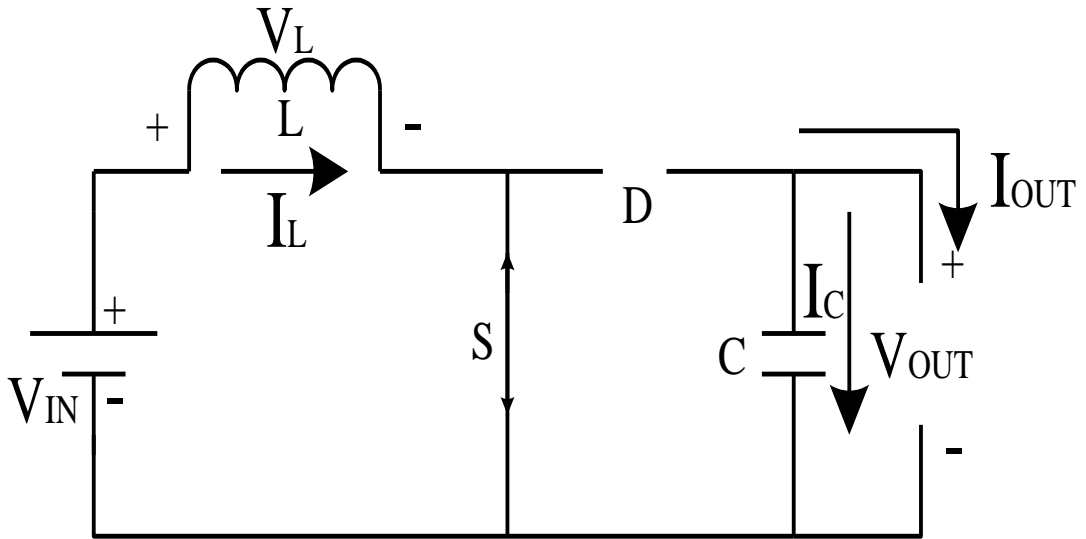
Fig. 3.13 Representation of boost converter while the switch is at closed circuit condition

Inductance is connected in series to meet the load voltage requirements and the minimum required inductance value (L_{MIN}) is calculated from the Eq. (3.10) with the continuous conduction operation mode of the inductor.

$$L_{MIN} = (\frac{V_0(1-D)^2 \times D}{2}) \times f_S \times I_A \tag{3.10}$$

Where V_0 is output DC voltage, D is duty cycle, f_S is converter's switching frequency, I_A is array average output current. Similarly, capacitance is connected in parallel in order to meet the load required current. The minimum required capacitance value ($C_{MIN)}$ is deducted using the Eq. (3.11).

$$C_{MIN} = \frac{V_0 \times D}{R \times \Delta V_0 \times f_S} \tag{3.11}$$

The switching frequency (f_S) value is taken by considering the switching losses, cost of switch and the converter efficiency. DC-DC converter boost ups the array output voltage upto to the requirements of the inverter as well the asynchronous motor load.

- ❖ Additional shunt capacitance for boost converter is used to compensate the DC link voltage oscillations and also to reduce the current ripple given by the PV array.
- ❖ Then the required output to the inverter and the load can be supplied by the PV system with MPPT and DC-DC boost converter.
- ❖ So filtered DC output can be given to the inverter.
- ❖ Inverter feeds the converted ac quantity to the ac motor drive.

In order to reduce the oscillations in the outputs of the DC-DC boost converter the space vector modulation (SVM) technique is used in the inverter, as a inverter controlling technique.

3.10 Conclusion

Modified MPPT and conventional P&O MPPT algorithms for photovoltaic system are developed in the simulation and the results produced by the modified MPPT are compared with the conventional P&O MPPT. Voltage, current and power values generated by the modified MPPT are better than the conventional P&O. Due to this, fast and accurate tracking, the tracking efficiency of the PV system is increased from 94-98% with the modified MPPT. Upon 252 validations from morning 8:00 am to evening 5:30 pm, the locus of practically calculated power is plotted. Also maximum voltage, current and power values obtained from the modified MPPT as well as conventional P&O MPPT with simulation, theoretical and practical observations are tabulated.

ASYNCHRONOUS MOTOR DRIVE PERFORMANCE WITH MODIFIED MPPT AND SVM

4.1 Introduction

Space vector modulation (SVM) controlling technique is the predominantly used technique in the pulse width modulation for voltage fed inverter ac drives. Because it reduces the harmonic content and also provides the consequential flexibility in giving the better switching waveforms compared to other modulation techniques. The better performance of an asynchronous motor drive parameters are observed with the comparison of the conventional and modified MPPT technique along with the SVM controlling technique of the inverter, at starting state, steady state, transients with step change in load torque and speed reversals operating conditions.

4.2 Mathematical Modeling of Asynchronous Motor Drive

A dynamic model of the machine which is valid for any instantaneous variation of voltage and current and adequately describing the performance of the machine under starting, steady state and transient state operating conditions can be obtained by representing the machine voltages and currents in terms of actual phase variables or in terms of two axis variables or using space phasor theory. The three phase motor is a balanced load because of the absence of zero sequence components and therefore it is possible to represent variables of one phase in terms of the other two thereby reducing the total number of equations describing the system. Thus, in such a model, a three phase machine is replaced by an equivalent two phase model with the both phases in quadrature. This helps in eliminating the mutual coupling that exists among the stator phases and rotor phases. The time varying self and mutual inductances can be made constant by referring all the variables to a common reference frame.

This common reference frame can be of two types i.e.

- ❖ i). fixed to stator,
- ❖ ii). fixed to rotor or fixed to the synchronously rotating magnetic field.

The realization of a variable frequency asynchronous motor drive with the high performance comparable to that of a separately excited DC motor requires a suitable mathematical model. The dynamic model of asynchronous motor drive will be useful in estimating the flux of the motor to determine the torque angle, the phase difference between the flux axes. And the stator current vector to fix up the flux axis and to enable the stator current to decompose into two components, i.e. one along with the flux axis and the other perpendicular to the flux axis. Basically, asynchronous motor can be seen as a transformer with a moving secondary, where the coupling coefficients between the stator and rotor phases change continuously with the change of rotor position θ_R.

The machine model can be described by differential equations with time varying mutual inductances, but such a model tends to be very complex. In order to minimize the complexity, the machine in three phase quantities can be represented as an equivalent machine in two phase quantities. Even though it is made simple, the problem of time varying quantities still persists. Hence, the required quantities are referred to a common frame of reference and by doing so; the above problem is taken care of. Three different techniques have been proposed for referring the machine quantities to a common reference frame. The techniques proposed by Kron's method deals with referring quantities of stator and rotor, for a common synchronously rotating reference frame. This makes the motor parameters equivalent to that of a DC motor.

The mathematical modeling of a dynamic asynchronous motor drive is done with the following assumptions as

- ❖ The stator and rotor slotting produces highly negligible variation with the respective inductances.
- ❖ Mutual inductances are equal.
- ❖ Voltage and current harmonics are neglect.
- ❖ Saturation, hysteresis and eddy current effects negotiable.
- ❖ Stator windings are distributed to produce the sinusoidal MMF along with air gap, i.e. space harmonics are negligible (Sinusoidal induction repartition).

The mathematical models of the machine used in this thesis are either in the

synchronously rotating reference frame or in the stator reference frame depending upon the situation. The Voltage Source Inverter (VSI) fed model is used for estimating the flux linkages from voltages and currents and for simulating the motor for maintaining direct coupling between the inverter and the motor.

Stator and rotor flux linkages in terms of current can be expressed as:

$$\Psi_{QS} = L_{lS}I_{QS} + L_M(I_{QS} + I_{QR}) \tag{4.1}$$

$$\Psi_{QR} = L_{lR}I_{QR} + L_M(I_{QS} + I_{QR}) \tag{4.2}$$

$$\Psi_{QM} = L_M(I_{QS} + I_{QR}) \tag{4.3}$$

$$\Psi_{DS} = L_{lS}I_{DS} + L_M(I_{DS} + I_{DR}) \tag{4.4}$$

$$\Psi_{DR} = L_{lR}I_{DR} + L_M(I_{DS} + I_{DR}) \tag{4.5}$$

$$\Psi_{DM} = L_M(I_{DS} + I_{DR}) \tag{4.6}$$

Here: Ψ_{QS}, Ψ_{QR}, Ψ_{DS}, Ψ_{DR} are the Q-axis and D-axis stator and rotor fluxes respectively. Ψ_{QM}, Ψ_{DM} are the mutual fluxes of Q-axis and D-axis respectively. L_{lS}, L_{lR} are the stator and rotor self inductances for respective axis. L_M is the mutual inductance for respective axis of stator and rotor. I_{QS}, I_{QR} are Q-axis stator and rotor currents. I_{DS}, I_{DR} are D-axis stator and rotor currents.

Voltage equations from the Kron's model by the stator field coils i.e. (DS and QS) with the armature coils i.e. (DR and QR). If the resistance R$_{DS}$ and total inductance L$_{DS}$ i.e. (L$_{DS}$=M$_D$+l$_{DS}$). It is manually coupled with the other D-axis coil. The mutual inductance effect of the coil is considered in the voltage equation of DS circuit. Q-axis coil will have no effect on DS and no rotational voltages appear in it, since the coil DS is on stationary element. Then the applied V$_{DS}$ voltage is as follows

$$V_{DS} = R_{DS}I_{DS} + L_{DS}PI_{DS} + M_D PI_{DR} \tag{4.7}$$

Similarly the applied voltage on Q-axis is identical to DS coil as:

$$V_{QS} = R_{QS}I_{QS} + L_{QS}PI_{QS} + M_Q PI_{QR} \tag{4.8}$$

The rotational induced voltages in the armature DR and QR coils are as:

$$V_{DR} = R_{DR}I_{DR} + L_{DR}PI_{DR} + M_DPI_{DS} - E_{DR} \qquad (4.9)$$

Negative sign for the rotational induced voltage (E_{DR}) is due to neglecting of other voltage drops, then the induced voltage is equal and opposite to the applied voltage (E_{DR}) as:

$$E_{DR} = +w_R\Psi_Q \qquad (4.10)$$

Here:

E_{DR} = rotational induced voltage (emf) in volts

w_R = speed in rpm

Ψ_Q = total armature flux linkages at Q-axis in webers

By substituting equation (4.4) in equation (4.3) we get is

$$V_{DR} = R_{DR}I_{DR} + L_{DR}PI_{DR} + M_DPI_{DS} - w_R\Psi_Q \qquad (4.11)$$

Where: $\omega_R = \dfrac{d\theta}{dt}$ and $P = \dfrac{d}{dt}$

Suffixes 'S' and 'R' represents stator and rotor respectively. V_{DS} and V_{QS} are D-Q axis stator voltages respectively, I_{DS}, I_{QS} and I_{DR}, I_{QR} are D-Q axis stator currents and rotor currents respectively. R_{DS}, R_{QS} and R_{DR}, R_{QR} are stator and rotor resistances per phase. L_{DS}, L_{QS} and L_{DR}, L_{QR} are self inductances of stator and rotor and M_D, M_Q are mutual inductances. As we know that Ψ_Q is the total armature flux linkage at Q-axis as:

$$\Psi_Q = M_Q(I_{QS} + I_{QR}) + l_{QR}I_{QR} \qquad (4.12)$$

Thus we get V_{DR} as:

$$V_{DR} = R_{DR}I_{DR} + L_{DR}PI_{DR} + M_DPI_{DS} - w_RM_Q(I_{QS} + I_{QR}) - w_Rl_{QR}I_{QR} \qquad (4.13)$$

$$V_{DR} = R_{DR}I_{DR} + L_{DR}PI_{DR} + M_DPI_{DS} - w_RM_QI_{QS} - w_RL_{QR}I_{QR} \qquad (4.14)$$

i.e. $L_{QR} = M_Q l_{QR} \qquad (4.15)$

Similarly,

$$V_{QR} = R_{QR}I_{QR} + L_{QR}PI_{QR} + M_QPI_{QS} + w_RM_DI_{DS} + w_RL_{DR}I_{DR} \qquad (4.16)$$

Then the matrix representations of the above equations are:

$$\begin{bmatrix} V_{DS} \\ V_{QS} \\ V_{DR} \\ V_{QR} \end{bmatrix} = \begin{bmatrix} R_{DS} + PL_{DS} & 0 & PM_D & 0 \\ 0 & R_{QS} + PL_{DS} & 0 & PM_Q \\ PM_D & -\omega_R M_Q & R_{DR} + PL_{DR} & -\omega_R L_{QR} \\ \omega_R M_D & PM_Q & \omega_R L_{DR} & R_{QR} PL_{QR} \end{bmatrix} \begin{bmatrix} I_{DS} \\ I_{QS} \\ I_{DR} \\ I_{QR} \end{bmatrix} \qquad (4.17)$$

Three phase ac machine voltages can be directly transformed into two phase with the equivalent D-Q axis voltages, which are oriented at "θ" angle i.e. directly from ABC reference frame to the arbitrary frame by using the Park's transformation with respect to Q and D-axis are as:

$$\begin{bmatrix} V_{AS} \\ V_{BS} \\ V_{CS} \end{bmatrix} = \begin{bmatrix} \cos\theta & \sin\theta & 1 \\ \cos(\theta - 120) & \sin(\theta - 120) & 1 \\ \cos(\theta + 120) & \sin(\theta + 120) & 1 \end{bmatrix} \begin{bmatrix} V_{QS1} \\ V_{DS1} \\ V_{OS1} \end{bmatrix} \qquad (4.18)$$

Where: V_{AS}, V_{BS}, V_{CS} are three phase voltages and V_{QS1}, V_{DS1} are the stator Q-axis and D-axis voltages. V_{OS1} is the zero sequence component.

By using the inverse relation we get is

$$\begin{bmatrix} V_{QS1} \\ V_{DS1} \\ V_{OS1} \end{bmatrix} = \frac{2}{3} \begin{bmatrix} \cos\theta & \cos(\theta - 120) & \cos(\theta + 120) \\ \sin\theta & \sin(\theta - 120) & \sin(\theta + 120) \\ 0.5 & 0.5 & 0.5 \end{bmatrix} \begin{bmatrix} V_{AS} \\ V_{BS} \\ V_{CS} \end{bmatrix} \qquad (4.19)$$

Two axis stationary reference frame is transformed into two axis rotating reference frame with the rotating speed "W$_E$" with respect to stator D-Q axis. Then "θ_E" can be as:

$$\theta_E = W_E t \qquad (4.20)$$

Two phase stator D-Q axis windings are transformed into hypothetical windings mounted on rotating D-Q axis. Then the rotating D-Q axis voltages are represented as:

$$V_{QS2} = V_{QS1} \cos\theta_E - V_{DS1} \sin\theta_E \qquad (4.21)$$

$$V_{DS2} = V_{QS1} \sin\theta_E + V_{DS1} \cos\theta_E \qquad (4.22)$$

Here: V_{QS2}, V_{DS2} are the rotating Q and D-axis voltages

By transforming the rotor reference frame into stator reference frame, we get the

following voltages as:

$$V_{QS1} = V_{QS} \cos\theta_E + V_{DS} \sin\theta_E \qquad (4.23)$$

$$V_{DS1} = V_{QS} \sin\theta_E + V_{DS} \cos\theta_E \qquad (4.24)$$

So the three phase voltages are represented as:

$$V_A = V_M \cos Wt \qquad (4.25)$$

$$V_B = V_M \cos(Wt - 120) \qquad (4.26)$$

$$V_C = V_M \cos(Wt + 120) \qquad (4.27)$$

Where: V_A, V_B, V_C are three phase stator reference phase voltages. Similarly the current equations are represented as:

$$I_A = I_M \cos Wt \qquad (4.28)$$

$$I_B = I_M \cos(Wt - 120) \qquad (4.29)$$

$$I_B = I_M \cos(Wt + 120) \qquad (4.30)$$

For balanced load, the zero sequence voltage and current are absent. So, this helps to represent the three phase by an equivalent two phase machine. Then the stator phase voltages are expressed in the quadrature D-Q axis as:

$$V_{QS} = R_S I_{QS} + W_E \Psi_{DS} + P\Psi_{QS} \qquad (4.31)$$

$$V_{DS} = R_S I_{DS} - W_E \Psi_{QS} + P\Psi_{DS} \qquad (4.32)$$

Where:

V_{QS}, V_{DS} are stator D-Q axis voltages

I_{DS}, I_{QS} are stator D-Q axis currents

R_S is the stator per phase resistance and Ψ_{DS}, Ψ_{QS} are the stator D-Q axis flux linkages. Similarly, the rotor equations are given with the consideration of transformation angle for the rotor quantities i.e. $(\theta_E - \theta_R)$ as:

$$V_{QD0R} = R_R \begin{bmatrix} 1 & 0 & 0 \\ 0 & 1 & 0 \\ 0 & 0 & 1 \end{bmatrix} [I_{QD0R}] + (W_E - w_R) \begin{bmatrix} 0 & 1 & 0 \\ -1 & 0 & 0 \\ 0 & 0 & 0 \end{bmatrix} [\Psi_{QD0R}]$$

62

$$+P[\Psi_{QD0R}] \tag{4.33}$$

Similarly, with removing the zero quantity, the voltages are presented as:

$$V_{QR} = R_R I_{QR} + (W_E - W_R)\Psi_{DR} + P\Psi_{QR} \tag{4.34}$$

$$V_{DR} = R_R I_{DR} - (W_E - W_R)\Psi_{QR} + P\Psi_{DR} \tag{4.35}$$

Here:

V_{QR}, V_{DR} are rotor D-Q axis voltages

I_{DR}, I_{QR} are rotor D-Q axis currents

R_R is the rotor per phase resistance

Ψ_{DR}, Ψ_{QR} are the rotor D-Q axis flux linkages.
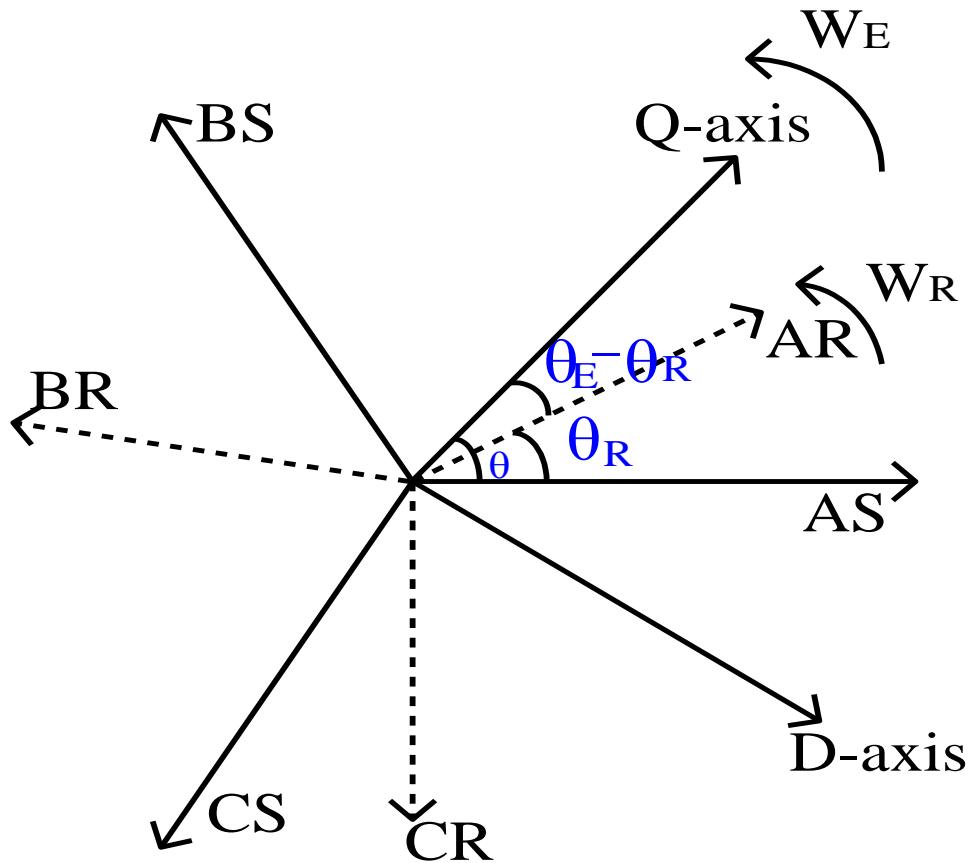
Fig. 4.1 Representation of 3-phase ABC to 2-phase arbitrary rotating D-Q axis

And finally at the steady state electromagnetic torque Te of the asynchronous motor is given by:

$$T_e = \frac{3}{2}\left(\frac{P}{2}\right)\left(\Psi_{QR} I_{DR} - \Psi_{DR} I_{QR}\right) \tag{4.36}$$

63

From this, the rotor flux will coincide with the D-axis and makes the Q-axis rotor flux equals to zero (0) i.e. $\Psi_{QR}=0$. Then the electromagnetic torque of the motor drive is deduced as followed:

$$T_e = \frac{3}{2}\left(\frac{P}{2}\right)\frac{L_M}{L_R}\left(\Psi_{DR}I_{QS}\right) \tag{4.37}$$

Due to this, torque is independently controlled by the stator Q- component current I_{QS}, if the rotor flux linkage Ψ_{DR} is not interrupted. And it leads to $\Psi_{QR}=0$ and $\Psi_{DR}=\Psi_R$, then the speed is represented as:

$$\omega_{Sl} = \frac{L_M R_R}{\Psi_R L_R}I_{QS} \tag{4.38}$$

The rotor angle θ_E is estimated using the measured rotor speed ω_R and slip speed ω_{Sl}

$$\theta_E = \int \omega_E dt = \int (\omega_R + \omega_{Sl})dt = \theta_R + \theta_{Sl} \tag{4.39}$$

4.3 Space Vector Modulation (SVM) Technique for The Two Level Inverter

Space vector modulation (SVM) technique is the important technique among all PWM techniques for three phase voltage source inverter. It was originally developed as a vector approach to pulse width modulation (PWM) for three phase voltage source inverter. It is more sophisticated technique that provides higher voltage with fewer harmonic. The main aim of any modulating technique is to obtain variable output having a fundamental component with minimum harmonics. SVM method is an advanced, computation intensive PWM method and possibly the best techniques for variable frequency drive applications. The carrier wave is modulated by reference wave and the switching points of inverter are determined.

The main intension of PWM implementation in power electronics is for controlling of motor drive speed, by incorporating with the inverter. When the analogue signals are generated then there will be a disadvantage of pulse width resolution, which promptly decreases the required signal bandwidth. In order to overcome such demerits, the space vector modulation technique is introduced which is the most enlightened control technique for the inverter and asynchronous motor

drive as discussed in the upcoming sub topics.

4.3.1 Working of SVM with two level voltage source inverter

The circuit model of three phase voltage source inverter is shown in Fig. 4.2. There are six power MOSFET switches to give the output and these switches are controlled by the provided pulses of SVM with variables A, A', B, B', C and C'. When upper switches are on i.e. A, B and C are "ON" then that the "ON" position is denoted as "1". Then the corresponding lower switches are switched OFF i.e. the corresponding A', B', and C' are "OFF" and that "OFF" position is denoted as "0". Therefore, the "ON" and "OFF" state of the upper switches S1, S3 and S5 can be used to determine and to produce the required output voltage.

The switches must be controlled so that two switches cannot be turned "ON" at the same time in the same leg, otherwise leg will be short circuited. This requirement may be acquired by the corresponding operation of the switches within the same leg i.e. if "A+" is "under conduction" then "A-" will be "under non-conduction" and vice-versa. Similarly the rest of other switching patterns are tabulated in Table 4.1. This technique generates less harmonic distortion in the output voltages or currents applied to the phases of asynchronous motor drive. Voltage vectors in each sector are represented in Fig. 4.3.
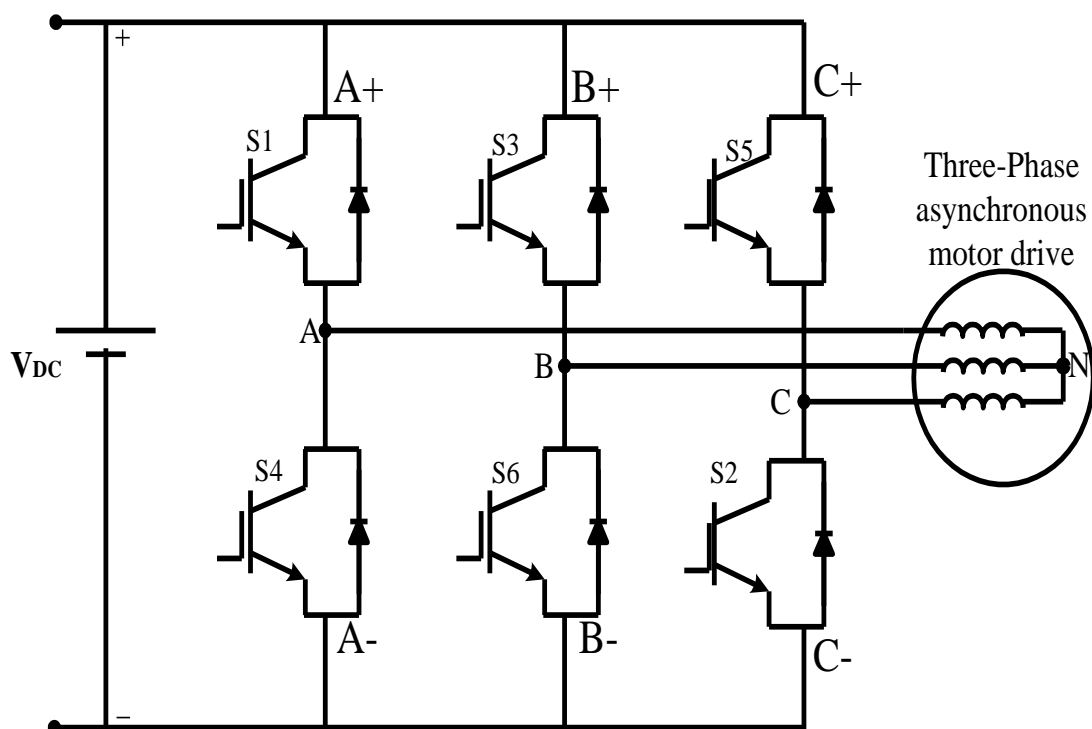
Fig. 4.2 Two level inverter fed asynchronous motor drive
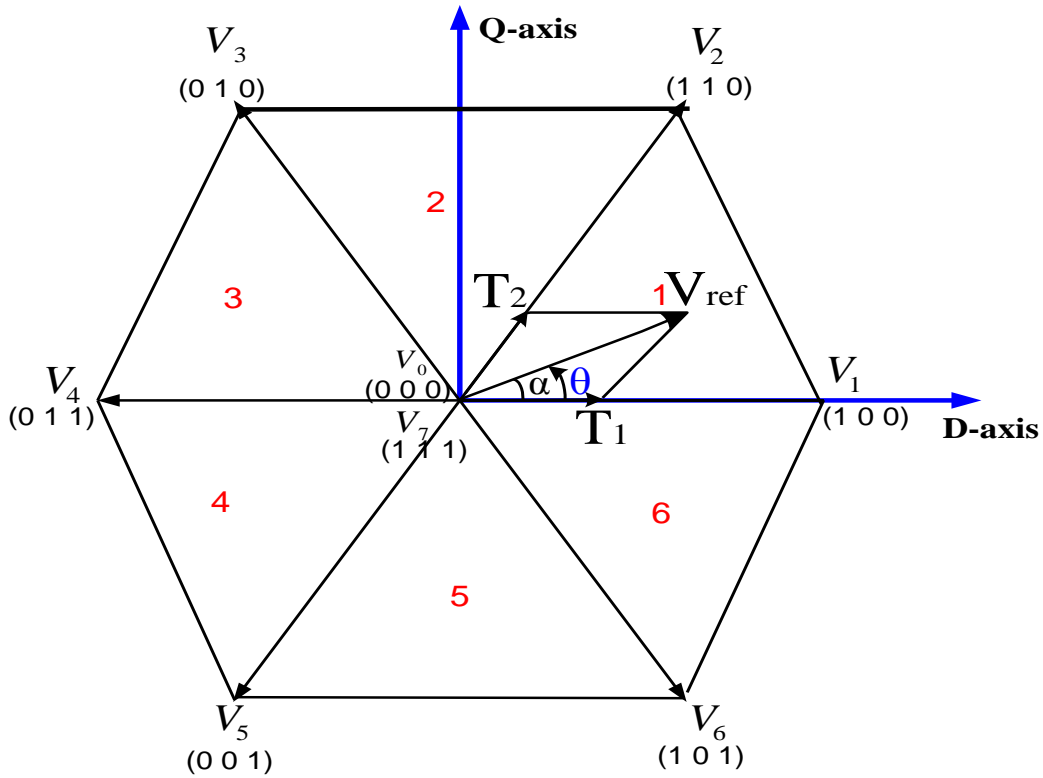
Fig. 4.3 Representation of space vector diagram of two-level inverter with effective vectors

4.3.2 Switching state topologies

This space vector modulation technique has six active (non-zero) vectors i.e. [100 110 010 011 001 101] and two non-active (zero) vectors i.e. [000 111], which are used for producing the required reference output voltages. Space Vector Modulation (SVM) technique is applied to minimize the overall switching changes when the nearest three space vectors are used. The identical properties of switching states and their redundancies enable the improvement of the SVM technique in order to reduce the switching loss and operating under fault conditions. The eight available vector switching state diagrams i.e. (V_0-V_7) of six switches are depicted in Fig. 4.4.

State-1: V_1(1 0 0)   State-2: V_2(1 1 0)
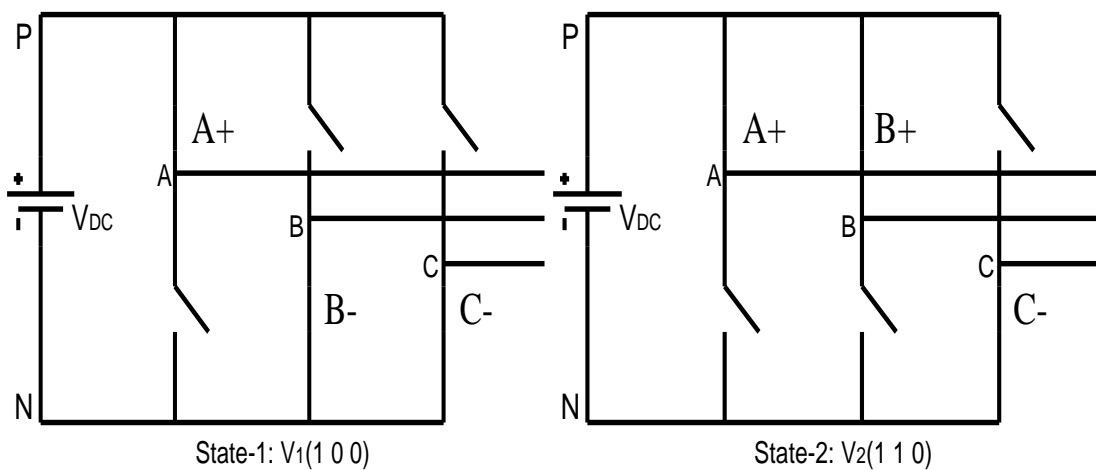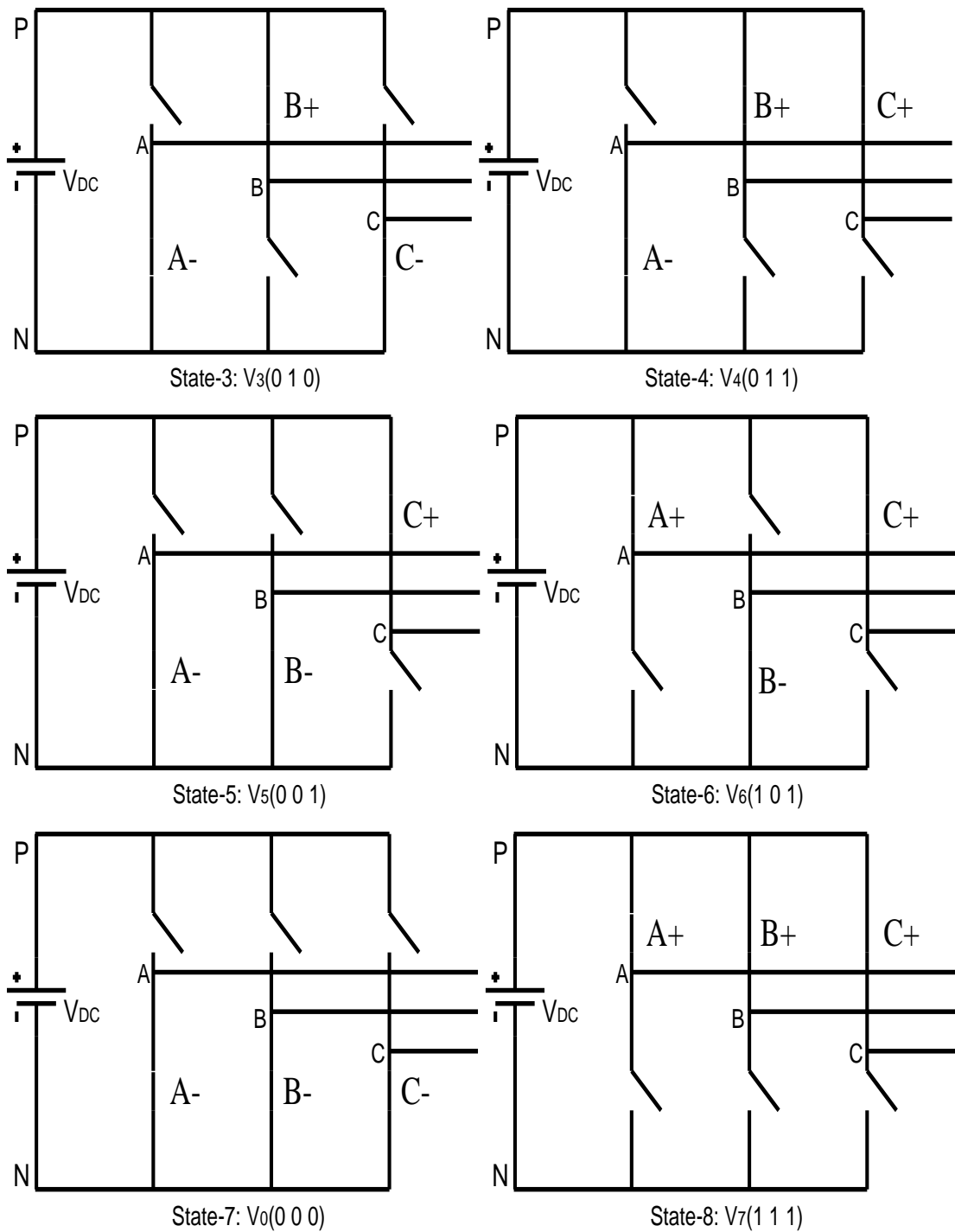
Fig. 4.4 Representation of 8-switching states

4.3.3   Output voltages from the vector topologies

Considering from the topology-1 with the state space-1 as shown in Fig. 4.4 that the output line voltages are generated as:

$$
\left.
\begin{aligned}
V_{AB} &= V_{DC} \\
V_{BC} &= 0 \\
V_{CA} &= -V_{DC}
\end{aligned}
\right\}
\tag{4.40}
$$

This is represented in the D-Q plane as depicted in Fig.4.5. Here the line voltage vectors are displaced by 120° in the space. The effective voltage vector produced with this topology is denoted by V_1 (100) as shown in Fig. 4.5.

From this notation (100) it refers that the three legs or phases A, B, C are either connected to the positive DC link or to the negative DC link. Thus "100" resembles that "A" is connected to the positive DC link and "B" and "C" are connected to the negative DC link.

Q-axis
V_{BC}
$-V_{CA}$
$-V_{DC}$
$V_1(1\ 0\ 0)$ D-axis
V_{DC}
V_{CA}
V_{AB}
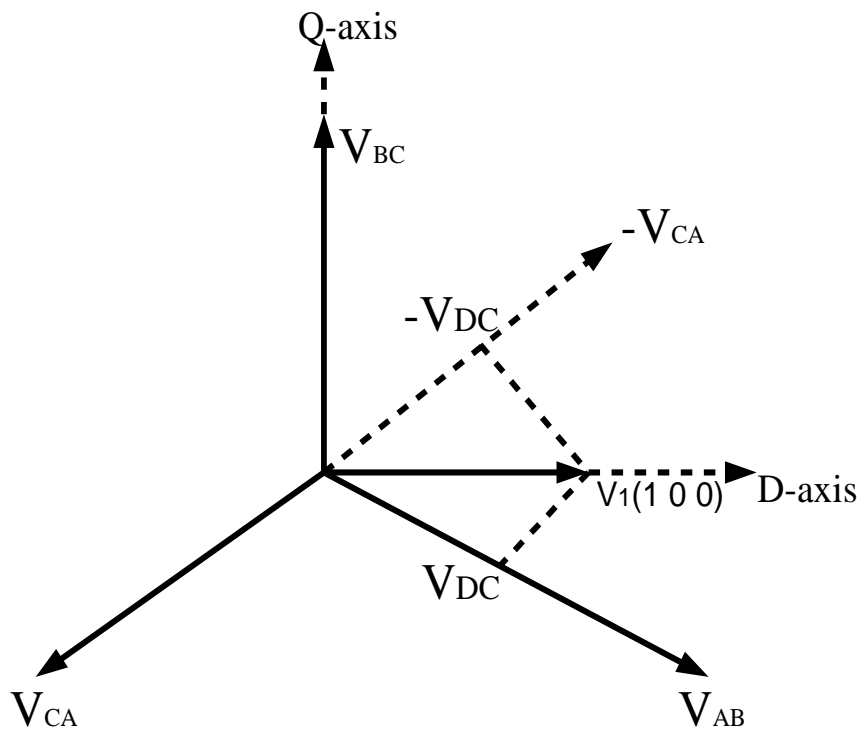
Fig. 4.5 Vector V_1 representation from topology-1 in D-Q plane

Similarly with the same working procedure six non-zero voltage vectors (V_1-V_6) are generated as shown in Table 4.1. The tips these six vectors form a regular hexagon. Then the remaining vectors with zero magnitudes are termed as zero switching or non-active state vectors.

They assume their positions at the origin in the D-Q plane. The vectors V_0-V_7 are called as switching state vectors. Vectors V_0 and V_7 are produced from the last two topologies as shown in the Fig. 4.6. That the respective last two topologies are represented in the Fig. 4.4
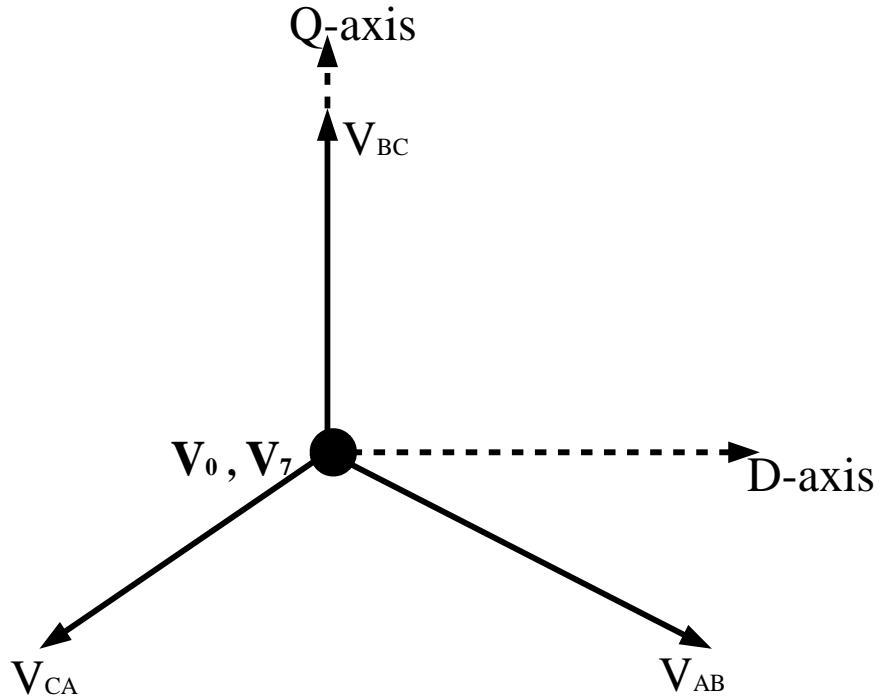
Fig. 4.6 Representation of vectors V_0 & V_7 from the topologies 7 & 8 in the D-Q plane

The output line voltages obtained from the last two topologies with zero magnitude are shown below:

$$\left.\begin{array}{l} V_{AB} = 0 \\ V_{BC} = 0 \\ V_{CA} = 0 \end{array}\right\} \tag{4.41}$$

Table 4.1 Switching voltage vector states with their voltage values

Voltage Vectors	Switching vectors			Phase voltages			Line-line voltages		
	A	B	C	V_{AN}	V_{BN}	V_{CN}	V_{AB}	V_{BC}	V_{CA}
V_0 (000)	OFF	OFF	OFF	0	0	0	0	0	0
V_1 (100)	ON	OFF	OFF	$\frac{2}{3}V_{DC}$	$-\frac{1}{3}V_{DC}$	$-\frac{1}{3}V_{DC}$	V_{DC}	0	$-V_{DC}$
V_2 (110)	ON	ON	OFF	$\frac{1}{3}V_{DC}$	$\frac{1}{3}V_{DC}$	$-\frac{2}{3}V_{DC}$	0	V_{DC}	$-V_{DC}$
V_3 (010)	OFF	ON	OFF	$-\frac{1}{3}V_{DC}$	$\frac{2}{3}V_{DC}$	$-\frac{1}{3}V_{DC}$	$-V_{DC}$	V_{DC}	0
V_4 (011)	OFF	ON	ON	$-\frac{2}{3}V_{DC}$	$\frac{1}{3}V_{DC}$	$\frac{1}{3}V_{DC}$	$-V_{DC}$	0	V_{DC}
V_5 (001)	OFF	OFF	ON	$-\frac{1}{3}V_{DC}$	$-\frac{1}{3}V_{DC}$	$\frac{2}{3}V_{DC}$	0	$-V_{DC}$	V_{DC}
V_6 (101)	ON	OFF	ON	$\frac{1}{3}V_{DC}$	$-\frac{2}{3}V_{DC}$	$\frac{1}{3}V_{DC}$	V_{DC}	$-V_{DC}$	0
V_7 (111)	ON	ON	ON	0	0	0	0	0	0

4.4 Three Phase to Two Phase Transformation

❖ It is based on the representation of the three phase quantities as vectors in a two-dimensional (D-Q) plane

The space vector concept is being derived from the rotating field of asynchronous motor drive and it is used to modulate the inverter output voltages.

In this modulation the three phase quantities can be transformed into their equivalent two phase quantity with the help of Park's transformation either in synchronously rotating frame or stationary frame. While considering the stationary reference frame let the three phase sinusoidal voltage component be represented as:
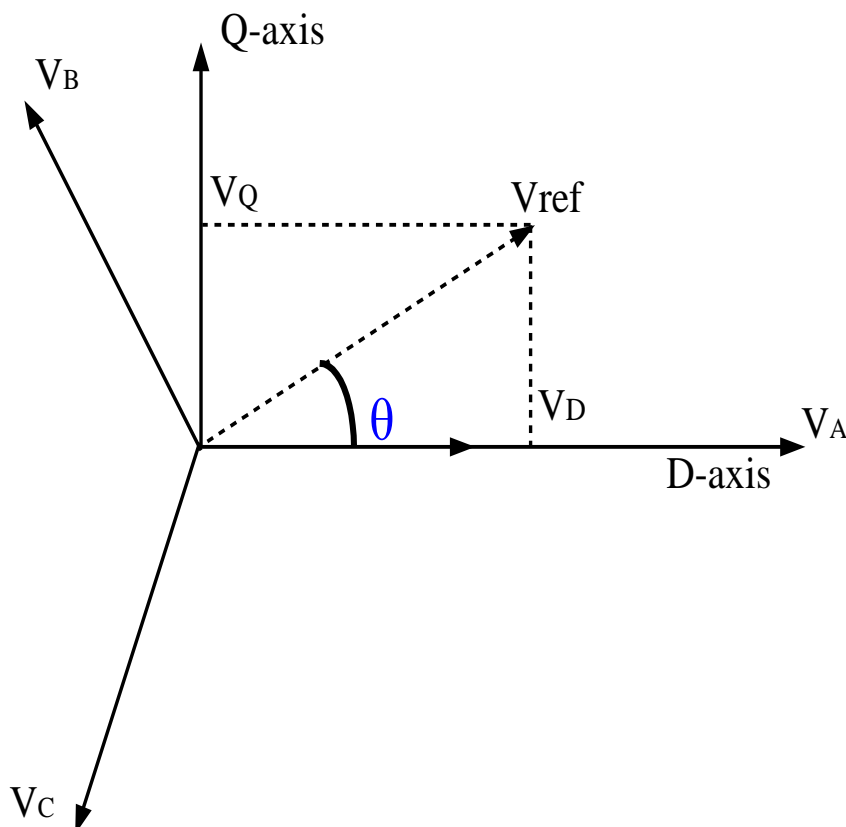
Fig. 4.7 Representation of three phase ABC reference voltages in a stationary D-Q axis

By considering the operation of the inverter under three phase balanced load then we get, that the sum of all the phase voltages equals to zero (0) as:

$$V_{AN} + V_{BN} + V_{CN} = 0 \tag{4.42}$$

Where: V_{AN}, V_{BN} and V_{CN} are the instantaneous phase voltages.

From the Park's transformation two axis (D-Q) frame voltages are represented with respect to the three phase (ABC) stator reference instantaneous voltages as:

$$\begin{bmatrix} V_D \\ V_Q \end{bmatrix} = \frac{2}{3} \begin{bmatrix} 1 & \frac{-1}{2} & \frac{-1}{2} \\ 0 & \frac{\sqrt{3}}{2} & \frac{\sqrt{3}}{2} \end{bmatrix} \begin{bmatrix} V_{AN} \\ V_{BN} \\ V_{CN} \end{bmatrix} \tag{4.43}$$

Where: V_D and V_Q are the D-axis and Q-axis voltages respectively.

$$V_D = \frac{2}{3} \left[V_A - 0.5(V_B + V_C) \right] \tag{4.44}$$

$$V_Q = \frac{\sqrt{3}}{3} (V_B - V_C) \tag{4.45}$$

Then the reference voltage "V$_{ref}$" is denoted as:

$$V_{ref} = V_D + jV_Q \tag{4.46}$$

$$V_{ref} = \sqrt{(V_D^2 + V_Q^2)} \tag{4.47}$$

$$\propto = \tan^{-1} \frac{V_Q}{V_D} \tag{4.48}$$

By substituting the Eq. (4.41) in (4.44) then we get is

$$V_{ref} = \frac{2}{3} [V_{AN} e^{j\theta} + V_{BN} e^{\frac{j2\pi}{3}} + V_{CN} e^{\frac{j4\pi}{3}}] \tag{4.49}$$

From topology 1, with the active switching state (100) that the obtained phase voltages are given as:

$$V_{AN} = \frac{2}{3} V_{DC}, \ V_{BN} = -\frac{1}{3} V_{DC}, \ V_{CN} = -\frac{1}{3} V_{DC} \tag{4.50}$$

Then the corresponding space vector V$_1$ is obtained by substituting the Eq. (4.48) in (4.47) as:

$$V_1 = \frac{2}{3} V_{DC} e^{j\theta} \tag{4.51}$$

By following the same procedure that the six active state space vectors can be obtained as:

$$V_K = \frac{2}{3}V_{DC}e^{\frac{j(K-1)\pi}{3}} \tag{4.52}$$

Where: K=1, 2, 3..6

4.5 Switching Time Calculations

❖ The volt-seconds produced by the vectors V_1, V_2 and V_7/V_0 along Q and D axes are the same as those produced by the reference vector v_{ref} as:

$$V_{ref}\angle\alpha° * T_S = V_1\angle0° * T_1 + V_2\angle60° * T_2 + 0 * T_Z \tag{4.53}$$

$$V_{ref}(\cos \propto + j \sin \propto) * T_S = \frac{2}{3}V_{DC}T_1 + \frac{2}{3}V_{DC}(\cos 60° + j \sin 60°) * T_2 \tag{4.54}$$

T_1 and T_2 values are found by the separation of real and imaginary values as:

$$\frac{2}{3}V_{DC}T_1 + \frac{2}{3}V_{DC}\cos\frac{\pi}{3}T_2 = |V_{ref}|\cos\alpha\, T_S \tag{4.55}$$

$$\frac{2}{3}V_{DC}\sin\frac{\pi}{3}T_2 = |V_{ref}|\sin\alpha\, T_S \tag{4.56}$$

Then the switching time periods are denoted as:

$$T_1 = \frac{|V_{ref}|.T_S}{\frac{2}{3}V_{DC}}.\frac{\sin(\frac{\pi}{3}-\alpha)}{\sin\frac{\pi}{3}} \tag{4.57}$$

$$T_2 = \frac{|V_{ref}|.T_S}{\frac{2}{3}V_{DC}}.\frac{\sin(\alpha)}{\sin\frac{\pi}{3}} \tag{4.58}$$

$$T_0 = T_S - T_1 - T_2 \tag{4.59}$$

Where: T_1, T_2 and T_0 are the time widths for the vectors V_1, V_2 and V_0 respectively. T_0 is the time period of zero (null) vectors i.e. for V_0 as well as V_7, i.e. the zeroth state time will be shared between two zero states as T_0 for V_0 and T_7 for V_7 respectively, and they can be expressed as:

$$T_0 = K_0T_Z \tag{4.60}$$

$$T_7 = (1 - K_0)T_Z \tag{4.61}$$

The various SVM controlling techniques are produced by adjusting the K_o value in between 0 and 1. However, in this SVM controlling technique, the zeroth voltage

72

vector time period is disseminated equally between V_0 and V_7. Hence, for the implementation and completion of this research, that the K_0 value is assigned as 0.5.

- ❖ Space vector modulation (SVM) algorithm is applied for two level inverter as a inverter controlling technique, for which the solar panels are connected to provide the dc supply.
- ❖ SVM is applied to minimize the overall switching changes when the nearest three space vectors are used.
- ❖ In PWM technique each phase voltage is produced separately according to its reference, while SVM technique transforms three phase reference voltage into a rotational vector in space vector domain and synthesizes it through the appropriate switching sates of the inverter.
- ❖ Switching sequence is given in order to get symmetrical algorithm pulses and voltage balancing. This is used to control the output voltages of the two level inverter with the modified MPPT controller.
- ❖ The D-axis and Q-axis voltages are converted into three-phase instantaneous reference voltages.

The voltage vectors with the switching times are presented in Fig. 4.8.
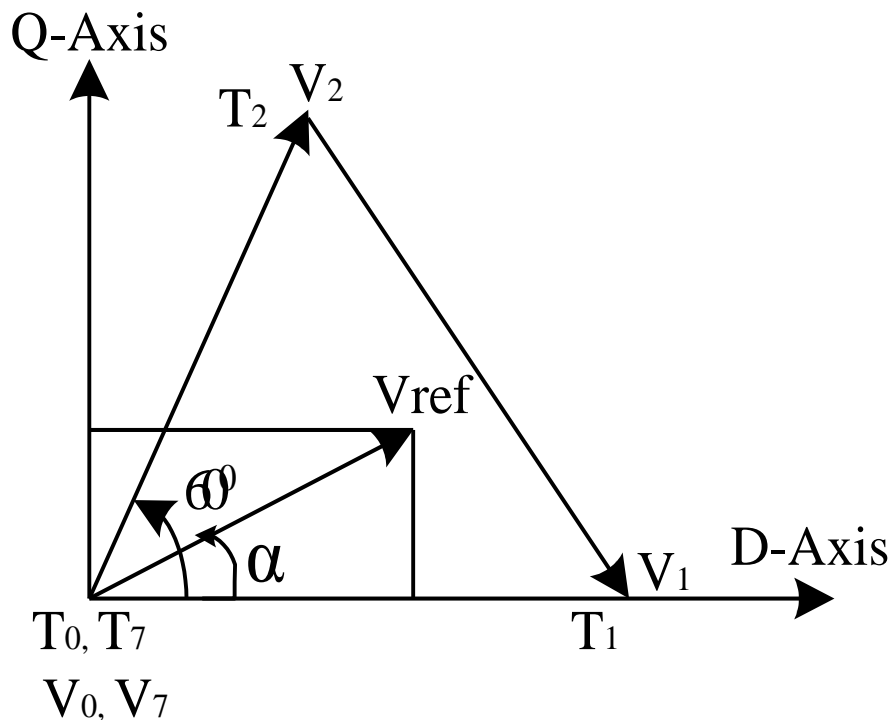
Fig. 4.8 Voltage vectors with the switching times

73

4.6 Simulation Results

Simulation results are obtained with the reference speed of 1480 RPM and switching frequency of 5 KHz. Performance of the inverter with the %THD line-line voltage values are observed. And also the performance of asynchronous motor drive is observed at starting state, steady state, step change in load torque and speed reversals operating conditions, with the connection of two level inverter by the conventional as well as modified MPPT using SVM controlling technique in Fig. 4.10-4.30.

4.6.1 Responses of inverter output voltages

PV array operating point is obtained or reached to a maximum suitable value by varying the duty cycle. DC-DC boost converter is used to increase the PV output and also to provide the maximum utilization for the PV system by operating at MPP. Array output voltage is boosted to 400 volts with the SVM based inverter controlling technique. Here the motor drive is being fed with 400 Volts supply with the help of boost converter and inverter. That the inverter output voltages are depicted in Fig. 4.9.
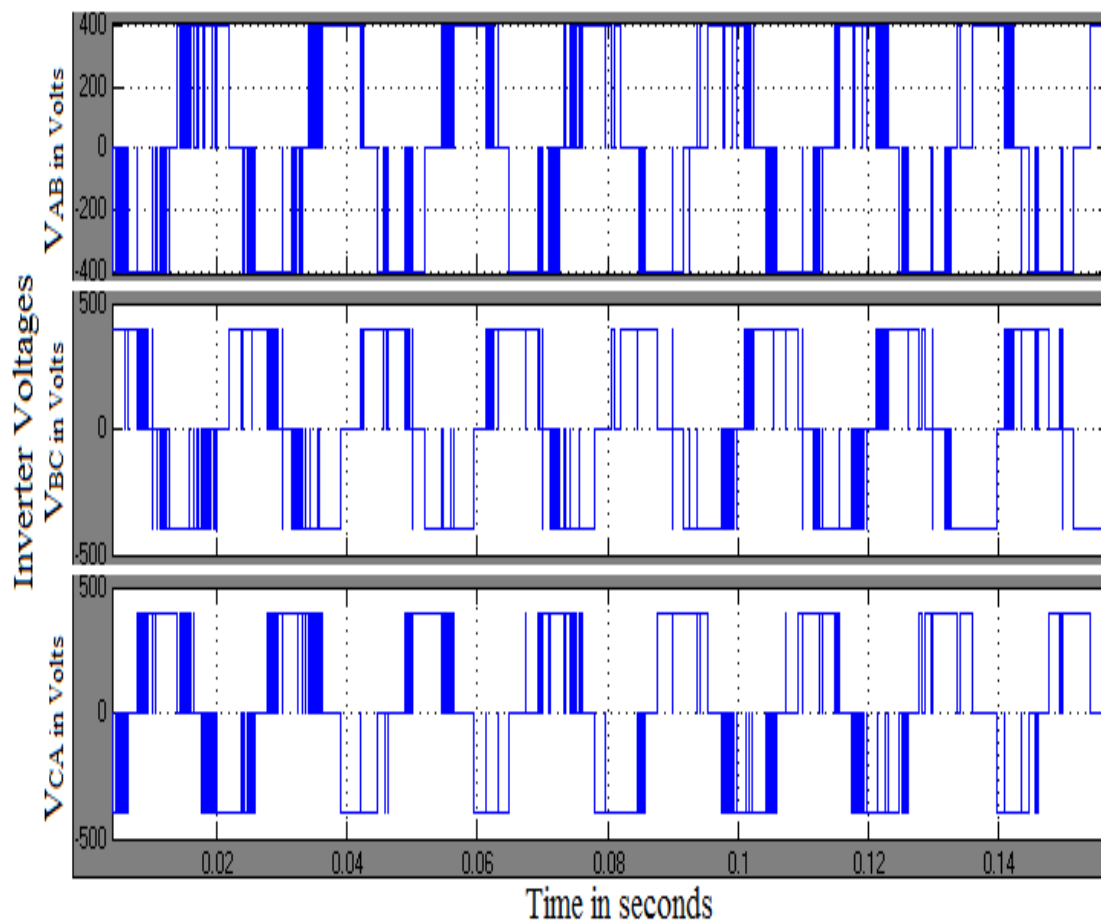
Fig. 4.9 Inverter output voltages

74

4.6.1.1 Inverter performance at switching frequency of 5 KHz with the conventional MPPT

The harmonic spectrums of SVM controlled inverter with the conventional MPPT at the switching frequency of 5 KHz are illustrated in Fig. 4.10-4.12. It is observed that the THD values of 3 line-line inverter voltages with the conventional MPPT SVM are 17.08%, 16.60% and 17.08% respectively.
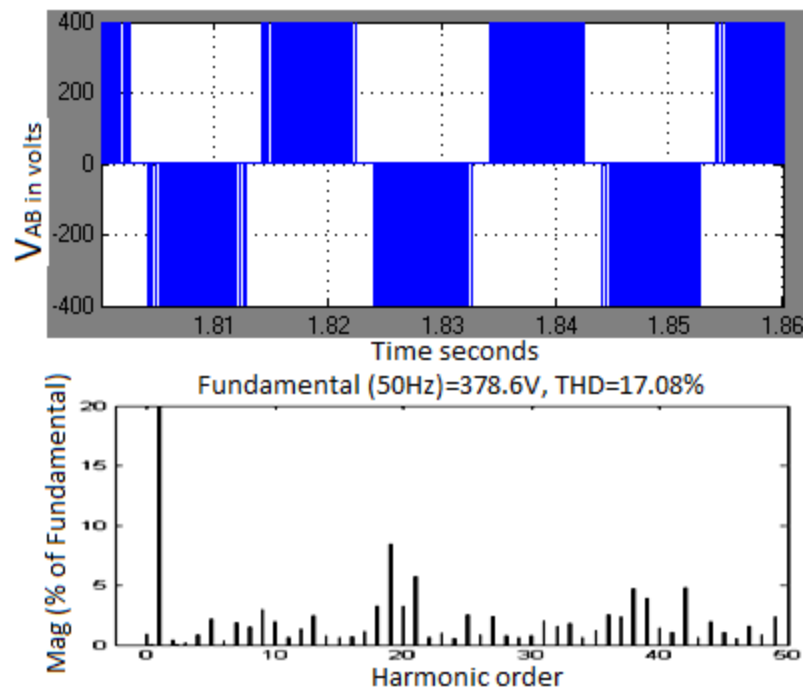
Fig. 4.10 Inverter V_{AB} line-line voltage with conventional MPPT at 5 KHz
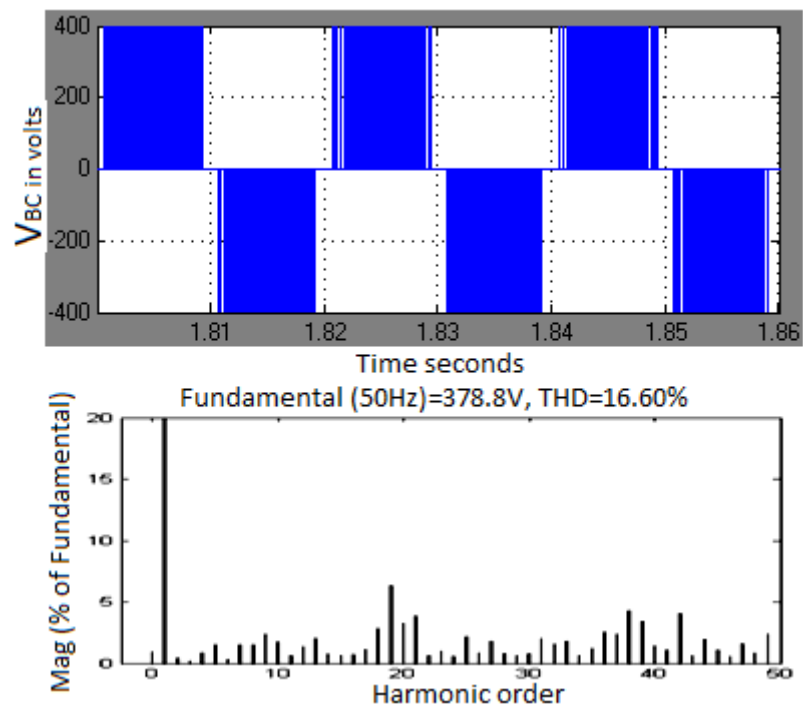
Fig. 4.11 Inverter V_{BC} line-line voltage with conventional MPPT at 5 KHz
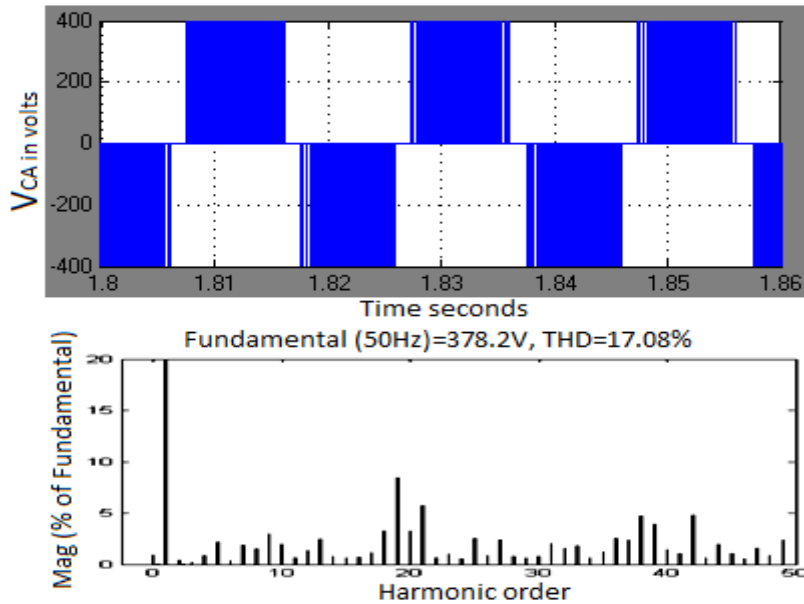
Fig. 4.12 Inverter V_{CA} line-line voltage with conventional MPPT at 5 KHz

4.6.1.2 Inverter performance at switching frequency of 5 KHz with the modified MPPT

Line-line voltages, harmonic spectrums and THD values using FFT waveforms of SVM controlled inverter with the modified MPPT at the switching frequency of 5 KHz is represented in Fig. 4.13-4.15. It is observed that the THD of 3 line-line voltages with the modified MPPT SVM gives the better output voltages with the more reduction of harmonics. The inverter line-line voltages THD values are observed as 14.23%, 14.36% and 14.23% respectively. From these results it is analyzed that the modified MPPT connected SVM reduces the THD of line-line voltages by 15-20%.
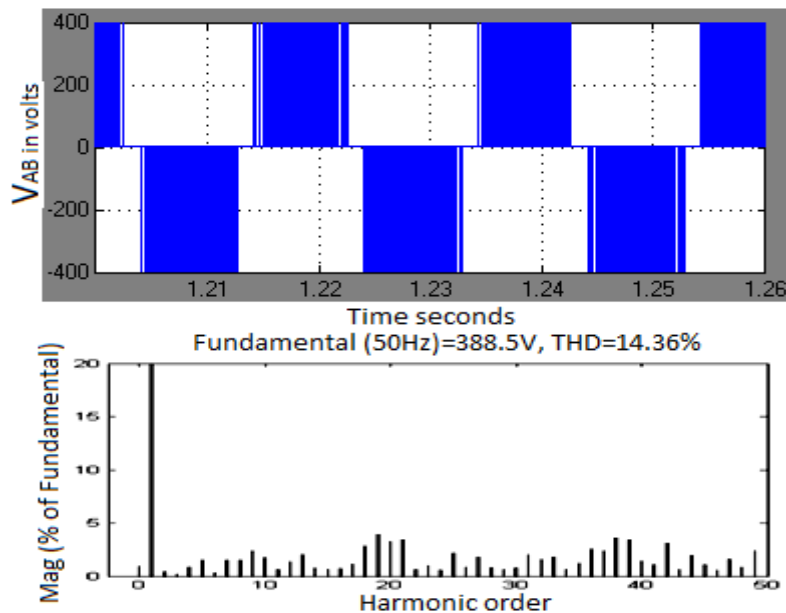
Fig. 4.13 Inverter V_{AB} line-line voltage with modified MPPT at 5 KHz

76
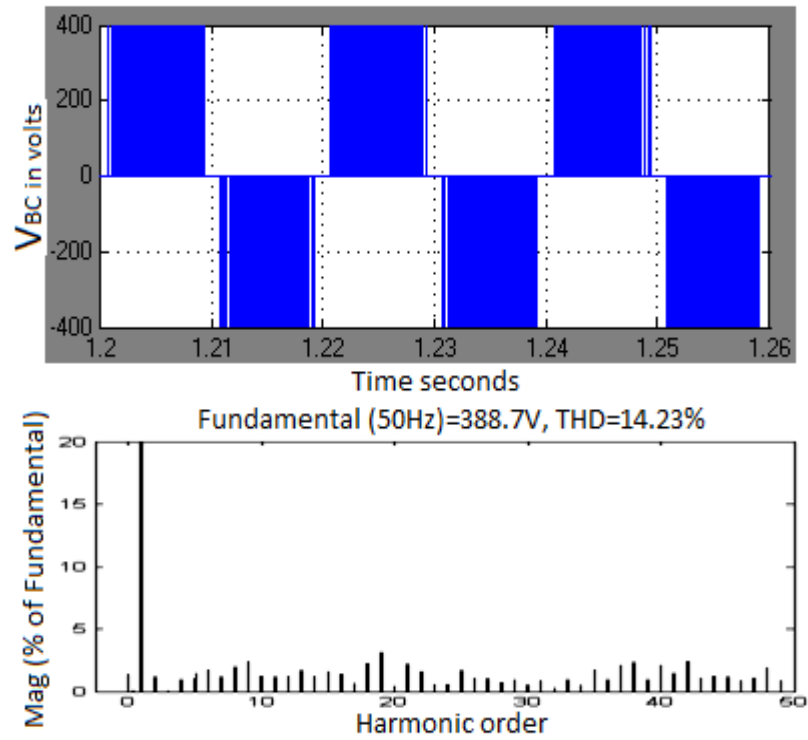
Fig. 4.14 Inverter V_{BC} line-line voltage with modified MPPT at 5 KHz
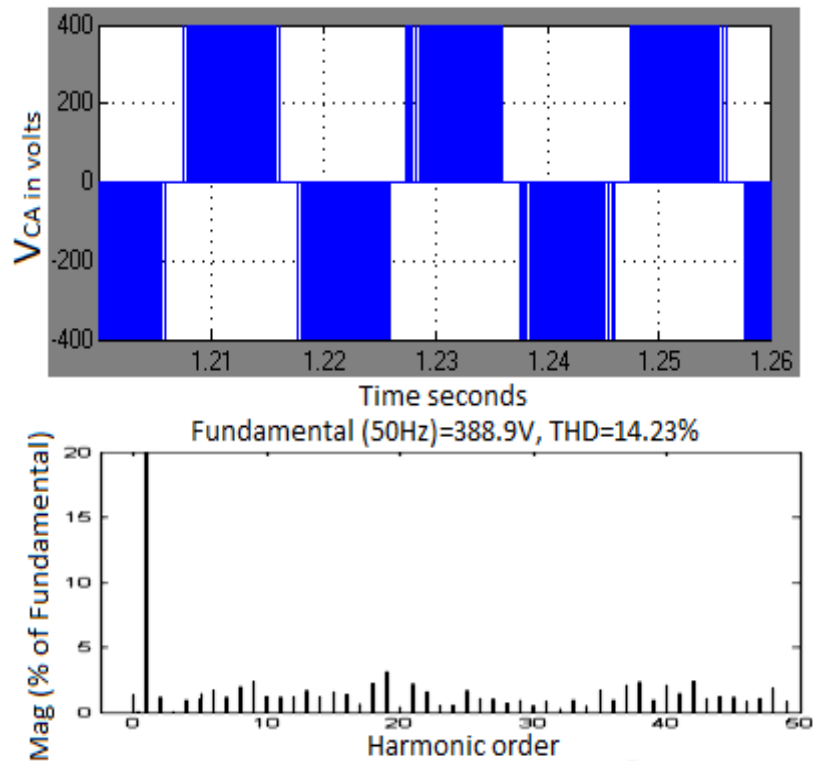
Fig. 4.15 Inverter V_{CA} line-line voltage with modified MPPT at 5 KHz

4.6.2 Performance of an asynchronous motor drive with 5 KHz at starting state

For the asynchronous motor drive the maximum current and the ripple content in the torque is reduced during starting in order to reach the early steady state. With the modified MPPT along with SVM, the maximum torque, maximum stator phase

77

current and the speed are obtained as 8.35 N-m, 5.061 Amps and 1424 RPM respectively.

It is observed that the ripple contents of stator phase current and torque with the conventional method are 0.38 and 0.32 respectively. Similarly with the modified method are 0.29 and 0.26 respectively. Here, it can be observed that lot of reduction compared to the conventional method i.e. current ripple 31.03% and torque ripple 23.07% is reduced. These results are presented in Fig. 4.16-4.18.
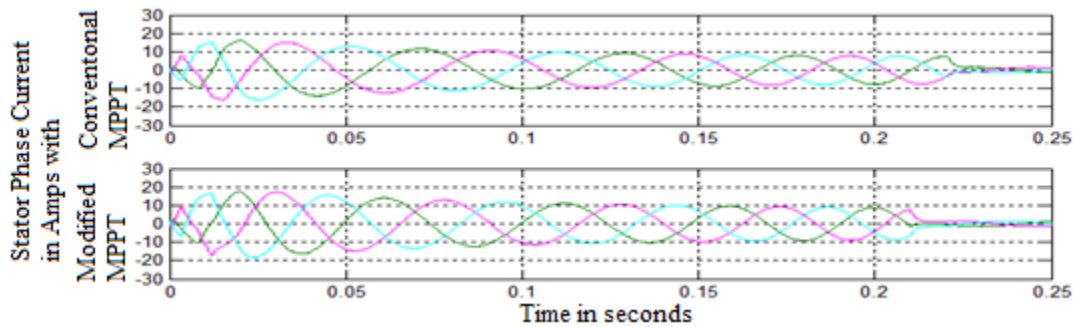
Fig. 4.16 Stator phase current responses with the conventional and modified MPPT controllers at starting
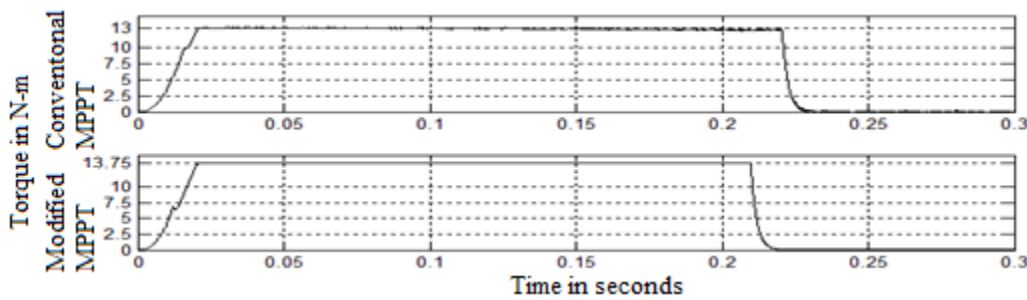
Fig. 4.17 Torque responses with the conventional and modified MPPT controllers at starting
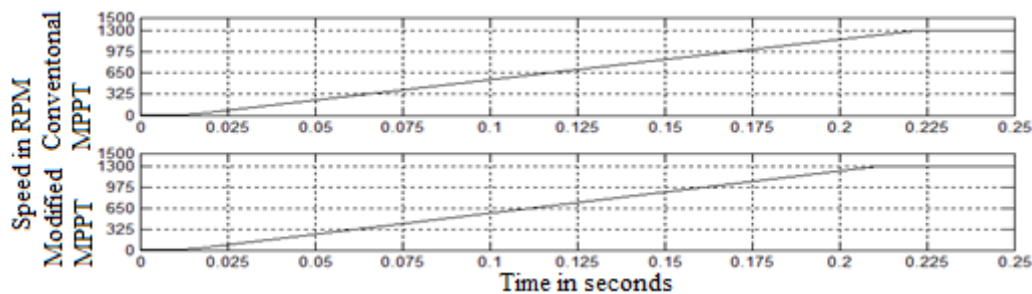
Fig. 4.18 Speed responses with the conventional and modified MPPT controllers at starting

4.6.3 Performance of an asynchronous motor drive with 5 KHz at steady state condition

The steady state responses of the stator phase currents, torque and speed with conventional and modified MPPT along with SVM are depicted in Fig. 4.19-4.21.

78

Here torque ripple with the modified MPPT is reduced a lot i.e. it is observed that the torque ripple contents with the conventional and modified MPPT are 0.35 and 0.27 respectively, i.e. 29.62% of torque ripple content is reduced during steady state. And the better speed response is obtained with the modified MPPT controller.
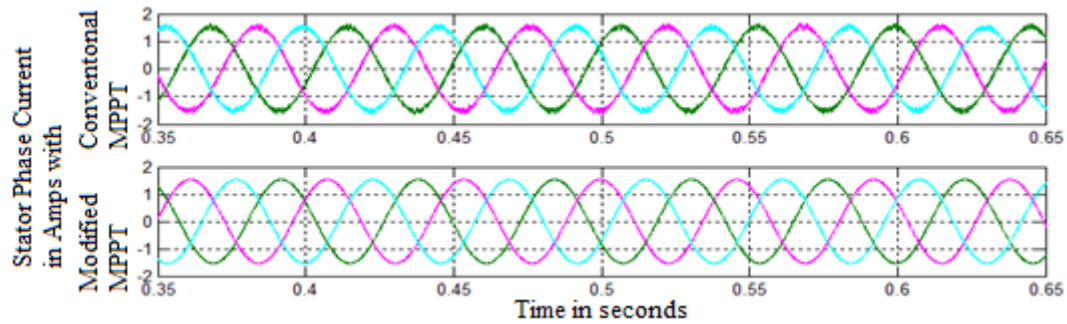
Fig. 4.19 Stator phase current responses with the conventional and modified MPPT controllers at steady state
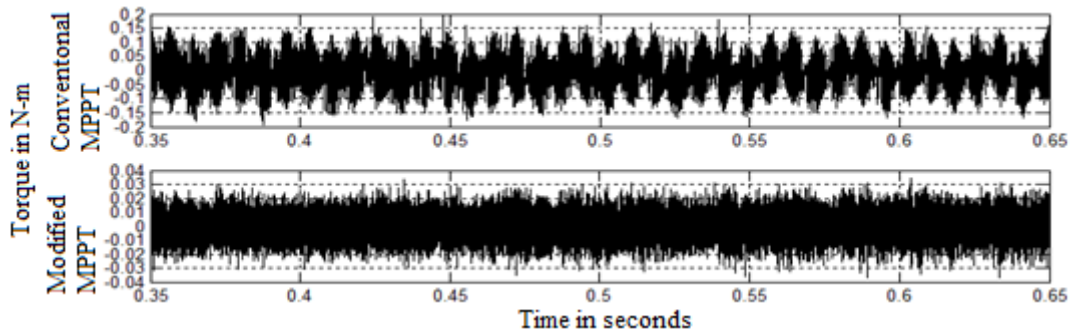
Fig. 4.20 Torque responses with the conventional and modified MPPT controllers at steady state
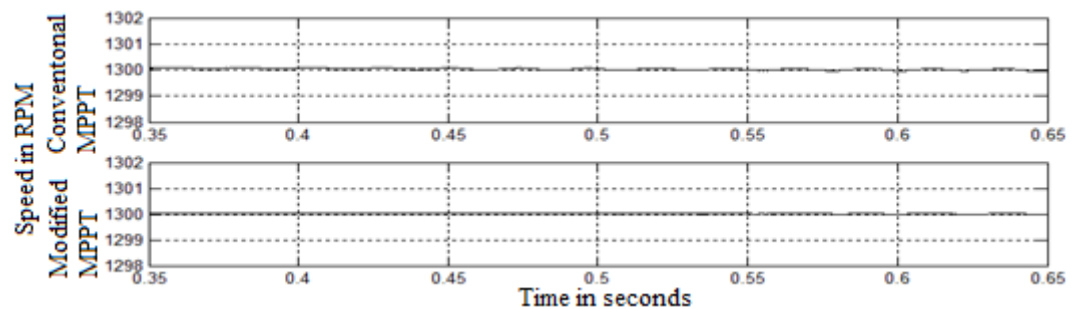
Fig. 4.21 Speed responses with the conventional and modified MPPT controllers at steady state

4.6.4 Responses of an asynchronous motor drive at transients with the step change in load

Responses of the motor drive at the transients during the step change in load torque are analyzed with the load of 8 N-m, which is connected at 0.7 seconds and removed at 0.9 seconds as available in Fig. 4.22-4.24. Ripple contents in the current and torque are reduced by the usage of modified MPPT. Also the speed decrement is

little less with the modified MPPT along with SVM control technique during the load change.
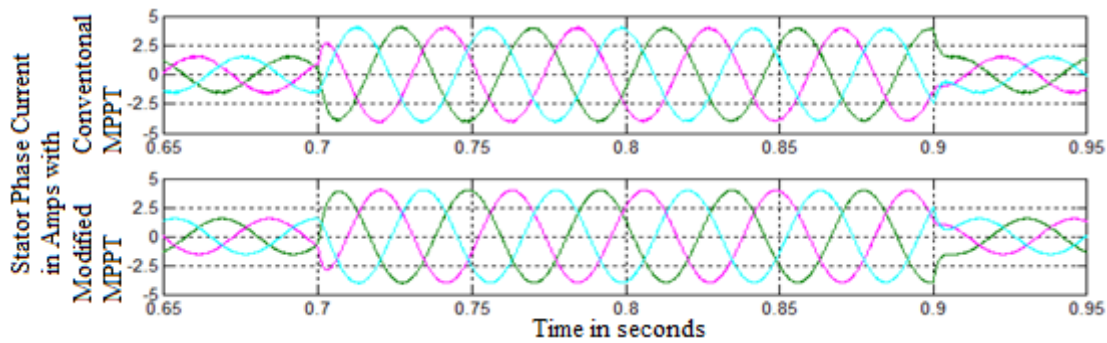
Fig. 4.22 Stator phase current responses with the conventional and modified MPPT controllers at transients with the step change in load
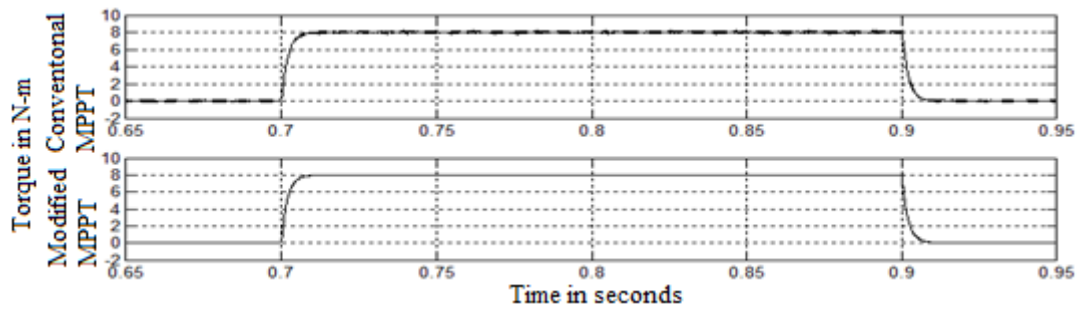
Fig. 4.23 Torque responses with the conventional and modified MPPT controllers at transients with step change in load
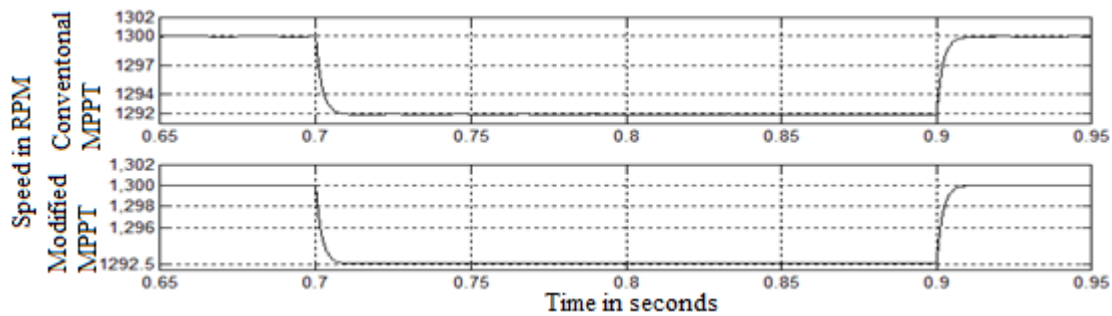
Fig. 4.24 Speed responses with the conventional and modified MPPT controllers at transients with step change in load

4.6.5   Performance of asynchronous motor drive with 5 KHz at transients with speed reversal operation from +1300 to -1300 rpm

The drive performances during speed reversals operation from +1300 to -1300 RPM are illustrated in Fig. 4.25-4.27.

Here, that the motor drive produces the smaller amount of ripple content in phase current and torques respectively and the earlier speed reference value is being reached by the usage of modified MPPT along with SVM control technique during

80

the speed reversal.
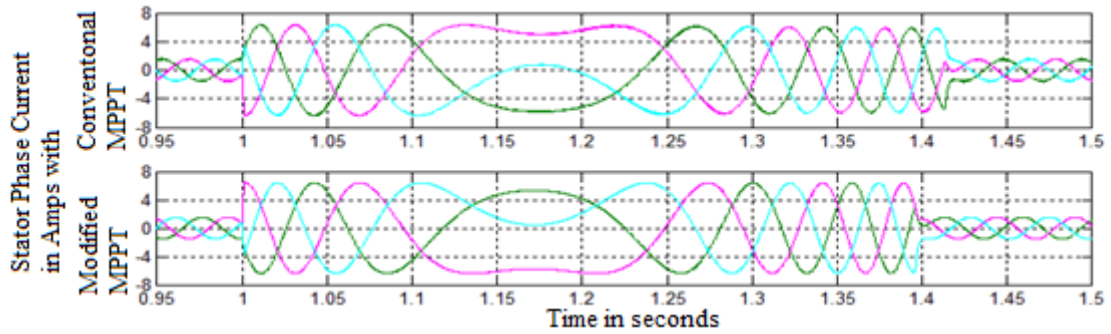
Fig. 4.25 Stator phase current responses with conventional and modified MPPT controllers at transients with speed reversal
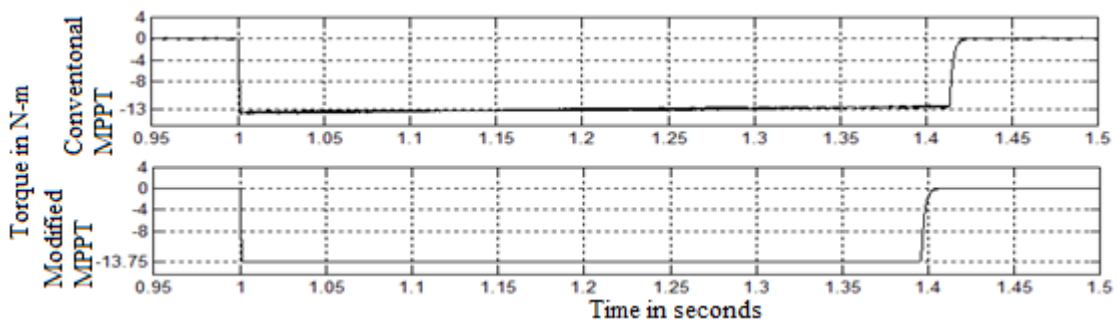
Fig. 4.26 Torque responses with conventional and modified MPPT controllers at transients with speed reversal
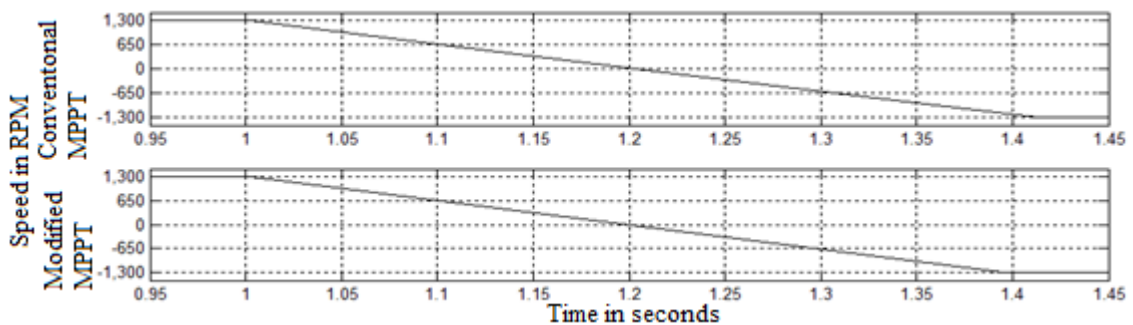
Fig. 4.27 Speed responses with conventional and modified MPPT controllers at transients with speed reversal

4.6.6 Performance of asynchronous motor drive with 5 KHz at transients with speed reversal operation from -1300 to +1300 rpm

The responses of the motor drive at speed reversals from -1300 to +1300 RPM are observed in Fig. 4.28-4.30. The overall parameters behavior of the drive is increased by the usage of modified MPPT controller.

Due to this better speed response is obtained along with attaining of early steady state when compared to other existed methods.
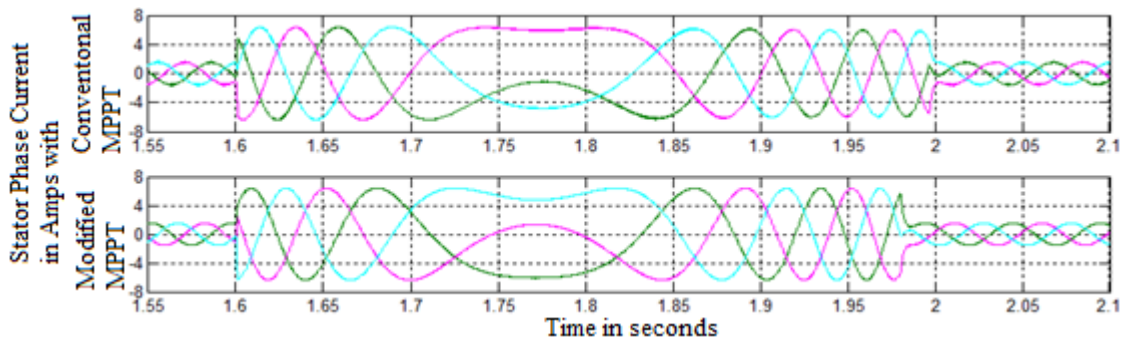
Fig. 4.28 Stator phase current responses with conventional and modified MPPT controllers at transients with speed reversal
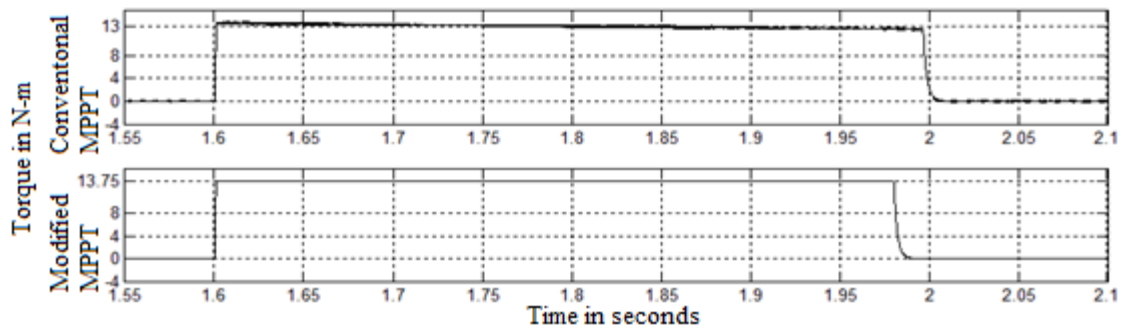
Fig. 4.29 Torque responses with conventional and modified MPPT controllers at transients with speed reversal
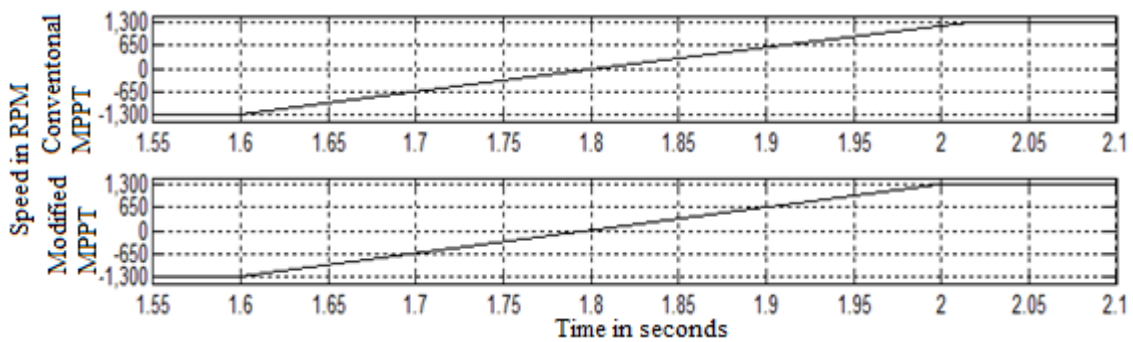
Fig. 4.30 Speed responses with conventional and modified MPPT controllers at transients with speed reversal

4.7 Performance of Asynchronous Motor Drive with the Comparisons of %THD at 5 KHz Switching Frequency

The % THD values of SVM controlled inverter line-line voltages i.e. V_{AB}, V_{BC} and V_{CA} are observed at the switching frequency of 5 KHz.

And these comparisons with the conventional MPPT along with SVM and the modified MPPT along with SVM are tabulated in the Table 4.2.

Table 4.2 Inverter % THD line-line voltage values

Switching frequency	Line-line Voltage Parameters	*Conventional P&O based MPPT along with SVM*	*Modified MPPT along with SVM*
5 kHz	V_{AB}	17.08%	14.23%
	V_{BC}	16.60%	14.36%
	V_{CA}	17.08%	14.23%

4.8 Performance of Asynchronous Motor Drive with the Modified MPPT and SVM

❖ Rating of the motor drive is available in Appendix-C.

❖ The responses of an asynchronous motor drive at steady state and step change in the load torque with 8 N-m are observed.

❖ Stator phase current and torque ripples obtained with conventional and modified methods are tabulated in the Table 4.3 and in the Table 4.4.

Table 4.3 Current and torque ripple contents at starting

Switching frequency	Parameters	*Conventional P&O based MPPT along with SVM*	*Modified MPPT along with SVM*
5 kHz	Current	0.38	0.29
	Torque	0.32	0.26

❖ The ripple content in the current and torque is reduced to nearly 31.03% and 23.07% respectively, with modified MPPT along with the inverter SVM controlling technique with help of modified MPPT.

Table 4.4 Torque ripple contents at steady state

Switching frequency	Parameters	*Conventional P&O based MPPT along with SVM*	*Modified MPPT along with SVM*
5 kHz	Torque	0.35	0.27

❖ It is observed that the torque ripple content with the conventional and modified MPPT are 0.35 and 0.27 respectively, i.e. 29.62% of torque ripple content is reduced during steady state.

❖ Due to this, that the fluctuations in the speed responses are decreased compared to conventional method.

4.9 Conclusion

Space vector modulation (SVM) controlling technique for the two level inverter is developed in simulink and tested with the modified MPPT PV array model at variable irradiance and variable temperature. From this, the performance of the asynchronous motor drive is analyzed by comparing both conventional and modified MPPT controller SVM results. Modified MPPT SVM enhances the system performance with improving the inverter output voltages and by reducing the THD of line voltages. Using modified MPPT SVM the THD of line voltages is reduced about 15-20%.

And also the ripple contents in the torque and stator phase currents are reduced to nearly 31.03% and 23.07% at staring and it is observed that the torque ripple contents with the conventional and modified MPPT are 0.35 and 0.27 respectively, i.e. 29.62% of torque ripple content is reduced during steady state with the modified MPPT. Here, step changes in load torque are performed at 8 N-m between 0.7 and 0.9 seconds. Due to this, early steady state response of the motor drive is also reached along with attaining of better speed response. Thus the utilization of asynchronous motor drive is improved much with the reduction of harmonics (THD) and ripples.

ASYNCHRONOUS MOTOR DRIVE PERFORMANCE WITH ANN BASED MODIFIED MPPT AND SVM TECHNIQUES

5.1 Introduction

Soft computing techniques include the artificial intelligent techniques like artificial neural networks (ANN) and fuzzy logic control techniques. In this chapter artificial neural network based MPPT is implemented to the PV system. Output of PV system is connected to the dc-dc boost converter and the converter output is given to the inverter. Here an artificial neural network based SVM is incorporated as a controlling technique for the inverter. This technique gives better inverter outputs to the asynchronous motor drive with the reducing harmonics and ripples.

It is introduced to overcome the drawbacks of conventional based SVM and to increase the performance of the asynchronous motor drive. So that the better performances of the motor drive are observed with the comparison of conventional based MPPT SVM to the ANN based MPPT SVM at starting state, steady state, transients with step change in load torque and speed reversals operations.

5.2 Artificial Neural Network Architectures

The artificial neural network architecture is termed as the data processing system consisting of a large number of highly interconnected processing elements. It describes about the arrangement of several neurons with their interlink relationship to each other. These arrangements are necessarily structured by indicating the neurons synaptic connections. In general, this network is categorized into three parts, called layers, which are stated as input layer, hidden layer and output layer.

a)   Input layer

This layer is used for the receiving of source information or data, features, signals or measurements from outside.

b)   Hidden layers

These layers are also said to be as intermediate or invisible layers which comprised of neurons to extract the patterns associated with the process or system to be analyzed. Most of the internal processing is being performed with the help of these layers.

c)   Output layer

This layer is used to produce the final output of the network by performing or processing of all previous layers. The neural network architectures are generally categorized as: i). Single layered networks, ii). Multi layered networks, iii). Mesh type networks. In this, research work is carried with the first two types.

5.2.1   Single layered feed forward structures

These networks will have just one input layer and one output layer. These are composed with 'N' inputs and 'M' outputs. In these structures that the information is always flown in single direction (unidirectional) from input layer to output layer. Number outputs are equal to number of neurons in these networks. Generally these networks are used for the attribute (pattern) classification and linear filtering with the help of perceptron or ADALINE structures as illustrated below.
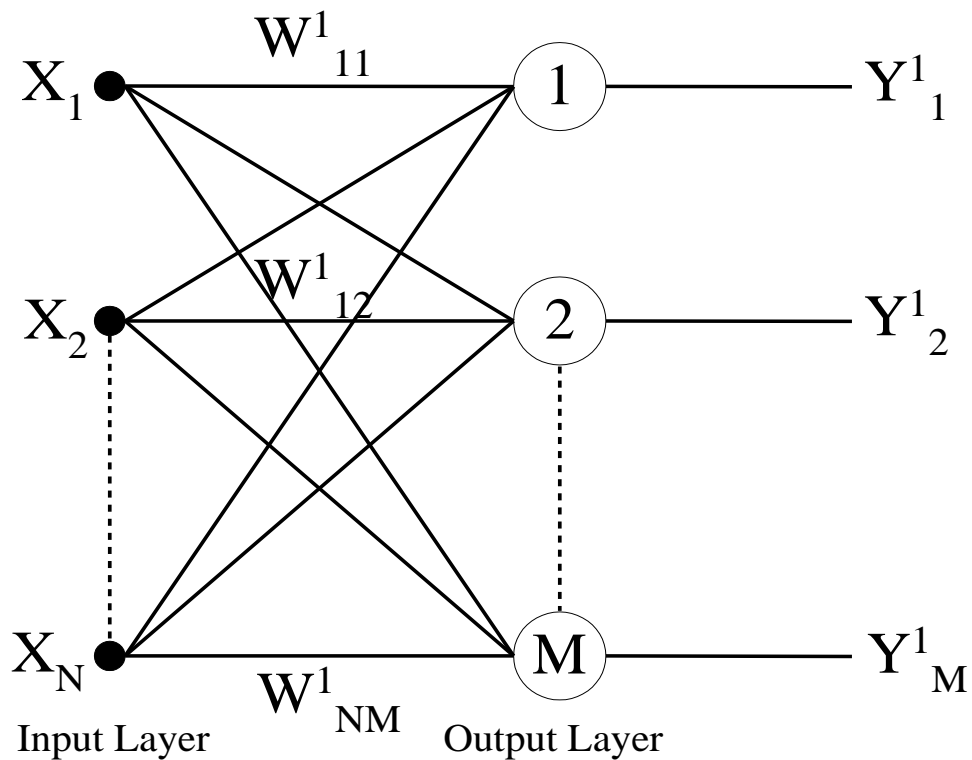
Fig. 5.1 Single layered feed forward neural network

5.3   Multi Layered Neural Network Structures

In this, ANN structure will have many layers. First layer is said to be input layer and the last layer is output layer. The layers in between these two are considered to be the hidden layers. Hidden layer is the place where an appropriate multiplication and weighing of each neuron takes place in order to provide the prescribed output. Multilayered networks categorized as:

- ❖ 1). Intralayered structures: neuron connections are made within the layer
- ❖ 2). Interlayered structures: neuron connections are made with different layers

Similarly organization of the multilayered structures are divided into two types

- ❖ 1). Multilayered feed forward network and
- ❖ 2). Feedback network

5.3.1   Multi layered feed forward network

Feed forward network is the single direction network that feeds the information in only one way i.e. from input to output without any feedback. The input layer neurons take the input pattern information or measurements from the external source. These input patterns are normalized within the limit values to be produced by the activation functions (AF).

These normalized activation functions result in performing the more desirable mathematical operations of the network. Hidden layers are present between to input and output. These are intermediate layers are consisting of neurons that are responsible for extracting the interconnected patterns (attributes) within the process of the system by performing the major process work of the network. Last layers are called as output layers, which produce the output by the sum of all integrated inputs of all the layers.

Here synaptic links are used to carry the information from one neuron to another. Each element of the input vector (X) is connected to each neuron input through the weigh matrix (W). The sum of all integrated inputs with the appropriate weights (W*X) forms the activation function (AF). Then finally it produces the output (Y). Multi layered feed forward neural network is represented in the Fig 5.2.
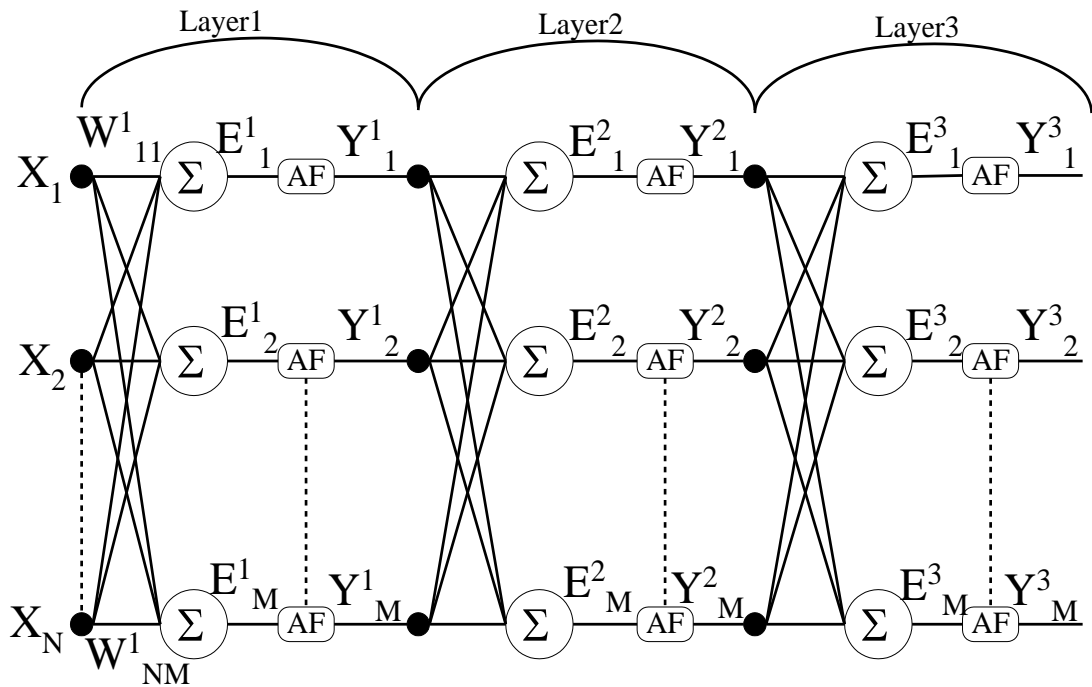
Fig. 5.2 Multilayered feed forward neural network

From above diagram each layer has weight matrix "W_K^L", a weighted input E^L and the output vector Y^L. Where: L is no. of layers. Here weighted sum of all integrated inputs will be given to the last layer i.e. out layer to produce the optimum required output.

Among the networks using multiple layered feed forward structures, the Multilayer Perceptron (MLP) training techniques used in their training process based on the generalized conditions and the competitive statements. It is possible to understand that the amount of neurons present in the first hidden layer, which are usually different from the number of signals consisting with the input layer of the network.

To the fact, the number of hidden layers and their respective neurons depend on their nature and severity of the problems being associated by the network, as well as the total number and property of the available data patterns about the problem. The amount of output signals will always dovetail with the number of neurons from the respective layer.

5.3.2 Multi layered feedback (recurrent) network

In this network a part of output will be taken in the form of feedback and that feedback loop is connected back to the other neurons. Feedback makes network for

dynamic information processing with the provision of additional input data patterns when the required output is not up to the requirement, i.e. it is also used for time variant systems, such as time series prediction, system identification, optimization and process control etc. Among the main feedback networks the Hopfield and the Perceptron networks are preferred with the feedbacks between neurons from distinct layers.

These learning techniques are used in their training process based on energy function minimization and generalized delta rules respectively. These networks with the feedback structures produce the outputs by taking the consideration of the previous output values. Feedback neural network is also said to be recurrent neural network as represented in the Fig.5.3.
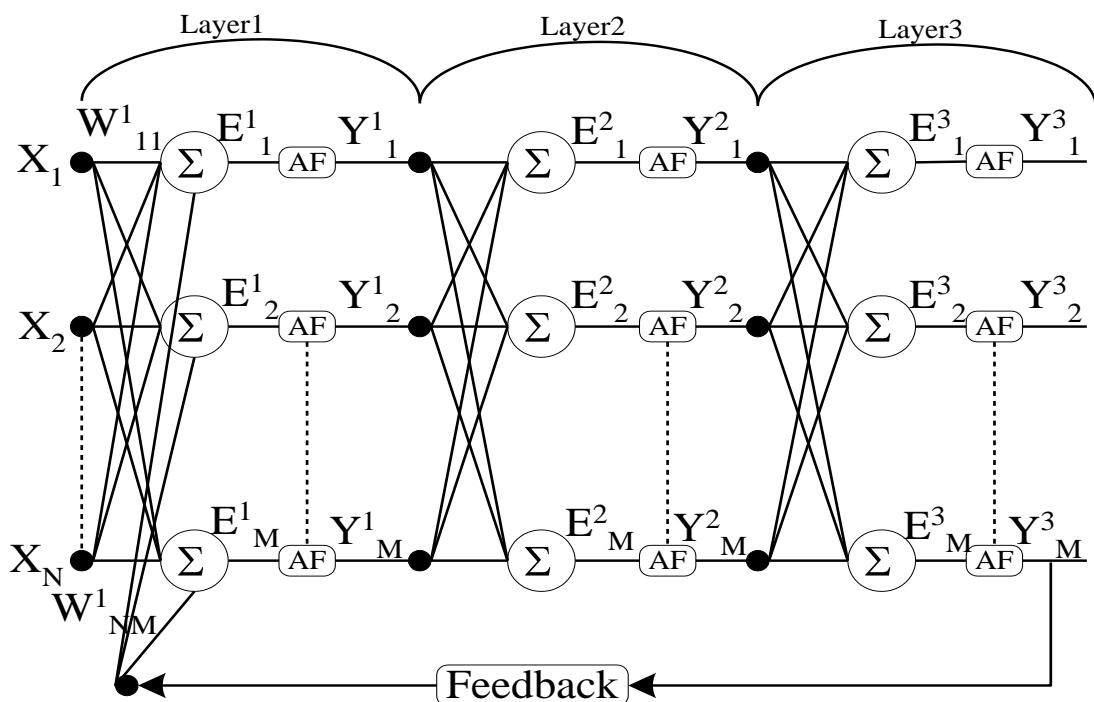
Fig. 5.3 Multilayered feedback neural network

5.4 Training Procedure with Learning Properties of ANN

Major pertinent properties of a network are by their capability of learning from the provided input attributes that represents the performance of the system. After completion of the traing relationship in between the inputs and outputs, network generalizes the desired solutions for the given input patterns. The training process of the network is done by the controlled tuning steps with the synaptic weights and threshold of its neurons to produce the expected outputs. This process of controlled

steps with tuning is called learning algorithm. During its execution process, the network extracts the discriminant features of the system mapping samples to observe the system behavior. During the training, the network completes the presentation of all the samples belonging to the training set, for the purpose to adjust the weights and threshold values called "epochs".

5.4.1 Supervised training

Supervised learning algorithm is the controlling process to get the required output from the given input patterns. It is necessarily needed a table with the generalized amount of neuron patterns with their values which we call as attributes to process the system and its behavior. In case of supervised learning, it totally depends on the given pattern or attribute or table value as if a teacher or a trainer is being trained and controlling the network with the help of a supervisor.

The synaptic weights or threshold values of a system are continuously modified with the help of comparative actions throughout the execution process. If there exists any discrepancy between the obtained outputs and the required outputs, then the algorithm adjusts the weights to the appropriate required value so as to obtain the desired output. It is possible only when the discrepancy is within the acceptable range of the generalized solutions by knowing the desired outputs.

5.4.2 Unsupervised training

In this process of unsupervised learning, the process of execution is done without supervisor or teacher. It not at all contains any knowledge of respective needed required outputs. This technique organizes itself without any existing attributes (patterns) between the neurons to comprise the entire observed data with recognizing the (clusters) or subsets.

The synaptic weights and the threshold values are modified within the algorithm to reflect the attributes (patterns). The network designer specifies the prior required maximum quantities of possible attributes for specifying the task.

5.4.3 Reinforced training

Reinforced training methods are considered with the variant of supervised training. These learning methods are consistently representing the difference between the responses, obtained by the algorithm and the corresponding most required output.

Reinforced learning algorithm modifies the internal neural parameters depending on any qualitative or quantitative information. It is acquired through the direct involvement of the system mapping by using the particular data to undergo the training process.

This training is done based on the trial and error method, depending on whether the existed retaliations for a given input are satisfactory or not. If they are satisfactory, then the synaptic weights and threshold values are gently increased to reinforce (reward) the behavioral of the system. These learning algorithms are based on the random pattern methods which prospectly selects the alternative actions with a limited set of attainable solutions. These solutions are rewarded by the possible prospects to generate the very adequate results.

5.4.4 Back propagation learning technique

This technique is used for the multilayered feed forward networks. In this, training is given by one of the supervised learning called 'Back propagation algorithm,' which uses the real time data patterns to adjust the weights and threshold values so as to minimize the errors in the training set.

If the weights are connected between X_N and X_M then that respective weight pattern between those two different neurons is represented as W_{NM}. Unit in the output layer determines the activity by the following procedures:

❖ Computes the total weight input X_N as following:

$$X_N = \Sigma_M Y_M W_{NM} \tag{5.1}$$

Where: Y_M is the activity level of the Nth unit in the previous layer and

W_{NM} is the weight connections between M^{th} and N^{th} neurons with the sigmoid activation function, the activity function Y_M is calculated as:

$$Y_N = [1 + e^{-X_N}]^{-1} \tag{5.2}$$

If the activities of the all individual units have been done, then, the network computes the error "e" as:

$$error\ (e) = \frac{1}{2}\Sigma_M(Y_M - D_M)^2 \tag{5.3}$$

Where: Y_M is the activity level of the M$^{\text{th}}$ unit in the top layer and D_M is the desired output of M$^{\text{th}}$ unit. Then the back propagation working is observed in further sections

❖ Computes in fast as the error changes from the total input received to a changed output unit. Then the error derivative is the difference between actual and desired activity.

$$eA_M = \frac{de}{dY_N} = Y_N - D_N \tag{5.4}$$

5.5 Artificial Neural Network (ANN) based MPPT Technique

A number of algorithms were developed to track the maximum power point efficiently. Most of the existing MPPT algorithms suffer from the drawbacks of 'slow tracking, wrong tracking and oscillations' during rapidly changing weather conditions with reducing the utilization efficiency. To overcome these drawbacks, an ANN based MPPT Control technique is introduced in this paper as it improves the performance of the system and efficiency with much better than any other conventional methods. In this technique a multi layered neural network is used and a multi layered trained artificial neural network based MPPT is added to estimate the temperature & irradiance levels from the PV array voltage and current signals.

A multi layered feed-back neural networks with back propagation trained network is used to give better performance even under rapidly changing environmental conditions for both steady and transient instants. To reduce the training set usually multi layer is adopted for implementing the MPPT to improve the non-uniform irradiance on the PV modules. As it is independent of time dependency and trade property, MPP can be tracked without time increment through PV characteristics changes. To overcome the problem of nonlinear characteristics of PV array with rapidly changing irradiation and temperature using conventional MPPT to track the maximum power point, an ANN based MPPT is introduced. This method solves the time dependence and trade off as tracking time is very fast compared to conventional incremental conductance and P&O methods even in sudden change of the weather conditions.

The mean square error is introduced to give better performance and accuracy of the network. This multi layered neural network algorithm is also used to estimate

battery power influencing factors like 'light intensity, temperature, battery junction and temperature.' It estimates the temperature and irradiance levels from array voltage and current signals in order to determine the optimum peak operating point, by approximating the maximum power point locus. It is of high speed, low-complexity MPPT technique, which always controls the PV panel output voltage in order to give the good response due to sudden changes of irradiance levels and helps to improve the tracking efficiency. This network is tested for series and parallel connected solar panels to produce the load required power with overcoming the drawbacks of slow, wrong tracking and to operate it at maximum power point and to reduce the oscillations during rapidly changing weather conditions.

With the help of a boost converter and an inverter by incorporating an ANN based SVM controlling technique, the maximum required voltage and power are obtained with fewer oscillations and reduced harmonics. Here back propagation feed forward trained network is introduced to overcome the non-linearities of PV arrays. It minimizes the long term system losses due to which it increases the conversion efficiency even under variable temperature and variable irradiance. Multi layered feed forward neural network based MPPT algorithm flow chart is represented in Fig. 5.4.
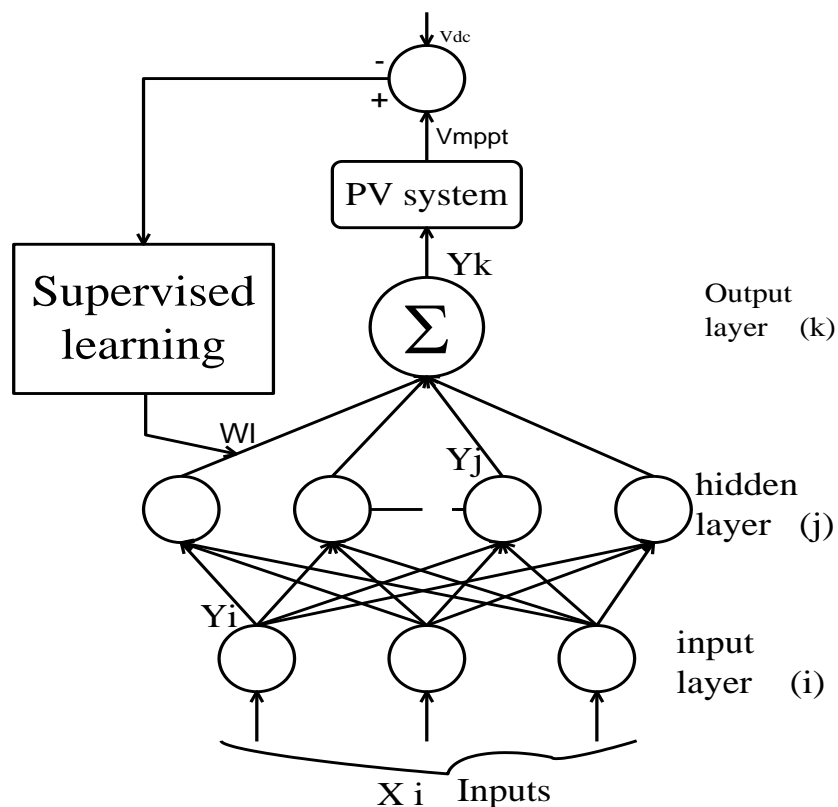
Fig. 5.4 Representation of ANN based MPPT flow chart

93

❖ Multi layered feed-back neural network with back propagation trained network is used to estimate the temperature & irradiance levels from the PV array voltage and current signals.

❖ It gives better performance even under rapidly changing environmental conditions for both steady and transient instants while reducing the training set.

❖ It is independent of time dependency due to which MPP can be tracked without time increment through PV characteristics changes.

❖ Here, a blocking diode is connected in series to a PV string to prevent reverse current flow from load. A bypass diode is also used to improve the power capture.

❖ To evaluate the effectiveness of the training network, the mean square error is used.

5.6 Working and Implementation of ANN based MPPT with Back Propagation Algorithm

Supervised learning is implemented to nullify the error with providing the required multiplication factors to the weights at the hidden layer. This technique gives the better performance even under rapidly changing environmental conditions for both steady and transient instants while reducing the training set. The boost converter and inverter are used to provide maximum output voltage to the load. Here a supervised learning feed forward trained network is introduced to overcome the non-linearities of PV array.

For the implementation of this algorithm, it needs all the required input and output real time data patterns. These required output data patterns are provided with the help of modified perturb and observation algorithm. ANN based MPPT produces the optimum duty cycle in order to get maximum power of the PV system. And that duty cycle is used for switching operation of the DC-DC boost converter switch. Inductance and capacitance parameters of the DC-DC converter produce the maximum required load voltage and current respectively.

For any load voltage discrepancy, inductance values are to be adjusted with proper weights. Similarly for load current discrepancy, capacitance values are

adjusted with proper weighing attributes. This technique has a very good pattern recognition capability. Three layer neural networks can fairly & perfectly estimate any nonlinear function to a random accuracy. Three layer feed forward back propagation ANN is used with an input, hidden and an output layer to produce the optimum duty cycle.

The input layer consists of a two dimensional vector, one is the DC output voltage of PV array and the other is the PV array current, output layer is one dimensional vector consisting of duty cycle. Temperature and irradiance are provided as the input parameters. In the hidden layer all the individual neurons activation functions are trained with the suitable weights. Finally with the help of sum of all the integrated inputs duty cycle output is generated. In order to generate the duty cycle and also to train the network, the modified PV array model, utilizes the all actual PV array data sheet values.

Here 1.5 KW with six SSI-3M6-250W poly-crystalline solar modules are used for the development of matlab-simulation model. The array involves 6 panels with 60 cells each where 10 cells are connected in series and such 6 strings are connected in parallel i.e. 250*6=1500 watts. ANN acquires the maximum power by sensing temperature and irradiance of the array. And ANN is trained to predict and also to acquire the required voltage and current values.

So for every instant comparison of power with the present iteration power to the previous iteration power is calculated to find the power difference. The iteration process goes on continued till the power difference is available and stops at the zero power difference state. ANN based MPPT produces the duty cycle as the output and that output duty cycle is given to the DC-DC boost converter.

5.6.1 Training procedure of ANN

For training of ANN set of samples are required with appropriate network behavior inputs and target outputs. Training of neural network includes the modification of the weights and biases of the network to enhance network performance.

Throughout the training execution process, the connection weights are modified until the best requirement is obtained for the provided input–output patterns based on

the minimum errors. In order to minimize the error for the multilayered feed forward networks, mean square error (MSE) is introduced which provides the fastness for the execution of the network along with reduction of errors. It is measured with the average squared difference between the desired and obtained outputs as denoted below:

$$F = MSE = \frac{1}{N}\sum_{M=1}^{N}(e_M)^2 \tag{5.5}$$

Here: 'e' is the error

$$\frac{1}{N} = \sum_{M=1}^{N}(Y_M - D_M)^2 \tag{5.6}$$

Where:

Y_M is the obtained output and

D_M is the desired output.

5.7 Performance of ANN based MPPT with its Obtained Output Curves

Performance of ANN based MPPT is observed by its voltage-current and voltage-power characteristic curves at two operating conditions as:

- ❖ 1). With variable irradiance at constant temperature and
- ❖ 2). With variable temperature at constant irradiance.

5.7.1 Performance of ANN based MPPT with variable irradiance at constant temperature

When the irradiance varies from 100, 250, 500, 800 and 1000 W/m^2 it is observed that the PV current and voltage will get increased with the irradiance levels. Due to this net PV array power also gets increased till the irradiance rise and voltage, current and power values get decreased as the irradiance falls.

So here voltage and current are directly proportional to the irradiance. If the voltage and current values are increased then power value automatically gets increases. The characteristic curves of PV module and array are presented in Fig. 5.5-5.6.
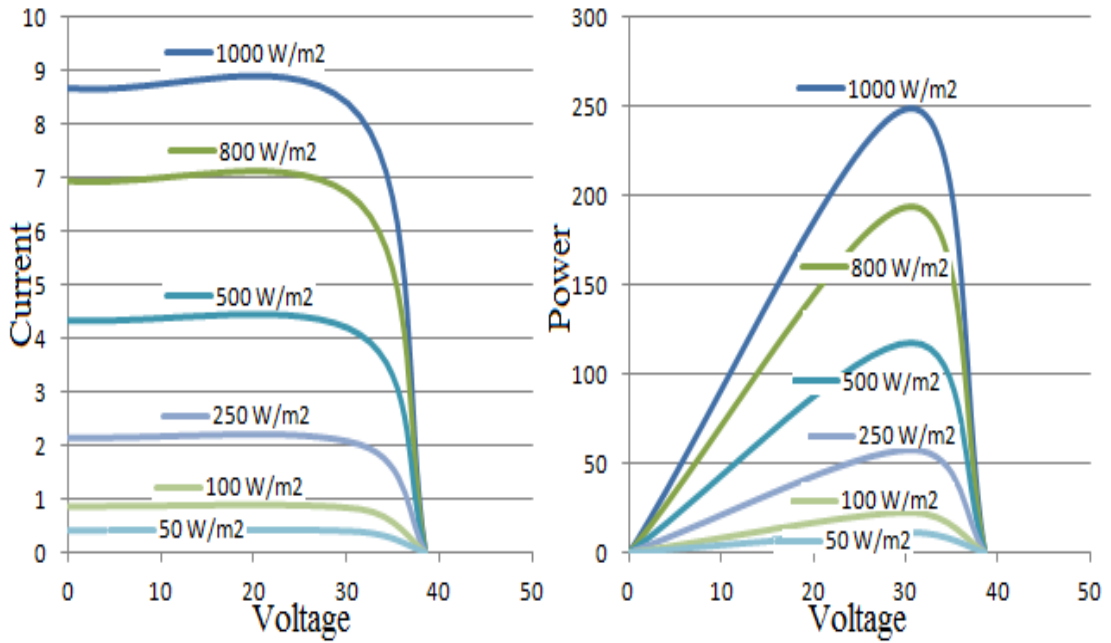
Fig. 5.5 Module characteristic curves at variable irradiance and constant temperature
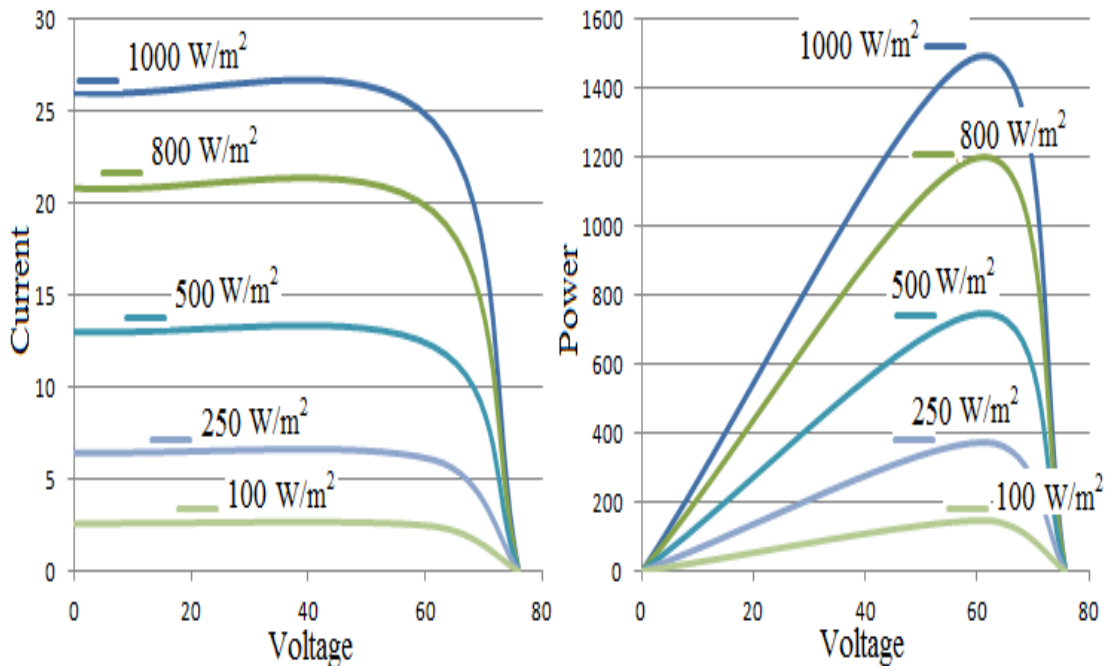
Fig. 5.6 Array characteristic curves at variable irradiance and constant temperature

5.7.2 Performance of ANN based MPPT with variable temperature at constant irradiance

When the temperature varies from 20° C, 30° C, 40° C, 50° C and 60° C, it increases the PV current marginally with drastically decrease in PV array voltage. Due to this, net PV array output power reduces. Array current is directly proportional to the temperature and voltage is inversely proportional to the temperature. These characteristics are observed in Fig. 5.7.
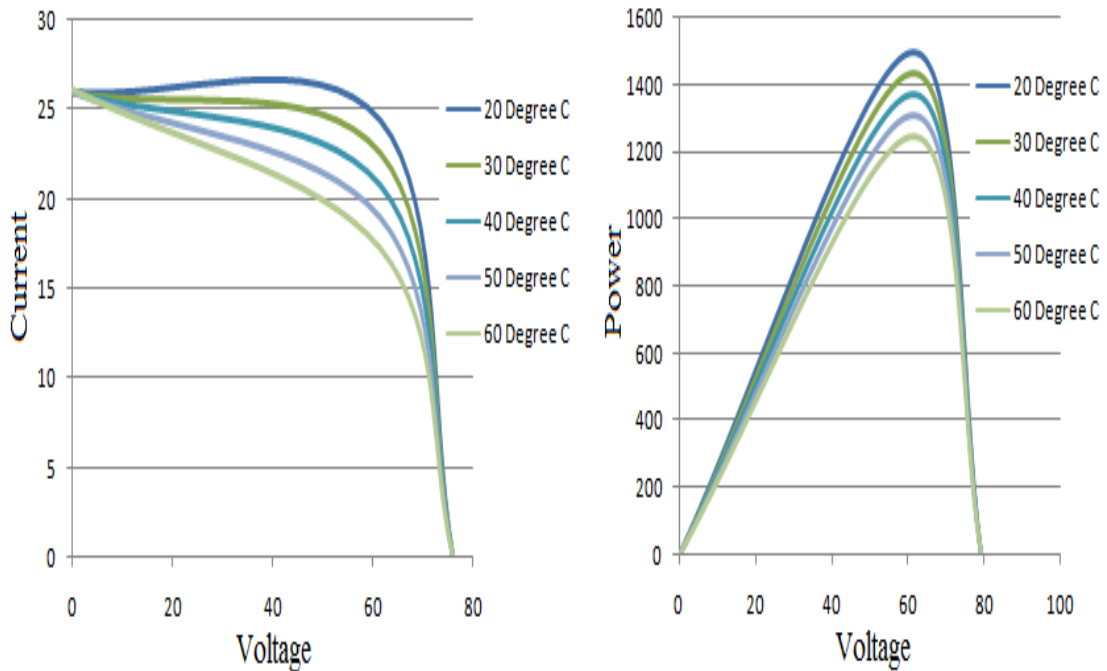
Fig. 5.7 Array characteristic curves at variable temperature and constant irradiance

5.8 Artificial Neural Network based MPPT with SVM

MPPT output will be given to the DC-DC converter to boost up the PV output and that boosted output will be given to the inverter. With the help of space vector modulation (SVM) as a controlling technique for the inverter, it converts the DC quantity to AC quantity and that AC will be fed to the asynchronous motor drive. In case of conventional SVM, inverter produces the output with some oscillations and harmonics. To overcome those drawbacks, ANN based MPPT with SVM has been introduced in this chapter.

5.8.1 Drawbacks of conventional MPPTs with SVM

❖ Approximation of non-linear function in SVM as a linear function leads to harmonics.

❖ The use of a look-up table and interpolation limits the maximum switching frequency of the inverter.

❖ ANN based method is used for training the individual layers of the network to overcome the complexity of the network.

❖ Requires complex online computation while executing the network with the given data patterns.

❖ To overcome this, soft computing technique methods like ANN and ANFIS based MPPTs with SVM are used.

5.8.2 Working and implementation of ANN based MPPT with SVM

ANN based MPPT with SVM is discussed in the present chapter and ANFIS based MPPT with SVM is going to be discussed in the next chapter. SVM with ANN MPPT is used for two level inverter. It uses hyperbolic tan (tan sigmoid) activation function for hidden layers. It is linear, for which the minimum error is obtained with the linear approximation in the output layer. Input to this network is V_{ref} with angle θ to generate the duty ratios as an output, and also to generate the pulses. Those duty ratios are compared with the repetitive counter which is generated by the required sampling frequency.

The obtained values are then processed in the relay circuit to generate the switching pulses for the SVM controlled inverter. For training of the network back propagation algorithm is used in matlab-simulink neural network toolbox. The training is used for 73121 epochs with the mean square error value of 0.0002. To overcome the disadvantage of repeated training, ANN MPPT with SVM is implemented to train and build the network with the independent of switching frequency. The switching operation from this ANN based SVM is characterized into eight switching states $S_I = (S_A, S_B, S_C)$ as discussed in the previous chapter.

Here I= 0, 1,……7 and S_A, S_B, S_C are states of an inverter in A, B and C legs of a three phase respectively. When switch one is ON then switch 4 is OFF and vice-versa. Similarly for switches 2 & 5 and for switches 3 & 6 respectively. Output voltage of the inverter is being controlled by these eight switching states. The main purpose of this ANN based SVM is approximate the reference voltage vector "V_{ref}" using these eight switching patterns as explained clearly in the previous chapter. The eight vectors from the voltage vector space is divided into six sectors as explained in chapter 4.

Output of the inverter is given by the proper sequence switching of six switches in the inverter with the controlling of ANN method with SVM by the switching pulses (S_A, S_B and S_C) of the inverter. This phenomenon is based on the generation of three consecutive switching voltage vectors with the sampling time period T_S. So that the average output voltage produced tries to match with the inverter reference voltage. The performance of this SVM is characterized mainly by the modulation index, switching frequency and harmonic distortion. The modulation index is the ratio of

reference voltage vector to the voltage produced by the inverter six switching voltage vectors. ANN MPPT with SVM is implemented majorly for the following factors:

- ❖ To produce the modulation index and reference angle"θ";
- ❖ To calculate the switching time periods T_1, T_2, T_S, T_0;
- ❖ To determine the cycle and switching time periods for all the switches of the inverter and;
- ❖ To generate the required output voltages of the inverter.

Steps for the implementation of feed forward back propagation algorithm with space vector modulation technique are described by a flow chart illustrated in Fig. 5.8. ANN MPPT along with SVM is used for training the individual layers of the network to overcome the complexity of the network, i.e. the algorithm is suitable for a very simple practical implementation, and can gain almost linear characteristic, and also avoids the look up table. The number of layers, number of neurons in the hidden layer and the activation functions are to be chosen for the network topology.

The input/output real time data patterns are provided by the modified MPPT matlab-simulation results. The network is initialized with positive and negative weights to avoid the saturation, before the training of the network by provision of output data patterns to compares with the desired pattern. Required weights are modified to get the very minimum acceptable error between the calculated values to a desired value. Training and execution process will get continued for all the neuron patterns so that the error matching is obtained from all the patterns.

During this condition the network is to be trained satisfactorily with all the required attributes (patterns) in order to get required output patterns. If the error is unable to be converted to a small acceptable value then, the numbers of neurons in the hidden layers are modified with the appropriate weights, and sometimes if required the additional neurons or additional hidden layers are added to the network. Instead of single patterned single neuron training at a particular time, group (batch) training can be done. Where all the patterns are presented simultaneously and final weight updates are made after processing all the patterns with the required weight modifications.

The weight adjustment for the reduction of error (i.e. a cost function is given by the squared error) is done by the gradient descent technique where the weights are

iterated one at a time starting backward from the output layer. A backward trip for such calculations is known as a reverse pass. Round trip calculations, consisting of a pair of a forward pass and reverse pass called an epoch. If the neural network is trained with the "M" input patterns then squared output error from the all output layer neurons of the network is given by:

$$e_M = (D^M - Y^M)^2 = \sum_{N=1}^{Z}(D_N^M - Y_N^M)^2 \tag{5.7}$$

Here: D_N^M is the desired output of the N^{TH} neuron in the output layer

Y_N^M is the corresponding actual obtained output

Z is the dimension of the output vector

D^M is the "M" pattern desired output and

Y^M is the "M" pattern actual obtained output.

The sum of the squared errors for the set of 'M' patterns can be expressed as:

$$SSE = e = \sum_{M=1}^{X} e_M = \sum_{M=1}^{X}\sum_{N=1}^{Z}(D_N^M - Y_N^M)^2 \tag{5.8}$$

If the weights of the neurons are altered to minimize the value of the objective function SSE by the gradient descent method then the weight update equation can be given as:

$$W_{MN}(K+1) = W_{MN}(K) - (\frac{\delta e_M}{\delta W_{MN}(K)} \tag{5.9}$$

Where: is the learning rate,

$W_{MN}(K+1)$ is new weight between M and N^{th} neuron and

$W_{MN}(K)$ is the corresponding old weight.

5.9 Simulation Responses of an Asynchronous Motor Drive with ANN based MPPT and SVM

Simulation results are obtained with the reference speed of 1400 RPM at starting and steady state operating conditions. And 1200 RPM is set as a reference speed for the transients with step change in load torque and speed reversal operating conditions to analyze the performance of asynchronous motor drive in reducing the ripple contents of the stator phase current and torques. Inverter from the boost converter output, feeds the motor drive with 400 V supply at the switching frequency

of 5 KHz by incorporating the ANN method with SVM as a controlling technique. These all responses of the motor drive with the conventional and ANN based MPPT along with SVM are observed in Fig. 5.8-5.21.

5.9.1 Performance of an asynchronous motor drive at starting

For the asynchronous motor drive the maximum current and the ripple content in the torque is reduced during starting in order to reach the early steady state. With the ANN based MPPT and SVM the maximum torque, stator phase current and speed are obtained as 12.28 N-m, 7.596 Amps and 1400 RPM respectively. It is observed that the ripple content in the torque is 0.49 with the reduction compared to the other existed method as 0.54. Due to this better speed response is obtained. These results are available in Fig. 5.8-5.10.
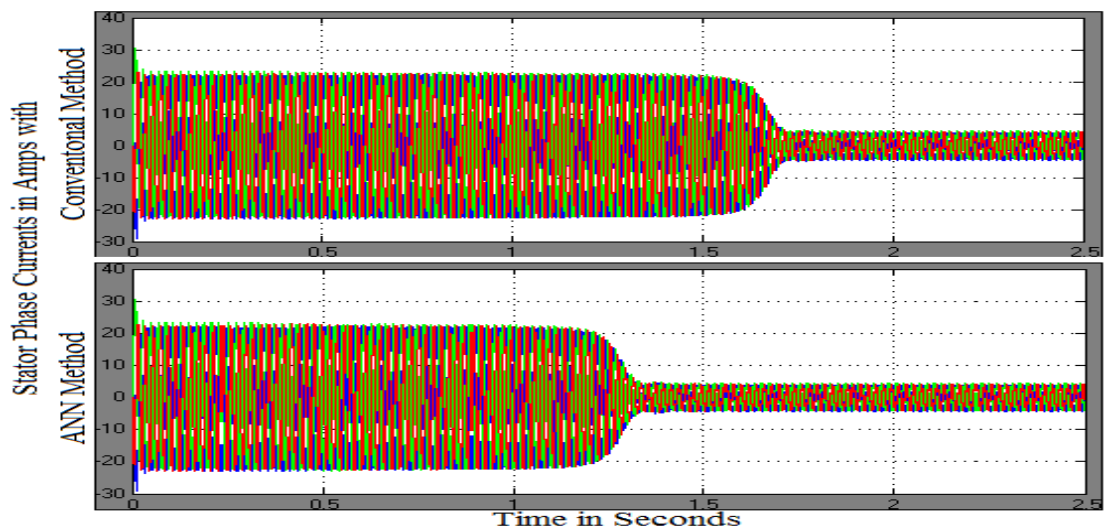
Fig. 5.8 Stator phase current responses with conventional and ANN based MPPT with SVM at starting
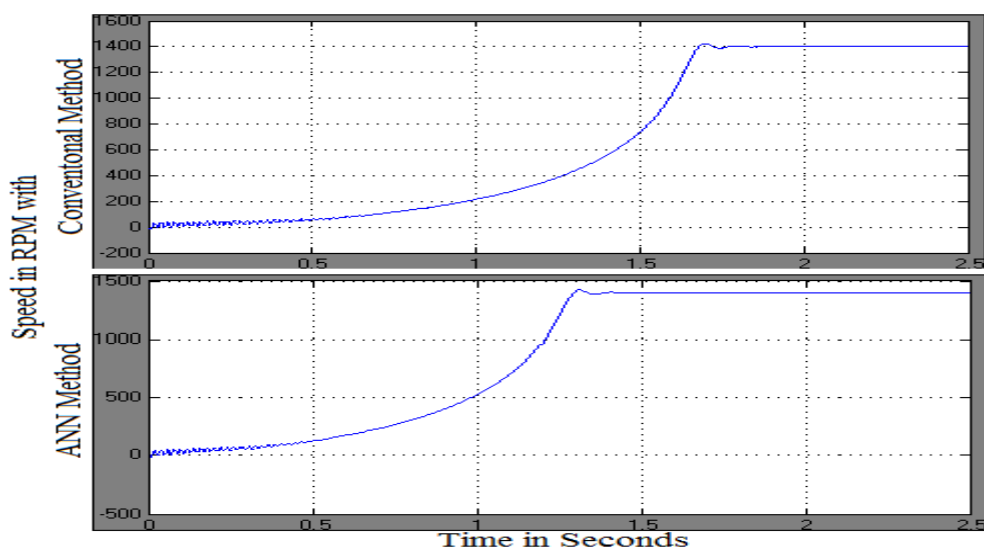
Fig. 5.9 Speed responses with conventional and ANN based MPPT with SVM at starting
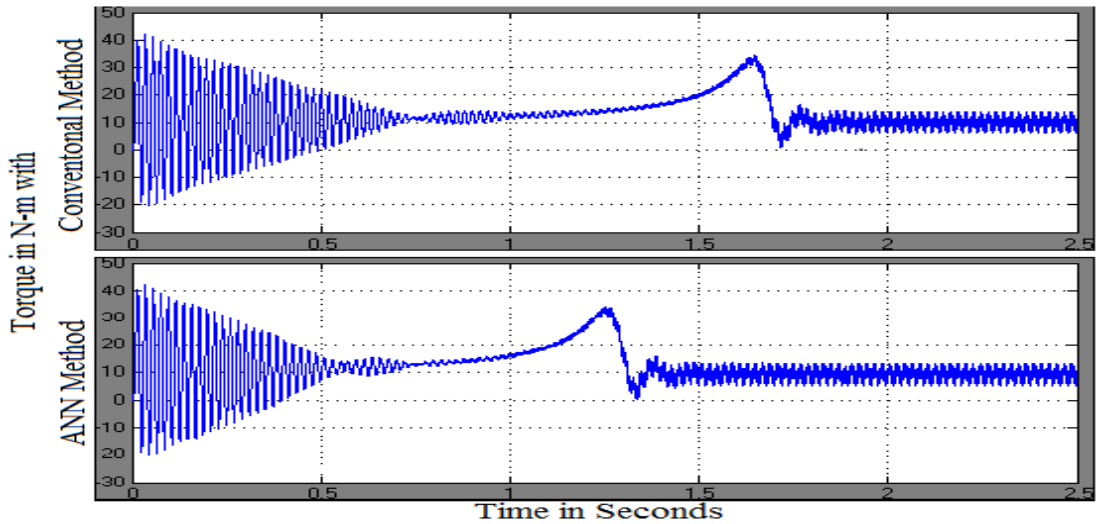
Fig. 5.10 Torque responses with conventional and ANN based MPPT with SVM at starting

5.9.2 Performance of an asynchronous motor drive at steady state condition

The steady state responses of the stator phase currents, torque and speed with conventional and modified ANN based MPPT along with SVM are observed in Fig. 5.11-5.12. Here torque ripple with the modified ANN based MPPT is reduced a lot i.e. it is observed that the current and torque ripples with the conventional based SVM are 0.34 and 0.32 respectively. Similarly with ANN method are 0.25 and 0.23 respectively, i.e. the ripple content in current is reduced to 36% and the torque is reduced to 39.13%. Due to this better speed response is obtained with the ANN based MPPT controller along with SVM.
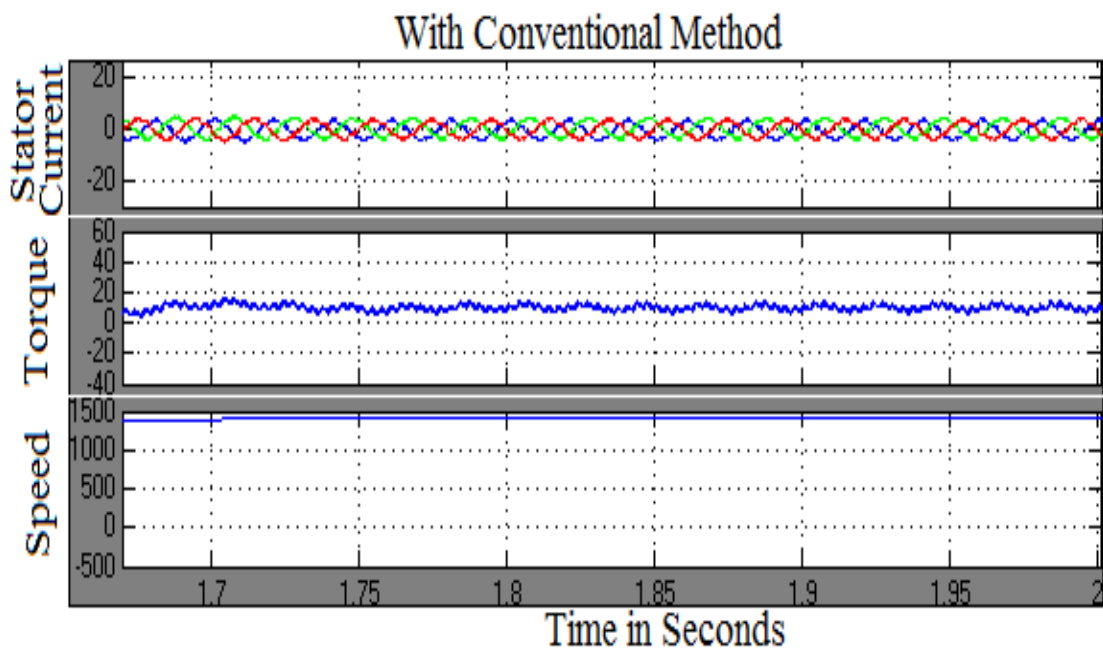
Fig 5.11 Stator phase current, torque and speed responses with the conventional based MPPT and SVM at steady state

103
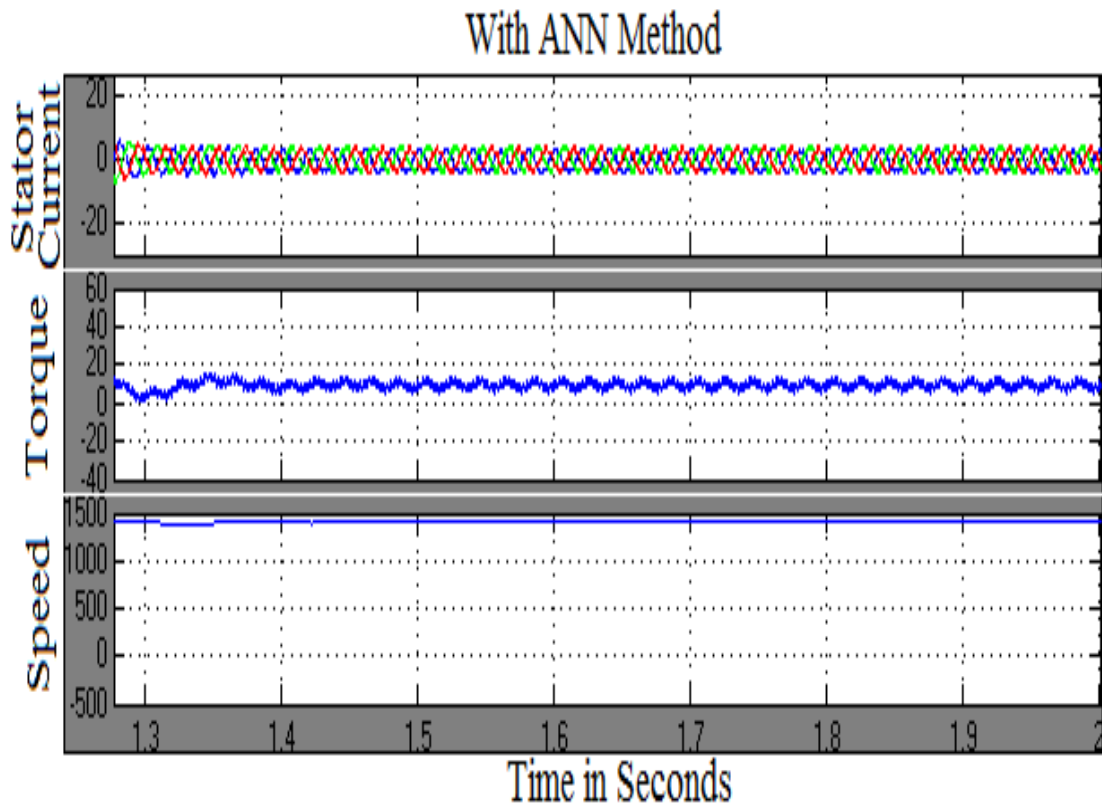
Fig 5.12 Phase current, torque and speed responses with ANN based MPPT and SVM at steady state

5.9.3 Performance of asynchronous motor drive at transients with step change in load

The ripple contents in current and torque are reduced with the ANN based MPPT and SVM. Also the speed decrement is little less with the ANN based MPPT during the transients with step change in load torque. For the responses during the transients with step change in load torque with 8 N-m is applied at 0.6 sec and removed at 0.8 sec and those respective results are shown in Fig. 5.13-5.15.
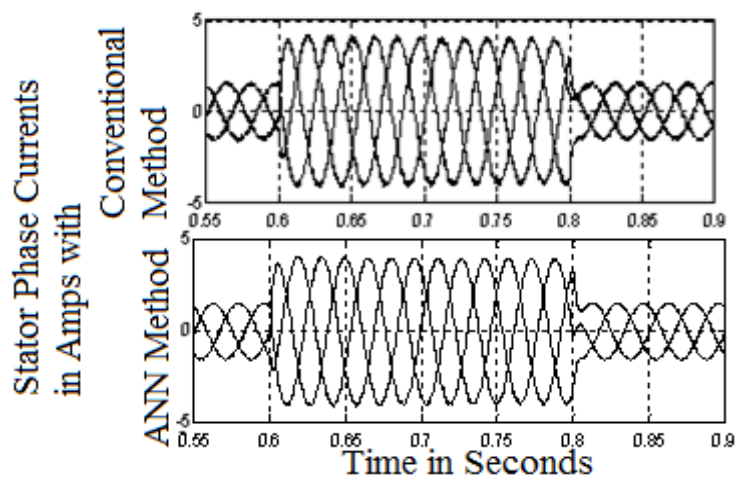
Fig. 5.13 Stator phase current responses with conventional and ANN based MPPT and SVM at

transients with step change in load
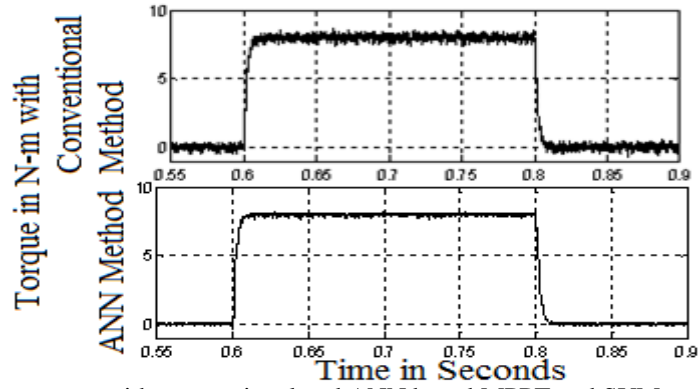
Fig. 5.14 Torque responses with conventional and ANN based MPPT and SVM at transients with step change in load
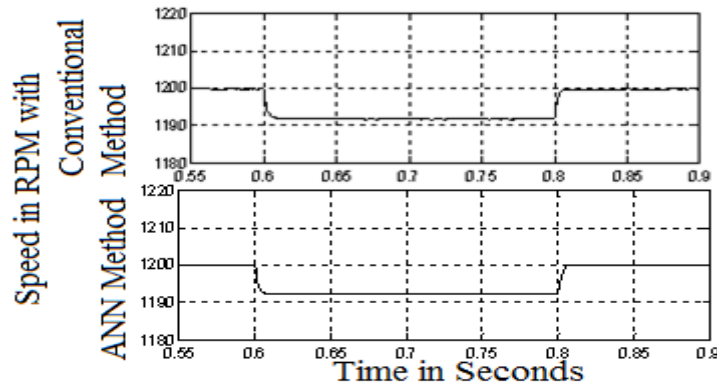
Fig. 5.15 Speed responses with conventional and ANN based MPPT and SVM at transients with step change in load

5.9.4 Performance of asynchronous motor drive at transients with speed reversal operation from +1200 to -1200 rpm

The overall performance of the drive is improved with the ANN based MPPT along with SVM controller. And the speed response reaches the reference value earlier compared to other existed methods. The results of the drive during speed reversals from +1200 to -1200 RPM are depicted in Fig. 5.16-5.18.
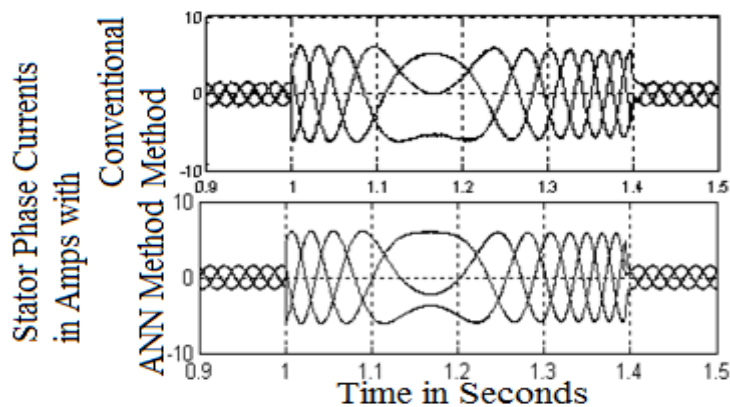
Fig. 5.16 Stator phase current responses with conventional and ANN based MPPT and SVM at transients with speed reversal

105
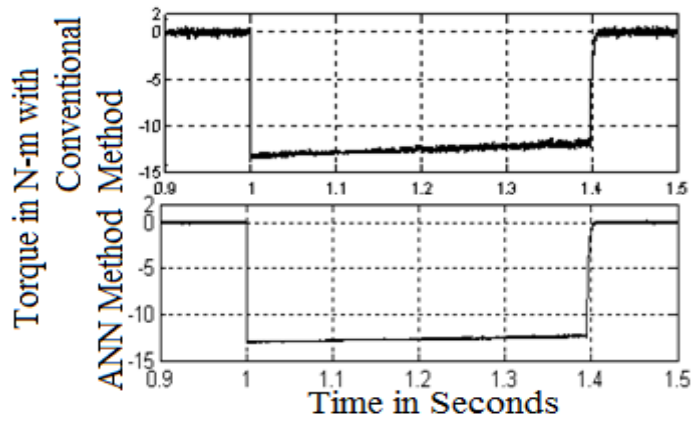
Fig. 5.17 Torque responses with conventional and ANN MPPT SVM at transients with speed reversal
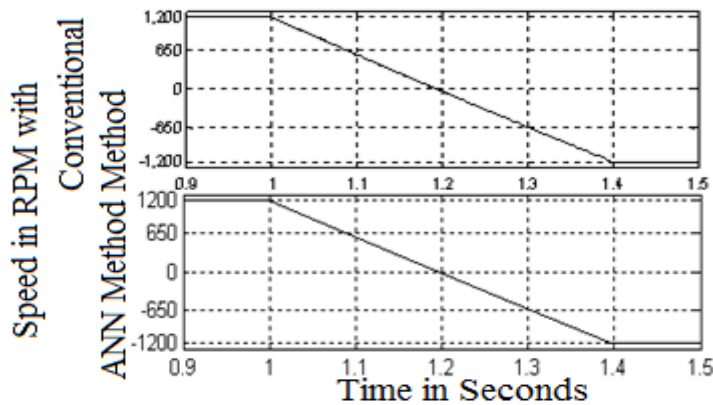
Fig. 5.18 Speed responses with conventional and ANN MPPT and SVM at transients with speed reversal

5.9.5 Performance of asynchronous motor drive at transients with speed reversal operation from -1200 to +1200 rpm

The overall performance of the drive is improved with the modified ANN based MPPT controller along with SVM controlling technique, the speed response reaches the little earlier compared to conventional methods. The results of the drive during speed reversals from -1200 to +1200 RPM are presented in Fig. 5.19-5.21.
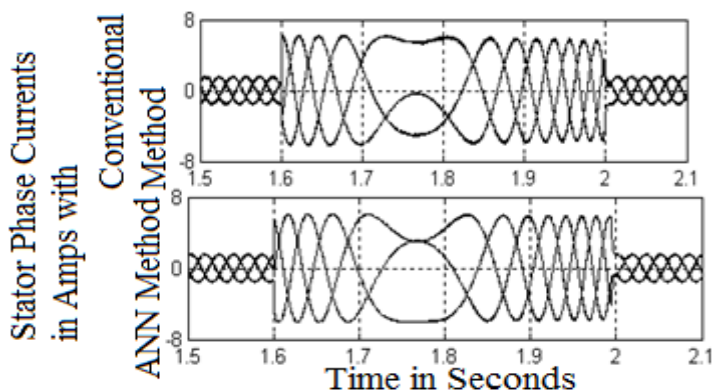
Fig. 5.19 Stator phase current responses with conventional and ANN based MPPT and SVM at transients with speed reversal

106
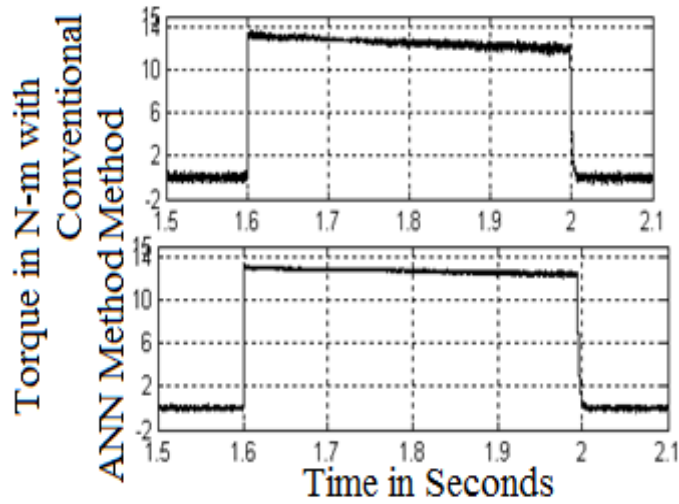
Fig. 5.20 Torque responses with conventional and ANN based MPPT SVM at transients with speed reversal
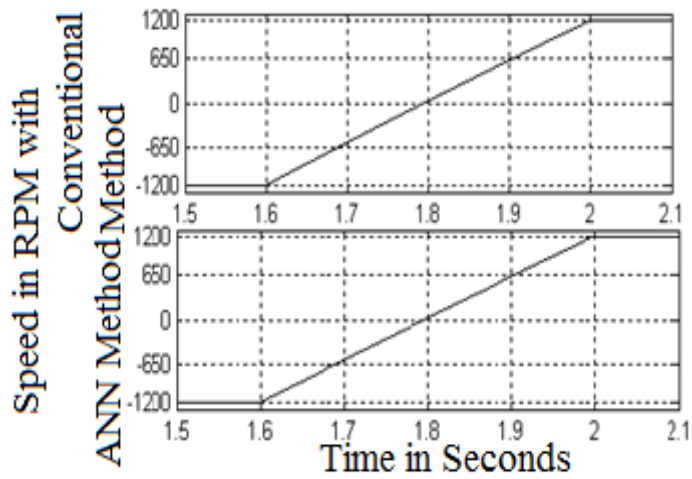
Fig. 5.21 Speed responses with conventional and ANN based MPPT SVM at transients with speed reversal

5.10 Performance of an Asynchronous Motor Drive with the Comparison of Ripple Content

❖ The ripple content in the current and torque is more with P&O based SVM method compared to artificial neural network MPPT with SVM method as tabulated in the Table 5.1.

Table 5.1 Current and torque ripple contents

Switching frequency	Parameters	Conventional P&O based MPPT along with SVM	ANN based MPPT along with SVM
5 kHz	Current	0.34	0.25
	Torque	0.32	0.23

❖ The ripple content in the current and torque is reduced to 36% and 39.13% with the ANN based MPPT along with SVM method compared to Conventional P&O based MPPT along with SVM.

❖ Due to this, oscillations in the speed response get decreased compared to conventional method.

❖ Early steady state response is also obtained with the ANN MPPT and SVM compared to the conventional MPPTs along with SVM.

5.11 Conclusion

The PV array model with the artificial neural network (ANN) based MPPT controller is tested by the ANN based SVM controlling technique. From this, the performance of the asynchronous motor drive is improved much with reducing of current and torque ripples at steady and transients with step change in load torque, i.e. current and torque ripples at steady state with the conventional based SVM are observed 0.34 and 0.25 respectively.

Similarly, with ANN based MPPT and SVM are as 0.32 and 0.23 respectively, i.e. current ripple is reduced to 36% and torque ripple is reduced to 39.13%. Due to this, oscillations of the motor drive also get reduced, which meanwhile makes the motor drive to get the better speed response along with attaining of early steady state response. Thus performance of the motor drive is improved even in the abnormal weather conditions with the ANN based MPPT along with SVM controlling technique. Thus the utilization and efficiency of the system is also improved much with an ANN based MPPT controller along with SVM technique, compared to the conventional methods.

ADAPTIVE NEURO FUZZY INFERENCE SYSTEM (ANFIS) BASED MPPT WITH SVM

6.1 Introduction

Another soft computing technique in addition to ANN based MPPT is Adaptive Neuro Fuzzy Inference System (ANFIS) based MPPT. ANFIS based MPPT extracts the maximum power even at abnormal weather conditions with very fast accurateness. Compared to conventional MPPT, ANFIS based MPPT increases the tracking efficiency of PV system with greater than 98%. ANFIS based MPPT is used to generate the optimum duty cycle for switching device of DC-DC boost converter.

It is a five layered network consisting of input, hidden and output layers with number of neurons for proper training of the network. Training for each neuron is done by adding of appropriate weights in order to produce required duty cycle. Boost converter boosts up the array output voltage by the optimum duty cycle which is obtained from the ANFIS based MPPT, and it feeds boosted output to the inverter. Inverter converts that boosted DC quantity to a pulsating AC quantity with the help of an ANFIS based space vector modulation (SVM) controlling technique of the inverter.

This technique gives better inverter output voltages to the asynchronous motor drive with the minimized harmonics and reduced ripples. It is introduced to overcome the drawbacks of conventional based SVM in order to increase the performance of the asynchronous motor drive. Due to these, minimized harmonics and reduced ripple contents, an enhanced performance of an asynchronous motor drive is observed during starting, steady state, transients with step change in load torque and speed reversals operations.

6.2 ANFIS based MPPT

ANFIS based maximum power point tracking (MPPT) is a technique, that extracts the maximum possible power from one or more photovoltaic devices, typically solar panels. The purpose of the MPPT system is to sample the output of the

solar cells and apply the proper resistance (load) to obtain maximum power for any given environmental conditions.

MPPT devices are typically integrated into an electric power converter system that provides voltage or current conversion, filtering and regulation for driving various loads, including inverters and batteries or motors drives. It extracts maximum capable power from PV modules or arrays for the available temperature and solar insolation by the MPPT controller.

The appearance of multi peak output curves of partial shading in PV arrays is common, where the development of an algorithm for accurately tracking the true MPPs of the complex and non-linear output curves is crucial. A typical solar panel converts only 30-40 percent of the incident solar irradiation into electrical energy. Maximum power point tracking is used to increase the efficiency of the panel. The major requirement to get the maximum power is that the source resistance should be equal to that of the load resistance.

In the source side, a boost converter is connected to a solar panel in order to enhance the output voltage so that to use for different applications like motor loads by changing the duty cycle of the boost converter. Most of the existing MPPT algorithms suffer from the drawbacks of slow tracking, wrong tracking and oscillations during rapidly changing weather conditions, due to which, the utilization efficiency is getting decreased.

To overcome these, an ANFIS based MPPT control technique is introduced in this chapter. Here, it improves the performance of PV system and increases the tracking efficiency much better than any other conventional methods. The boost converter and the inverter are used to provide maximum output voltage to the load requirements. Adaptive neuro fuzzy inference system based MPPT techniques with their structure and Matlab code representation are analyzed and that are illustrated in Fig. 6.1.
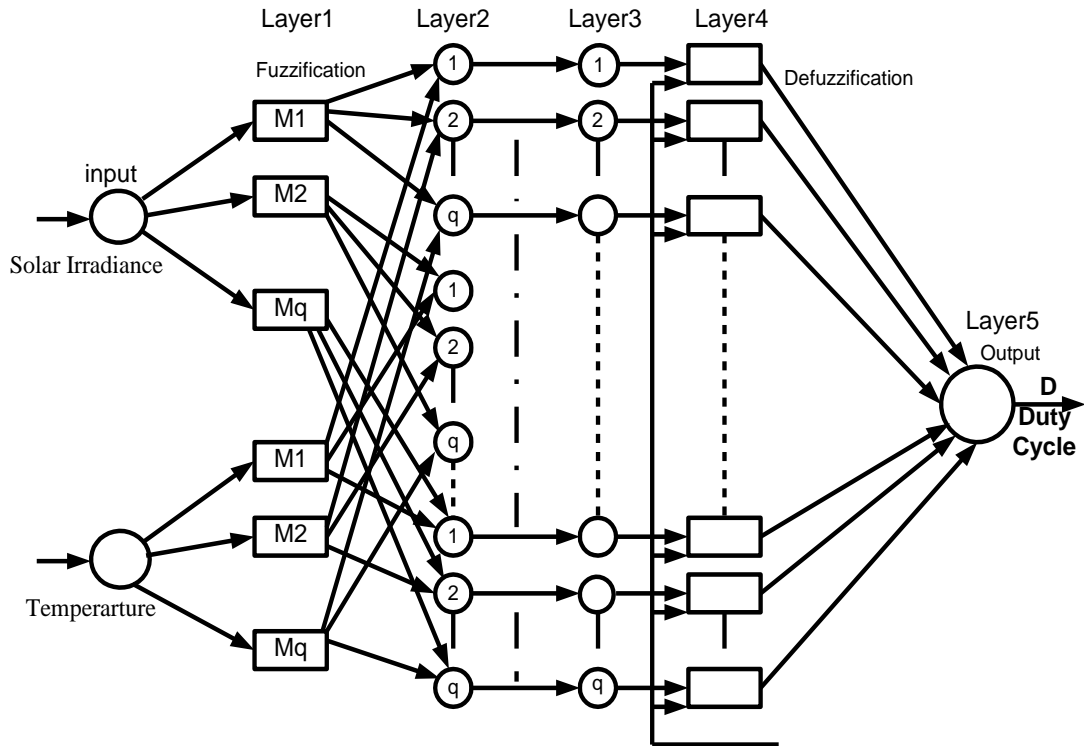
Fig. 6.1 ANFIS based MPPT structure

Solar voltage and current with respect to temperature and irradiance are taken as input training data patterns for ANFIS based MPPT. It gives the optimum required outputs from the solar PV array with respect to the provided input pattern values of temperature and solar irradiance. The actual output power from the PV array is calculated by the multiplication of sensed operating voltage and current values, by adding the proper weights while training the MPPT algorithm. ANFIS generates the set of fuzzy rules in order to produce the appropriate output for different values of given input pattern values. Membership function pattern parameters are adjusted or modified till the error value is reduced to a minimum value.

Once all the pattern parameters of membership function are adjusted, the ANFIS model becomes the trained model with the supervisor and the network is ready to be used in MPPT control method. Obtained results are always compared with desired values. This modification of weights, adjustment of neuron pattern values and sometimes adding of additional neurons to the hidden layers of the network gets continued until the required value of optimum duty cycle is generated. That generated duty cycle is given to the DC-DC converter, which is connected in-between the solar array and inverter in order to boost the array output voltage to the inverter required voltage by adjusting the duty cycle of the boost converter. Thus; ANFIS based MPPT

is developed to obtain the optimum duty cycle for the DC-DC converter by maintaining the maximum power point (MPP) of the PV system.

The battery also helps to regulate the power flow from the PV panel to the motor drive. The ANFIS is employed with an optimization algorithm in order to modify the each individual layer parameter pattern values of the fuzzy inference system. The topologies with DC-DC converters are usually employed for battery charging applications. The temperature is varied from $20°$ C to $60°$ C in a step of $10°$ C and the solar irradiance is varied from 10 W/m^2 to 1000 W/m^2 in a step of 50 W/m^2. Thus total two hundred data patterns are used to train the network. The network is trained for 73121 epochs. The target error is specified or set in order to maintain the error at 6% and the training execution process gets continued.

After completion of the training, it is observed that at 6% error the output of ANFIS matches very close to the actual output. The training stops when either the predefined epoch number or error rate epoch number is obtained. The gradient descent algorithm is mainly implemented to tune the non-linear premise parameters, while the basic function of the mean least-squares is used to optimize or to adjust the linear consequent parameters. The input membership functions are then translated into fuzzy rules. These are observed as one for the temperature and the other for solar irradiance. The rules are framed as per the specific output requirement of the network.

6.3 Importance of an ANFIS based MPPT

❖ ANFIS based MPPT is developed in order to overcome the non-linearities of PV cell due to temperature and irradiance variations.

❖ To generate the optimum duty cycle in order to provide the switching pulse to the DC-DC boost converter switching device.

❖ To provide the required DC output to the inverter with the help of ANFIS based MPPT and DC-DC boost converter.

❖ Fast and accurate tracking with the enhanced energy conversion technique possible with the very low settling time, even compared to the conventional P&O algorithm.

❖ Mean relative error (MRE) with ANFIS produces very accurate estimation between the actual and the predicted data with error not exceeding of 1%.

❖ Controllers efficiency is increased by 5 to 25% with the ANFIS based MPPT, recovering the following losses as

❖ PV panel mismatch losses (3 to 5 %).

❖ Suboptimal MPPT losses (3 to 10 %).

❖ Simpler system design and alleviates fault tolerance (0 to 15 %).

6.4 Provision of Required Data Values to the ANFIS based MPPT

Required input and output data pattern values for training of the ANFIS based MPPT in order to get the desired maximum output power from the PV system with always maintaining the maximum power point (MPP) with respect to irradiance and temperature are tabulated in the Table 6.1.

Table 6.1 Input and output data patterns given for ANFIS based MPPT

Time in (Hours)	Temperature in (^{0}C)	Power in (Watts)	
		For ANFIS based MPPT	*For ANN based MPPT*
08.00	30.75	259.33	232.02
08.30	32.55	478.94	475.55
09.06	33.35	695.68	680.93
09.30	35.25	815.96	791.75
10.00	38.25	848.49	823.68
10.30	39.35	883.33	855.33
11.00	39.55	954.96	920.62
11.30	40.02	1048.07	1008.71
12.00	40.50	1096.48	1051.65
12.10	40.68	1159.15	1109.54
12.30	41.10	1212.19	1158.90
13.00	41.35	1264.69	1207.41
13.30	40.45	1159.15	1110.21
14.00	40.08	1053.86	1013.75
14.30	39.00	953.56	920.13
15.00	38.42	822.25	798.13
15.30	37.95	652.05	639.58
16.00	37.32	518.54	513.34
16.30	37.06	240.73	237.60
17.08	33.25	122.74	120.30
17.30	32.85	46.35	45.74

6.5 ANFIS based MPPT with SVM

To overcome the drawbacks of the conventional SVM as mentioned in the previous chapter, an ANFIS based SVM is implemented and its working is explained in this chapter. This chapter presents the simulation modeling along with the experimental validation of asynchronous motor drive with the dSPACE RTI-1104 real time controller. It is used to control and improve the parameters like stator phase current, torque and speed. These asynchronous motor drives are non-linear machines with complex and dynamic with time variations.

Control of asynchronous motor drive is a challenging one, i.e. especially speed control. ANFIS based MPPT develops the control signal for firing the rule base with the proper selection of membership functions. ANFIS based SVM is implemented with proper rule base by the back propagation algorithm, which is an integrated approach to improve the performance of the motor drive. The simulation and practical validation results are presented at the end of the chapter with faster responses and early setting times.

ANFIS controller will take care of sudden fluctuations in the speed and obtains the early reference value or the prescribed value. ANFIS has a strong learning capability with good interpretability and can also integrate the expert's knowledge. It is used to learn membership values while constructing If-Then rules. It has the network architecture constructed from the fuzzy reasoning, structured codified knowledge with fuzzy rules while adapting the learning capabilities.

6.6 Implementation of ANFIS based MPPT with SVM

Implementation of ANFIS based MPPT along with SVM is done by describing its five layers working and generation of reference angles and duty cycles. Here, the angle θ and change in angle θ' are used to feed the SVM for generating the duty cycles, which are independent of sampling time. Duty ratios along with the required sampling time period T_S are given to the relay circuit to generate the switching pulses for the switching devices of the inverter in order to generate the required voltages to the asynchronous motor drive.

6.6.1 Layer description of ANFIS based MPPT with SVM

ANFIS based SVM consists of five layers including 0th layer or input layer as:

❖ Layer 0 : Input Layer (passive in nature)

❖ Layer 1 : Membership Function Layer (Fuzzification Layer)

❖ Layer 2 : Rule Layer (Firing Layer)

❖ Layer 3 : Type Reduction Layer

❖ Layer 4 : Out Layer or Normalization layer (Defuzzification Layer)

❖ Layer 5 : Output Layer

Layer 0: It an input layer, is passive in nature in which temperature and irradiance are provided as the input pattern values at different time instants in a day from morning 8:00 am to evening 5:30 pm. ANFIS controller is developed with the Sugeno Fuzzy model.

Layer 1: It is the layer in which θ and θ' are provided for each individual set of containing nodes N_1 to N_5 i.e. for 5 nodes. It is also said to be a membership layer, where all the neurons are provided with the membership data pattern values. Here N_1 to N_5 are the linguistic variables that are used for the fuzzy theory to describe the membership functions. All the variables in this layer 1 are called as adoptive nodes and the respective particulars in this layer are called premise or pre-conditioned particulars (specifications). Relations between the input and output membership functions of this layer are denoted as:

$$Y'_{1i} = \mu_i N_i(\theta) \qquad i = 1,2,..5 \tag{6.1}$$

$$Y'_{1j} = \mu_j N_j(\theta') \qquad j = 1,2,..5 \tag{6.2}$$

Where: Y'_{1i}, Y'_{1j} represents the layer 1 output nodes and $\mu_i N_i, \mu_j N_j$ represents the layer 1 membership functions. These memberships are bell shaped with maximum value of "1" and minimum value of "0". Bell shaped membership function is represented with the required parameters as:

$$F(\theta; A\ B\ C) = \frac{1}{1+|\frac{\theta-C}{A}|^{2B}} \tag{6.3}$$

$$F(\theta'; A\ B\ C) = \frac{1}{1+|\frac{\theta'-C}{A}|^{2B}} \tag{6.4}$$

Where: A, B parameters vary the width of the curve and the parameter C locates the centre of the curve. For this, the parameter B should be positive. A, B and C

parameters are also said to be as premise parameters. This layer checks the weight of each membership function. It takes all its inputs from the 0th layer. Computing of the membership values specified the particular degree to all the input pattern values. Here all crisp values are converted into fuzzy sets by the process called fuzzification.

Layer 2: Pre-condition matching of fuzzy rules is performed in this layer, i.e. activation level of each rule gets computed in this layer. Number of layers is equal to the number of fuzzy rules. All pattern values are fired and those fired values are normalized in this layer. This layer is also called as rule layer. All the node outputs of this layer are the product of all incoming inputs.

All the individual outputs of this layer resemble as the firing power of the rule, the calculation of firing strengths is represented in the Fig. 6.2. Neurons receive the input information from the previous layers, which represents the fuzzy sets. If a neuron has more number of inputs then the conjunction of all rules are processed by the fuzzy operation. This operation is used to combine the multiple inputs to form suitable fuzzy rules. Here, the numbers of neurons that are processed are 25.

$$Y_2' = \mu M_i(\theta) \text{ And } \mu M_i(\theta') \tag{6.5}$$
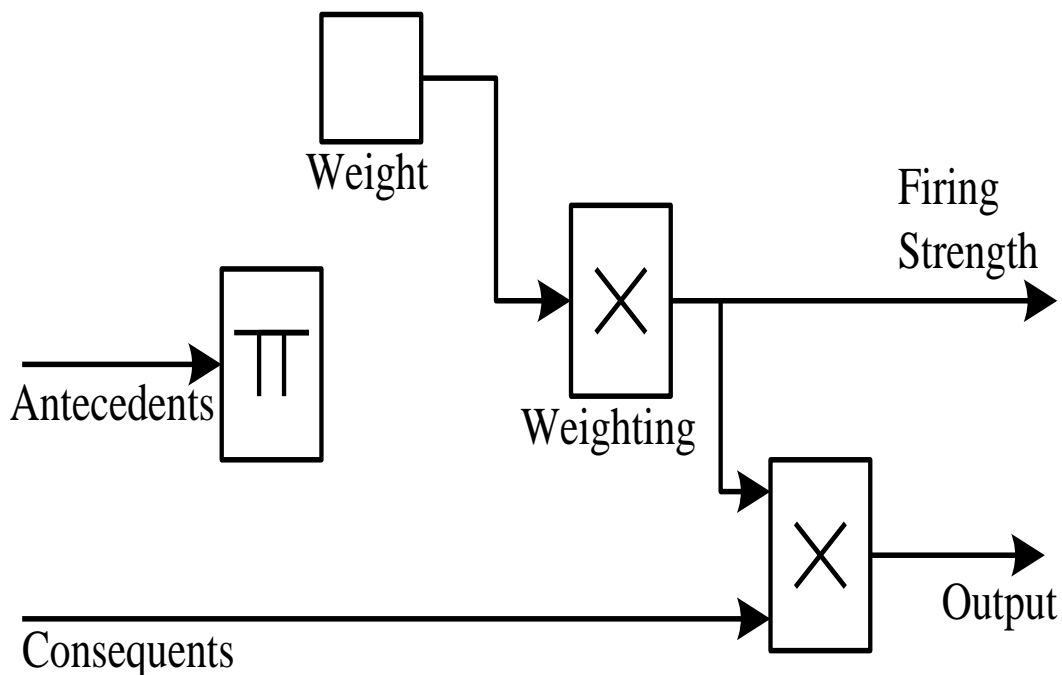
Fig. 6.2 Firing Strength representation

Layer 3: This layer is also called as Norm layer, which provides the output values from the weighted sum of previous inputs from inference of the rules. Each

neuron of this layer performs the normalization, and those outputs are called normalized firing strengths that are given by:

$$Y_3' = \frac{Y_{2i}'}{\Sigma_i Y_{2i}'} \qquad where\ i = 1,2\ ..\ ..$$ (6.6)

It is a fixed node where it also calculates the ratio of ith rule activation level to that of all the fuzzy rules.

Layer 4: This layer is called an Out layer, which is integration of all the weighted sum of previous inputs. It is an adaptive node that calculates the contribution of ith rule towards the overall output, i.e. in this defuzzification process of fuzzy system takes place with the weighted average method.

So it gives the crisp output by defuzzifying of the entire layer's fuzzy output. ANFIS applies a standard defuzzification process by including the centroid technique. And the overall output is represented in Eq. (5.7). In this layer all the neurons are trained by least square estimation to produce the optimum output.

$$Y_4' = Y_3' \sum_{i-1}^{M} M_i\theta + N_i\theta' + R_i\ where\ i = 1.2, ... M$$ (6.7)

Where: M_1, M_2,…M_M, N_1, N_2,…N_M and R_1,R_2,…R_M are the consequent parameters of the layer.

Layer 5: It has a single neuron that produces the final output that has the weighted sum of all integrated outputs of the previous layers and hence termed as an Output layer. Then the final output is given as:

$$Y_5' = \sum_i Y_4^i$$ (6.8)

Where: Y_5' is the 5th layer output and Y_4^i is the 4th layer output. Overall output generated from the ANFIS is compared with the repetitive counter or up-down counter and that is processed through the relay to generate the optimum switching pulses to S_A, S_B and S_C, which are used for proper switching of inverter switching devices.

Then finally required and produced output from inverter is supplied to the asynchronous motor drive with the help of ANFIS based MPPT and SVM controlling technique. ANFIS controller layout with the layers description is shown in Fig. 6.3.
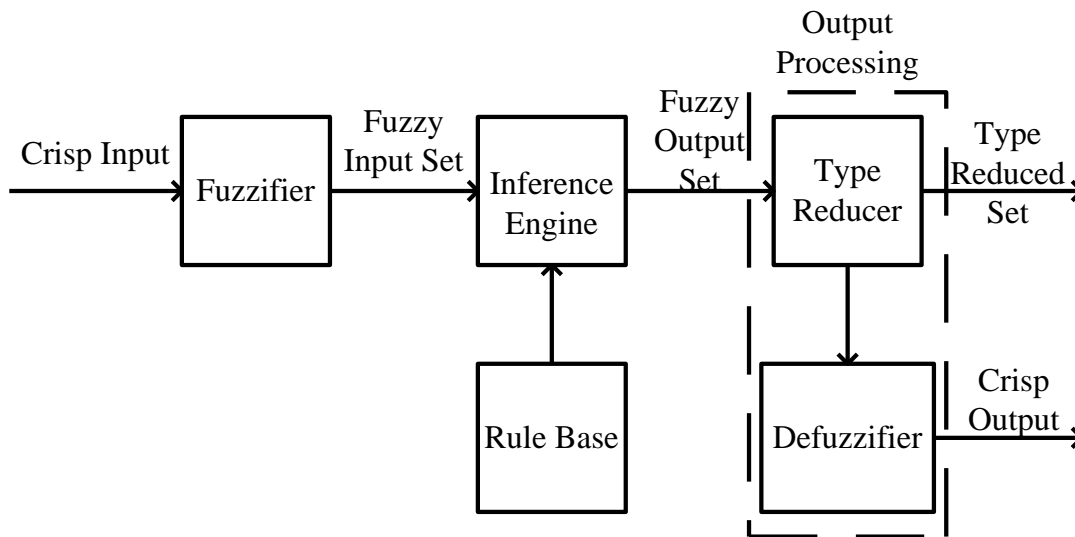
Fig. 6.3 ANFIS controller representation

6.6.2   Learning algorithm steps

❖ It is a hybrid learning technique, combining gradient descent back propagation & mean least square optimization algorithms.

❖ At each epoch an error (an error measure is the sum of the squared difference between actual and desired output) measure is reduced.

❖ Training stops when the pre-defined epoch number or error rate is reached.

❖ The gradient descent algorithm is mainly implemented to tune the non-linear premise parameters.

❖ The basic function of the mean least-squares is to optimize or adjust the linear consequent parameters.

Hybrid learning technique of ANFIS with forward pass and backward pass is explained below

6.6.2.1   Forward pass

The training set of inputs for forward pass input pattern values as input vectors i.e. θ and θ' are given to the ANFIS. Node outputs are calculated on the basis of layer by layer and rule consequent parameters, observed by the least-square estimator. In this, Sugeno type fuzzy inference, an output vector and duty ratios are linear functions. Thus, given pattern values for the membership parameters i.e. triangular membership with 3 membership parameters, training set of 73121 inputs i.e. θ and θ' and output duty ratios pattern values are linear equations in terms of consequent parameters as:

118

$$D_{1-M} = \overline{W}_1(1)F_1(1) + \overline{W}_1(1)F_2(1) + \cdots + \overline{W}_N(1)F_N(1)$$

$$D_{1-M} = \overline{W}_1(2)F_1(2) + \overline{W}_1(2)F_2(2) + \cdots + \overline{W}_N(2)F_N(2)$$

.

.

.

$$D_{1-M} = \overline{W}_1(M)F_1(M) + \overline{W}_1(M)F_2(M) + \cdots + \overline{W}_N(M)F_N(M) \tag{6.9}$$

$$D_1(1) = \overline{W}_1(1)[M_1\theta(1) + N_1\theta'(1) + R_1]$$

$$\overline{W}_2(1)\left[M_2\theta(1) + N_2\theta'^{(1)} + R_2\right] + \ldots\ldots +$$

$$\overline{W}_N(1)\left[M_N\theta(1) + N_N\theta'^{(1)} + R_N\right]$$

$$D_1(2) = \overline{W}_1(2)[M_1\theta(2) + N_1\theta'(2) + R_1]$$

$$\overline{W}_2(2)[M_2\theta(2) + N_2\theta'(2) + R_2] + \cdots +$$

$$\overline{W}_N(2)N[M_N\theta(2) + N_N\theta'(2) + R_N]$$

.

.

.

$$D_1(M) = \overline{W}_1(M)[M_1\theta(M) + N_1\theta'(M) + R_1]$$

$$\overline{W}_2(M)[M_2\theta(M) + N_2\theta'(M) + R_2] + \cdots +$$

$$\overline{W}_N(M)[M_N\theta(M) + N_N\theta'(M) + R_N] \tag{6.10}$$

Where: M is the input/output pattern values and N is the nodes in the layer.

D_{1-M} is the predicted duty ratio of ANFIS for the given input pattern values. From Eq. (5.10) the matrix form is written as:

$$D_{1-M} = AK \tag{6.11}$$

Where: D_{1-M} is a M×1 = 73121×1, which the predicted duty ratio vector as:

$$D_{1-M} = \begin{bmatrix} D_{1-M}(1) \\ \vdots \\ D_{1-M}(M) \end{bmatrix} \tag{6.12}$$

Where: A is a M×N (1+ number of input variables)=73121×75 matrix as:

$$\begin{bmatrix} \overline{W}_1(1) & \overline{W}_1(1)\theta(1) & \overline{W}_1(1)\theta'(1) & . & . & \overline{W}_N(1) & \overline{W}_N(1)\theta(1) & \overline{W}_N(1)\theta'(1) \\ \overline{W}_2(2) & \overline{W}_1(2)\theta(2) & \overline{W}_1(2)\theta'(2) & . & . & \overline{W}_N(2) & \overline{W}_N(2)\theta(2) & \overline{W}_N(2)\theta'(2) \\ . & . & . & . & . & . & . & . \\ . & . & . & . & . & . & . & . \\ \overline{W}_1(M) & \overline{W}_1(M)\theta(M) & \overline{W}_1(M)\theta'(M). & . & . & \overline{W}_N(M) & \overline{W}_N(M)\theta(M) & \overline{W}_N(M)\theta'(M) \end{bmatrix} \tag{6.13}$$

Here: K is N (1+ input variables ×1)×1=75× 1 vector of unknown consequent parameters as:

$$K = [M_1 N_1 R_1 \quad M_2 N_2 R_2 \quad ... ... \quad M_N N_N R_N]^T \tag{6.14}$$

Least squared estimate of K should be identified to find out the exact solution with minimizing squared error as:

$$||AK - D_{1-M}||^2 \tag{6.15}$$

Then the least squared estimate using the pseudo inverse technique is as follows:

$$K^* = (A^T A)^{-1} A^T D_{1-M} \tag{6.16}$$

Where: $(A^T A)^{-1} A^T$ is pseudo inverse of A.

The moment when the consequent parameters are established, then, computing of actual network process starts with the final output vector D_1 and the error vector (e), is calculated as:

$$e = D_{1-M} - D_1 \tag{6.17}$$

6.6.2.2   Backward pass

Back propagation algorithm is applied for the backward pass. Here error signals are propagated in back and antecedent parameters are updated according to the chain

rule. For a consideration a correction is applied to the parameter A of bell shaped membership function, the chain rule is calculated as:

$$\Delta a = -\frac{\partial p}{\partial a} = -\frac{\partial p}{\partial e} \times \frac{\partial e}{\partial D_1} \times \frac{\partial D_1}{\partial (\overline{W_i} F_i)} \times \frac{\partial (\overline{W_i} F_i)}{\partial \overline{W_i}} \times \frac{\partial \overline{W_i}}{\partial W_i} \times \frac{\partial W_i}{\partial W_{Ai}} \times \frac{\partial W_{Ai}}{\partial a} \tag{6.18}$$

Where: n is the learning rate and p is the instantaneous value of the squared error of the output neuron as:

$$p = \frac{1}{2} e^2 = \frac{1}{2} (D_{1-M} - D_1)^2 \tag{6.19}$$

$$\Delta a = -(D_{1-M} - D_1)(-1) \times F_i \times \frac{\overline{W_i}(1-W_i)}{W_i} \times \frac{W_i}{W_{Ai}} \times \frac{\partial W_{Ai}}{\partial a} \tag{6.20}$$

Where: $\frac{\partial W_{Ai}}{\partial a} = \frac{1}{[+(\frac{\theta-a}{c})^{2b}]} \times \frac{1}{c^{2b}} \times 2b \times (\theta - a)^{2b-1} \times (-1) \tag{6.21}$

$$= W_{Ai}^2 \times \frac{2b}{c} \times (\frac{\theta-a}{c})^{2b-1} \tag{6.22}$$

In this total number of layers L is fixed at 5 (five), the number of nodes in each layer depends mainly on number of inputs and the number of individual neurons associated with each input and the number of fuzzy rules. Finally there will be a single output at the 5th layer to provide the duty ratios for the switching devices of two level inverter. So that the inverter provides the required supply to the asynchronous motor drive with the help of ANFIS based SVM controlled technique.

6.7 Main Features of ANFIS based MPPT and SVM

❖ Adaptive Neuro Fuzzy MPPT with SVM is trained in under modulation region for generating duty ratios. The switching frequency used is 5 kHz.

❖ The training data for ANFIS is obtained by simulating the conventional SVM.

❖ It is trained for 73121 epochs.

❖ The training time for one epoch is typically 0-5 minutes and training error obtained is less than 0.00015.

❖ The number of membership functions for the input variables is 5 and 5 respectively.

❖ The number of rules are 25(5*5=25)

❖ Bell shape membership functions are used for two input variables. So Adaptive Neuro Fuzzy contains a total of 105 fitting parameters, i.e. 30(5*3+5*3=30) are premise parameters

75(3*25=75) are consequent parameters

6.8 Simulation Responses of an Asynchronous Motor Drive with ANFIS based MPPT and SVM

Simulation results are obtained with the reference speed of 1300 RPM and switching frequency of 5 KHz. The performance of motor drive parameters stator phase current, speed and torque, are analyzed at starting, steady state, transients with step change in load torque and speed reversal operations. Motor is fed by 400 V supply with the help of a boost converter and an inverter in incorporating ANFIS based SVM controlling technique. These all responses of the motor drive with the conventional and ANFIS based MPPT along with SVM are presented in Fig. 6.4-6.18.

6.8.1 Performance of an asynchronous motor drive at starting

For the asynchronous motor drive the maximum current and the ripple content in the torque is reduced during starting in order to reach the early steady state. With the ANFIS method and SVM, the maximum torque and the speed are obtained as 13.58 N-m and 1300 RPM respectively. It is observed that the ripple content in the torque is reduced to 0.17 compared to conventional method. Due to this, better speed response is attained. These results are observed in Fig. 6.4-6.6.
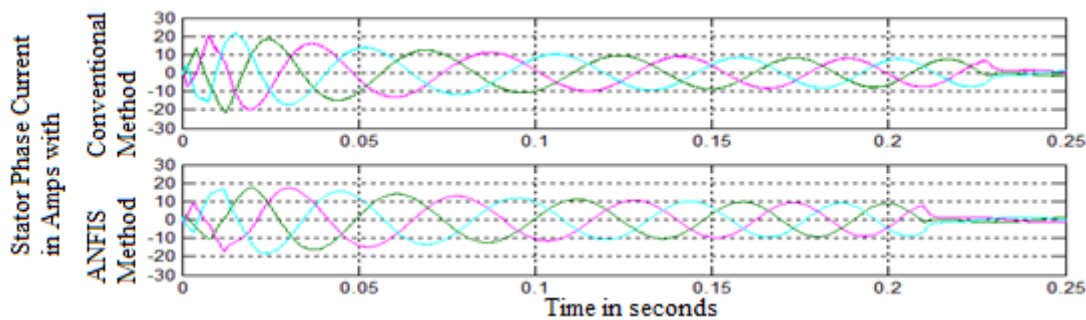
Fig. 6.4 Stator phase current responses with conventional and ANFIS methods at starting
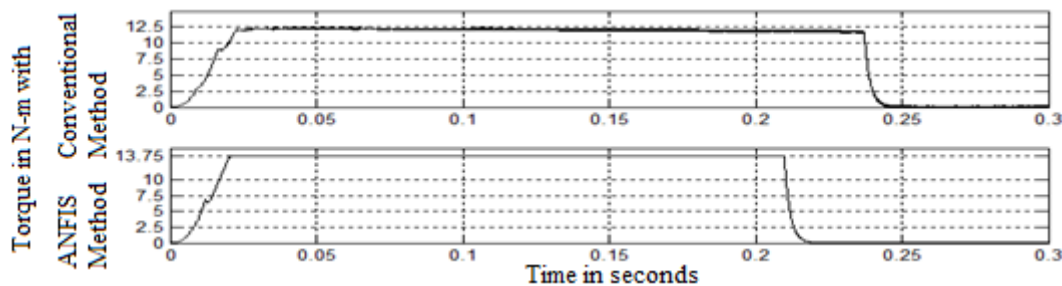
Fig. 6.5 Torque responses with conventional and ANFIS methods at starting
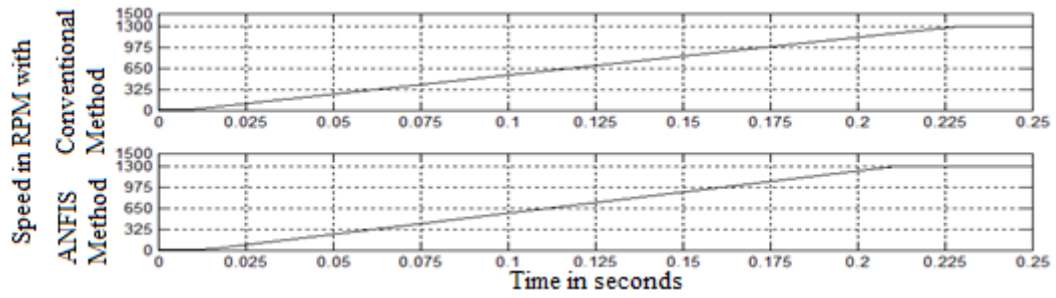
Fig. 6.6 Speed responses with conventional and ANFIS methods at starting

6.8.2 Performance of an asynchronous motor drive at steady state

The steady state responses of stator phase currents, torque and speed with conventional and ANFIS method are shown in Fig. 6.7-6.9. Here torque ripple with the proposed MPPT is reduced a lot i.e. it is observed that the torque ripple with the conventional and modified MPPT are 0.35 and 0.20 respectively.
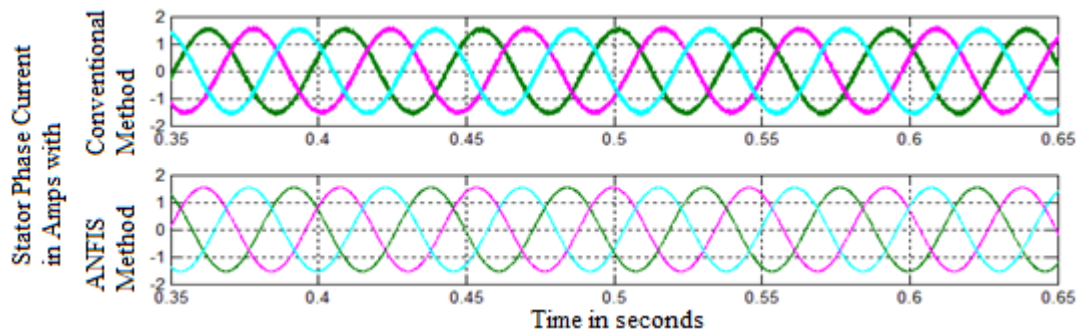
Fig. 6.7 Stator phase current responses with conventional and ANFIS methods at steady state
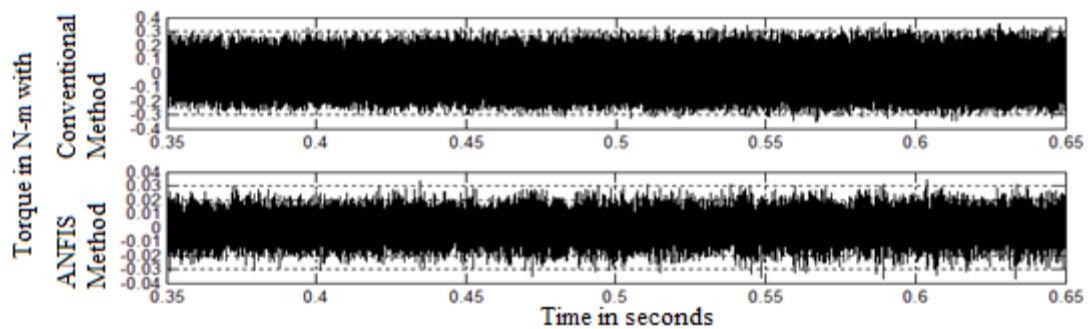
Fig. 6.8 Torque responses with conventional and ANFIS methods at steady state
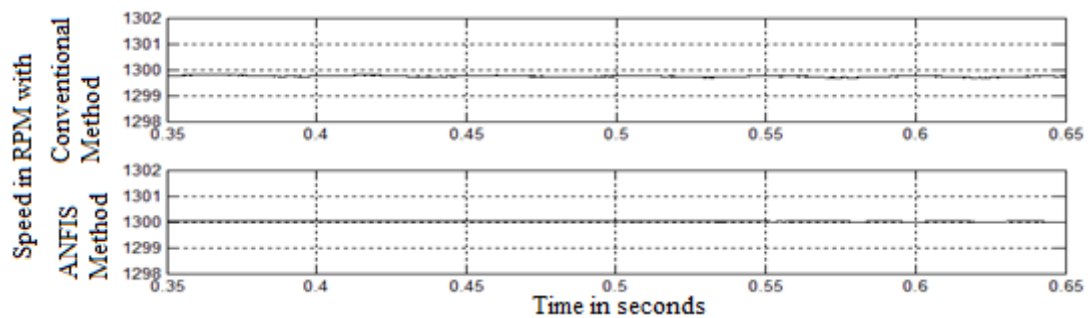
Fig. 6.9 Speed responses with conventional and ANFIS methods at steady state

123

6.8.3 Performance of an asynchronous motor drive at transients with step change in load

The responses during the transients with step change in load torque of 8 N-m is applied at 0.7 sec and removed at 0.9 sec as represented in Fig. 6.10-6.12. The ripple content in current and torque is reduced a lot with the ANFIS method. And also the speed decrement is less with the ANFIS method during the load change.
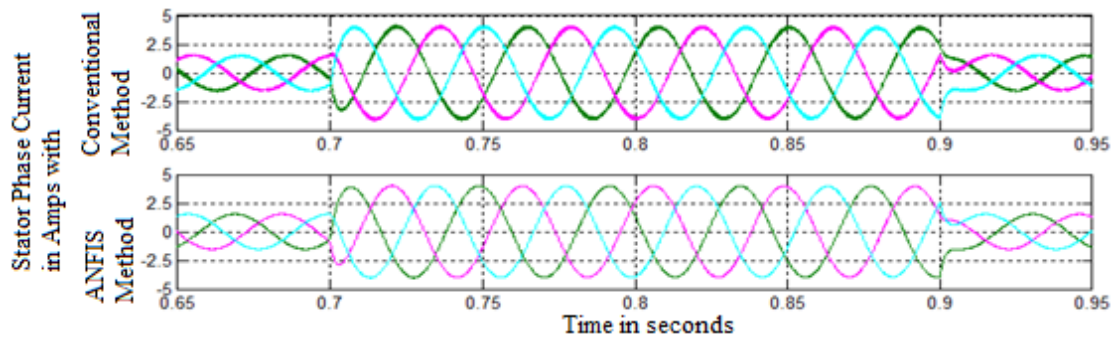
Fig. 6.10 Stator phase current responses with conventional and ANFIS methods at transients with step change in load
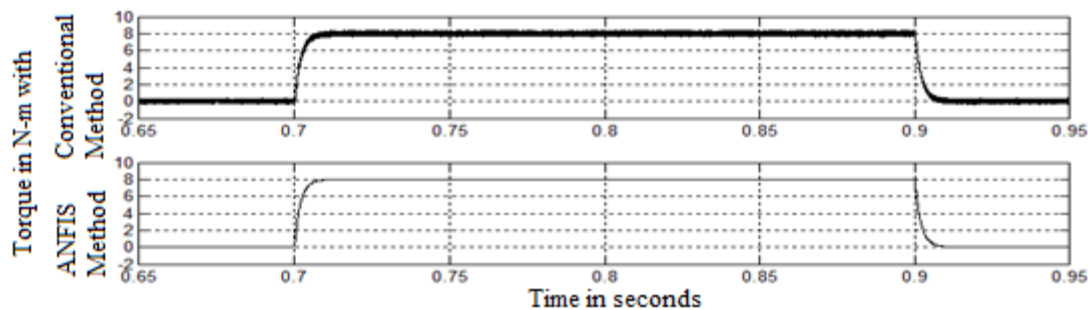
Fig. 6.11 Torque responses with conventional & ANFIS methods at transients with step change in load
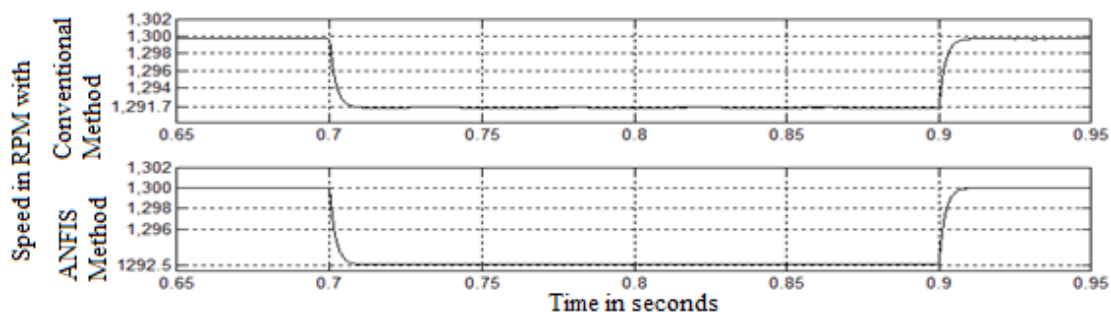
Fig. 6.12 Speed responses with conventional & ANFIS methods at transients with step change in load

6.8.4 Performance of an asynchronous motor drive at transients with speed reversal from +1300 to -1300 rpm

The results of the drive during speed reversals from +1300 to -1300 RPM are available in Fig. 6.13-6.15. The drive gives less ripple content in stator phase current and torques. Early speed reference value is reached with the ANFIS method.
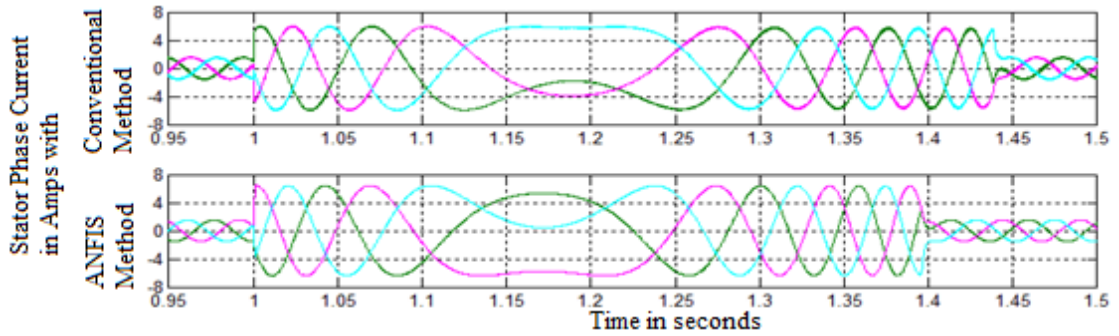
Fig. 6.13 Current responses with conventional and ANFIS methods at transients with speed reversal
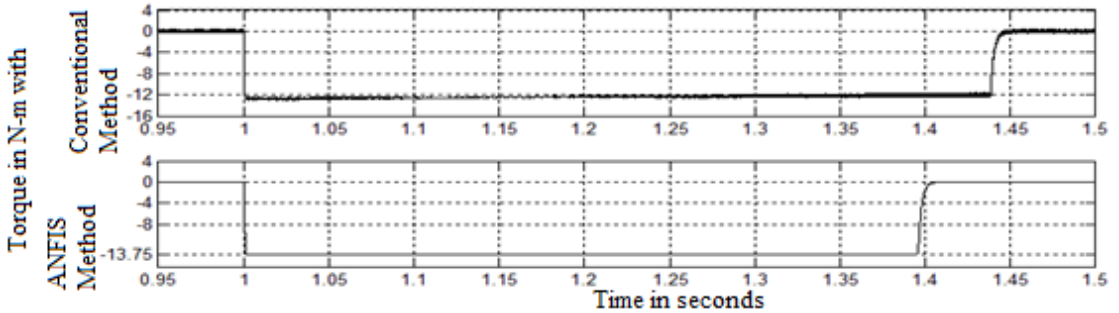
Fig. 6.14 Torque responses with conventional and ANFIS methods at transients with speed reversal
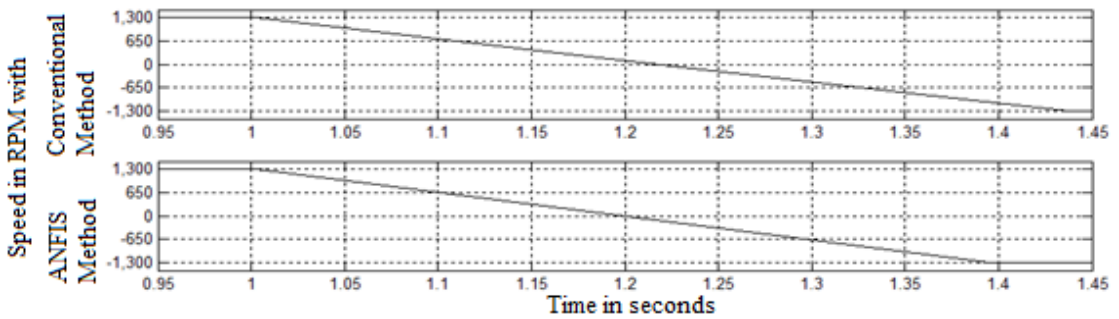
Fig. 6.15 Speed responses with conventional and ANFIS methods at transients with speed reversal

6.8.5 Performance of an asynchronous motor drive at transients with speed reversal from -1300 to +1300 rpm

When the results of the drive during speed reversals from -1300 to +1300 RPM are analyzed in Fig. 6.16-6.18, it is observed that the overall performance of the drive is improved much by the ANFIS method along with the better speed response.
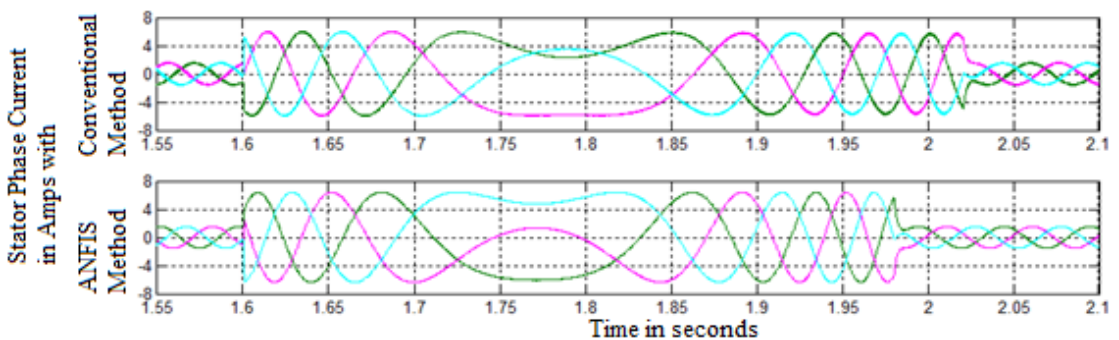
Fig. 6.16 Current responses with conventional and ANFIS methods at transients with speed reversal

125
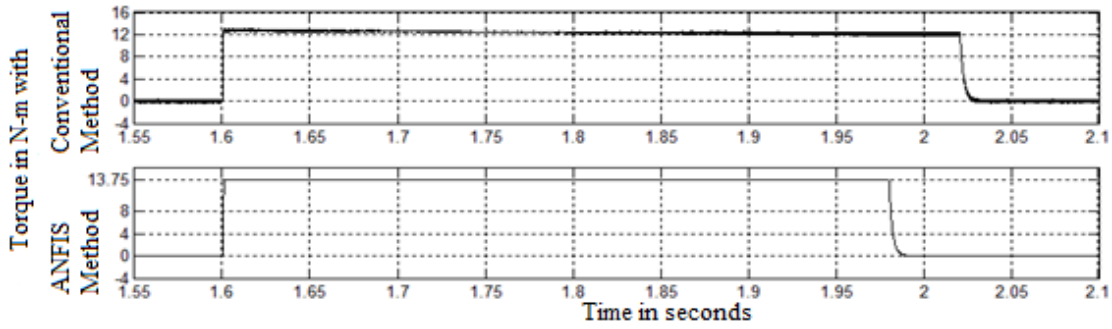
Fig. 6.17 Torque responses with conventional and ANFIS methods at transients with speed reversal
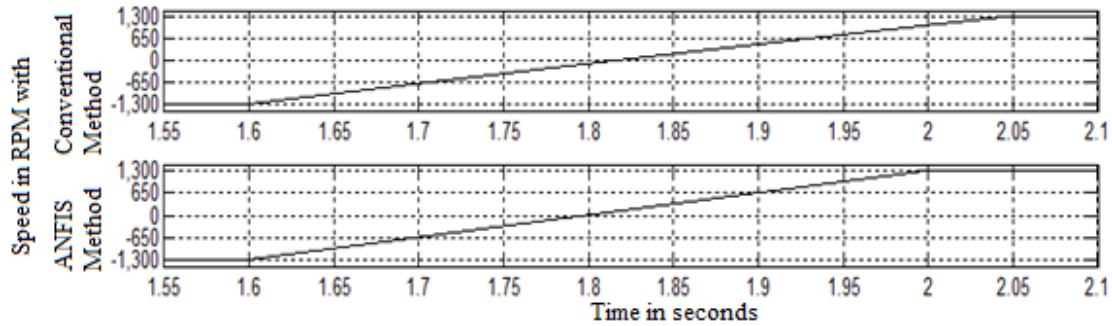
Fig. 6.18 Speed responses with conventional and ANFIS methods at transients with speed reversal

6.8.6 Performance of an asynchronous motor drive with torque ripple

The torque ripple is reduced to 47.05% during starting and 75% during steady state respectively with the ANFIS method compared to other conventional methods. The results of the drive with torque ripple are presented in Fig. 6.19-6.20.
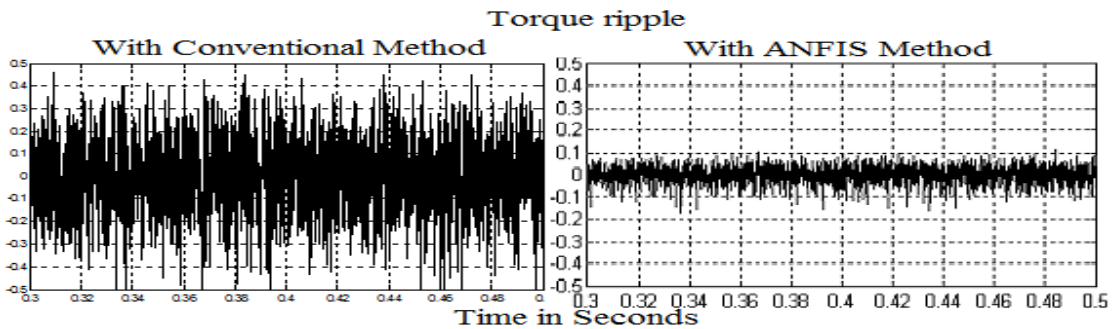
Fig. 6.19 Torque ripple responses with conventional and ANFIS methods during starting
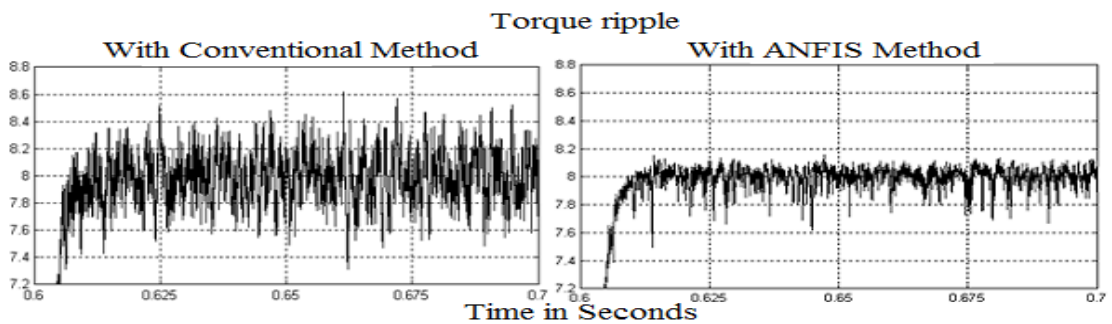
Fig. 6.20 Torque ripple responses with conventional and ANFIS methods during steady state

126

6.8.7 Performance of an asynchronous motor drive with D-Q axis current ripple

The current ripple is reduced to 43.75% during starting and 66.66% during steady states respectively with the ANFIS method compared to other conventional methods. The results of the drive with D-Q axis current ripples are presented in Fig. 6.21.
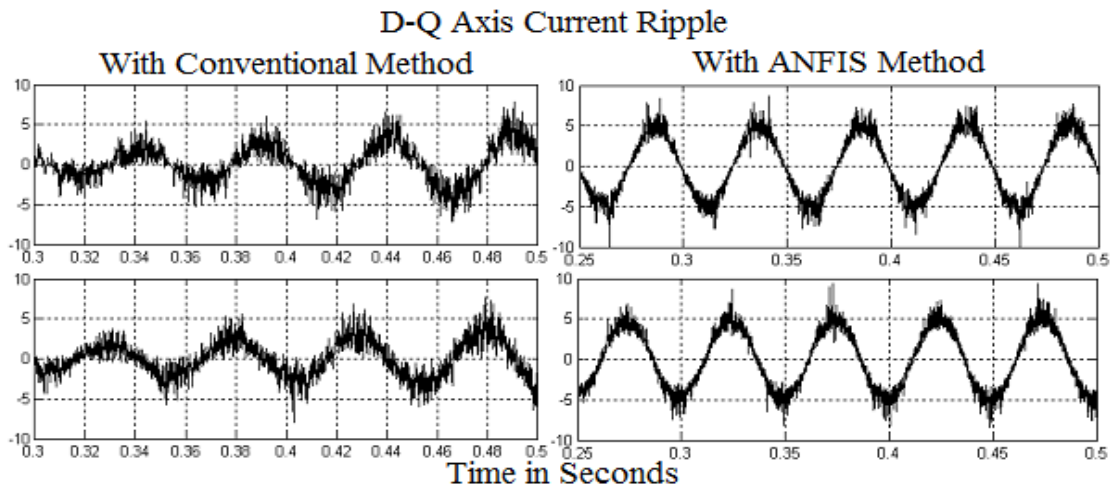
Fig. 6.21 D-Q axis current ripple with conventional and ANFIS methods during starting and steady states

6.8.8 SVM controlled inverter performance with conventional MPPT

The harmonic spectrums of SVM controlled inverter with the conventional MPPT at the switching frequency of 5 KHz are illustrated in Fig. 6.22-6.24. It is observed that the THD values of 3 line-line voltages with the conventional MPPT SVM are 8.81%, 8.62% and 8.62% respectively.
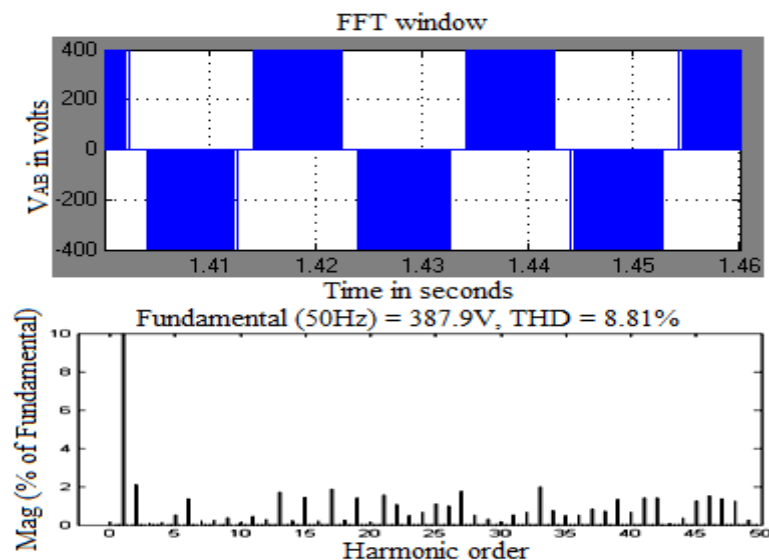
Fig. 6.22 Inverter V_{AB} line-line voltage with conventional MPPT
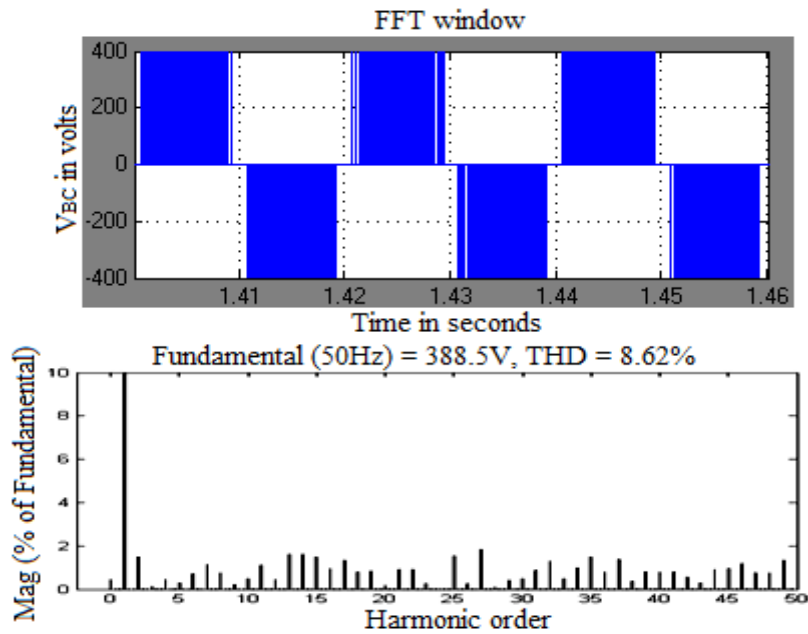
Fig. 6.23 Inverter V_{BC} line-line voltage with conventional MPPT
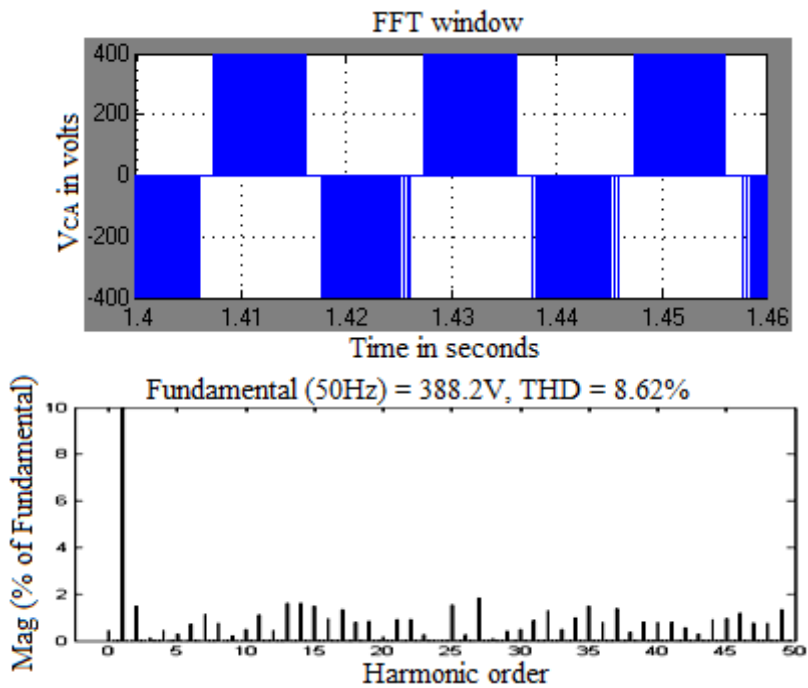
Fig. 6.24 Inverter V_{CA} line-line voltage with conventional MPPT

6.8.9 SVM controlled inverter performance with modified MPPT

Line-line voltages, harmonic spectrums and THD values using FFT waveforms of SVM controlled inverter with the modified MPPT at the switching frequency of 5 KHz are represented in Fig. 6.25-6.27. It is observed that the THD of 3 line-line voltages with the modified MPPT SVM gives the better output voltages with more reduction of harmonics. The inverter line-line voltages THD values are observed as 6.21%, 6.65% and 6.21% respectively.

128
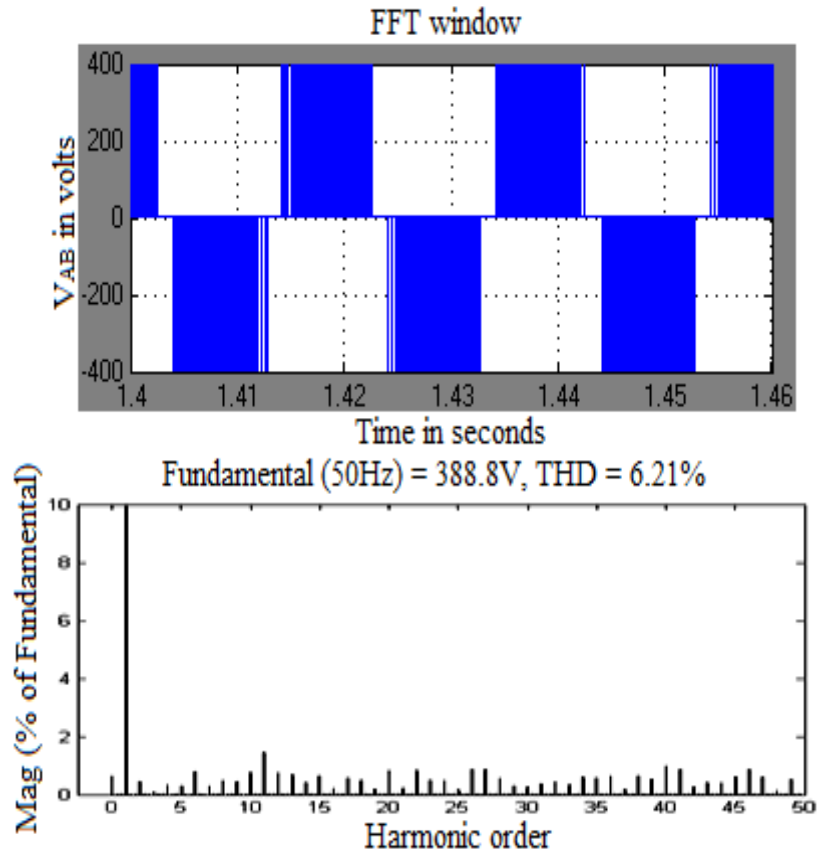
Fig. 6.25 Inverter V_{AB} line-line voltage with modified MPPT
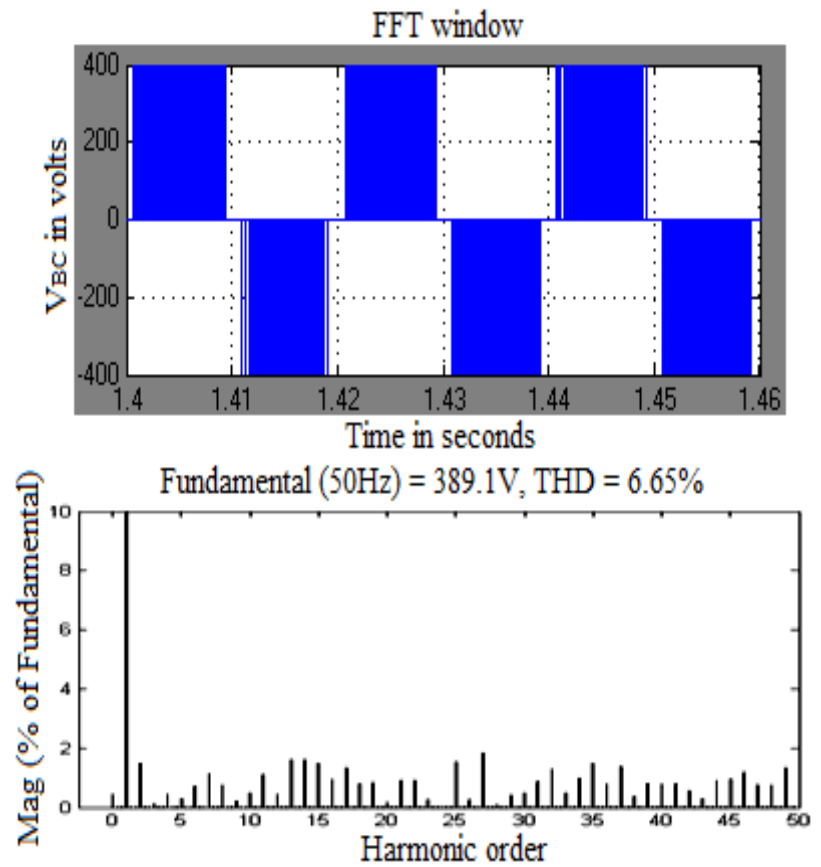
Fig. 6.26 Inverter V_{BC} line-line voltage with modified MPPT
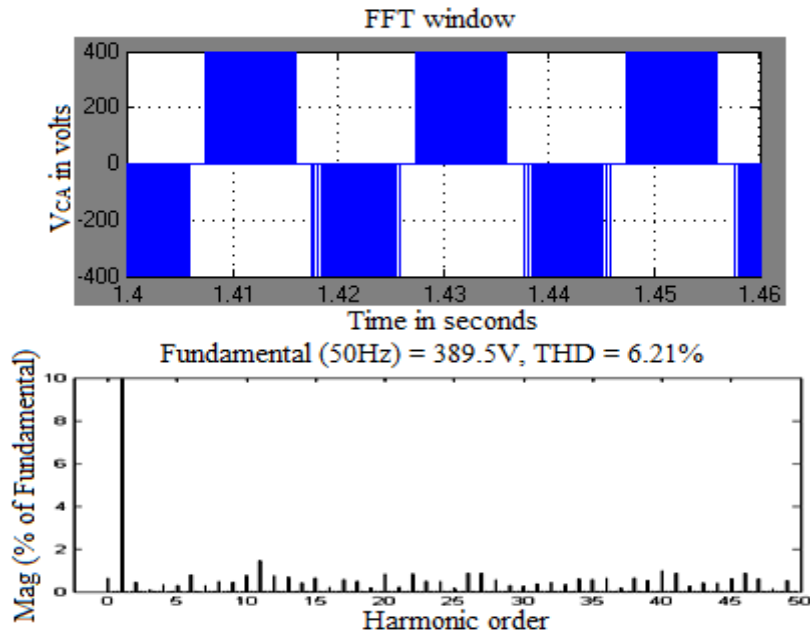
Fig. 6.27 Inverter V_{CA} line-line voltage with modified MPPT

6.9 Experimental Validations with dSPACE RTI-1104

A dSPACE RTI-1104 controller is used as a control platform to enable the linkage between the Matlab-simulation models and the real time hardware implementation for the experimental validations by using the dSPACE RTI-1104 input-output (I/O) connecting blocks into the simulink models. The I/O blocks are like analog to digital converter (ADC), digital to analog converters (DAC) and BIT-OUT-CX blocks. Simulink model with dSPACE is converted into C-code automatically by using the Matlab-simulink real time workshop (RTW) function. And the codes are compiled by a compiler and linked to the real time dSPACE RTI-1104 processor board. The dSPACE graphical user interface (GUI) is used to monitor the inverter performance and behavior in the real time application.

The dSPACE-1104 controller board is effectively used for the design of high frequency link inverter. A proportional integral (PI) controller is used an alternative way to control and to stabilize the ac output voltages in the dSPACE. Figure 26 illustrates about the working in the block diagram of the dSPACE-1104 that comprises of a main processor power PC603 with 250 MHz including the 16-bit slave DSP-TI TMS320F240 microcontroller and a 64-bit floating point processor. This controller is also used for the ideal hardware system development with the reasonable cost rapid control. Which is prominently chosen for the high speed

130

multivariable digital controllers development and real time simulations in various applications. The dSPACE-1104 controller is represented in Fig. 6.28.
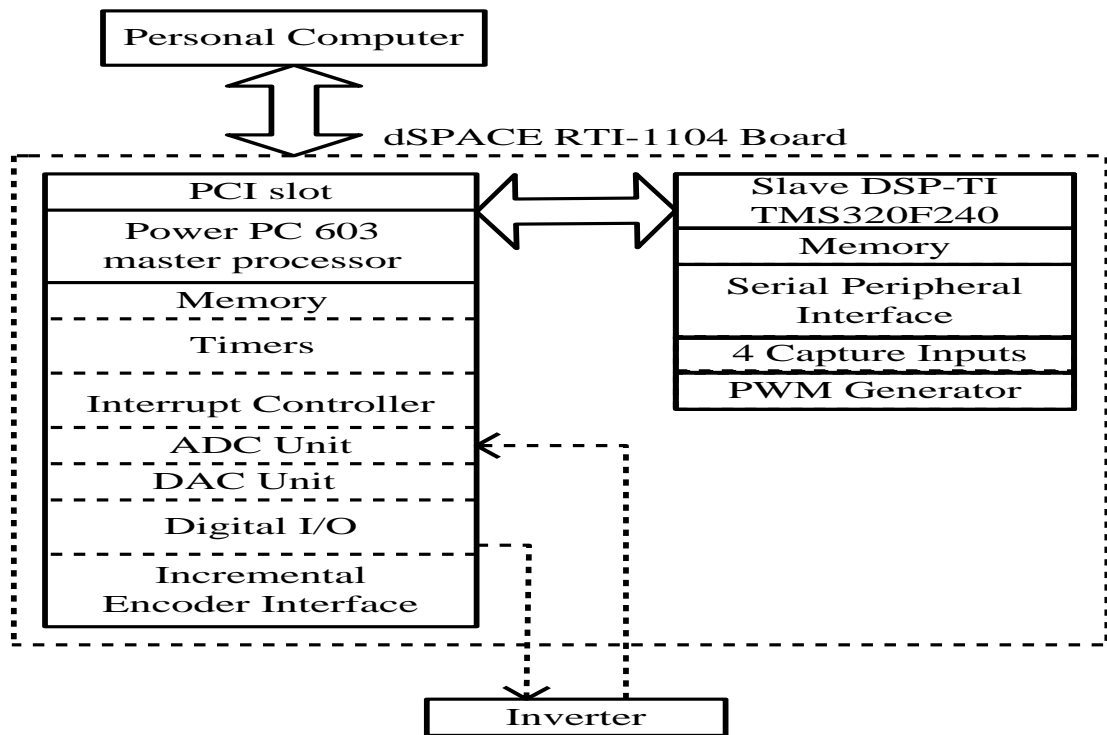
Fig. 6.28 Representation of the dSPACE RTI-1104 controller board

6.9.1 dSPACE RTI-1104 control procedure

For the purpose of PV inverter control system designing, it requires majorly 3 blocks i.e. the sensors for voltage and current divisions, the dSPACE RTI-1104 controller and the inverter. Output of the inverter is given to the load for the controlling process. dSPACE RTI-1104 controlled inverter is shown in Fig. 6.29.
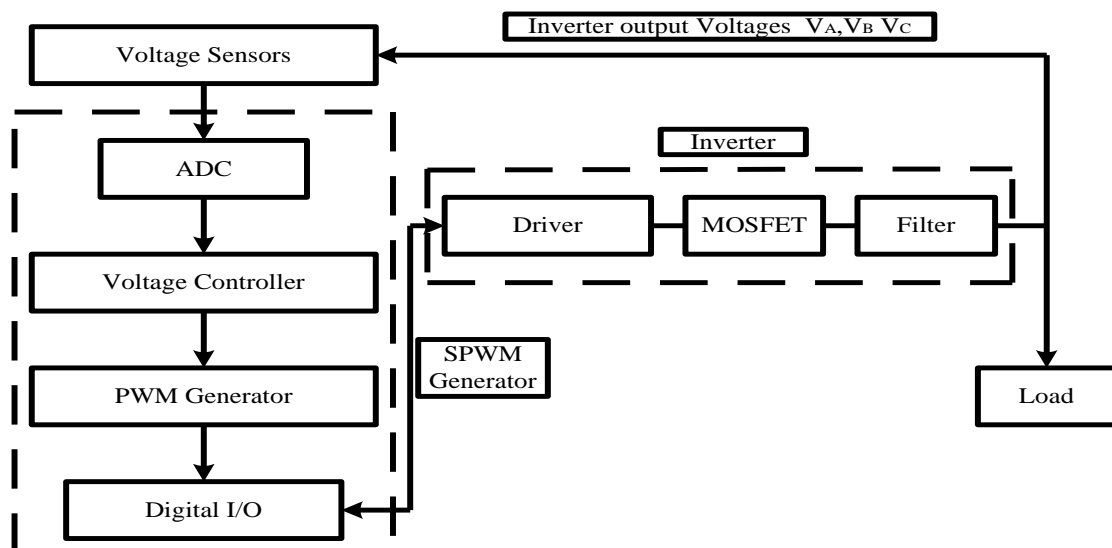
Fig. 6.29 Representation of the dSPACE controlled inverter

131

Due to three phase inverter, the three voltage sensor circuitry functions are used as an interfacing device for the controller board of dSPACE-1104 and the inverter. Output voltages of an inverter i.e. V_A, V_B and V_C are used to read voltages for sensors with the unity power factor as discussed in Chapter-4. These sensed voltages are decreased to minimum workable voltage value with the safe scaling as per the requirement before giving to the controller board of dSPACE. Because, the higher voltages damages the controller board. And that array obtained output analog signals are given to the ADC channels of the dSPACE controller to control and to maintain the voltage as per the requirement as presented in Fig. 6.30.
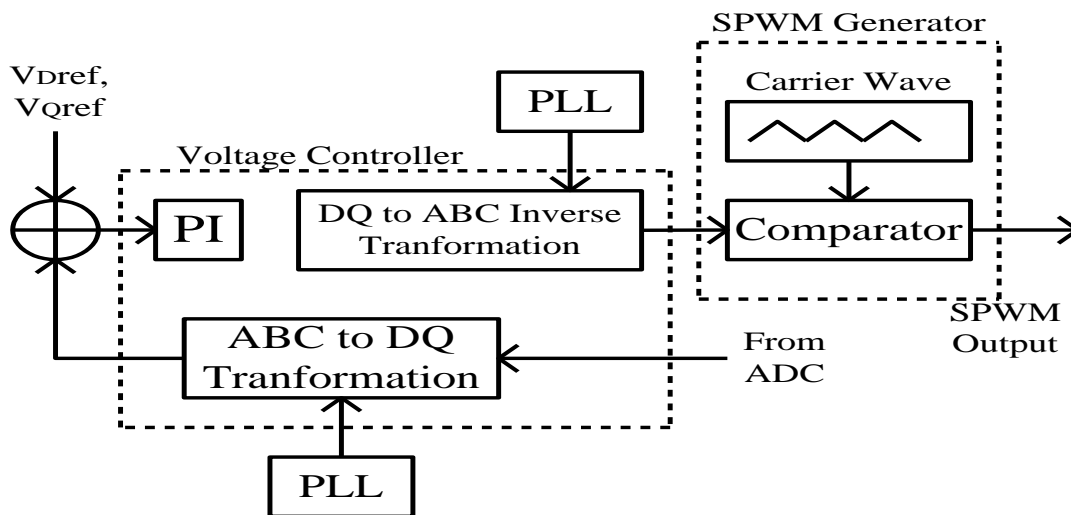
Fig. 6.30 Process of voltage control scheme implementation in the dSPACE RTI-1104 controller board

By the Park transformation method the sampled three phase signals are transformed to 'DQ$_0$' reference frame as explained in Eq. (4.19) from chapter 4. This transformation is applicable for only 3-phase balanced load. Due to this, V_0 in the 'DQ' co-ordinated frame is removed with containing only V_D and V_Q terms as denoted in Eq. (4.19) in the chapter 4. 50 Hz synchronization signal is used for transformation from the phase locked loop. Then, the voltages are compared with the V_{Dref} and V_{Qref} reference voltages to generate the voltage errors and to feed PI controllers in order to regulate the output voltages. PI control algorithm in time domain is represented as in Eq. (6.23).

$$U(t) = k_p e(t) + k_i \int_0^t e(t)dt \qquad (6.23)$$

Here, U(t) is the PI controller's output, k_i and k_p are the integral and the proportional gains and *e(t)* is the error i.e. the difference between the measured and

the actual voltage values. Here, PI controller reduces the rise time inverter output steady state error. It also calculates the error integral and compares it to the required value to generate the control signal in order to maintain the minimum error signal (Z. Salam et al, 2006, H, Saadat et al, 2004). Thus, system is said to be under proper maintenance with balancing when the output voltages are as close to the reference value. Due to this, inverter output voltage is controlled and also stabilized. Then, the output signals are transformed back to the 3-phase system to make the inverter output waveforms as close to the sinusoidal waveforms, using the inverse Park transformation with PI controller.

It requires the 50 Hz synchronization signal from the PLL to transform the ABC coordinates. Finally, these ABC signals are provided to the SPWM generator to provide the switching signals for the inverter. The SPWM modulates the switching signals and shapes the output ac voltages as close to a sine wave. Then, the switches duty ratios are modulated by the control signal with the desired fundamental frequency. In this generator, a 50 Hz control signal is compared with the 25 KHz triangular wave to generate the switching signals. The triangular wave frequency entrenches the inverter switching frequency. The modulation index (M_a) is the control variable which is responsible for the inverter output RMS voltage values. The modulation index (M_a) is the ratio of signal (A_{ref}) to the carrier signal (A_{tri}) i.e. triangular wave signal as given below:

$$M_a = \frac{A_{ref}}{A_{tri}} \tag{6.24}$$

By proliferation of the modulation index the desired output control signal gets changed. The RMS line output voltage of the fundamental value is directly proportional to the modulation index and input DC voltage (V_{DC}) as noted below::

$$V_{Line,RMS} = \frac{V_{Phase,Peak}}{\sqrt{2}} = \frac{\left(M_a \times \frac{V_{DC}}{2}\right) \times \sqrt{3}}{\sqrt{2}} \tag{6.25}$$

$$0.612 \times M_a \times V_{DC} \tag{6.26}$$

The modulation index range lies in between zero and one. If the modulation index (M_a) is greater than one then, it causes over modulation resulting severe harmonics in the inverter high output voltages. The modulation index is taken as less

133

than one in this research work. Here, the inverter comprises of three sections i.e. the driver circuit, MOSFETSs and filter. In between the controller board SPWM signals and the MOSFETs the driver circuit is used as an interfacing device. It is very important to produce the required switching signals to correct the inverter output voltage levels for its performance and also to provide isolation between the control system and the inverter for the adjustment of low and high voltages, which is achieved by the opto-coupler driver circuit.

The controller produces the required gate sequential signals for switching the ON and the OFF of the MOSFETs to generate the output voltages of the inverter. Then, the inverter output voltages are passed through the second order LC low pass filter to reduce the harmonic components as well as to attain the nearest sinusoidal output waveforms i.e. LC filters are used reduce the harmonic distortions by connecting the coupling point as a common for the distribution system. Then, the required inductance 'L' capacitance 'C' values in the time domain are represented as:

$$V_R = L \frac{di(t)}{dt} \tag{6.27}$$

$$i(t) = C \frac{dv(t)}{dt} \tag{6.28}$$

Here: 'V_R' is the receiving end voltage and i(t) is the periodic current of the system. Here, it is suggested to set the cut-off frequency of the filter is chosen to be one or two octaves above the fundamental frequency, here, the input DC voltage small. So it is to be increased in order to meet the inverter requirements. And that is to be given to the isolation transformer in order to provide the supply to the load. Initially, the reference speed is adjusted to 1300 RPM in both conventional and ANFIS based MPPT, SVM controlled methods of the asynchronous motor drive under no-load condition.

The PWM pulses are generated to the inverter by the incremental build with the provision of DC-link voltage. Hence, the drive picks up its speed to the required value by attaining the steady state under no-load condition. The corresponding waveforms of torque (T_e), speed (N_r), flux (ψ_e) and current (I_a) with the conventional and ANFIS based MPPT methods are observed from the digital storage oscilloscope (DSO) as depicted in Fig. 6.31-6.34 along with experimental validation set up diagrams.

Fig. 6.31 PV array practical set up diagrams

Fig. 6.32 Experimental setup diagrams of dSPACE RTI-1104

135
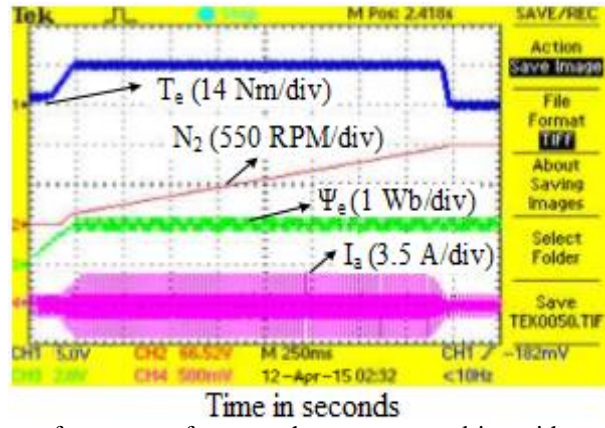
Fig. 6.33 Starting performances of an asynchronous motor drive with conventional method
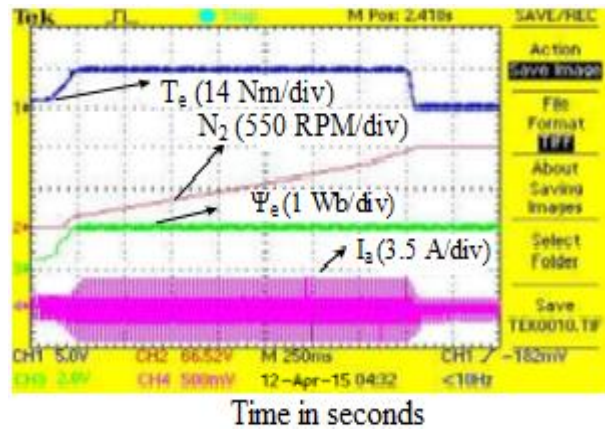
Fig. 6.34 Starting performances of an asynchronous motor drive with ANFIS method

The sudden load of 8 N-m is enacted and released at 0.2s and 0.7s. Then the corresponding modifications in the asynchronous motor drive waveforms are presented in Fig.6.35-6.36. The torque and currents, suddenly rises and falls due to load perturbation. Proposed MPPT has good ripple reduction in the asynchronous motor drive parameters during the load change.
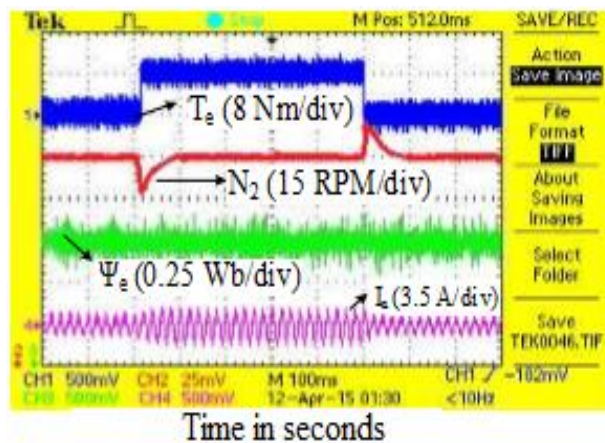
Fig. 6.35 Responses of an asynchronous motor drive with the conventional method, during a sudden
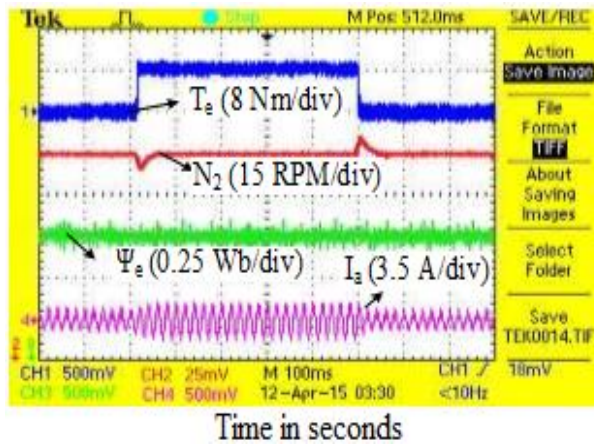
change in load

Fig. 6.36 Responses of an asynchronous motor drive with the ANFIS method, during a sudden change in load

6.10 Performance of an Asynchronous Motor Drive

❖ Rating of the motor drive is available in Appendix-C.

❖ The behavior of an asynchronous motor drive at steady state and step change in the load torque (8 N-m) are observed.

❖ The current and torque ripples obtained are represented as:

Table 6.2 Comparison of current and torque ripple with the conventional and ANFIS methods

Switching frequency	Parameters	*Conventional P&O based MPPT along with SVM*	*AANFIS based MPPT along with SVM*
5 kHz	Current	0.23	0.16
	Torque	0.25	0.17

❖ The ripple content in the current and torque are reduced to 43.75% and 47.05% respectively with the ANFIS based MPPT along with SVM method compared to Conventional P&O based MPPT along with SVM.

❖ Due to this, oscillations in the speed response get decreased with the ANFIS based MPPT and SVM method compared to other two methods.

Table 6.3 Performance of asynchronous motor drive with the comparison of inverter %THD

Switching frequency	Parameter	Conventional MPPT with SVM	ANFIS based MPPT with SVM
	V_{AB}	8.81%	6.21%
5 kHz	V_{BC}	8.62%	6.65%
	V_{CA}	8.62%	6.21%

137

❖ It is observed that the %THD is reduced about 35-42% with the help of ANFIS based MPPT compared to conventional P&O based MPPT and SVM.

6.11 Conclusion

The PV array model with the adaptive neuro fuzzy inference system (ANFIS) based MPPT controller is tested. From this the performance of the asynchronous motor drive is analyzed comparing both conventional and ANFIS MPPT controller. ANFIS based MPPT has improved the tracking efficiency from 92% to greater than 98%. ANFIS based MPPT generates very optimum duty cycle due to which the converters switching of boost converter is provided. By the variations of duty cycle, DC-DC boost converter boosts the PV output voltage and that is fed to the inverter, controlled by the SVM controlling technique. ANFIS based MPPT with SVM overcomes the all non-linearities of the PV system with the variations of temperature and irradiance in a day. It also reduces the ripple contents with minimizing the harmonics in the stator phase current and torques of an asynchronous motor drive. During the steady state, the ripple contents in current and torque with conventional method are as 0.23 and 0.25 respectively. These ripple quantities with ANFIS method are reduced to a large extent and observed as 0.16 and 0.17 respectively.

The ripple content in the current and torque is reduced to 43.75% and 47.05% with the ANFIS based MPPT along with SVM method compared to Conventional P&O based MPPT along with SVM. Due to this, oscillations in the motor drive are reduced with attaining of early steady state and better response of the drive. The performance of the asynchronous motor drive is evaluated by Matlab/Simulink along with experimental implementation. Experimental validations are done with the help of dSPACE RTI-1104 real time controller with the hardware setup. Data acquisition and codes of the successfully simulated model can be linked and loaded directly to the dSPACE RTI-1104 controller for real-time hardware operation. Simulation and practical results are analyzed very neatly. From the obtained results it is well known now that the ANFIS based MPPT has given the very improved performance with reducing of THD and ripples. Thus, the utilization and efficiency of the system is improved much with the ANFIS based MPPT controller along with SVM controlling technique.

CONCLUSIONS AND FUTURE SCOPE

7.1 General Introduction

The part of this thesis reflects the reviewing process about the soft computing based MPPT techniques for the PV system along with space vector modulation (SVM) techniques to the inverter control. This method is implemented to reduce the THD in the outputs of the inverter. An open loop speed control procedure is developed to analyze the performance of an asynchronous motor drive, which is fed from two-level inverter using the modified perturb & observe based MPPT, artificial neural network (ANN) based MPPT, and adaptive neuro fuzzy inference system (ANFIS) based MPPT incorporated with SVM method. Its performance is compared to the above individual methods, with the conventional MPPT based SVM method by the developed matlab-simulation model. Experimental validations are also conducted from that of the dSPACE RTI-1104 controller by the implementation of ANFIS based MPPT along with SVM inverter controlling technique.

7.2 Concluding Remarks

Semiconductor technologies and control methods for adjustable speed drives have been given much priority in industrial applications due to enhanced and improved inverter topologies. Asynchronous motor drives are majorly used as adjustable speed control drives. For these, voltage source inverters (VSI) are chosen as best and standard configurations for the pulse width modulation (PWM) controlled inverter drives compared to current source inverters, because various PWM controlling techniques are proposed for controlling VSI. Out of various techniques, SVM controlling technique is predominantly used for the voltage fed inverter ac drives, because the harmonic content is diminished and also offers the consequent ability to improve the switching in the waveforms compared to other controlling techniques. However, SVM method has the difficulty in getting the complex online computations that usually limits its operation up to few kilohertz of switching frequency. To overcome this problem, inverter is fed with the modified MPPT, ANN based MPPT and ANFIS based MPPT incorporated with SVM, in order to feed the

minimized harmonics and reduced rippled output of inverter to the asynchronous motor drive.

SVM is incorporated with the photovoltaic (PV), MPPT outputs of DC-DC boost converter and inverter to the asynchronous motor drive in order to improve the performance of the asynchronous motor drive in the parameters of the stator phase current, torque and speed. Generally PV system converts only 30-40% of solar irradiation into electricity and that the PV system energy conversion efficiency lies in between 12-20%. Photovoltaic systems are vastly preferred, because of their major benefits like, low maintenance, noise free, eco friendly and also the vast decrement in the photovoltaic cell cost. The growth rate of PV system during the period 2004-2009 was 60% and in 2011 it has been increased to 80%. Since PV system energy conversion efficiency is less (minimum), hence the overall system expenditure has got decreased and to overcome this, high efficiency power converters are designed for extracting maximum possible power from the photovoltaic system. For this, PV array is formed by connecting PV modules in series and parallel combinations in order to yield more output voltage and current. Power generation using this PV system is based on the principle of photoelectric effect. Here, in this, PV array is formed with the 6 modules connected in series and parallel combination i.e. two modules are connected in series combination in order to meet the voltage requirements and such three pair combinations are connected in parallel in order to meet the current requirements. Each module has the capacity of 250 watts by consisting of 60 cells for each panel at which 10 cells are connected in series and such 6 parallel paths are connected in parallel. Each cell open circuit voltage is about 0.7 volts with less than 2 watts of power at open circuit condition. Open circuit voltage of each panel is about 37.98 volts with short circuit current of 8.67 amps.

Solar energy is a vital untapped resource in a tropical country like ours. India plans to produce 20 Giga watts of solar power by 2020. From above explanation, it can be observed that the energy conversion efficiency is very low for the solar PV system, in order to increase the energy conversion efficiency the perturb and observe based maximum power point tracking (MPPT) controlling technique is introduced. MPPT extracts the maximum available power of the PV system with respect to the provided irradiance and temperature. MPPT controllers with the provided algorithm

increases the PV output power by maintaining the maximum power point voltage (V_{MPP}) and maximum power point current (I_{MPP}). This MPPT controller increases the energy conversion efficiency by 80-92%. But, PV array maximum power point changes with climatical conditions. To overcome this drawback and to increase the energy conversion efficiency, the modified perturb and observe based MPPT is introduced. By varying the duty cycle in the duty cycle This MPPT technique increases the energy conversion efficiency of the PV system to 94-98%. With the help of modified MPPT, that the PV array produces the maximum capable power about 1500 watts by having of maximum operating voltage (V_{MPP}) of module is about 30.69 volts and maximum operating current (I_{MPP}) of 8.15 amps. Similarly from the developed matlab-simulation model, that the array produces the maximum power point voltage (V_{MPP}) about 61.38 volts with the open circuit voltage (V_{OC}) of 75.96 volts. Similarly with the maximum power point current (I_{MPP}) about 24.45 amps with the short circuit current (I_{SC}) of 26.01 amps and the maximum power of 1500 watts.

Practical calculations of PV system power validations are also conducted and tabulated out of 252 validations from morning 8:00 am to evening 5:30 pm. Output obtained from the PV system along with MPPT does not get sufficient input supply to feed the asynchronous motor drive. So this PV MPPT output is given to the DC-DC boost converter in order to boost up the output to a higher value, so as to supply the inverter and asynchronous motor drive. Inverter takes the boosted PV output as a input and converts that DC quantity to a AC quantity, as per the requirements of the asynchronous motor load with the proper controlling technique of the inverter. With the help of space vector modulation (SVM) controlling technique, the two level inverter produces the output voltage of 400 volts (line-line) to the motor load. And the performance of the asynchronous motor drive is analyzed with the parameters such that, the stator phase current, the torque and the speed by the comparison of conventional MPPT based SVM to the modified MPPT based SVM. Modified MPPT based SVM gives the better performance of the motor drive by decreasing the ripple content in the stator phase current and torque with minimizing the harmonic content i.e. total harmonic distortions (THD). It is perceived that the ripple content in the stator phase current and torque with the conventional method are 0.38 and 0.32 respectively.

These ripple quantities are reduced to 0.29 and 0.26 respectively for stator phase current and torque. So there is a lot of reduction in the ripple contents with the modified MPPT along with SVM compared to the other existed methods i.e. current ripple 31.03% and torque ripple 23.07% is reduced during starting and 29.62% of torque ripple is reduced during steady state. Similarly, the THD is also minimized with the help of modified MPPT along with SVM controlling technique, i.e. It is observed that the, harmonic values of inverter 3 line-line voltages with the conventional MPPT using SVM are 17.08%, 16.60% and 17.08% respectively. These values with the modified MPPT using SVM are reduced to 14.23%, 14.36% and 14.23% respectively. From this analyzation, it is observed that, the THD is minimized to 15-20% by the modified method compared to that of the conventional method at the switching frequency of 5 KHz. Due to this, the oscillations in the speed response are decreased. Non-linearities in the PV output characteristics could unable to be removed due to the variations in the temperature and irradiance or by the abnormal weather conditions with the MPPT controller. So, to overcome these non-linearities in the PV output voltage-current and voltage-power characteristics, the soft computing based MPPT techniques like ANN based MPPT and ANFIS based MPPT techniques are introduced.

These techniques are also incorporated with the DC-DC boost converter and SVM controlled inverter in order to feed the asynchronous motor drive and to analyze the behavior of the asynchronous motor drive parameters. Values obtained from the modified perturb and observe based MPPT simulation model are given to the ANN based MPPT as input patterns. 73121 epochs are trained with the mean square error value of 0.0002 by the activation function of tan sigmoid. Each neuron is trained effectively with the appropriate weights so as to produce the optimum duty cycle as well as to maintain the linear approximation. Mean square error is introduced in order to minimize the error with the multi layer back propagation technique. ANN based MPPT maintains the maximum power point constantly with the help of optimum duty cycle, though the weather variations occur. Training procedure with the addition of proper weights will be continued during the execution unless until the error is nullified. If not all the input, output patterns are modified with the required weights so as to reach the desired value. After this, the output of PV system with the ANN based MPPT is given to the DC-DC boost converter and that the boosted output is fed to the

two level inverter. Again that the two level inverter is incorporated with the SVM controlling technique in order to reduce the ripple contents and to minimize the harmonics.

Due to this, performance of an asynchronous motor drive is improved much with its parameters like stator phase current, torque and speed. From ANN based MPPT with SVM controlling technique of the inverter it is observed that the ripple contents in the stator phase current and torque with the conventional method are 0.34 and 0.32 respectively. Then these quantities are reduced to 0.25 and 0.23 respectively with the ANN based MPPT along with SVM controlling technique of the inverter, i.e. current ripple is reduced to 36% and torque ripple is reduced to 39.13%. Due to this, oscillations are decreased by attaining of early steady state response along with better the speed response of the motor drive. Similarly the performance of an asynchronous motor drive is also observed with the ANFIS based MPPT along with SVM controlling technique of the inverter. Conversion efficiency for greater than 98% is obtained with ANFIS based MPPT controlling technique. It has very fast and accurate tracking with very low settling time than any other conventional tracking methods. The actual output power from the PV array is calculated by the multiplication of sensed operating voltage and current values, by adding the proper weights while training the MPPT algorithm. ANFIS generates the set of fuzzy rules in order to produce the appropriate output for different values of given input pattern values. Membership function pattern parameters are adjusted or modified till the error value is reduced to a very minimum value.

Once all the pattern parameters of membership function are adjusted, then the ANFIS model becomes the trained model with the supervisor and the network is ready to be used in MPPT control method. The network is trained for 73,121 epochs. The target error is specified or set, in order to maintain the error at 6% and the training execution process gets continued. After completion of the training, it is observed that at 6% error the output of ANFIS matches very close to the actual output. The training stops when either the predefined epoch number or error rate epoch number is obtained. So, that the optimum output from PV system with the ANFIS based MPPT is given to DC-DC converter to boost up the PV output. Boosted DC output is supplied to the two level inverter by the SVM controlling technique.

Due to this, all the non-linearities in the PV output characteristic curves as well as the inverter outputs are to be overcomed by making the linear approximation. And that controlled inverter output of 400 volts line-line voltage is fed to the asynchronous motor drive. Due to this, the parameters enhanced performance of an asynchronous motor drive is analyzed from the developed matlab-simulation model along with the experimental validations. From the simulation execution, it is observed that the ripple contents in the stator phase current and torque are far reduced i.e. 43.75% of current ripple is reduced with that of the torque ripple by 47.05%.

Due to this, better performance of the motor drive is obtained with the reduced oscillations, reaching of better speed response and early steady state. Experimental validations are done with the help of dSPACE RTI-1104 real time controller with the hardware setup. Data acquisition and codes of the successfully simulated model can be linked and loaded directly to the dSPACE RTI-1104 controller for real-time hardware operation. Simulation and the practical results are analyzed very neatly. From the both obtained results it is giving the clear observation that, the ANFIS based MPPT with SVM controlling technique of the inverter has given the very improved performance with reducing of THD, ripples and non-linearities. Thus the utilization and efficiency of the system is improved much with the ANFIS based MPPT controller along with SVM controlling technique.

7.3 Future Scope

Though the important conclusions are stated above, still some more extended research work can be done with the combination of PV MPPT controlling techniques and asynchronous motor drive as

- ❖ SVM controlling techniques can also be implemented with the soft computing techniques along with indirect and direct vector control methods.
- ❖ Multi level inverter topologies can also be implemented for the asynchronous motor drive along with SVM controlling technique of the inverter fed with ANFIS based MPPT PV system.

PUBLICATIONS BASED ON THIS RESEARCH WORK

Refereed International Journal:

1. B. Pakkiraiah and G. Durga Sukumar, "A New Modified MPPT Controller for Improved Performance of an Asynchronous Motor Drive under Variable Irradiance and Variable Temperature," *International Journal of Computers and Applications*-***Taylor & Francis Publisher***, vol.38, no.2-3, (2016), pp.61-74. **(Scopus).**

2. B. Pakkiraiah and G. Durga Sukumar, "Enhanced Performance of an Asynchronous Motor Drive with A New Modified Adaptive Neuro Fuzzy Inference System Based MPPT Controller in Interfacing with dSPACE DS-1104," *International Journal of Fuzzy Systems*-***Springer Publisher***, vol.8, no.6 (2017), pp.1-16. **(SCI-Expanded).**

3. B. Pakkiraiah and G. Durga Sukumar, "Research Survey on Various MPPT Performance Issues to Improve the Solar PV System Efficiency," *Journal of Solar Energy*, vol.2016, no.2016, Article ID 8012432, (2016), pp.1-20, doi:10.1155/2016/8012432. **(EI, INSPEC).**

4. B. Pakkiraiah and G. Durga Sukumar, "A New Modified Artificial Neural Network Based MPPT Controller for the Improved Performance of an Asynchronous Motor Drive," *Indian Journal of Science and* Technology, vol.9, no.45, (2016), pp.1-10. **(Scopus Indexed).**

5. B. Pakkiraiah and G. Durga Sukumar, "A Modified MPPT Controller for Indirect Vector Controlled Induction Motor Drive with Variable Irradiance and Variable Temperature in Interfacing with dSPACE DS-1104," (2017), *Accepted for Journal of Electrical Engineering and Technology*-***JEET***. **(SCI-Expanded).**

International Conference:

6. B. Pakkiraiah and G. Durga Sukumar (2015), "A New Modified MPPT Controller for Solar Photovoltaic System," *2015 IEEE International Conference on Research in Computational Intelligence and Communication Networks (ICRCICN)*, pp. 294-299.

7. B. Pakkiraiah and G. Durga Sukumar (2016), "Isolated Bi-directional DC-DC Converter's Performance and Analysis with Z-Source by Using PWM Control

Strategy," *Accepted for IEEE 3rd International Conference on Electronics and Communication Systems (ICECS-2016), 25-26th February 2016 Conference Proceedings*.

8. B. Pakkiraiah and G. Durga Sukumar (2017), "A New Modified Adaptive Neuro Fuzzy Inference System Based MPPT Controller for the Enhanced Performance of an Asynchronous Motor Drive," *Advancement of Computer Communication & Electrical Technology (ACCET-2016) 21st – 22nd October 2016-**Taylor & Francis CRC Press***, pp.349-356.   **(GOT BEST PAPER AWARD)**

9. B. Pakkiraiah and G. Durga Sukumar (2017), "Survey on Solar Photovoltaic System Performance with Various MPPT Techniques to Improve the Efficiency," *Advancement of Computer Communication & Electrical Technology (ACCET-2016) 21st - 22nd October 2016-**Taylor & Francis CRC Press**,* pp.295-306.

10. K. Pandu Ranga, G. Durga Sukumar, B. Pakkiraiah and M. Subba Rao (2016), "Neuro Fuzzy Based Indirect Vector Control Doubly Fed Induction Generator," *for IICPE 2016 has been accepted and presentation completed in 2016 IEEE Seventh India International Conference on Power Electronics (IICPE-2016)*, held at Thapar University, Patiala, Punjab, India on November 17-19.

11. K. Pandu Ranga, G. Durga Sukumar, B. Pakkiraiah and M. Subba Rao (2016), "Neuro Fuzzy based P_S & Q_S Controller for Doubly Fed Induction Generator with Wind Turbine," *Accepted for IEEE International Conference on Electrical Power and Energy Systems (ICEPES-2016)*, to be held at Maulana Azad National Institute of Technology, Bhopal, Madhya Pradesh on 14th-16th December.

International / National Workshops:

12. B. Pakkiraiah, Three day National Work Shop on, "Advancements in Green Energy and Automation Control of Electrical Power (AGEACEP)," at VFSTRU, Vadlamudi-Andhra Pradesh, held on 16th – 18th October (2014).

13. B. Pakkiraiah, Two day National Workshop on, "Solar Technologies," at VFSTRU, Vadlamudi-Andhra Pradesh, held on 20th -21st August (2015).

14. B. Pakkiraiah, Three day International Pre Conference Tutorial on, "Programming Simulation and Optimization using MATLAB/SIMULINK," at RCCIIT, Kolkata-West Bengal, held on 20th -22nd November (2015).

15. B. Pakkiraiah , Two day International Workshop on " Power Control, Communication and Computational Technologies for Sustainable Growth (PCCCTSG)," at G. Pulla Reddy Engineering College (Autonomous), Kurnool-Andhra Pradesh, held on 11th -12th December (2015).

16. B. Pakkiraiah, Five day Faculty National Workshop on, "Real Time Control of Electrical Machine Drives with dSPACE and FPGA, at VFSTRU, Vadlamudi-Andhra Pradesh, held on 1st -5th June (2016).

17. B. Pakkiraiah, International Conference/Workshop on, "Allied Electrical and Communication Systems (ICAECS), at VFSTRU, Vadlamudi-Andhra Pradesh, held on 8th -10th December (2016).

REFERENCES

A. A. Kulaksiz and O. Aydogdu, "ANN based Maximum Power Point Tracking of Photovoltaic System using Fuzzy Controller", *IEEE innovations in Intelligent Systems and Applications*, (2012), pp.1-5.

A. Al Nabulsi, R. Dhaouadi and H. Rehman, "Single Input Fuzzy Controller (SFLC) based maximum power point tracking", *IEEE Modeling, Simulation and Applied Optimization 4th International Conference on*, (2011), pp.1-5.

A. Al-Amoudi and L. Zhang, "Optimal control of a grid-connected PV system for maximum power point tracking and unity power factor", *in Processing 7th International Conference on power Electronics Variable Speed Drives IEEE*, (1998), pp.80-85.

A. Durgadevi, S. Arulselvi and S. P. Natarajan, "Photovoltaic Modeling and Its Characteristics", *IEEE Emerging Trends in Electrical and Computer Technology*, (2011), pp.469-475.

A. F. Cupertino, J. T. De Resende, H. A. Pereira and S. I. Seleme Junior, "A Grid Connected Photovoltaic System with A Maximum Power Point Tracker using Passivity based Control Applied in a Boost Converter", *IEEE Transactions on Industrial Applications*, (2012), pp.1-8.

A. Iqbal, H. Abu-Rub and S. M. Ahmed, "Adaptive Neuro-Fuzzy Inference System based Maximum Power Point Tracking of a Solar PV Module," IEEE Energy Conference and Exhibition, (2010), pp.51-56.

A. Mbarushimana and Xin Ai, "Real time digital simulation of PWM converter control for grid integration of renewable energy with enhanced power quality," *IEEE Electric Utility Dereglation and Restructing and Power Technologies (DRPT)*, (2011), pp.712-718.

A. Mellit and S. A. Kalogirou, "Neuro-Fuzzy based Modeling for Photovoltaic Power Supply System", *IEEE Power Energy Conference*, (2006), pp.88-93.

A. Mellit, A. Hadjarab, N. jhorissi and H. Salhi, "An ANFIS based forecasting for solar radiation data from sunshine duration and ambient temperature", *IEEE Transactions on Power Engineering*, (2007), pp.1-6.

A. O. Ibrahim and O. Basir, "A Novel Sensor Less Support Vector Regression Based Multi Stage Algorithm to Track the Maximum Power Point for Photovoltaic Systems", *IEEE Power and Energy Society General Meeting*, (2013), pp.1-5.

A. Safari and S. Mekhilef, "Simulation and hardware implementation of incremental conductance MPPT with direct control method using Cuk converter", *IEEE Transactions on Industrial Electronics*, (2011), 58, pp.1154-1161.

A. Trejos, C. A. Ramos-Paja and S. Serna, "Compensation of DC link voltage oscillations in grid connected PV systems based on high order DC/DC converters", *IEEE Alternative Energies and Energy Quality,* (2012), pp.1-6.

A. Yafaoui, B. Wu and R. Cheung, "Implementation of maximum power point tracking algorithm for residential photovoltaic systems", *in proceedings of the 2nd Canadian Solar Building Conference*, (2007).

Ajay Patel, Vikas Kumar and Yogendra Kumar, "Perturb and observe maximum power point tracking for Photovoltaic cell", *International Conference on research trends in applied sciences with Engineering Applications*, (2013), 4(6).

C. Bo-Chiau and L. Chun-Liang, "Implementation of maximum power point tracker for photovoltaic arrays", *in 6th IEEE Conference on Industrial Electronics and Applications (ICIEA)*, (2011), pp.1621-1626.

C. Liu, B. Wu and R. Cheung, "Advanced Algorithm for MPPT Control of Photovoltaic Systems", *Canadian Solar Buildings Conference*, (2004).

C. Liu, K. T. Chau and X. Zhang, "An efficient wind photovoltaic hybrid generation system using doubly excited permanent magnet brushless machine", *IEEE Transactions on Industrial Electronics*, (2010), 53(3), pp.831-839.

C. Sreeja and S. Arun, "A novel control algorithm for three phase multilevel inverter using SVM," *IEEE PES Innovative Smart Grid Technologies-India (ISGT India)*, (2011), pp.262-267.

Chia Seet chin, Yit Kwong Chin, Bih Lii Chua, A. Kiring, and K. T. K. Teo, "Fuzzy logic based MPPT for PV array under partially shaded conditions", *IEEE Transactions on advanced computer science applications and Technologies*, (2012), pp.133-138.

Chian-Song Chiu and Ya-Lum Ouyang, "Robust maximum power point tracking control of uncertain photovoltaic systems: A unified T-S Fuzzy model based approach sensor less maximum power point tracking control in wind energy generation using permanent magnet synchronous generator", *IEEE Transactions on Control Systems Technology*, (2011), 19(6), pp.1516-1526.

Dong Hwa Kim, "GA-PSO based vector control of indirect three phase induction motor," *Elsevier Science Direct Applied Soft Computing*, (2007), 7(2), pp.601-611.

Durga Sukumar, Jayachandranath Jitendranath, Suman Saranu, "Three-level Inverter-fed Induction Motor Drive Performance Improvement with Neuro-fuzzy Space Vector Modulation," *Electrical Power Components and Systems*, (2014), 42(15), pp.1633-1646.

E. Koutroulis, K. Kalaitzakis and N. C. Voulgaris, "Development of a Micro controller-based photovoltaic maximum power point tracking control system", *IEEE Transactions on Power Electronics*, (2001), pp.46-54.

E. Michael Ropp and S. Gonzalez, "Development of a MATLAB/Simulink Model of a Single-Phase Grid-Connected Photovoltaic System", *IEEE Energy Conversion*, (2009), pp.195-202.

Fangrui Liu, Yong Kang, Y. U. Zhang and Shaxu Duan, "Comparison of P&O and Hill Climbing MPPT Methods for Grid Connected PV Converter", *Industrial Electronics and Applications IEEE 3rd conference*, (2008), pp.804-807.

G. Brando, A. Dannier and R. Rizzo, "A Sensor Less Control of H-bridge Multilevel Converter for Maximum Power Point Tracking in Grid Connected Photovoltaic Systems", *IEEE Transactions on Clean Electrical Power*, (2007), pp.789-794.

G. H. Yordanov, O. M. Midtgard and T. O. Saetre, "Ideality factor behavior between the maximum power point and open circuit", *IEEE Photovoltaic Specialists Conference*, (2013), pp.0729-0733.

G. Petrone, G. Spagnuolo and M. Vitelli, "A Multivariable Perturb and Observe Maximum Power Point Tracking Technique Applied to a Single Stage Photovoltaic Inverter", *IEEE Transactions Industrial Electronics*, (2011), 58(1), pp.76-84.

G. Spiazzi, S. Buso and P. Mattavelli, "Analysis of MPPT Algorithms for Photovoltaic Panel Based on Ripple Correlation Techniques in Presence of Parasitic Components", *IEEE Power Electronics Conference*, (2009), pp.88-95.

Guo Xiao Yun, Chen jinmei and Liu Qihui, "Real-time and grid connected control of PV power system", *IEEE Advanced Power System Automation and Protection*, (2011), 2, pp.923-928.

H. A. B. Siddique, S. M. Ali and R. W. De Doncker, "DC Collector Grid Configurations for Large Photovoltaic Parks", *IEEE Power Electronics and Applications*, (2013), pp.1-10.

H. Afghoul, F. Krim and D. Chikouche, "Increase the photovoltaic conversion efficiency using Neuro-Fuzzy control applied to MPPT", *IEEE Renewable and Sustainable Energy Conference*, (2013), pp.348-353.

H. Al-Bahadili, H. Al-Saadi, R. Al-Sayed and M. A. S. Hasan, "Simulation of: Maximum Power Point Tracking of Information Technology", *Renewable Energy Processes and Systems*, (2013), pp.79-84.

H. Patel and V. Agarwal, "MPPT Scheme for a PV-fed single phase single stage grid connected inverter operating in CCM with only one current sensor", *IEEE Transactions on Energy Conversion*, (2009), 24(1), pp.256-263, 2009.

H. Radwan, and M. Orabi, "The Non Ideality Effect of Optimizing the P&O MPPT Algorithm for Stand Alone Applications", *IEEE Telecommunications Energy Conference*, (2012), pp.1-7.

H. Saadat, "Power System Analysis," *2nd edition, McGraw-Hill*, (2004), New York, NY, USA.

Hong Hee Lee, Le Minh Phuong, Phan Quoc Dzung, Nguyen Truong Dan Vu and Le Dinh Khoa, "The New Maximum Power point Tracking Algorithm using ANN-based Solar PV Systems", *IEEE TENCON 2010*, (2010), pp.2179-2184.

I. K. Song, "Simulation and analysis of existing MPPT control methods in a PV generation system", *Journal of International Council Electrical Engineering*, (2011), 1(4), pp.446-451.

J. Appelbaum, "The Quality of Load Matching in a Direct Coupling Photovoltaic System", *IEEE Transactions on Energy Conversion*, (1987), 2(4), pp.534-541.

J. Huusari and T. Suntio, "Interfacing Constraints of Distributed Maximum Power Point Tracking Converters in Photovoltaic Applications", *IEEE Power Electronics and Motion Control Conference*, (2012), pp.DS3d.1-1-DS3d.1-7.

J. J. Joshi, P. Karthick and R. S. Kumar, "A solar panel connected multilevel inverter with SVM using fuzzy logic controller," *IEEE International Conference on Energy Efficient Technologies for Sustainability (ICEETS)*, (2013), pp.1201-1206.

J. M. Enrique, J. M. Andujar and M. A. Bohorquez, "A reliable, fast and low maximum power point tracker for photovoltaic applications", *Solar Energy*, (2010), 84(1), pp.79-89.

J. M. Kwon and K. H. Nam, "Grid connected photovoltaic multi string PCS with PV current variation reduction control", *IEEE Transactions on Industrial Electronics*, (2009), 56(11), pp.4381-4388.

J. Selvaraj and N. A. Rahim, "Multilevel inverter for grid- connected PV system employing digital PI controller," *IEEE Transaction on Industrial Electronics*, (2009), 56(1), pp. 149-158.

J. Suganya, and M. Carolin Mabel, "Maximum Power Point Tracking for a Photovoltaic System", *IEEE Computing, Electronics and Electrical technologies*, (2012), pp.463-465.

Jinbang Xu, Anwen Shen, Cheng Yang, Wenpei Rao and Xuan Yang, "ANN based on Incremental Conductance Algorithm for MPP Tracker", *IEEE Bio-Inspired Computing: Theories and Applications (BIC-TA)*, (2011), pp.129-134.

Jun Pan, Chenghua Wang and Feng Hong "Research of Photovoltaic Charging System with Maximum Power Point Tracking", *IEEE Transaction on Electronic Measurement and Instruments*, (2009), pp.4-471-4-481.

K. Y. Khouzam and P. Groumpos, "Optimum Matching of Ohmic Loads to the Photovoltaic Array", *Solar Energy*, (1991), 46(2), pp.101-108.

K. Y. Khouzam, "Optimum Load Matching in Direct Coupled Photovoltaic Power Systems Applications to Resistive Loads", *IEEE Transactions on Energy Conversion*, (1990), 5(2), pp.265-271.

K. Yamauchi, "Incremental Learning on a budget and its application to quick maximum power point tracking of photovoltaic systems", *IEEE Soft Computing and Intelligent Systems Joint 6th International Symposium on Advanced intelligent Systems, 2012 joint International Conference on*, (2012), pp.71-78.

Kok Soon Tey and Saad Mekhilef, "Modified Incremental Conductance MPPT Algorithms to Mitigate Inaccurate Responses under Fast-changing Solar Irradiation Level", *Power Electronics and Renewable Energy Laboratory PEARL, Science Direct Solar Energy (101)*, (2014), pp.333-342.

L. Ciabattoni, M. Grisostomi, G. Ippoliti and S. Longhi, "Neural Networks based Home Energy Management System in Residential PV Scenario", *IEEE Photovoltaic Specialists Conference*, (2013), pp.1721-1726.

L. Cristald, M. Faifer, M. Rossi and S. Toscani, "MPPT Definition and validation a new model based approach", *IEEE Instrumentation and Measurement Technology Conference*, (2012), pp.594-599.

L. Fangrui, D. Shanxu, L. Fei, L. Bangyin and K. Yong, "A variable step size Incremental Conductance MPPT", *IEEE Transactions on Industrial Electronics*, (2008), 55, pp.2622-2628.

L. M. Elobaid, A. K. Abdelsalam and Zakzouk, "Artificial Neural Network Based Maximum Power Point Tracking Technique for PV Systems", *38th Annual Conference on IEEE Industrial Electronics Society*, (2012), pp.937-942.

L. Piegari and R. Rizzo, "Adaptive perturb and observe algorithm for Photovoltaic maximum power point tracking", *IET Renewable Power Generation*, (2010), 4(4), pp.317-328.

L. Zhang, A. Al-amoudi and Y. Bai, "Real time maximum power point tracking for grid connected photovoltaics systems", *in processing 8th International Conference Power Electronics Variable Drives IEEE*, (2000), pp.124-129.

Lian jiang, D. R. Nayanasiri, D. L. Maskell and D. M. Vilathgamuwa, "A Simple and Efficient Hybrid Maximum power point tracking method for PV systems under partially shaded condition", *IEEE Industrial Electronics Society*, (2013), pp.1513-1518.

Lian Jiang, D. R. Nayanasri, D. L. Maskell and D. M. Vilathgamuwa, "A Simple and Efficient Hybrid Maximum Power Point tracking Method for PV Systems Under Partially Shaded Conditions", *IEEE Industrial Electronics Society*, (2013), pp.1513-1518.

Liang-Rui Chen, Chih-Hui Tsai, Yuai-Li Lin and Yen-Shin Lai, " A Biological Swarm Chasing Algorithm for Tracking the PV Maximum Power Point Energy conversion", *IEEE Transactions on Energy Conversion,* (2010), 25(2), pp.484-493.

Lili Han and Lanying Jia, "Photovoltaic Power Generation System MPPT", *IEEE Advanced Computational Intelligence*, (2012), pp.919-922.

Long Jie and Chen Ziran, "Research on the MPPT Algorithms for Photovoltaic System Based on PV Neural Network", *IEEE Control and Decision Conference*, (2011), pp.1851-1854.

M. Adly, M. Ibrahim and H. El Sherif, "Comparative Study of Improved Energy Generation Maximization Techniques for Photovoltaic Systems", *IEEE Power and Energy Engineering Conference*, (2012), pp.1-5.

M. Aleenejad, H. Iman-Eini and S. Farhangi, "A minimum loss switching method using space vector modulation for cascaded H-bridge multilevel inverter," IEEE *20th International Conference on Electrical Engineering (ICEE)*, (2012), pp.546-551.

M. I. Hossain, S. A. Khan, M. Shafiullah and M. J. Hossain, "Design and Implementation of MPPT Controlled Grid Connected Photovoltaic System", *IEEE Computers and informatics (ISCI) 2011 IEEE Symposium on*, (2011), pp.284-289.

M. M. Saied and M. G. Jaboori, "Optimal Solar Array Configuration and DC Motor Field Parameters for Maximum Annual Output Mechanical Energy", *IEEE Transactions on Energy Conversion*, (1989), 4(3), pp.459-465.

M. Qiang, S. Mingwei, L. Liying and J. M. Guerrerro, "A novel improved variable step-size incremental-resistance MPPT method for PV systems", *IEEE Transactions on Industrial Electronics*, (2011), 58, pp.2427-2434.

M. Quamuzzam and K. M. Rahaman, "A Modified Perturb and Observe Maximum Power Point Tracking Technique for Single Stage Grid Connected Photovoltaic Inverter", *WSEAS transaction on power systems*, (2014), 9.

M. Sheraz, and M. A. Abido, "An Efficient MPPT Controller using Differential Evolution and Neural Network", *IEEE Power and Energy (PECon)*, (2012), pp.378-383.

M. Tauseef and E. Nowiki, "A Simple and Cost Effective Maximum Power Point Tracker for PV Array Employing as Novel Constant Voltage Technique", *IEEE Electrical and Computer Engineering*, (2012), pp.1-4.

N. A. Azli, Z. Salam, A. Jusoh, M. Facta, B. C. Lim and S. Hossain, "Effect of fill factor on the MPPT performance of a grid-connected inverter under Malaysian conditions", *in proceedings of the 2nd IEEE International Power and Energy conference (PECon-08)*, (2008), pp.460-462.

N. M. Razali, and N. A. Rahim, "DSP-Based Maximum Peak Power Tracker using P&O Algorithm", *Clean Energy and Technology IEEE First Conference on*, (2011), pp.34-39.

Nguyen Gia Minh Thao and K. Uchida, "Control the Photovoltaic Grid-Connected System Using Fuzzy Logic and Backstepping Approach", *IEEE Control Conference*, (2013), pp.1-8.

Nian Zhang, P. K. Behera and C. Williams, "Solar Radiation Prediction Based on Particle Swarm Optimization and Evolutionary Algorithm using Recurrent Neural Networks", *IEEE Systems Conference*, (2013), pp.280-286.

Nicola Femia Giovanni Spagnuolo and Massimo Vitelli, "Optimization of Perturb and Observe Maximum Power Point Tracking Method", *IEEE Transactions on Power Electronics*, (2005), 20(4), pp.963-973.

O. Cigdem, E. Kayacan and O. Kaynak, "Experimental Study of an Interval Type-2 Fuzzy Neural Network using Sliding-Mode Online Learning Algorithm", *IEEE Control Conference*, (2011), pp.1181-1186.

P. Mattavelli, S. Saggini, E. Orietti and G. Spiazzi, "A Simple Mixed-Signal MPPT Circuit for Photovoltaic Applications", *IEEE Applied Power Electronics Conference and Exposition (APEC)*, (2010), pp.953-960.

Phan Quoc Dzung, Le Dinh Khoa, Hong Hee Lee, Le Minh Phuong and Nguyen Truong Dan Vu, "The New MPPT Algorithm Using ANN-Based PV", *IEEE Strategic Technology (IFOST)*, (2010), pp.402-407.

Q. Kou, S. A. Klein and W. A. Beckman, "A Method for Estimating the Long Term Performance of Direct Coupled PV Pumping Systems", *Solar Energy*, (1998), 64(1), pp.33-40.

R. B. A. Koad and A. F. Zobaa, "Comparative Study of Five Maximum Power Point Tracking Techniques for Photovoltaic Systems," International Journal on Energy Conversion (IRECON), (2014), 2 (1), 17-25.

R. Giral, C. A. Ramos-Paja, D. Gonzalez, J. Calvente, A. Cid-Pastor and L. Martinez-Salamero, "Minimizing the effects of shadowing in a PV module by means of active voltage Sharing", *IEEE Industrial Technology*, (2010), pp.943-948.

R. Khadri, J. P. Gaubert and G. Champenois, "An Improved Maximum Power Point Tracking for Photovoltaic Grid-Connected Inverter based on Voltage-Oriented control", *IEEE Transactions on industrial Electronics*, (2011), 58(1), pp.66-75.

R. Ramaprabha, B. L. Mathur and M. Sharanya, "Solar Array Modeling and Simulation of MPPT using Neural Network", *IEEE Transactions on Control, Automation, Communication and Energy and Conservation*, (2009), pp.1-5.

Roberto Faranda and Sonia Leva, "Energy Comparison of MPPT techniques for PV systems", *WSEAS Transactions on Power Systems*, (2008), 3.

S. A. Khan and M. I. Hossain, "Design and Implementation of Microcontroller Based Fuzzy Logic Control for Maximum Power Point Tracking", *IEEE International Conference on Electrical and Computer Engineering*, (2010), pp.322-325.

S. Chin, J. Gadson and K. Nordstrom, "Maximum power point tracker", *Tufts University Department of Electrical Engineering and Computer Science*, (2003), pp.1-66.

S. D. Anitha and S. B. J. Prabha, "Artificial Neural Network based Maximum Power Point Tracker for photovoltaic System", *IEEE Sustainable Energy and Intelligent Systems*, (2011), pp.130-136.

S. Duryea, S. Islam and W. Lawrance, "A Battery Management System for Stand-Alone Photovoltaic Energy Systems", *IEEE Industrial Applications Magazine*, (2001), 7(3), pp.67-72.

S. Hadjammar and F. Bouchafaa, "Performance of PV System Connected to the Grid with MPPT Controlled by Fuzzy control", *IEEE Transactions on Smart Energy Grid Engineering*, (2013), pp.1-7.

S. Kamaruzzaman, "Optimization of a Stand- Alone wind/PV Hybrid System to Provide Electricity for a household in Malaysia", *Proceedings of 4th IASME/WSEAS International Conference on Energy and Environment*, (2009), pp.435-438.

S. Kazmi, H. Goto, O. Ichiokura and H. J. Guo "An Improved and very efficient MPPT controller for PV systems subjected to rapidly varying atmospheric conditions and partial shading", *in Proceedings of the Power Engineering Conference*, (2009), pp.1-6.

S. Mekhilef and N. A. Rahim, "Xilinx FPGA based three-phase PWM inverter and its application for utility connected PV system," *in Proceedings of the IEEE*

Region 10 Conference on Computers, Communications, Control and Power Engineering (TENCON '02), (2002), pp. 2079-2082.

S. Patel and W. Shireen, "Fast converging digital MPPT control for Photovoltaic applications", *IEEE power and Energy Society General Meeting*, (2011), pp.1-6.

S. Sreekumar and A. Benny, "Maximum Power Point Tracking of Photovoltaic System using Fuzzy Logic Controller based Boost Converter", *IEEE Current Trends In Engineering and Technology (ICCTET)*, (2013), pp.275-280.

Shun-Feng Su, Yao-Chu Hsueh, Cio-Ping Tseng, Song-Shyong Chen, and Yu-San Lin, "Direct Adaptive Fuzzy Sliding Mode Control for Under-actuated Uncertain Systems," *International Journal of Fuzzy Logic and Intelligent Systems*, (2015), 15(4), pp.240-250.

Subiyanto, A. Mohamed and M. A. Hanna, "Maximum Power Point Tracking in Grid Connected PV System using a Novel Fuzzy Logic Controller", *IEEE transactions on Research and Development*, (2009), pp.349-352.

Subramanian Krithiga, Nanjappa Gounder and Ammasai Gounden "Power Electronic Configuration for the Operation of PV systems in Combained Grid-Connected and Stand Alone modes", *IET Power Electronics*, (2014), 7(3), pp.640-647.

T. D. Hund and B. Thomson, "Amp-Hour Counting Charge control for Photovoltaic Power Systems", *26th IEEE Photovoltaic Specialists Conference*, (1997), pp.1281-1284.

T. H. Tuffaha, M. Babar, Y. Khan and N. H. Malik, "Comparative study of different hill climbing MPPT through simulation and experimental test bed", *Research Journal of Applied sciences, engineering and technology*, (2014), pp.4258-4263.

W. Libo, Z. Zhengming and L. Jianzheng, "A single stage three phase grid connected photovoltaic system with modified MPPT method and reactive power compensation", *IEEE Transactions on Energy Conversion*, (2007), 22(4), pp.881-886.

Wang Nian Chun, WU MeiYue and Shi GuoSheng, "Study on characteristics of photovoltaic cells based on Matlab Simulation", *IEEE Power and Energy Engineering Conference*, (2011), pp.1-4.

Weiping Luo and Gujing Han, "Tracking and Controlling of Maximum Power Point Application in Grid Connected Photovoltaic Generation System", *IEEE Knowledge acquisition and Modeling*, (2009), 3, pp.237-240.

Xiaojin Wu, Zhiqiang Cheng and Xueye Wei, "A study of maximum power point tracking in novel small-scale photovoltaic LED lighting systems", *IEEE Artificial Intelligence and Computational Intelligence*, (2009), pp.40-43.

Y. Zhou, F. Liu, J. Yin and S. Duan, "Study on realizing MPPT by Improved Incremental Conductance Method with variable step size", *in 3rd IEEE Conference on Industrial Electronics and Applications*, (2008), pp.547-550.

Yi-Hsun Chiu, Yi-Feng Luo, Jia-Wei Huang and Yi-Hua Liu, "An ANN-based Maximum Power Point Tracking Method for Fast Changing Environments", *IEEE Soft Computing and Intelligent System (SCIS) and 13th International Symposium on advanced Intelligent system (ISAIS), 2012 joint International Conference on* (2012), pp.715-720.

Youngseok Jung, junghun So, Gwonjong Yu and J. Choi, "Improved perturbation and observation method of MPPT control for photovoltaic power systems", *IEEE Photovoltaic Specialists Conference*, (2005), pp.1788-1791.

Yuan Wang, Hongming Yang, Anjun Li and Yingxiang wang, "Research of photovoltaic and PHEV hybrid management based on hierarchical fuzzy control", *Electrical Engineering Computing Science and Automatic Control*, (2011), pp.1-5.

Z. Salam, T. L. Soon and M. Z. Ramil, "Hardware implementation of the high frequency link inverter using the dSPACE DS-1104 digital signal processing board," *in proceedings of the 1ˢᵗ International Power Energy Conference (PECon'06)*, (2006), pp.348-352.

Zhao Yong, Li Hong, Liu Liqun and Gao XiaoFeng, "The MPPT Control Method BY using BP Neural Networks on PV Generating Systems", *IEEE Transactions on Industrial Control and Electronics Engineering*, (2012), pp.1639-1642.

Zhigang Liang, A. Q. Huang and Rong Guo., "High Efficiency Switched Capacitor Buck-Boost Converter for PV Applications", *IEEE Applied Power Electronics Conference and Exposition*, (2012), pp.1951-1958.

BIBLIOGRAPHY

A. O. Ibrahim and O. Basir, "A Novel Sensor Less Support Vector Regression Based Multi Stage Algorithm to Track the Maximum Power Point for Photovoltaic Systems," IEEE Power and Energy Society General Meeting, (2013), pp.1-5.

A. P. Mark, G. C. R. Irudayaraj, R. Vairamani and K. Mylsamy, "Dynamic Performance Analysis for Different Vector-Controlled CSI-Fed Induction Motor Drives," Journal of Power Electronics, (2014), 14 (5), 989-999.

A. Panda, M. K. Pathak and S. P. Srivastava, "Solar direct torque controlled induction motor drive for industrial applications," International Journal of Renewable Energy Research, (2013), 3(4), pp.794-802.

Anil Chandrakanth S, Thanga Raj Chelliah and S. P. Srivastava, "Efficiency Determination of Induction Motor and its Sensitivity Analysis towards Parameter Variation," Int. Journal of Artificial Intelligence and Soft Computing, (2014), 4(2-3), pp.144-163.

B. Chokkalingam and J. L. Munda, "Simplified SVPWM for Z Source T-NPC-MLI including neutral point balancing," 2016 IEEE Symposium on Computer Applications & Industrial Electronics (ISCAIE), Penang, (2016), pp.132-138.

Bhim Singh, Man Mohan & S. P. Srivastava, "Experimental Investigations on Starting of Inverter fed cage motor ," Journal of Electric Machines & Power System (USA), (1995), 23(2), pp.119-140.

C. Bharatiraja, J. L. Munda, R. Bayindir and M. Tariq, "A common-mode leakage current mitigation for PV-grid connected three-phase three-level transformer less T-type-NPC-MLI," 2016 IEEE International Conference on Renewable Energy Research and Applications (ICRERA), Birmingham, (2016), pp.578-583.

C. N. Arun kumar. M, M. Kaliamoorthy, P. Brindha and V. Rajasekaran, "A novel single-phase cascaded h-bridge inverter with new cell configuration and reduced power electronics components with low THD," International Journal of Research in Engineering and Technology, (2014), 3 (7), pp.523-530.

C. Thanga Raj, S. P. Srivastava and P. Agarwal, "Energy efficient control of three phase induction motor- A review ," Int. journal of computer and electrical engg., IJCEE, Singapore, (2009), 1(1), pp.61-70.

D. M. Vinod Kumar, "Fast Approach to Artificial Neural Network Training and its Applications to Economic Load Dispatch," Electric Machines and Power Systems (USA), (1995), 23(1), pp. 13-24.

D. M. Vinod Kumar, "Power System Network Topology Processing based on Artificial Neural Networks," Electric Machines and Power Systems (USA), (1998), 26(3), pp.249-263.

D. M. Vinod Kumar, "Power System State Forecasting using Artificial Neural Networks," Electric Machines and Power Systems (USA), (1999), 27(6), pp.653-664.

D. M. Vinod Kumar, "Topology Processing and Static State Estimation using Artificial Neural Networks," IEE Proceedings-Generation, Transmission and Distribution, (1996), 143(1), pp.99-105.

Dharmasa, "Cost Effective Analysis of Solar and Wind Power in Oman", The union of Electronics and Electrical Engineering and Telecommunication, Bulgaria, `EU, (2013), 48(5-6), 1-14.

E. K. Appiah, A. A. Jimoh, A. S. O. Ogunjuyigbe and J. L. Munda, "Dynamic and steady state performance of higher phase order (HPO) squirrel cage induction machine," 2014 16th International Power Electronics and Motion Control Conference and Exposition, Antalya, (2014), pp.466-471.

G. H. Yordanov, O. M. Midtgard and T. O. Saetre, "Ideality factor behaviour between the maximum power point and open circuit," IEEE Photovoltaic Specialists Conference, (2013), pp.0729-0733.

Gan Dong and Olorunfemi Ojo, "Efficiency Optimizing Control of Induction Motor Using Natural Variables," IEEE Transactions on Industrial Electronics, (2006), 53(6), pp.1791-1798.

H. A. B. Siddique, S. M. Ali and R. W. De Doncker, "DC Collector Grid Configurations for Large Photovoltaic Parks," IEEE Power Electronics and Applications, (2013), pp.1-10.

H. Chaieb and A. Sakly, "Comparison between P&O and P.S.O methods based MPPT algorithm for photovoltaic systems," 2015 16th International Conference on Sciences and Techniques of Automatic Control and Computer Engineering (STA), Monastir, (2015), pp. 694-699.

J. Leuchter, V. Rerucha and A. F. Zobaa, "Mathematical modelling of photovoltaic systems," Proceedings of 14th International Power Electronics and Motion Control Conference EPE-PEMC 2010, Ohrid, (2010), pp.S4-1-S4-4.

K. Kusakana, J. L. Munda and A. A. Jimoh, "Feasibility study of a hybrid PV-micro hydro system for rural electrification," AFRICON 2009, Nairobi, (2009), pp.1-5.

K. Tejne Sachin, and S. P. Srivastava, "Comparative performance analysis of vector controlled induction motor drive for neural controller and DSP implemented PI controller," IEEE international conf on comm. systems and network technologies (CSNT),11-13 May 2012,Rajkot(India), (2012), pp.274-281.

L. K. Letting, J. L. Munda and A. Hamam, "Particle swarm optimized T-S fuzzy logic controller for maximum power point tracking in a photovoltaic system," 2010 Conference Proceedings IPEC, Singapore, (2010), pp.89-94.

Lili Han and Lanying Jia, "Photovoltaic Power Generation System MPPT," IEEE Advanced Computational Intelligence, (2012), pp.919-922.

M. Hala Mohamed Abdel, Z. Ahmed Faheem, R. Mohamed Helmy Abdel, "Temperature effects on the electrical performance of large area multicrystalline silicon solar cells using the current shunt measuring technique.", Engineering Journal, (2010), 2(11), pp.888-894.

M. Kaliamoorthy, R. M. Sekar and I. Gerald Christopher Raj, "Solar powered single stage boost inverter with ANN based MPPT algorithm," 2010 INTERNATIONAL CONFERENCE ON COMMUNICATION CONTROL AND COMPUTING TECHNOLOGIES, Ramanathapuram, (2010), pp.165-170.

M. Kaliamoorthy, V. Rajasekaran and G. PraveenRaj, "A novel single phase cascaded multilevel inverter for hybrid renewable energy sources," 2015 International Conference on Advanced Computing and Communication Systems, Coimbatore, (2015), pp.1-10.

M. Kaliamoorthy, V. Rajasekaran and I Gerald Christopher Raj, "Single-phase fifteen-level grid-connected inverter for photovoltaic system with evolutionary programming based MPPT algorithm," Solar Energy, (2014), 105, pp.314-329.

M. Venkatesan, R. Rajeshwari, N. Deverajan, and M. Kaliyamoorthy, "Comparative Study of Three Phase Grid Connected Photovoltaic Inverter Using PI and Fuzzy Logic Controller with Switching Losses Calculation," International Journal of Power Electronics and Drive Systems, (2016), 7 (2), 543-550.

Madhusudan Singh, Bhim Singh and A. K. Tandon, "Transient performance of Series Compensated Three-Phase Self-Excited Induction Generator", in IEEE Petroleum & Chemical Industry Conference (PCIC'04), New Delhi, (2004), Nov.9-10.

Madhusudan Singh, Bhim Singh and A. K. Tandon, "Experimental Investigations on VAR Requirement of three Phase Self-Excited Induction Generator Driven by Variable Speed Prime Mover", Proceeding of International Conference on Energy and Environmental Technologies for Sustainable Development, (2003), October, 8-10.

Madhusudan Singh, Bhim Singh, and A. K. Tandon "Steady State and Transient Characteristics of Three Phase Self-Excited Induction Generator Driven by Variable Speed Prime Mover", Proceeding of All India Jasmia Electrical Engineering Conference, (2003), August, 16-17.

Olorunfemi Ojo and I. E. Davidson, "PWM-VSI Assisted Stand-alone Dual Stator Winding Induction Generator," IEEE Trans. on Industry Applications, (2000), 36(6), pp.1604-1611.

Olorunfemi Ojo, "The Generalized Discontinuous PWM Modulation Scheme for Three-Phase Voltage Source Inverters," IEEE Trans. on Industrial Electronics, (2004), 51(6), pp.1280-1289.

Olorunfemi Ojo, Obasohan Omozusi, A. Ginart and B. Gonoh, "The Operation of a Stand-Alone, Single-Phase Induction Generator Using a Single-Phase, Pulse-Width Modulated Inverter with a Battery Supply," IEEE Transactions on Energy Conversion, (1999), 14(3), pp.526-531.

Olorunfemi Ojo, Sheetal Asuri, Gan Dong and Z. Wu, "Control of Induction Motor Drive Fed with a Single-Phase Sparse PWM Rectifier- Inverter," IEE Proceedings – Electrical Power and Applications, (2005), 152(3), pp. 526-534.

Olorunfemi Ojo, Zhiqiao Wu and Gan Dong, "High Performance Speed-Sensorless Control of an Induction Motor Drive Using a Minimalist Single-Phase PWM converter," IEEE Transactions on Industry Applications, (2005), 41 (4), pp. 996-1004.

P. Palanivel, S. S. Dash, N. Chellammal, AF Zobaa, "Performance Analysis of Three Phase Multilevel Inverters Using Sinusoidal Pulse Width Modulation with Zero Sequence Signal," International Review of Electrical Engineering, (2011), 6 (2), pp.1-6.

P. Parthiban, P. Agarwal and S.P. Srivastava, "A simplified Space-Vector Modulated Control Scheme for CSI fed IM Drive," 3D-21,IEEE International Conf. Power Electronics, Electric Drive and Energy System, PEDES-2006, held at IIT Delhi on 12-15 Dec. 2006, (2006), pp.1-6.

R. Giral, C. A. Ramos-Paja, D. Gonzalez, J. Calvente, A. Cid-Pastor and L. Martinez-Salamero, "Minimizing the effects of shadowing in a PV module by means of active voltage Sharing," IEEE Industrial Technology, (2010), pp.943-948.

R. Billinton, B. Karki, R. Karki, Ramakrishna Gokaraju, "Operating Reserve Assessment of Wind Integrated Power Systems,"CIGRE Canada Conference on Power Syste ms, Winnipeg, (2008), pp.1-6.

R. B. A. Koad, A. F. Zobaa, A. El-Shahat, "A novel MPPT algorithm based on particle swarm optimization for photovoltaic systems," IEEE Transactions on Sustainable Energy, (2017), 8 (2), 468-476.

T. R. Ayodele, A. A. Jimoh, J. L. Munda and J. T. Agee, "Impact of variation of wind speed in a wind integrated power system," 2010 International Conference on Advances in Energy Engineering, Beijing, (2010), pp.110-114.

T. Sawatzky, Gokaraju Ramakrishna and S. O. Faried, "Application of Support Vector Machines to Identify a Loss of Excitation Condition on a Power System," IEEE Power Engineering General Meeting, Minneapolis, (2010), pp.25-29.

Titu Bhowmick and Dharmasa, "Development of Prototype Protection Setup for Standalone Solar Power System," American Journal of Electrical Power and Energy Systems, (2015), 4(6), pp.100-105.

APPENDIX-A

SSI-3M6-250W poly-crystalline solar module parameters

S. No	Parameter	Parameter value
1	Maximum power (P rated)	250 W (tolerance $\pm$ 3%)
2	Maximum power point voltage (V_{MPP})	30.68 V
3	Maximum power point current (I_{MPP})	8.14 A
4	Open circuit voltage (V_{OC})	37.98 V
5	Short circuit current (I_{SC})	8.67 A
6	Series fuse rating	15 A
7	Diode rating	15 A
8	Application class	A
9	Fire hazard rating	C
10	Number of series cells	10
11	Number of parallel cells	6
12	Total number of cells	60

APPENDIX-B

Selection of diode ideality factor for PV panel with different materials

S. No	Material	Ideality factor
1	Si-mono	1.2
2	Si-poly	1.3
3	a-Si-H	1.8
4	a-Si-H-Tandem	3.3
5	a-Si-H-Triple	5
6	CdTe	1.5
7	CTs	1.5
8	AsGa	1.3

APPENDIX-C

❖ **Three-phase, 400 V, 3 hp (2.2 KW), 50, Hz and 1480 rpm induction motor**

Parameters:

❖ Stator resistance Rs = 4.1 Ω,

❖ Stator inductance Ls=0.545 H,

❖ Rotor resistance Rr = 2.5 Ω,

❖ Rotor inductance Lr=0.542 H,

❖ Mutual inductance Lm=0.51 H,

❖ Moment of inertia J=0.04 Kg-m^2.